Cerebral characterization of sensory gating in disconnected dreaming states during REM sleep and propofol sedation using hd-EEG and fMRI

Coma Science Group
GIGA Consciousness
University and University Hospital Liége

Author:

Benedetta Cecconi

Promotor:

Prof. Dr. Steven Laureys
ULiége

Co-Promotor:

Dr. Jitka Annen
ULiége

Committee:

Prof. Vincent Bonhomme	University of Liége
Prof. Christina Schmidt	University of Liége
Prof. Didier Ledoux	University of Liége
Dr. Marianna Bevova	University of Luxembourg
Prof. Thomas Andrillon	Paris Brain Institute
Prof. Charline Urbain	Université Libre de Bruxelles

Thesis presented in partial fulfilment of the requirements for the degree of Doctor in Biomedical and Pharmaceutical Sciences

Liége, November 2024

In loving memory of Giovanna, also known as Nonna Ninni

This research was supported by Fonds de la Recherche Scientifique (mandat d'aspirante - FNRS ASP), the MindScience Foundation (Tom Slick Research Award), the GIGA Doctoral School for Health Sciences and other personal grants from the University of Liége (MODUS and Prix Dunan) and from Fondation Léon Fredericq.

Acknowledgements

The work presented in this thesis would not have been possible without the support and collaboration of many people, to whom I owe my sincere gratitude.

First, I would like to thank my supervisors, Dr. Jitka Annen and Prof. Melanie Boly, and my promotor, Prof. Steven Laureys. Jitka, your guidance has been invaluable both to this research and to my personal growth. You took me under your wing when I was a young, 24-year-old intern, and since then, you have been my constant reference point. The person I most wanted to speak with when experiments didn't go as planned or when results were not making sense. Your infectious optimism, sharp wit, and scientific curiosity (always asking just the right questions) kept me moving forward. We had our fair share of disagreements - my stubborn nature and all - but in the end, we always found common ground. Our discussions (and occasional bickering) will be something I will miss deeply. Thank you for everything you've taught me, both in science and in life; you've had a big (positive) influence on my life.

Melanie, it goes without saying that this project would not exist without your ideas. I am deeply thankful that you believed in me from the very beginning, even when I barely knew the basics. You did not get discouraged but taught me so much with great patience. I admire the ease with which you could solve all the (seemingly impossible) problems I faced with the EEG project. You were my problem-solver who could turn my day around in a second. You always showed compassion and kindness when I needed it most. Thank you for welcoming me into your lab with such warmth!

Steven, without you, I probably wouldn't be here today. Thank you for

offering me this position and so many opportunities, which allowed me to travel the world and enriched me as a person. You taught me so much about navigating difficult situations and maintaining a positive mindset. Your support, guidance, and constant protection over these years are something I am deeply grateful for.

I am grateful to Prof. Giulio Tononi for his invaluable ideas, guidance, and support throughout this project.

A very heartfelt thank you also goes to the President of my thesis committee, Prof. Vincent Bonhomme. Your invaluable medical and anesthesiology knowledge formed the foundation of my thesis. I will always fondly remember the time we spent together during data acquisition, all the things you taught me that I hold dear, and your boundless kindness, positivity, and generosity. Similarly, a special thank you goes to Dr. Javier Montupil. Thank you for sharing your scientific and medical knowledge with me, for helping design the experiment, and for your help in acquiring nearly 60 subjects! I will always treasure the patience you showed and the fun we had together - especially your unforgettable "uuuh, uuh" technique for awakening participants (:D).

Thanks to the members of my Committee, Prof. Didier Ledoux, Dr. Marianna Bevova and Prof. Christina Schmidt (who also kindly agreed to serve as the secretary of my defense). Your input throughout my PhD was valuable to the achievements presented here. I would also like to thank the external jury members, Prof. Charline Urbain and Prof. Thomas Andrillon, for the time and effort they invested in evaluating my work. Furthermore, this work would not have been possible without the support of the CRC platform and its dedicated technical team.

A special thanks to the directors of the CSG, Prof. Olivia Gosseries and Prof. Aurore Thibaut, and of the Conscious Care Lab, Prof. Audrey Vanhaudenhuyse. I also extend my gratitude to the post-docs of the GIGA-CONSCIOUSNESS unit: Dr. Nicolas Lejeune, Dr. Pablo Núñez Novo, Dr. Charlène Aubinet, Dr. Charlotte Martial, Dr. Aminata Bicego, and Dr. Charlotte Gregoire. Thank you all for your guidance and support.

Among my current and past colleagues at the CSG, a special thanks goes to: Glenn, thank you for being my friend, confidant, and the one who's made me laugh from day one. Your humor, kindness, and intelligence (let alone poetic talent) are truly one of a kind. Sepehr, girl (as we would say)

you taught me so much, and our talks during those hours of listening to beeps will always stay with me. You're an amazing friend and colleague. A heartfelt thank you to my friends Naji (you highly educated me on meal composition) and Fatemeh - without you, this project would still be stuck at subject 10! Thank you for your kindness and for all the help during those wild acquisitions. I really had some of my best laughs. Thanks for keeping it light and fun. Simona, your sweetness, Neapolitan charm, and our gossip sessions were highlights of many days. Thank you for being the pure soul you are! Special thanks to my dear friends Estelle and Alice (my bohemian girl), who welcomed me into the lab and have been incredible colleagues and friends since the first day. Our talks about THE life and love are memories I'll carry with me. A special thank you also to Pablito - I'll miss not catching all your jokes and musical references. You made the lab a lighter place. Thank you for your friendship and helping with the paperwork (:D). Arianna, the few projects we worked on together were some of the best collaborations I've had. Your talent, efficiency, humor, and direct style are invaluable. Here's to many more, I hope! Thanks to my office mates, Marie and Amandine, for all our conversations, dinners, and light-hearted moments. Emma, you were the best intern a PhD could ask for - resourceful, independent, and full of ideas. I have no doubt you'll go on to do great things, and I'm glad we became friends along the way. Michiel, I still try to avoid pronouncing your name (whenever possible) since I've accepted that I'll never land it correctly! Thank you for all your help with MATLAB codes and for our talks in New York. You're a great scientist!

I'd also like to express my gratitude to the friends, former colleagues, and co-authors from the GIGA-CONSCIOUSNESS unit. Thank you for your contributions, support, and the moments we've shared over the years: Stéphane C., Raja, Pauline, Nolwenn, Audrey, Stephen L., Andrea P., Helena, Aldo, Leandro, Laurence, Anais G., Paolo, Melanie, Geraldine, Nathalie, Emilie and Cecile.

Thank you to my Madison colleagues - now friends - who were with me during my year in Madison. Atakan, my (first) flatmate in Madison, thank you for your genuine spirit. I'll always remember our endless discussions about everything and nothing, our grams of mother nature, and the broccoli with mustard. Beril, thank you for being a wonderful friend and colleague. You welcomed me to Madison at that coffee shop when I first arrived and have been caring ever since. Will thanks for teaching me so much about domestic tasks (if I know how to properly load a dishwasher, it's thanks

to you, you know), the fun times, the pizza, the pesto made from your 100 basil plants, and all the support. You truly made me feel at home. Mariel, thank you for our long, inspiring conversations and for your warm welcome. Garret, thanks for all you've taught me (or at least tried to) about philosophy and for being the natural comedian you are, it's nearly impossible not to laugh with you for more than five minutes. And as your beloved cup says, live, laugh, love, right? Thank you, Giuseppe, for our afternoons of chit-chat and all the support. Matteo, thanks for your patience in explaining IIT to me, and I hope there's more to come! And a big thank to all the other incredible colleagues I had the chance to meet at UW, Graham, Urszula, Alirezta, Elena, Robert, Joanna, and Rong.

Un grazie speciale va alla mia amica, ormai sorella, Fiammetta. Grazie per esserci sempre, per ascoltare i miei ragionamenti contorti senza mai giudicarmi. Siamo davvero due gocce d'acqua! Mamma, senza di te non so chi sarei o dove sarei (a zappare la terra come diresti te). Sei sempre stata un punto di riferimento fondamentale, e senza il tuo sostegno continuo e incondizionato probabilmente non avrei concluso questo PhD. Grazie anche a mio padre, per i suoi consigli preziosi che mi hanno guidata per molto tempo. Un ringraziamento va di dovere a Carlo: grazie per il tuo aiuto, per il supporto informatico 24/7 e per la pazienza infinita. Ti devo molto, e te ne sono infinitamente grata. Un grazie anche alla mia Nonna Franca, che mi hai sempre ascoltata e tirata su con il tuo amore incondizionato. Sei la nonna numero 1! Un grazie anche ai miei zii, zia Francesca e zio Alberto, che mi sono sempre stati vicini, pronti a sostenermi (e soprattutto a sopportarmi) e al mio cuginetto Pippo, grande tifoso che sono certa diventerà un grande arbitro. Infine, un grazie speciale ai parenti di 'Arlo e a Giorgia e Graziano, che mi hanno fatta sentire fin da subito una di famiglia: Maria, Giuseppe, Enrico, i due Adriani, Francesco, Marilina e Vincenzo, Graziella e Beatrice.

Matilde, Francesco e Tommaso, siete la mia gioia più grande. Vedervi crescere e diventare pian piano adulti è stata una delle esperienze per cui sono più grata nella vita. Siete parte di me, e vi vorrò sempre un bene infinito.

Stefan, meeting you was probably the most unexpected thing in my life. You became my home and anchor in such a short time that I still sometimes can't believe it. I will never be able to thank you enough for all the patience and care you show me. This PhD definitely owes a lot to you. I'd be happy to be even half the person and scientist you are.

Abstract

Consciousness, defined as any form of subjective experience, can often detach from the external environment, placing the individuals in a state of sensory disconnection with preserved consciousness. Despite its prevalence, the neural mechanisms underlying sensory disconnection remain poorly understood, due to the difficulties in behaviorally distinguishing between states of consciousness where sensory awareness is present (connected consciousness (CC)) and those where it is absent (disconnected consciousness (DC)). Previous studies comparing wakefulness to sleep or anesthesia have been limited by the inherent differences between these physiological states and the intermittent nature of CC and DC within sleep and anesthesia.

To address these limitations, this study employed auditory stimulation during REM sleep and propofol sedation, followed by serial awakenings to collect subjective reports on participants' state of consciousness and sound perception before waking. The auditory paradigm used was an oddball paradigm, where a regular sequence of sounds (standard) is interrupted by a sound of a different frequency (deviant or oddball). Brain activity was recorded using high-density EEG during REM sleep and fMRI during propofol sedation. We compared brain activity of CC and DC participants — different phenomenological states within the same physiological state — to investigate the mechanisms behind sensory disconnection. Additionally, we compared brain activity during CC with that recorded during wakefulness, while participants listened to the same auditory paradigm, to quantify the impact of physiological state on sensory connection, as CC and wakefulness share sensory awareness but differ in the underlying physiology.

EEG analyses during REM sleep revealed distinct scalp-level differences between CC and DC participants. CC participants exhibited more pronounced

event-related potential (ERP) components traditionally associated with consciousness, suggesting a more elaborate processing and differentiation of standard and deviant sounds. These ERP differences were accompanied by a decrease in delta power (1-4 Hz) and an increase in beta2 power (18-30 Hz) in the CC state. Dynamic Causal Modeling revealed that these scalp differences likely originated from distinct connectivity patterns between CC and DC states. Specifically, DC exhibited an overall reduction in feedback and feedforward connectivity within a temporo-parietal circuit encompassing the inferior parietal lobule and superior temporal gyrus. The comparison between CC and wakefulness showed enhanced processing of deviant sounds in wakefulness, marked by increased amplitude of a late ERP component. This scalp difference was attributed to stronger connectivity during wakefulness compared to CC in a fronto-parietal circuit, involving the inferior frontal gyrus and inferior parietal lobule.

During propofol sedation, we observed unexpected activation increases in DC compared to CC in response to all sounds combined, primarily in temporal and pre-/post-central regions. In contrast, CC participants exhibited widespread decreases and focused increases in the precuneus and a distinct network involving prefrontal regions, hippocampal gyrus, and middle occipital gyrus. This paradoxical pattern reversed for deviant sounds, where CC showed widespread activity increases in fronto-parietal and temporal areas, while DC showed minimal changes, potentially suggesting that deviant perception may be exclusive to CC states. fMRI spectral analysis revealed increased high-frequency oscillations in DC in sensory and attention regions, potentially indicating higher slow-wave activity compared to CC participants in these regions. Interestingly, differences between CC and wakefulness emerged only in general auditory processing, while no differences were observed in deviant sound processing, suggesting similar processing of deviant sounds in CC during sedation and wakefulness.

The current work represents one of the first demonstrations that differential sound processing occurs between self-reported CC and DC within the same physiological state, providing distinct neural signatures of sensory disconnection during REM sleep and propofol anesthesia.

Résumé

La conscience, définie comme toute forme d'expérience subjective, peut souvent se détacher de l'environnement externe, plaçant les individus dans un état de déconnexion sensorielle avec une conscience préservée. Malgré sa prévalence, les mécanismes neuronaux sous-jacents à la déconnexion sensorielle restent mal compris en raison de la difficulté à distinguer comportementalement les états de conscience où la perception sensorielle est présente (conscience connectée (CC)) de ceux où elle est absente (conscience déconnectée (CD)). De ce fait, les études comparant l'éveil au sommeil ou à l'anesthésie ont souvent été limitées par les différences inhérentes entre ces états physiologiques et par la nature intermittente des états de CC et CD dans le sommeil et l'anesthésie.

Pour répondre à ces limitations, cette étude a utilisé une stimulation auditive pendant le sommeil paradoxal et durant un état de sédation au propofol, suivie de réveils en série permettant de recueillir des rapports subjectifs sur l'état de conscience des participants et leur perception des sons avant le réveil. Le paradigme auditif utilisé était un paradigme 'oddball', où une séquence régulière de sons (standard) est interrompue par un son d'une fréquence différente (déviant ou son inattendu). L'activité cérébrale a été enregistrée à l'aide d'un EEG haute densité pendant le sommeil paradoxal et à l'aide d'une IRMf pendant la sédation au propofol. Nous avons comparé l'activité cérébrale des participants en CC et CD — différents états phénoménologiques au sein du même état physiologique — afin d'étudier les mécanismes à l'origine de la déconnexion sensorielle. De plus, nous avons comparé l'activité cérébrale pendant la CC à celle enregistrée pendant l'éveil, tandis que les participants écoutaient le même paradigme auditif, afin de quantifier la façon dont l'état physiologique impacte la connexion sensorielle, étant donné que la CC et l'éveil partagent la conscience sensorielle mais sont

différents en termes de physiologie sous-jacente.

Les analyses EEG pendant le sommeil paradoxal ont révélé des différences distinctes au niveau des signaux provenant du cuir chevelu entre les participants en CC et en CD. Les participants en CC présentaient des composantes de potentiels évoqués (PE) plus prononcées, traditionnellement associées à la conscience, suggérant un traitement plus élaboré et une différenciation des sons standards et déviants. Ces différences dans les PE étaient accompagnées d'une diminution de la puissance delta (1-4 Hz) et d'une augmentation de la puissance beta2 (18-30 Hz) dans l'état de CC. La modélisation causale dynamique a révélé que ces différences neurophysiologiques provenaient probablement de schémas de connectivité distincts entre les états de CC et de CD. Plus précisément, la CD présentait une réduction générale de la connectivité feedback et feedforward au sein d'un circuit temporo-pariétal englobant le lobule pariétal inférieur et le gyrus temporal supérieur. La comparaison entre la CC et l'éveil a montré un traitement renforcé des sons déviants en éveil, marqué par une augmentation de l'amplitude d'une composante PE tardive. Cette différence de PE a été attribuée à une connectivité plus forte pendant l'éveil par rapport à la CC dans un circuit fronto-pariétal, impliquant le gyrus frontal inférieur et le lobule pariétal inférieur.

Pendant la sédation au propofol, nous avons observé des augmentations paradoxales de l'activation en CD par rapport à la CC en réponse à tous les sons combinés, principalement dans les régions temporales et pré-/post-centrales. En revanche, les participants en CC présentaient des diminutions généralisées et des augmentations focalisées d'activation dans les régions auditives primaires ainsi qu'au sein d'un réseau distinct impliquant le précuneus, les régions préfrontales, le gyrus hippocampique et le gyrus occipital moyen. Ce schéma paradoxal s'inversait pour les sons déviants, où la CC montrait des augmentations généralisées de l'activité dans les régions fronto-pariétales et temporales, tandis que la CD montrait peu de changements, suggérant que la perception des sons déviants pourrait être exclusive aux états de CC. L'analyse spectrale de l'IRMf a révélé une augmentation des oscillations à haute fréquence dans les régions sensorielles et d'attention chez les participants DC, ce qui pourrait indiquer une activité à ondes lentes plus élevée par rapport aux participants CC dans ces régions. De façon intéressante, les différences dans le traitement des sons entre les groupes CC et éveil n'ont émergé que dans le traitement auditif général, tandis qu'aucune difference n'a été observée dans le traitement des sons déviants, suggérant ainsi un traitement similaire des sons déviants en CC pendant la sédation et

l'éveil.

Ce travail représente l'une des premières démonstrations qu'un traitement différentiel des sons se produit entre les états de CC et CD auto-rapportés au sein du même état physiologique, fournissant des signatures neuronales distinctes de la déconnexion sensorielle pendant le sommeil paradoxal et l'anesthésie au propofol.

List of Publications

Discussed in the thesis

Cecconi, B., Laureys, S., & Annen, J. (2020). Islands of Awareness or Cortical Complexity? [Letter to the editor]. *Trends in Neurosciences*, *43*, 545–546. https://doi.org/10.1016/j.tins.2020.05.007

Cecconi, B., van der Lande, G., & Sala, A. (2023). Neural Correlates of Consciousness. *Coma and Disorders of Consciousness*, 1–15. https://doi.org/10.1007/978-3-031-50563-8_1

Cecconi, B., Montupil, J., Mortaheb, S., Panda, R., Sanders, R. D., Phillips, C., Alnagger, N., Remacle, E., Defresne, A., Boly, M., Bahri, M. A., Lamalle, L., Laureys, S., Gosseries, O., Bonhomme, V., & Annen, J. (2024). Study protocol: Cerebral characterization of sensory gating in disconnected dreaming states during propofol anesthesia using fMRI. *Frontiers in Neuroscience*, *18*, 1306344. https://doi.org/10.3389/FNINS.2024.1306344/BIBTEX

Cecconi, B., Annen, J., & Laureys, S. (2019). Can human neurological tests of consciousness be applied to octopus? *Animal Sentience*, *4*. https://doi.org/10.51291/2377-7478.1667

Cecconi, B., Gorska, U., Mat, B., Aparicio, M. K., Cilento, R., Selte, A., Monai, E., Moffet, E., Laureys, S., Gosseries, O., Schnakers, C., Annen, J., Tononi, G., & Boly, M. (2024). *Ethical and neuroscientific implications of high perturbational complexity in patients in a minimally conscious state* [In preparation]

Cecconi, B., Mortaheb, S., Bahri, M. A., Boly, M., Laureys, S., Gosseries, O., Bonhomme, V., & Annen, J. (2024). *Cerebral characterization of sensory gating in disconnected dreaming states during propofol sedation using fMRI* [In preparation]

Cecconi, B., Riedner, B., Smith, R., Annen, J., Laureys, S., Tononi, G., Boly, M., & Baird, B. (2024). *High density EEG signatures of connected vs disconnected consciousness during REM sleep* [In preparation]

Other publications

Farisco, M., Pennartz, C., Annen, J., Cecconi, B., & Evers, K. (2022). Indicators and criteria of consciousness: ethical implications for the care of behaviourally unresponsive patients. *BMC Medical Ethics*, *23*. https://doi.org/10.1186/s12910-022-00770-3

Thibaut, A., Panda, R., Annen, J., Sanz, L. R., Naccache, L., Martial, C., Chatelle, C., Aubinet, C., Bonin, E. A., Barra, A., Briand, M. M., Cecconi, B., Wannez, S., Stender, J., Laureys, S., & Gosseries, O. (2021). Preservation of Brain Activity in Unresponsive Patients Identifies MCS Star. *Annals of neurology*, *90*, 89–100. https://doi.org/10.1002/ANA.26095

Panda, R., López-González, A., Gilson, M., Gosseries, O., Thibaut, A., Frasso, G., Cecconi, B., Escrichs, A., Deco, G., Laureys, S., Zamora-López, G., & Annen, J. (2023). Whole-brain analyses indicate the impairment of posterior integration and thalamo-frontotemporal broadcasting in disorders of consciousness. *Human Brain Mapping*, *44*, 4352–4371. https://doi.org/10.1002/HBM.26386

Ooms, F., Annen, J., Panda, R., Cecconi, B., Surlemont, B., & Laureys, S. (2024). Entrepreneurial neuroanatomy: Exploring gray matter volume in habitual entrepreneurs. *Journal of Business Venturing Insights*, *22*, e00480. https://doi.org/10.1016/J.JBVI.2024.E00480

Contents

List of Figures

List of Acronyms

A1 Primary Auditory Cortex

BMS Bayesian Model Selection

BOLD Blood-Oxygen-Level-Dependent

BOR Bayesian Omnibus Risk

CC Connected Consciousness

DC Disconnected Consciousness

DCM Dynamic Causal Modelling

DMN Default Mode Network

DoC Disorder of Consciousness

EEG Electroencephalography

EIB Excitation–Inhibition Balance

EMCS Emergence from Minimally Conscious State

EMG Electromyography

ERP Event-Related Potential

ERPs Event-Related Potentials

fMRI functional Magnetic Resonance Imaging

GA General Anesthesia

GLM General Linear Model

hd-EEG High-density electroencephalography

HG Heschl's gyrus

IA Intraoperative Awareness

ID Intraoperative Dreaming

IFG Inferior Frontal Gyrus

IFT Isolated Forearm Technique

IPL Inferior Parietal Lobule

LAMF Low-amplitude Mixed-Frequency

LOR Loss of Responsiveness

LOC Loss of Consciousness

MCS Minimally Conscious State

MCS- Minimally Conscious State *minus*

MCS+ Minimally Conscious State *plus*

MMN Mismatch Negativity

MRI Magnetic Resonance Imaging

NREM Non-rapid eye movement

PAS Perceptual Awareness Scale

PEB Parametric Empirical Bayes

PSD Power Spectral Density

REM Rapid Eye Movement

ROI Region of Interest

ROR Regain of Responsiveness

SI Supplementary Information

SMA Supplementary Motor Area

SSS Stanford Sleepiness Scale

STG Superior Temporal Gyrus

SWA Slow Wave Activity

UWS/VS Unresponsive Wakefulness Syndrome/Vegetative State

VAS Visual Analog Scale

Chapter 1

Introduction

What is lost at the point of death
that is essential to human nature?

Robert M. Veatch
Transplantation Ethics

Based on

Cecconi, B., Gorska, U., Mat, B., Aparicio, M. K., Cilento, R., Selte, A., Monai, E., Moffet, E., Laureys, S., Gosseries, O., Schnakers, C., Annen, J., Tononi, G., & Boly, M. (2024). *Ethical and neuroscientific implications of high perturbational complexity in patients in a minimally conscious state* [In preparation]

Cecconi, B., Laureys, S., & Annen, J. (2020). Islands of Awareness or Cortical Complexity? [Letter to the editor]. *Trends in Neurosciences*, *43*, 545–546. https://doi.org/10.1016/j.tins.2020.05.007

Cecconi, B., van der Lande, G., & Sala, A. (2023). Neural Correlates of Consciousness. *Coma and Disorders of Consciousness*, 1–15. https://doi.org/10.1007/978-3-031-50563-8_1

Cecconi, B., Annen, J., & Laureys, S. (2019). Can human neurological tests of consciousness be applied to octopus? *Animal Sentience*, *4*. https://doi.org/10.51291/2377-7478.1667

This chapter provides an operational definition of consciousness as non-reflective, subjective experience. I discuss evidence from anesthesia, sleep, and mind-wandering studies, demonstrating the frequent detachment of consciousness from external sensory inputs, resulting in states of sensory disconnection. The challenge of behaviorally distinguishing between conscious states with sensory perception (connected consciousness) and those without it (disconnected consciousness) is examined in light of current methods for assessing consciousness. I evaluate the effectiveness of objective and subjective measures, and behavioral responsiveness in differentiating between CC and DC states. The chapter concludes that, for studying sensory disconnection during states such as sleep and sedation, the most effective approach is to serially awaken participants, after sensory stimulation, to collect subjective reports on their state of consciousness and sensory perception prior to awakening. This methodology allows for a within-state examination of the neural signatures of sensory disconnection, which minimizes biases from between-state comparisons.

Keywords: *consciousness, sensory disconnection, measures of awareness.*

1.1 Human consciousness: a reflective or non-reflective experience?

Understanding the nature and origins of consciousness has always been a fundamental human pursuit. Existential questions such as "where do we come from? What are we? Where are we going?"[1] have likely been pondered since the dawn of human existence. Indeed, evidence from early Paleolithic burials suggests that even our most distant ancestors reflected on the nature of the soul and its fate after death (Riel-Salvatore & Clark, 2001). As technology advanced and our environment transformed, these questions were further adapted and refined. For instance, the 1950s witnessed a series of significant medical innovations and scientific discoveries (such as cardiac massage, electric cardioversion, and positive pressure ventilation) which created previously unimaginable conditions: today, these medical advancements allow patients in coma or with disorders of consciousness (DoC) (see Box 1.1) to survive for decades. However, these remarkable strides have not provided definitive answers to the most fundamental questions their families ask, such as "are they conscious?", "can they feel pain?", "can they hear me?". On cursory examination, consciousness may appear as a concept

[1]Title of the famous painting by French artist Paul Gauguin.

readily grasped through intuition and possessing a seemingly self-evident nature. However, when tasked with providing a definition precise enough to operationalize for scientific investigation, substantial disagreement emerges, resulting in a plethora of discordant definitions.

A prominent debate currently polarizes over two contending definitions of consciousness: consciousness as subjective experience and consciousness as self-report[2]. To elucidate the distinction between these two definitions of consciousness, consider the example of watching a captivating action film. As you become engrossed in the movie, you may not reflect on what you are seeing (e.g., you are not thinking "I am watching an action movie, the main character is doing this and that…"). However, after an especially thrilling action scene, you might regain self-reflection, i.e., you begin to reflect on your viewing experience, thus engaging in self-report. Were you consciously experiencing the movie before this reflective moment? Scientists who identify consciousness with self-report would argue that you were not conscious of the movie before you began to reflect on it (e.g., R. Brown et al., 2019). In their view, consciousness can only be a reflective experience. In contrast, proponents of consciousness as subjective experience (synonymous with phenomenology, i.e. "what's like to be you" (Nagel, 1974)) would contend that you were indeed conscious of the movie even before you began to reflect on it. In their view, consciousness can be non-reflective.

The definition of consciousness as subjective experience is a more inclusive definition than that of consciousness as self-report, which is inevitably restricted to a smaller sample. It is true that in principle the existence of non-reflective consciousness can be doubted: in fact, one might argue that now, as I am self-reporting, I am just deluding myself into thinking that I experienced the film when I was not self-reporting. I might just be fabricating a memory. However, it seems more plausible to infer that one was experiencing the film throughout the viewing, rather than becoming conscious of it only upon self-reflection. In other words, the existence of non-reflective consciousness is "an inference to a good explanation" (Ellia et al., 2021), which dismisses a highly implausible hypothesis (i.e., that I was unconscious throughout the viewing until I recovered self-reflection). Similarly, we cannot prove beyond any doubt the consciousness of those around us due to the inherently subjective/private nature of consciousness. Yet, we generally accept that others are conscious, as the alternative hypothesis seems highly implausible. In the

[2]Although there are many other contending definitions, see e.g., the consciousness entry in the Internet Encyclopedia of Philosophy: https://iep.utm.edu/consciousness/#H1.

clinical setting, particularly with comatose patients or those transitioning to a DoC (see Box 1.1), a diagnosis can be a matter of life and death. Therefore, it would seem more appropriate to favor the more plausible definition of consciousness over the less plausible one.

As pointed out by (Evers, 2016), "words shape perception, and perception is important in shaping how one decides to treat others, not least in clinical context". The diagnostic label has substantial repercussions on the clinical team's perception of the patient and, consequently, on the care provided (Evers, 2016; Young et al., 2021). It affects clinical as well as family decision-making; if the diagnosis is of unconsciousness, the risk of self-fulfilling prophecy is always latent (Young et al., 2021). Ultimately, this diagnostic parsimony (in the sense of attributing consciousness only to patients who can reflect on their experiences) might result in overlooking suffering. In the present work, we define consciousness as subjective, non-reflective experience.

Box 1 – Patients with Disorders of Consciousness

DoC include several conditions with varying degrees of arousal and absent or limited awareness (Bernat, 2006; Laureys, 2005). Coma is a temporary state characterized by absence of arousal and awareness and characterized behaviorally by absence of eye-opening (both spontaneous and following stimulation) (Plum & Posner, 1972). Coma persists for more than one hour and typically not more than a month. A patient exits coma when eye opening is regained, progressing to either unresponsive wakefulness syndrome/vegetative state (UWS/VS), characterized by reflexive motor behavior but lack of purposeful motor behavior or cognitive functions, or to minimally conscious state (MCS), characterized by non-reflexive and purposeful behavior (Giacino et al., 2002; Gosseries et al., 2014). When behavioral signs point to a recovery of perceptual awareness, the patient is diagnosed as MCS-, while if behavioral signs point to a recovery of language comprehension, the patient is diagnosed as MCS+ (Giacino et al., 2002, 2004). If the patient improves further and regains functional communication or functional use of objects, (s)he is diagnosed as Emerging from the MCS (EMCS), which is not considered as part of the spectrum of DoC (Giacino et al., 2004). A patient in EMCS is deemed fully conscious, while retaining varying degrees of motor and cognitive disability.

1.2 How to assess consciousness?

In awake, healthy subjects the state and contents of consciousness can be assessed directly through the collection of subjective reports or, indirectly, through behavior (see fig. 1.1). In the first case, consciousness is measured trough introspection. In experimental settings, this can be measured by letting participants report on their subjective perception of presented stimuli, for example in terms of clarity of the perceptual experience. An example of a subjective scale is the Perceptual Awareness Scale PAS, a 4-point scale with the following descriptive labels (Ramsøy & Overgaard, 2004; Sandberg et al., 2011): (1) no experience, (2) a brief glimpse, (3) almost clear experience, and (4) clear experience of the presented stimulus. In the second case instead, consciousness is experimentally measured based on the performance accuracy in a given behavioral task. For instance, participants might be asked to discriminate between uppercase and lowercase letters. Above-chance performance in the discrimination task is considered evidence that participants were aware of the stimuli. Yet, the relationship between consciousness and performance continues to be a topic of intense debate (Hassin, 2013; Mudrik & Deouell, 2022; Overgaard & Sandberg, 2012; Sandberg et al., 2011; Timmermans et al., 2010). Some contend that subjects can perform above chance without being aware of the stimuli, asserting that a wide range of tasks can be performed unconsciously, e.g., performing abstract mathematical computations, discriminating facial expressions, engaging in semantic processing (Hassin, 2013; Sklar et al., 2012). On the contrary, studies using scales validated to capture changes in phenomenology (e.g., the PAS) seem to suggest that performance and consciousness are closely associated, to the extent that when subjects report being unaware of the stimuli, performance is at chance (Balsdon & Clifford, 2018; Mazzi et al., 2016; Overgaard et al., 2008; Sandberg et al., 2011; Shanks, 2017).

Those favoring objective over subjective measures follow a long-standing tradition that dates back to the behaviorist revolution (Hughes & Watson, 1926; Pavlov, 1906, 1927; Skinner, 1938), which imposed a sharp conceptual divide between 'who we are' and 'what we do' - corresponding to the subjective and objective realms, respectively. Within this framework, the collection of introspective reports is regarded as nonscientific (Jacobsen et al., 2022; Watakabe et al., 2022). As philosopher Wittgenstein argued, a public language that is intersubjectively understandable cannot convey subjective experiences, as these are private and accessible, by definition, only to the individual experiencing them (Jacobsen et al., 2022; Wittgenstein, 1967). The

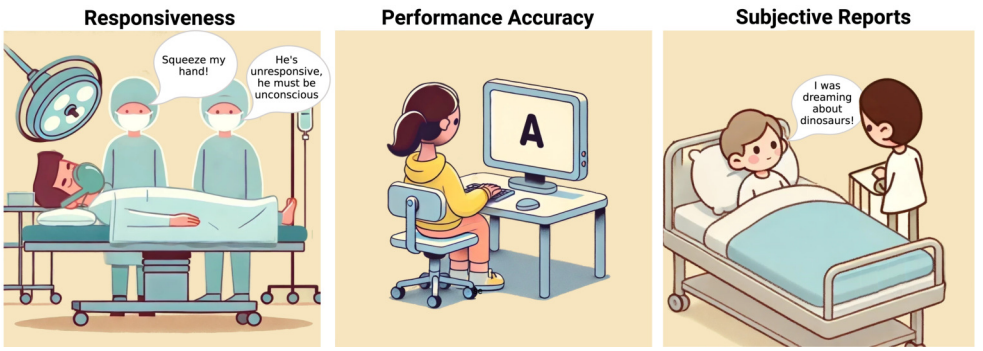

Figure 1.1: How to assess consciousness? Researchers estimate subjects' consciousness using responsiveness (first image), inferring consciousness based on patients' motor responses (or lack thereof) to simple commands; task performance (middle figure), assessing consciousness through task performance such as accuracy in distinguishing uppercase and lowercase letters; and subjective reports (last figure), based on subjects' (introspective) descriptions of their experiences. Researchers may also combine these measures, such as task performance with subjective reports. Created with Dall-E 3 and assembled in BioRender.com

'correctedness' of a subjective report cannot be verified, as there is no means from a third-person perspective to ascertain to which specific subjective experience the reported words correspond. Today, numerous studies have attempted to empirically demonstrate that subjective reports are unreliable. Typically, evidence supporting these claims highlights the abovementioned dissociation between subjective reports and task performance or shows that subjects substantially alter their reports when asked with different wording or upon repeated iterations of the experiment (Marcel, 2003; Overgaard & Sandberg, 2012; Peels, 2016).

It is important to emphasize that the chosen measure of consciousness has far-reaching consequences, as it directly influences the biomarkers or neural signatures of consciousness used in clinical setting e.g., to diagnose consciousness levels. These biomarkers are validated in fact by identifying, in healthy subjects, a specific neural response that correlates with the chosen measure of consciousness. Due to differing underlying assumptions about consciousness, objective and subjective measures often yield different biomarkers. For instance, the event-related potential P300, peaking around 300 ms after stimulus onset, is often proposed as a biomarker of consciousness (Dehaene et al., 2011; Mashour et al., 2020; Rutiku et al., 2015). This wave is elicited by presenting infrequent stimuli (deviants or oddballs) in a

repetitive background of frequent stimuli (standards). An established version of this so-called 'oddball' paradigm employs a combination of temporal regularities, both local in time and global across several seconds[3]. In the study where it was first introduced (Bekinschtein et al., 2009), the validation process involved participants performing the active task of counting the number of deviants, while in the control conditions, participants were asked to mind-wander or perform a distractive task. Violations of global regularities elicited a subcomponent of the P300 called the P3b only when participants were counting the deviants and paying attention to the stimuli, but not when they were mind-wandering or distracted. This led to the conclusion that the P3b is a sign of "conscious awareness of the stimulus" (Bekinschtein et al., 2009).

When researchers used similar paradigms but validated neural responses against subjective reports, they found earlier event-related components to consistently track reported versus unreported awareness of the stimuli (Dembski et al., 2021; Eklund & Wiens, 2019; Eklund et al., 2021), such as the N1 and mismatch negativity responses[4]. For reported stimuli the P3b was often not detected (Dembski et al., 2021) - e.g., in (Sergent et al., 2005), it was not detected for awareness ratings below 10 on a 21-point scale. Therefore, subjective and objective measures result in distinct signatures of consciousness due to different underlying assumptions. Proponents of the P3b as a biomarker of consciousness argue that detection of global irregularities indexes perceptual awareness, while detection of local irregularities (and the related early components) reflects "pre-attentive and automatic responses" (Bekinschtein et al., 2009). Conversely, proponents of earlier components as indicators of awareness contend that the ability to count deviants or detect global irregularities reflects post-perceptual processing and task performance rather than awareness (Eklund et al., 2020; Schröder et al., 2021). When the P3b-based measure was translated to clinical settings, it showed a sensitivity of 26.8%, as many DoC patients, despite consciously perceiving the stimuli, might not have had the cognitive resources necessary for sustaining attention for long periods and detecting global irregularities (Faugeras et al., 2012). In contrast, earlier components-based measures, specifically their enhancement,

[3]The paradigm consists of trials of five tones. The first four are identical in pitch and the fifth can be either identical to the preceding ones (locally standard trials) or of a different pitch (locally deviant trials). At the beginning of the experiment, a global regularity is established by repeating either the local standard or the local deviant trials twenty to thirty times. The established global regularity is then violated by the introduction of a different sound series.

[4]For a more detailed description of early components, see section 1.6.

have shown better accuracies (Engemann et al., 2018), such as 89% in a study by (K. Zhang et al., 2023).

As argued by (Ellia et al., 2021), if one wants to explain consciousness, one must address the “subjective properties of experience”. Focusing solely on the objective correlates of consciousness (i.e., cognitive functions like attention) does not explain consciousness but rather "explains it away” (Chalmers, 1996). To truly account for consciousness, it is essential to address its subjective properties using the objective methods of science. We cannot determine which objective measures index consciousness until we assess, for each paradigm, which cognitive functions/behavior require consciousness of the stimuli, with consciousness assessed using subjective scales validated to track changes in phenomenology, such as the PAS. It follows that the search for the biomarkers of consciousness should involve validation against subjective reports. This is due to the inherently inferential nature of consciousness from a third-person perspective and the still ongoing search for a definitive biological model of consciousness, complete with a robust biomarker serving as a "conscious meter" (Koch, 2017). Collection of introspective reports remain at present the most reliable proxy for tracking changes in the phenomenal experience of others.

Finally, it is important to clarify that the fact that these reports are retrospectively extended to the period immediately preceding the moment of reporting does not necessarily imply that they denote a reflective experience. Instead, they may capture the short-term memory of a non-reflective experience with involvement of reflective cognitive processes, only being involved once the participant accesses and begins to describe the experience. In sec. 1.1, we provided a working definition of consciousness as non-reflective experience, which is precisely what the current experiment aims to capture, given that experiences involving metacognition are typically reduced or minimal during sleep and propofol sedation (Gott et al., 2024; Gross et al., 2019; Scheinin et al., 2021; Siclari et al., 2013, 2017; Tononi et al., 2024). Nevertheless, further theoretical exploration systematically comparing reflective and non-reflective experiences lies beyond the scope of this thesis. Addressing this distinction would necessitate a different experimental protocol from the one employed here, and the incorporation of additional questions explicitly aimed at assessing participants’ levels of self-reflexivity, alongside questions measuring sensory connectedness. Instead, the present work focuses on investigating the neural correlates of sensory (dis)connection under conditions where participants are expected to be conscious in the majority of cases (Radek et al.,

2018; Scheinin et al., 2021; Siclari et al., 2017; Tononi et al., 2024; Valli et al., 2023), and report on the presence or absence of environmental connection.

1.3 Being conscious without being responsive

When transitioning to altered states of consciousness, whether physiologically or pharmacologically induced, inferring a person's level of consciousness becomes increasingly challenging. For instance, if participants are deeply anesthetized, collecting subjective reports or having them perform a task becomes virtually impossible. Previous research on anesthetized participants typically relied on responsiveness to assess the presence of consciousness (see fig. 1.1). That is, brain activity acquired during wakefulness was usually compared with activity observed during unresponsiveness, assuming that unresponsiveness equates to unconsciousness. Inferring the presence or absence of consciousness from (un)responsiveness has now been widely shown to be inaccurate, as unresponsiveness does not always correspond to unconsciousness (Sanders et al., 2012).

In unresponsive, paralyzed patients, accidental return of consciousness during general anesthesia (GA) is one of its most serious complications, usually referred to as intraoperative awareness (IA). IA episodes have been described as feeling helpless, experiencing pain, paralysis, suffocation and sense of impeding death together with hearing noise and sounds from the surgical setting (Errando et al., 2008; Moerman et al., 1993; Osterman et al., 2001). The incidence of IA was initially estimated between 0.0065% and 1.0% (Errando et al., 2008; Pandit et al., 2013), but new studies indicate it could occur in 34.8%/37% of surgeries (Linassi et al., 2018; Sanders et al., 2012). This discrepancy is mainly due to the adopted detection method (Mashour & Avidan, 2015). The more conservative estimates rely on explicit recall of IA episodes, questioning participants post-surgery. In this way, an episode of IA is considered to have occurred only if the patient reported it after operation, spontaneously (during standard postoperative evaluation) or directly questioned through structured interviews (e.g., Brice interview (Brice et al., 1970)). The second estimates rely instead on the isolated forearm technique (IFT), which, by preventing muscle relaxants from acting on one of the forearms, assesses responsiveness during GA in real-time, demanding patients from time to time to respond to commands (e.g., squeeze my hand). Studies using this technique revealed that up to 37% of anesthetized patients, despite looking deeply asleep, were conscious of external stimuli (Linassi

et al., 2018; Sanders et al., 2012). However, more recent estimates from clinical practice suggest that 5–10% of patients in routine clinical care experience these episodes (Lennertz et al., 2023; Sanders et al., 2017). In any case, in most of these studies, IFT responders could not remember the IA's event after emergence from GA, consistently demonstrating that IA is not necessarily tied to explicit recall (Gaskell et al., 2017; Mashour & Avidan, 2015; Russell & Wang, 2015; Sanders et al., 2012). While the psychological sequelae of IA without recall are still controversial (Mashour & Avidan, 2015; Tasbihgou et al., 2018; M. Wang et al., 2012), psychological consequences of IA with recall have been widely reported (e.g., nightmares, daytime anxiety, fear of hospitals) and can lead to post-traumatic stress disorder (Moerman et al., 1993; Osterman et al., 2001).

IA is not the only conscious state that anesthetized patients may experience while unresponsive. Between 22% and 58.6% of patients report intraoperative dreaming (ID) during GA (Errando et al., 2008; Leslie, 2010; Noreika et al., 2011). Distinguishing between IA and ID is not always straightforward (Leslie, 2010; Radek et al., 2018); patients often incorporate auditory and somatosensory stimuli into their dreams or report perceiving such stimuli in a dream-like state (Leslie, 2010; Leslie et al., 2007, 2009; Noreika et al., 2011; Radek et al., 2018). These episodes have sometimes been referred to as "near-miss awareness" (Leslie, 2010).

These studies collectively indicate that completely unresponsive patients can experience a wide range of conscious states. These states span from conscious, dreaming experiences without perception of the surrounding environment to episodes of full awareness of one's environment.

1.4 Being conscious without environmental perception: separating consciousness from environmental connection

The intuitive notion of consciousness often equates it with continuous awareness of the environment, making it seem counterintuitive to imagine someone being conscious while being disconnected from their surroundings. However, more than half of human experience is spent in a stream of internally generated content, from which the external environment tends to gradually fade away (Killingsworth & Gilbert, 2010; Seli et al., 2018; Tononi et al., 2024). The paradigmatic example of consciousness preservation without perception

of one's environment is dreaming sleep. During dreaming sleep, in fact, we undergo a variety of experiences, ranging from sensorily vivid, complex narratives to simpler scenarios or even isolated thoughts (Nir & Tononi, 2010; Siclari et al., 2013; Stickgold et al., 2001; Tononi et al., 2024). Only in less than a third of the time, participants report having had no experience prior to awakening (Tononi et al., 2024). However, even during dreaming experiences, studies have shown that subjects can sometime incorporate external stimuli into their dreams without awakening, maintaining a level of neural processing of external stimuli (e.g., Campbell and Kenny, 2002; Colrain and Campbell, 2007; Kakigi et al., 2003; Türker et al., 2023).

Dissociation between consciousness and environmental perception can also manifest during wakefulness. Studies estimate that we spend 46.9% of our waking time mind-wandering, engrossed in a stream of internally generated thoughts (Killingsworth & Gilbert, 2010; A. F. Ward & Wegner, 2013). During mind-wandering, one's consciousness becomes progressively less influenced by external stimuli and the task at hand, leading to a decreased engagement with the external world and increased absorption in one's internal world (Chun et al., 2011; Kam & Handy, 2013; Seli et al., 2018; A. F. Ward & Wegner, 2013). The level of absorption can vary depending on factors such as the saliency of external stimuli, the complexity of the task at hand or the emotional state of the subject (Barron et al., 2011; Gold & Ciorciari, 2020; Smallwood et al., 2009). In extreme cases, the internal absorption and environmental disconnection can be so profound as to result in car crashes (Yanko & Spalek, 2014). Multiple studies have investigated the neural correlates of perception of external stimuli during self-reported episodes of mind-wandering. These studies consistently reported a general reduction in processing of external stimuli (both salient and not salient) (Barron et al., 2011; Smallwood et al., 2008). However, as during sleep, the disconnection never seems to be complete: our mind, despite wandering, seems to always remain alert to detect critical stimuli that might necessitate us to re-interact with the environment (Kam & Handy, 2013).

Even though the disconnection from the external world can vary in degrees and duration, mind-wandering and dreaming states clearly highlight how consciousness is not necessarily tied to one's environment but can exist within purely internally generated content. An interesting question to consider would be the level of disconnection of DoC patients (see Box 1.1). For example, it remains unknown what is like to be an MCS patient (Gosseries et al., 2014). Due to episodic memory encoding dysfunctions, MCS patients

do not usually remember events occurred when MCS after emerging from this state (e.g., see the New York Times case report). Their experience could be characterized by more sustained periods of sensory disconnection or more transient ones, as observed during mind-wandering. Even in cases less challenging than DoC, distinguishing between environmentally disconnected and connected states of consciousness remains a difficult task. As previously mentioned, traditional markers like responsiveness or physiological state (e.g., sleep) are unreliable indicators, as connected, disconnected and unconscious states can manifest and fluctuate within these conditions. How can we then effectively differentiate between these states in scenarios like sleep or anesthesia, where traditional methods offer minimal insight?

1.5 Within-state experience sampling: a promising candidate to differentiate between connected, disconnected consciousness and unconsciousness

Fig. 1.2 illustrates the states of connected, disconnected consciousness, unconsciousness and wakefulness - the first two states being the focus of this thesis. While earlier sections have introduced these states, we now provide formal, operational definitions to ensure clarity on the subject of our investigation. We define disconnected consciousness (DC) as a state of consciousness with no perception of environmental stimuli and connected consciousness (CC) as a state of consciousness involving selective perception of environmental stimuli. Here, we do not differentiate between CC with incorporation, where external stimuli are reinterpreted into the ongoing experience[5], and CC without incorporation, where external stimuli are perceived in a dream-like state without being reinterpreted into the ongoing stream of consciousness. For the purposes of this thesis, we adopt a broader definition of CC that encompasses both these experiences.

During altered states of consciousness, such as sleep or anesthesia, a promising approach to distinguish between CC and DC is to collect retrospective reports (i.e., experience sampling) in a serial manner. With this approach, (unresponsive) anesthetized or asleep participants are awakened multiple times at designated intervals and questioned about the experience they were having immediately prior to awakening. This method, first implemented in sleep studies, featured progressively increasing the frequency of awakenings,

[5]E.g., an alarm sound reinterpreted in the dream as a barking dog.

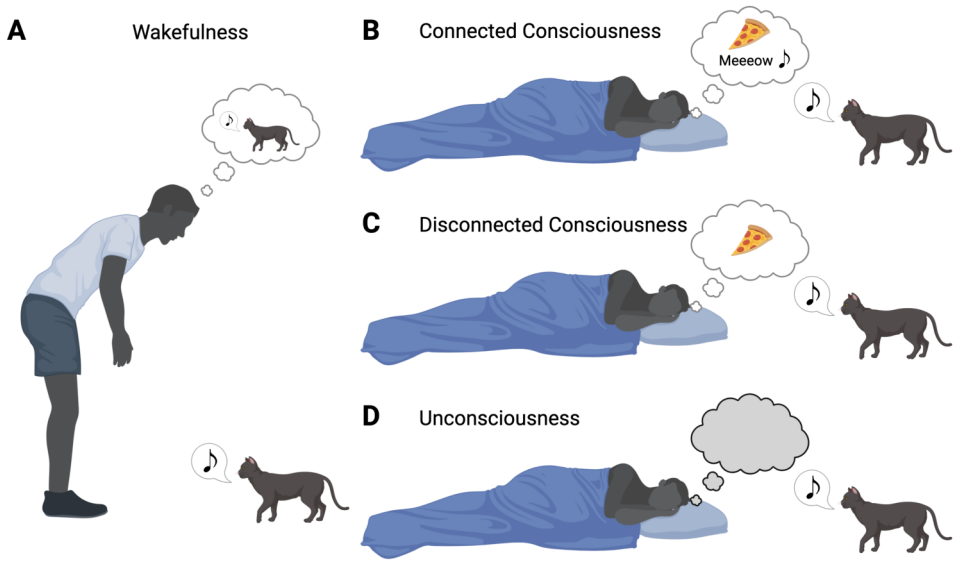

Figure 1.2: Wakefulness and states of consciousness during sleep. Panel A. The man is awake and connected to his environment, demonstrably seeing, hearing, and interacting with the cat. **Panel B.** The man is asleep and is dreaming of pizza. The cat's meow "percolates" through his consciousness, without causing awakening and making the man (partially) connected to his surroundings. **Panel C.** The man is asleep and dreaming of pizza. No environmental stimuli (e.g., cat meow) are incorporated into his dream content, indicating a lack of connection to his surroundings. **Panel D.** The man is unconscious, not experiencing any internally or externally generated content. Created with BioRender.com.

culminating in participants being awakened every 30-45 minutes during an overnight experimental session (Casagrande et al., 1996; Dement & Kleitman, 1957; Fosse et al., 2001; Goodenough et al., 1965; Kahan & LaBerge, 2011; Siclari et al., 2013; Stickgold et al., 2001).

Although the serial awakening paradigm is well-established in sleep research, it has been infrequently applied in anesthesia studies, partly due to the challenges of repeatedly awakening anesthetized participants. GA can in fact be divided into three main phases, each associated with varying depths of anesthesia and characterized by distinct physiological and behavioral markers: induction, maintenance, and emergence (E. N. Brown et al., 2010). The induction phase involves the transition from wakefulness to sedation. In the sedated state, patients are behaviorally unresponsive but can usually

be easily awakened, with eyes closed and in spontaneous ventilation (E. N. Brown et al., 2010; Smith et al., 2023). The serial awakening paradigm is most suited to this state, as the depth of sedation can be finely controlled and kept stable. However, as the depth of anesthesia increases beyond sedation, the patient's heart rate starts to rise and episodes of respiratory depression become more frequent, making breathing support devices necessary (E. N. Brown et al., 2010; Smith et al., 2023). Cessation of eye movements, progressive paralysis, and respiratory depression characterize the maintenance phase, also known as surgical anesthesia, as in this period surgical operations may be performed. This phase is not suited for a serial awakening paradigm, as the high anesthetic concentration makes frequent awakenings and reports collection difficult. Additionally, there are ethical concerns about exposing healthy individuals to GA solely for research purposes. Finally, emergence from anesthesia, marked by the return of spontaneous breathing, is also unsuitable for a serial awakening paradigm as it is typically very short-lasting and unstable in terms of anesthetic concentration.

As previously mentioned, traditional anesthesia research usually relied on post-recovery reports or responsiveness to infer the conscious state of a patient or subject. Implementing the serial awakening paradigm in sedated participants offers several advantages. First, by attempting to wake participants and querying them about their experience while still under anesthesia, the potential for lack of explicit recall is minimized. Second, by shortening the time window over which the report is retrospectively extended, this method ensures a more precise mapping of subjective experience onto brain activity. As shown by sleep studies using serial awakening paradigms, consciousness fluctuates significantly, with the type of experience changing considerably from one half-hour to the next (Siclari et al., 2013).

To mitigate limitations of between-state contrastive approaches, we employed (serial) experience sampling within a single state[6] (Tononi & Massimini, 2008). Traditional sleep or anesthesia studies have resorted to between-state comparisons, contrasting stimulus processing during wakefulness with stimulus processing during sleep or during the maintenance phase of GA (Colrain & Campbell, 2007; Krom et al., 2020). Even recent anesthesia studies

[6]It should be noted that the anesthesia study (chapter 3) used a serial awakening paradigm, while the sleep study (chapter 2) involved a single awakening at the end of the night. Thus, technically, the former employed a serial awakening paradigm while the latter used simple experience sampling. However, in both studies, CC and DC states occurred in a similar physiological background.

using serial awakening paradigms during sedation ultimately resorted to between-state comparisons (Casey et al., 2022; Radek et al., 2018; Scheinin et al., 2021; Valli et al., 2023). In (Scheinin et al., 2021; Valli et al., 2023) episodes of DC were contrasted with responsive wakefulness and in (Casey et al., 2022) with self-reported wakefulness. However, understanding the neural mechanisms that connect and disconnect us from the external world proves difficult through these contrasts, due to the multitude of differing factors between states. Wakefulness, in fact, involves not only consciousness but various other processes, such as metacognition, cognitive control, and behavioral arousal and is supported by a markedly different physiology compared to sleep or GA/sedation. In this work, episodes of CC and DC are contrasted within the same sleep stage or under near-identical anesthetic concentrations, allowing for the comparison of phenomenologically distinct states arising from the same underlying physiological state. This approach aims to minimize confounding variables and offers the potential to isolate the (true) neural correlates of sensory disconnection.

1.6 Sensory processing during sleep[7]

Scientific awareness that individuals can occasionally perceive environmental stimuli during sleep, without arousing, dates back to the late 18th century (e.g., (Freud, 1899)). Extensive laboratory research since the 1960s has corroborated this phenomenon, conducting experiments where somatosensory, auditory, visual, or olfactory stimulation was applied to sleeping participants (mostly during rapid eye movement (REM) sleep), who were subsequently awakened to report on their dreams and stimuli perception (e.g., (Berger, 1963; Ellman & Antrobus, 1991; Leslie & Ogilvie, 1996; Nielsen, 1993; Schredl et al., 2009)). These studies clearly showed that CC and DC can alternate within the same sleep stage, offering an excellent opportunity to investigate the neural mechanisms underlying sensory disconnection while avoiding between-state contrastive biases. However, no study has yet leveraged this alternation of CC-DC states within a single sleep stage to directly contrast these conditions using both neuroimaging and experience sampling (i.e., immediate post-stimulation collection of reports).

One line of research, comprising the studies mentioned above (Berger, 1963;

[7] As our study employed EEG during rapid eye movement sleep, this section will primarily focus on findings from EEG studies investigating sensory processing during sleep. Discussion of sleep studies using other neuroimaging modalities will not be included here.

Ellman & Antrobus, 1991; Leslie & Ogilvie, 1996; Nielsen, 1993; Schredl et al., 2009), investigated the extent to which dreams can be influenced by external stimulation, focusing on how external stimuli are incorporated and reinterpreted within the dream content (e.g., an alarm sound reinterpreted in the dream as a barking dog). Thanks to the collection of reports from participants after sensory stimulation, these studies demonstrated that a considerable portion of stimuli reach dreamers' consciousness more often than previously expected (for a review see e.g. Ellman and Antrobus, 1991; Salvesen et al., 2024). However, they do not provide insights into the neural mechanisms of stimulus incorporation due to the absence of neuroimaging data (Salvesen et al., 2024). Conversely, the other avenue of research that employed sensory stimulation during sleep has omitted the collection of reports, focusing on describing changes in brain activity triggered by sensory stimulation, across sleep stages or compared to wakefulness (Colrain & Campbell, 2007). An example of this literature involves studies combining high-density electroencephalography (hd-EEG and sensory stimulation to analyze event-related potentials (ERPs). These studies revealed that compared to ERPs in the waking state, ERPs during REM sleep generally exhibit increased latency and decreased amplitude, particularly for early components (Kakigi et al., 2003). Notably, N1, mismatch negativity (MMN), P2 and P50 waveforms to external stimulation are generally preserved during REM, albeit attenuated compared to wakefulness (Colrain & Campbell, 2007; Picton et al., 1974). The N1, strongly anticorrelated with sleep/anesthesia and responsiveness, has been proposed as a potential indicator of loss of consciousness and as a modulator of sensory sensitivity (Näätänen & Picton, 1987). P2 and P50 are instead likely involved in high-order aspects of sensory processing and in sensory gating of redundant stimuli, respectively (Aydin et al., 2024; Colrain & Campbell, 2007; Freunberger et al., 2007; Harel, 2020). Additionally, during REM sleep, new components may emerge, such as the N350, hypothesized to be engaged in inhibitory sensory processing aimed at facilitating sleep onset (Colrain & Campbell, 2007; Jemel et al., 1999; Sakellariou et al., 2020; Yang & Wu, 2007). Yet, the relationship between these different components and conscious states remains unknown. As in these studies subjective reports were not collected, the described sleep-induced distortion of ERP waveforms could reflect DC, unconsciousness, or CC. Similarly, studies investigating alterations of brain responses to stimuli of particular valence, involving higher-order cognitive processing, cannot definitively link these changes to the neural correlates of DC/CC, since subjective reports were not collected upon awakening. In these fascinating studies, researchers have shown differential activation to one's

own name compared to others, semantically congruent versus incongruent words, or informative versus meaningless speech in asleep participants (Bastuji et al., 1995; Koroma et al., 2020; Perrin et al., 1999). However, as discussed in section 1.2, which specific cognitive functions are intrinsically related to consciousness remains an open question. To address this challenge, each cognitive function should be validated against subjective reports. Assigning e.g. saliency to certain aspects of sensory input might require CC, occur during DC, or even happen during unconsciousness.

Observing how sleep modulates brain responses to external stimulation, however, has laid the groundwork for hypothesizing about the mechanisms responsible for sensory disconnection during sleep. A longstanding hypothesis proposed the existence of a 'thalamic gate' that blocks stimuli from reaching the cortex, thereby preventing their conscious processing (McCormick & Bal, 1994). However, the aforementioned studies demonstrating the presence of ERP (cortical) responses across sleep stages, convincingly refuted this initial hypothesis. Currently, two principal hypotheses dominate the discourse on the mechanisms underlying sensory disconnection during sleep (non-mutually exclusive) (Andrillon & Kouider, 2020; Tononi et al., 2024). The first, termed the 'cortical gating' hypothesis, posits that stimuli do reach the cortex during sleep but fail to propagate further due to a cortical gate. This gate would arise from neuronal bistability and slow wave oscillations common during sleep, causing cortical circuits to alternate between periods of synchronous activation and silencing, ultimately resulting in a breakdown of cortical effective connectivity (Andrillon & Kouider, 2020; Esser et al., 2009; Massimini et al., 2005). Specifically, a regional distribution of slow wave activity (SWA) - δ band (1-4 Hz) - may play a pivotal role in inducing sensory disconnection. It is important to clarify that sleep stages are not uniform across the cortical surface, but rather exhibit local and asynchronous activity (Siclari & Tononi, 2017). SWA has been observed in fact in humans (Bernardi et al., 2019; Funk et al., 2016; Langille, 2019; Siclari & Tononi, 2017) and in the primary sensory and motor cortices of rats (Funk et al., 2016)during REM sleep. As REM is a state in which, at least in humans, dreaming occurs virtually always (Tononi et al., 2024), SWA only in sensory-motor regions might ensure disconnection while preserving consciousness. The second hypothesis, known as the 'informational gating' hypothesis (Andrillon & Kouider, 2020; Nir & Tononi, 2010), proposes that the dreamer is disconnected due to an overflow of top-down activity over bottom-up. In other words, even though sleeping participants might exhibit some degree of processing of

environmental stimuli, the deeply hallucinatory, internally generated state in which they are immersed likely occupies critical cortical resources to a level that precludes further in-depth processing of external stimuli (Nir & Tononi, 2010).

1.7 Sensory processing during anesthesia

Studies examining sensory processing during anesthesia typically compared stimulus-evoked responses between wakefulness and various depths of anesthesia, such as light or deep sedation (Banks et al., 2018; Dueck et al., 2005; Heinke et al., 2004; Krom et al., 2020; Nourski et al., 2018; Plourde et al., 2006). These studies demonstrated that brain responses to external stimuli were altered in a dose-dependent manner, with gradual suppression up to complete abolition during deep sedation. While stimulus processing remained intact in primary sensory regions, higher-order associative cortices exhibited information processing degradation during light sedation and complete abolition during deep sedation, which was assumed to reflect loss of consciousness (LOC).

In the auditory domain, studies examined brain responses to deviant and standard sounds across a hierarchy of auditory regions, including the primary auditory cortex (posteromedial portion of Heschl's gyrus), secondary auditory regions (such as the planum temporale and anterior superior temporal gyrus), and related regions such as the insular cortex, superior temporal sulcus, middle temporal gyrus, supramarginal, and angular gyri, e.g., (Dueck et al., 2005; Krom et al., 2020; Nourski et al., 2018; Plourde et al., 2006). In (Nourski et al., 2018), integrating local and global levels of temporal irregularities as described in 1.2 (Bekinschtein et al., 2009), brain responses to local deviants were preserved (though attenuated) across all auditory regions under light sedation. However, at higher anesthetic concentrations and during presumed LOC, responses to local deviants were confined to the primary auditory cortex. Similar results were reported by (Krom et al., 2020) using both simple (e.g., click trains) and complex stimuli (e.g., words). In these studies, the different states compared were defined either by anesthetic concentration alone or by a combination of anesthetic concentration and responsiveness, assessed using measures such as the Observer's Assessment of Alertness/Sedation scale (Chernik et al., 1990). As previously mentioned in sections 1.3 and 1.2, the absence of collections of subjective reports to categorize the different contrasted states limits their ability to reliably differentiate between conscious

and unconscious states. Observed changes in brain activity could reflect a mixture of states (CC, DC, unconsciousness), as participants might have been unresponsive because DC or they could have been CC but lacked motivation to respond.

However, at very deep anesthetics concentrations it is likely that participants were unconscious. In studies comparing resting-state wakefulness with deep sedative states (supposedly inducing LOC), the neural correlates of LOC were found to involve broad deactivation and disconnection of mesial parietal regions, posterior cingulate cortex, precuneus, and frontal areas - for a review see (Alkire et al., 2008; Bonhomme et al., 2019). These findings, combined with results from anesthesia studies with sensory stimulation, indicating a dissociation between primary and secondary regions at deep sedative doses, led to the conclusion that anesthesia-induced LOC derives from a cortical gate, as referred to in the 'cortical gating' hypothesis (see sec.1.6). Similar to sleep, a mechanistic role for SWA in determining this cortical gate and leading to unconsciousness (or DC) has also been reported in anesthesia studies. (Mhuircheartaigh et al., 2013)'s results suggested in fact a modulatory role for SWA, with SWA saturation deactivating the thalamus and primary cortices, interrupting wake-like brain activity in response to external stimuli. Therefore, the cortical gate in anesthesia might be produced through mechanisms similar to those in sleep.

Another hypothesis on how subjects might become DC during anesthesia has been proposed by (Sanders et al., 2021), within the predictive coding framework. This hypothesis, which incorporates aspects of the 'informational gating' hypothesis discussed earlier, explains some paradoxical findings during anesthesia, which the cortical gating or informational hypotheses alone cannot explain. For instance, (Banks et al., 2018) observed enhanced stimulus representation in the primary auditory cortex under sedation compared to wakefulness. This enhancement was shown by increases in mutual information between stimuli and neural units, and increased precision and reliability in timing the stimuli. Similarly, (Darracq et al., 2018) reported increased alpha power, indicating heightened excitability (Moheimanian et al., 2021)[8], during presumed disconnected states of ketamine anesthesia and REM sleep. According to (Sanders et al., 2021), these paradoxical observations can be explained by increased prediction error signaling resulting from the mismatch between

[8]Alpha oscillations are an index of neural excitability with low alpha power indexing high cortical excitability (de Pesters et al., 2016; Jensen & Mazaheri, 2010; Klimesch et al., 2007; Lange et al., 2013; Mazaheri & Jensen, 2010; Romei et al., 2008).

feedforward and feedback information. The predictive coding framework in the sensory realm postulates that higher-order cortex continuously generates hypotheses about the environment, which are constantly updated by comparing them with incoming feedforward information. If the (higher-order cortex) predictions do not match the incoming sensory stimuli, a feedforward prediction error is propagated to the cortex to update those predictions. As feedback activity is higher compared to feedforward activity during DC (as per the informational gating hypothesis), feedforward prediction error signaling increases, resulting in the greater activation observed.

1.8 Aims and objectives

In this thesis, my objective is to characterize the neural mechanisms of sensory disconnection by comparing cerebral responses to external stimuli in distinct phenomenological conditions, i.e., CC vs DC, occurring during the same physiological state. I leveraged the physiological states of REM sleep and propofol sedation, as they alternate periods of CC and DC. This work consists of two main studies: the investigation of sensory disconnection during REM sleep using hd-EEG and the investigation of sensory disconnection during propofol sedation using functional magnetic resonance imaging (fMRI). In both studies, during stable REM sleep or unresponsive sedation, healthy controls were administered a series of sounds following the oddball rule (see sec. 1.2). After auditory stimulation, participants were awakened and asked to report on their subjective experience of the sounds (i.e., "did you hear the sounds before awakening?"). Based on the subjective reports collected, participants were categorized as CC if they reported hearing the sounds prior to awakening, and DC if they reported not hearing the sounds. hd-EEG and fMRI recordings were then contrasted between these two conditions. Additionally, in both studies, we recorded participants' brain activity during wakefulness, while they listened to the same auditory stimuli presented during sleep or sedation. By comparing the brain activity of CC participants during sleep/sedation with their activity during wakefulness, we were able to assess the impact of the physiological state on CC. CC and wakefulness are, in fact, similar phenomenological states (as in both cases participants heard the sounds) but differ in their underlying physiology.

Study 1's main objectives were the following:

1a) characterize time differences in sound processing between CC and DC, as well as CC and wakefulness, leveraging the enhanced temporal reso-

lution of hd-EEG. This analysis investigated whether stimulus blockage or modulation occurs at early or late stages of sound processing in DC relative to CC, and in CC relative to wakefulness.

1b) estimate differences in SWA (which, as discussed above, has recently been associated with states of sensory disconnection and unconsciousness) between CC and DC conditions. This analysis served as a first step to investigate the mechanisms behind sensory disconnection, revealing whether SWA plays a role in blocking sensory stimuli from conscious processing.

1c) explain the observed scalp differences in 1a) and 1b) by quantifying changes in effective connectivity between CC and DC and CC and wakefulness. This entailed constructing a neural model that included brain regions known to be relevant for processing oddball sounds during wakefulness, and estimating connectivity changes between these regions, for CC vs. DC, and CC vs. wakefulness. This analysis sought to identify the network of areas that sustain sensory connection during (dreaming) consciousness, independently of physiological state.

Study 2's main objectives were the following:

2a) spatially characterize differences in sound processing between CC and DC, as well as CC and wakefulness, by quantifying Blood-Oxygen-Level-Dependent (BOLD) activation time-locked to sounds both in regions of interest known to be relevant for auditory perception and, at the whole-brain level, in each voxel. These analyses complemented objective 1a) by providing a spatially fine-grained picture of sound processing differences between CC-DC and CC-wakefulness.

2b) attempt to quantify differences in the spatial distribution of SWA between CC and DC using high-frequency BOLD oscillations as an emerging, though still preliminary, proxy for SWA. This analysis potentially offered insight on 1) whether activations observed in 2a) were due to increases in SWA or increases in desynchronized, faster activity; and 2) complemented 1b) results by elucidating spatial locations of observed general increases or decreases in SWA in DC/CC.

This work aims to provide fundamental insights into how, during DC, subcortical and cortical regions block external stimuli from conscious processing. These findings could potentially contribute to the development of

(dis)connectedness biomarkers, promising for implementation in anesthesia monitoring. Monitoring episodes of DC and CC could not only assist in preventing intraoperative connectedness but might also contribute to reducing hypnotic drug dosages, which are known to increase delayed recovery (Vuyk et al., 1997), cardiovascular side effects (Sanders et al., 2012) and postoperative cognitive disorders (Ling et al., 2022; Mason et al., 2010). Finally, our findings may be used to improve diagnosis of DoC patients. Understanding the level of consciousness and the cognitive capacities retained by these patients is, in fact, problematic due to their (often) unresponsiveness. Knowing the neural correlates of (dis)connected consciousness may allow to innovate the procedures of diagnosis and classification of these patients.

Chapter 2

Cerebral characterization of sensory gating in disconnected dreaming states during REM sleep using hd-EEG

"Listen, my dear, she said, this can't go on, you can't live in two worlds at once, in the world of reality and the world of dreams, that kind of thing leads to hallucinations, you're like a sleepwalker walking through a landscape with your arms outstretched, and everything you touch becomes part of your dream, even me, a fat old woman weighing one hundred seventy-five, I can feel myself dissolving into the air at the touch of your hand, as if I was becoming part of your dream too"

Antonio Tabucchi
Requiem: A Hallucination

Based on:

Cecconi, B., Riedner, B., Smith, R., Annen, J., Laureys, S., Tononi, G., Boly, M., & Baird, B. (2024). *High density EEG signatures of connected vs disconnected consciousness during REM sleep* [In preparation]

In this chapter, we investigated EEG responses to an auditory oddball paradigm in CC and DC participants during REM sleep. CC participants demonstrated early differentiation between standard and deviant stimuli and increased amplitude of ERP components associated with conscious processing, such as the auditory awareness negativity, compared to DC participants. Dynamic Causal Modeling further revealed that these differences stemmed from reduced effective connectivity in DC relative to CC within a temporo-parietal circuit involving the superior temporal gyrus and inferior parietal lobule. The two groups also exhibited spectral differences, with CC participants showing decreased delta (1-4 Hz) and increased beta2 (18-30 Hz) power relative to DC. Finally, comparisons between CC and wakefulness revealed heightened deviant processing during wakefulness compared to CC, alongside increased effective connectivity in a fronto-parietal loop that included the inferior frontal gyrus and inferior parietal lobule.

Keywords: *EEG, ERP, Dynamic Causal modeling, sensory disconnection*

2.1 Introduction

The present study aims to elucidate the neural correlates of (dis)connected consciousness within-state, employing a combination of neuroimaging and experience sampling. Participants underwent continuous hd-EEG recording throughout the night, with an auditory sequence played at its conclusion. We employed an auditory roving paradigm, where trains of sounds at a constant frequency were followed by trains of sounds at a different frequency. In this paradigm, the initial sound in a trial served as a deviant but became a standard after a few repetitions. Following the auditory stimulation, participants reported whether they had perceived the sounds during the preceding sleep period. We exclusively selected recordings where the auditory stimulation occurred during REM sleep and contrasted brain activity between participants who reported CC and those who reported DC. By examining CC and DC within the same sleep stage, we aimed to investigate the neural mechanisms of sensory disconnection, while minimizing confounding factors of between-state comparisons (see sec. 1.5). Additionally, we recorded brain activity while participants were awake and exposed to the same auditory paradigm and contrasted brain activity during CC with that during wakefulness. This comparison evaluated the impact of physiological state on CC, as both conditions involved a similar phenomenological state (hearing the

sounds) but differed in their underlying physiology.

We first examined differences in ERPs between the CC and DC groups, and between CC and wakefulness, focusing on scalp-level variations. In the CC vs DC comparison, we analyzed pooled and individual responses to both standard and deviant tones, while for the CC vs wakefulness comparison, we focused on responses to standard and deviant tones. Separate ERP analyses were conducted on CC and DC recordings and, as a positive control, on wakefulness recordings to replicate established findings on auditory and oddball perception. Within the CC group, we hypothesized that all sounds would elicit well-structured early latency components, such as the P100 or N100, as well as potentially delayed middle latency components, such as the P200 (*Hypothesis I*). We further expected this pattern to intensify with deviant tones, eliciting additional middle-late latency components such as MMN and P300, reflecting differential processing of deviant and standard tones (*Hypothesis II*). In the DC group, we anticipated early modulation of ERP components in response to all tones (*Hypothesis III*) and, in response to standard and deviant tones individually, a lack of structured middle-late latency components, suggesting absence of differential processing of standard and deviant sounds (*Hypothesis IV*).

For the CC versus wakefulness contrast, we predicted no differences in early ERP components but expected reduced amplitude in the middle-to-late latency responses to deviant tones in CC compared to wakefulness (*Hypothesis V*), likely reflecting diminished cognitive and attentional engagement during sleep (Gott et al., 2024; Koroma et al., 2020). Conversely, for the CC vs. DC comparison, we hypothesized lower early-latency ERP amplitudes in the DC group in response to all sounds relative to CC (*Hypothesis VI*), alongside a marked reduction or absence of structured middle-to-late latency components in response to standard and deviant tones relative to CC (*Hypothesis VII*).

Power analyses were conducted across various frequency bands, as increased power in certain bands has been associated with sensory disconnection. In particular, increased power in the delta band may play a pivotal role in inducing sensory disconnection (Andrillon & Kouider, 2020; Funk et al., 2016), while power increases in the beta band may reflect enhanced stimulus processing and subject's responsiveness to stimuli (Hipp et al., 2011). Thus, we expected delta power to be elevated and beta power reduced in DC relative to CC (*Hypothesis VIII*).

Finally, we further investigated scalp-level differences by applying Dynamic Causal Modeling to the CC-DC and CC-wakefulness datasets. Modeling the deviant effect, this approach enabled us to explore commonalities and differences in effective connectivity between these states in response to deviant sounds, potentially explaining the observed scalp-level differences. In this regard, we anticipated increased connectivity between higher-order frontal regions and lower cortical regions in wakefulness compared to CC, due to the involvement of these areas in metacognition and attention processes (Bahmani et al., 2019; Chayer & Freedman, 2001; N. P. Friedman & Robbins, 2022; Frith & Dolan, 1996; Miller, 2000), which might be decreased during sleep (Gott et al., 2024) - (*Hypothesis IX*). Conversely, we expected stronger connectivity between primary and secondary regions in the CC group relative to the DC group (*Hypothesis X*).

In summary, we propose an EEG experiment to systematically differentiate between CC and DC states by delivering auditory stimuli and awakening participants to collect subjective reports on their perception of the sounds prior to awakening. Through a combination of scalp-level and effective connectivity analyses, we aimed to uncover the mechanisms behind auditory disconnection during sleep. This investigation explored whether DC is caused by a thalamic gate (McCormick & Bal, 1994), or whether, after reaching the cortex, stimuli are blocked from further processing due to a cortical gate. In particular, power analyses highlighted the potential role of SWA in influencing these mechanisms, while connectivity analyses revealed the underlying causal architecture supporting states of CC and DC, potentially explaining observed ERP differences.

2.2 Methods

2.2.1 Ethics

The study was approved by the institutional review board of the University of Madison. All participants provided written informed consent according to the Declaration of Helsinki and received financial compensation (300 dollars).

2.2.2 Subjects

Only participants who were not under any medication and had no history of sleep disorders or neurological conditions were recruited. They were also required to abstain from stimulants (e.g., caffeine) on the day of the exper-

iment. The database at our disposal encompassed 287 overnight hd-EEG recordings, each featuring participants exposed to a six-minute auditory sequence administered at the end of the night. From this pool, we selected the 28 recordings wherein the auditory sequence was played during REM sleep. Six participants were excluded from the analysis due to either excessive muscle artifacts as detected trough visual inspection of EEG raw recordings, uncertainty surrounding REM stage classification (see sec. 2.6.1), or responding "not sure" to inquiries about sound perception. Consequently, 22 subjects were retained for further analysis. Among these, 11 participants (mean: 44.18 ± 14.71 years old, min: 26.3, max: 65.1, 10 males) reported hearing the sounds during the sleep period and were classified as CC, while the remaining 11 (mean: 44.18 ± 15.51 years old, min: 25.3, max: 65, 3 males) reported not hearing the sounds and were classified as DC.

2.2.3 Experimental protocol

Participants visited the Center for Sleep and Consciousness (University of Wisconsin-Madison) for an overnight recording session. Before starting the overnight recording session, upon arrival and after hd-EEG net application, participants awake brain activity was recorded while a roving auditory oddball sequence (see sec. 2.2.4) was played. Before beginning the recording, participants were instructed to pay attention to the sounds: “Please do your best to pay attention to the sounds. You don’t need to make any responses during this section, your only task is to listen to the tones and rest your eyes on the cross in the center of the computer screen. This section will last approximately 8 minutes”. All sounds were played through sleep headphones that were taped to the hd-EEG net to keep them from moving between tasks and throughout the night. After the waking hd-EEG recording, participants completed the Stanford Sleepiness Scale (SSS) (Shahid et al., 2011) and a Visual Analog Scale (VAS) to assess sleepiness (Alqurashi et al., 2021) – questionnaires are provided in the Supplementary Information (SI). Participants were then instructed to fall asleep according to their individual bedtimes and were informed of the possibility of auditory stimuli being presented during the night. During the entire overnight experiment, participants rested in a dark, quiet room and wore the hd-EEG net along with polysomnography equipment. Throughout the night, subjects were serially awakened by an alarm and asked a series of questions about their state of consciousness during the preceding sleep period. The details of the serial awakening protocol used have been previously described in (Siclari et al., 2013, 2017). However, the data collected from these awakenings will not be analyzed in the present

study. At the end of the night, approximately 10 to 15 minutes before awakening, participants were exposed to a six-minute auditory sequence. The auditory paradigm was the same to the one used for waking recordings. After the end of the six-minute auditory sequence, participants were awakened by a tonal awakening sequence and queried about their perception of sounds during the sleep period through the microphone, i.e., "did you hear the series of tones played through your headphones before the alarm?". Finally, participants completed again the SSS and VAS scales. It is important to emphasize that a question probing their state of consciousness was not asked. Given the limited cognitive load immediately after awakening (Tononi et al., 2024), we prioritized asking the most essential question for the present study, specifically regarding the awareness of sounds. This approach was favored as most awakenings from REM sleep are known to involve consciousness (see sec. 2.5.5 for a more detailed discussion).

2.2.4 Auditory stimuli

Auditory stimuli were administered following the roving oddball rule, as previously described in (Boly et al., 2011; Garrido et al., 2008). The stimuli were pure sinusoidal waveforms. In each trial, all tones shared the same frequency and were followed by a series of tones of a distinct frequency (see fig. 2.1). The initial sound in a trial served as a deviant, which eventually became a standard sound after few repetitions. Accordingly, standard and deviant sounds possessed identical physical features, differing solely in the number of repetitions. The tones ranged in frequency from 500 to 800 Hz, with random intervals in integer multiples of 50 Hz. The number of repetition of the same tone within a trial was randomized between one and eleven. Each tone lasted for a duration of 70 ms, including 5 ms for both rise and fall times. The stimulus-onset asynchrony was set at 500 ms. On average, during each six-minute recording session, participants were presented with 615 standard sounds and 100 deviant sounds.

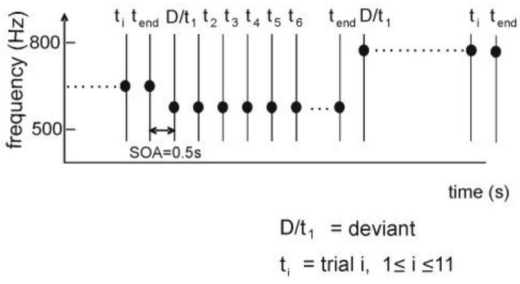

Figure 2.1: Experimental design. Schematic representation of the roving oddball paradigm. Reproduced with permission from (Boly et al., 2011).

2.2.5 EEG data acquisition and sleep scoring

hd-EEG was recorded using a 256-channel hd-EEG system (Electrical Geodesics, Inc., Eugene, OR). EEG recordings were sampled at 500 Hz (using vertex referencing) with the NetStation software and a NetAmps 300 amplifier. Additional polysomnography channels monitored submental electromyography (EMG), electrooculography, electrocardiography, snoring sounds, and blood oxygen levels (pulse oximetry) using Alice Sleepware equipment (Philips Respironics, Murrysville, PA). Sleep scoring was conducted by a certified American Board of Sleep Medicine Sleep Technologist, using standard 30-second epochs, based on the criteria established by the American Academy of Sleep Medicine (AASM) Manual for the Scoring of Sleep and Associated Events (Version 2.5). Only recordings containing either definite stage REM sleep epochs or adjacent epochs that met all criteria for definite REM stage, except for the presence of REMs, were retained. Definite stage REM sleep was defined by the concurrent presence of low-amplitude, mixed-frequency EEG activity without K complexes or sleep spindles, low chin EMG tone, and REMs (American Academy of Sleep Medicine, 2020). Recordings containing intervening arousals were excluded to ensure that the selected data represented continuous periods of stage REM sleep for both CC and DC conditions, with no ambiguity in sleep stage classification. For further details on the sleep-scoring criteria, refer to the SI, sec. 2.6.1.

2.2.6 Pre-processing

Preprocessing was conducted using software EEGLAB (Delorme & Makeig, 2004) – see fig. 2.2 for an overview.

Neck and face channels were excluded, reducing the total channels from 256 to 185. Data were band-pass filtered between 1 and 25 Hz for the scalp analysis/dynamic causal modeling and between 1 and 50 Hz for the power analysis. Bad channels and bad sections were manually identified and rejected. Adaptive Mixture Independent Component Analysis (Hsu et al., 2018) (AMICA) was employed to identify and eliminate artifacts originating from eye movements, cardiac activity, and muscle interference. Bad channels were interpolated - on average, the interpolated channels were 11 in CC; 20 in DC; and 7 in wakefulness. Finally, data were average referenced.

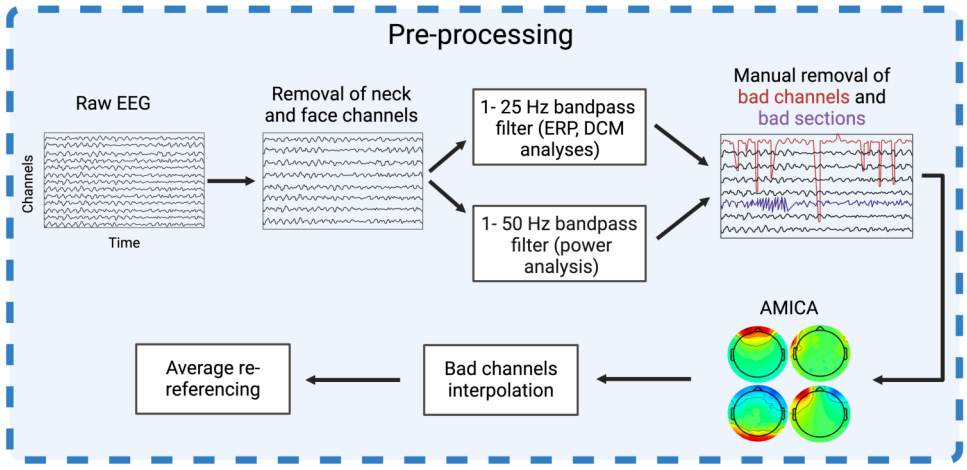

Figure 2.2: Pre-processing steps overview. Pre-processing included the removal of face and neck channels, reducing their number from 256 to 185; band-pass filtering the data from 1 to 25 Hz for ERP and Dynamic Casual modeling analyses and from 1 to 50 Hz for power analysis; manual removal of bad channels and segments, followed by the rejection of artifacts from eye movements, cardiac activity, and muscle interference using Adaptive Mixture Independent Component Analysis (AMICA); and finally, interpolation of bad channels and average referencing. Created with BioRender.com.

2.3 Analyses

2.3.1 Event-Related Potentials

See fig. 2.3 for an overview of the analyses carried out. ERP analyses were conducted in SPM12 (Statistical Parametric Mapping, 421 version 12, UCL Institute of Neurology, London, Britain, http://www.fil.ion.ucl.ac.uk/spm). Data were converted into SPM format files and epoched with a peristimulus window of 0 to 400 ms. We removed the 100 ms period before stimulus onset at 0 ms as it could have possibly reflected late-latency responses instead of serving as a baseline, given the short stimulus-onset asynchrony of 500 ms. Data were epoched selecting all deviant events and from the 6th to 11th standard events to achieve a more balanced ratio of standard versus deviant tones. In the preprocessed six-minute recordings, each subject had an average of 83 deviant events and 358 standard events (the minimum number of deviant events was 67 while the maximum was 100).

We conducted the analyses described below both on all sounds pooled

together (all deviant and 6th to 11th standard events) without distinguishing between standard and deviant events, and separately on deviant and standard events. Epoched data underwent two processing procedures: 1) direct conversion into 4D scalp-map images, resulting in one image for each trial (deviant and standard) for each subject; and 2) detrending (order 1) and robust averaging with the weighting function's offset set at 3 and weights computed by condition. The averaged data were then converted into 4D scalp-map images, resulting in two images (one for deviant and one for standard trials) for each subject. Subsequently, the 4D scalp-map images obtained from both processing procedures were split into 3D files. For trial

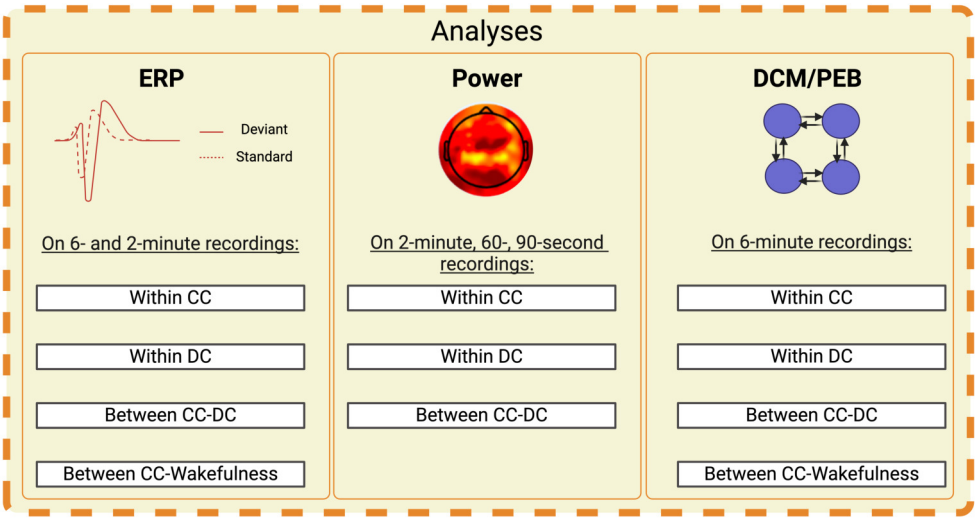

Figure 2.3: Analyses overview. ERPs were analyzed within groups by contrasting deviant and standard sounds and between groups by contrasting deviant, standard and standard-deviant difference waveforms. Additionally, we compared all sounds pooled together (i.e., without differentiating between standard and deviant sounds) between groups. Averaged power spectral density was analyzed within and between groups in the delta (1-4 Hz), theta (4-7.5 Hz), alpha (8-11.5 Hz), beta1 (12.5 – 18 Hz), beta2 (18–30 Hz), and gamma (30-50 Hz) frequency bands. Dynamic Causal Modeling was performed by estimating ten models of increasing complexity for each subject in each group (see sec. 2.3). Bayesian Model Selection was then used to identify the model that best explained the data in each group. At the second level, the Parametric Empirical Bayes approach was employed to analyze changes in connectivity strength in response to deviant sounds between and within groups, using the most probable models from the Bayesian Model Selection analysis (see sec. 2.3 for more details).

images obtained from procedure 1) a first level within-subject factorial design was specified using a two-sample t-test design. We assumed independence between the two conditions (standard and deviant events), while accounting for unequal variance. The onsets of standard and deviant events were included as covariates, interacting with stimulus type (Factor 1) and centered on Factor 1's mean. This approach aimed to examine whether the effects of interest intensified closer to awakening.

We then defined a series of contrasts to quantify the processing of standard and deviant tones separately, the differences in stimulus processing between standard and deviant tones, and determine whether these effects intensified closer to awakening. The obtained contrast images were subsequently input into a) a SPM second-level between-subjects two-sample t-test design, assuming independence and unequal variance between our conditions of connected vs disconnected consciousness; b) a second-level Statistical NonParametric Mapping 13 (SnPM13) (http://warwick.ac.uk/snpm) two-sample t-test design, with 5000 permutations and cluster inference, using overall grand mean scaling for global normalization. Scalp-images derived from robust averaged data were entered into a SnPM design with identical parameters as specified for design (b), wherein we contrasted brain activity time-locked to standard-alone and deviant-alone events in CC versus DC. Deviant and standard (average) scalp-images were also subtracted using the 'contrast' SPM function and fed into a second-level factorial one-sample t-test design within each condition. This additional analysis aimed to investigate more precisely the timing of differential processing of standard and deviant sounds within CC and DC participants. All results were corrected for multiple comparisons using a family-wise error rate as implemented in SPM/SnPM, thresholded at cluster-level or peak-level with $p<0.05$. SnPM was chosen for its enhanced power with small sample sizes: by leveraging weighted locally pooled variance estimates, it has greater power compared to conventional parametric methods (http://warwick.ac.uk/snpm). As we found a significant effect of time (the differences in processing of sounds between CC and DC participants intensified closer to awakening), we decided to trim the 6-minute recordings and conduct the aforementioned analyses separately on the last 2 minutes before awakening (average number of deviant events: 32; average number of standard events: 58; minimum number of deviant events: 29; maximum number of deviant events: 37). The 8-minute recordings acquired during wakefulness were truncated to six minutes for consistency with sleep recordings, analyzed for within-state differences between standard and de-

viant events and contrasted with the same participants recorded during CC using the analyses detailed above.

2.3.2 Spectral analysis

Spectral analysis was conducted using custom MATLAB scripts/functions on data stored in EEGLAB format. We quantified power spectral density (PSD) in the sleep recordings of the last 60, 90 seconds, and 2 minutes before awakening. Since the spectral analysis was carried out independently of the events, we were not constrained by the number of deviant/standard stimuli per cropped recording. This allowed us to analyze data closer to awakening, shortening the validity window of retrospective reports (i.e., reports collected upon awakening were extended back in time for a shorter period, such as 60 seconds, 90 seconds or 2 minutes before collection). PSD was estimated using the pwelch Matlab function: the signal was segmented into 1000 ms Hamming windows with a 50% overlap, employing 1000 discrete Fourier transform points for the PSD estimation. Averaged PSD was analyzed in the delta (1-4 Hz)[1], theta (4-7.5 Hz), alpha (8-11.5 Hz), beta1 (12.5 – 18 Hz), beta2 (18–30 Hz), and gamma (30-50 Hz) frequency bands. Averaged PSD for each band was then normalized by dividing it by the total power across all frequencies. Second-level analyses between connected and disconnected participants were conducted on normalized averaged power for each band separately using two-sided paired t-tests. We corrected for multiple comparisons employing a nonparametric cluster-based permutation test (Nichols & Holmes, 2002). A cluster-forming threshold of $t = 2.08$ was utilized, corresponding to a corrected significance level of $p = 0.05$. The same analyses were also performed on non-normalized averaged PSD to account for potential biases introduced by normalizing to total power, as this normalization might cause large group differences in specific frequency bands to shift or skew the observed effects. The results of these analyses are provided in the SI.

2.3.3 Dynamic Causal modeling

We employed the Dynamic Causal modeling (DCM) framework (David et al., 2006; Friston et al., 2003), as implemented in SPM12, to infer the causal architecture of regional dynamics in CC vs DC participants and in CC vs awake

[1]Studies in rodents and humans show that regional delta activity is an integral feature of REM sleep (Bernardi et al., 2019; Funk et al., 2016; Langille, 2019; Siclari & Tononi, 2017), manifesting as sawtooth waves or slow waves. Thus, potential increased delta power in one group does not contradict the classification of these recordings as REM sleep.

participants. In DCM, each source is represented using a neural mass model, which characterizes the responses of neuronal subpopulations, each with its unique intrinsic dynamics. The behavior and interactions between sources are described using first-order differential equations, which account for how neural activity in each region evolves over time, based on external inputs and connections to other regions (David et al., 2006; Friston et al., 2003; Kiebel et al., 2008). Importantly, DCM defines connectivity as the directed causal influence one source has on another, capturing both intrinsic (within a source) and extrinsic (between different sources) interactions. These connections are dynamic and can change depending on the experimental context. Variational Laplace is applied to estimate these connectivity parameters efficiently, integrating prior knowledge with observed data for accurate model inversion (Zeidman et al., 2023).DCM assumes that the observed EEG data result from the depolarization of pyramidal cell populations (Friston et al., 2003). The relationship between these neuronal signals and the recorded sensor data is modeled using a lead-field, which is a mathematical description of how neuronal currents in the brain (sources of activity) produce measurable signals in the sensors (David et al., 2006; Friston et al., 2003; Kiebel et al., 2008). This description determines how activity from different brain regions contributes to the signals captured by the sensors, essentially describing how the electromagnetic fields produced by neurons are detected by scalp sensors (David et al., 2006; Friston et al., 2003; Kiebel et al., 2008). The resulting DCM spatiotemporal model is a nonlinear state-space model linking unobserved neuronal dynamics to observed data via these lead-field equations (David et al., 2006; Friston et al., 2003; Kiebel et al., 2008). It includes temporal (connectivity) and spatial (sensor projection) parameters, which are estimated using Bayesian inference.

Being an hypothesis-driven method, DCM allows users to specify and compare different biophysically plausible models which are hypothesized to generate the observed data (David et al., 2006; Friston et al., 2003; Kiebel et al., 2008). Ultimately, it indicates which model offers the most accurate representation. This is accomplished by 1) defining a forward model to simulate time series under the specified neural architectures (i.e., neural models) and quantifying the fit of each model to the data (Bayesian inversion); and 2) by comparing the evidence for the specified models (Bayesian comparison) (David et al., 2006; Friston et al., 2003; Kiebel et al., 2008).

We performed DCM for evoked responses on the six-minute recordings. We set the peristimulus time window to 0-400 ms relative to the stimulus

onset, the detrend option to 1, the subsample option to the default value of 1, and the number of modes to 8 (resulting in DCMs being computed on a reduced representation of the data, corresponding to eight channel mixtures). For the forward model, we used the 'EEG BEM' head model (Boundary Elements Model (Geselowitz, 1967; Hämäläinen & Sarvas, 1989; Mosher et al., 1999), with location of sources described by a canonical cortical mesh (of size 'normal'). Before forward model calculation, the position of the EEG electrodes was coregistered to the head model in each subject. Evoked responses were spatially modelled using a single equivalent current dipole for each source (see fig. 2.8A). We quantified the evidence for 10 increasingly complex models, varying in their anatomical sources and connections (see figs. 2.8A-B). The full model included left and right primary auditory (A1) cortex, left and right superior temporal gyrus (STG), left and right inferior parietal lobule (IPL), left and right inferior frontal gyrus (IFG), connected with feedforward, feedback and intrinsic connections present on all sources. A1, IFG and STG sources were selected based on previous work showing the involvement of these regions in the processing of deviant sounds (Boly et al., 2011; Doeller et al., 2003; Garrido et al., 2008). IPL was included based on its broader involvement in bottom-up perception (Igelström & Graziano, 2017) and deviant detection as evidenced by EEG and fMRI studies (Justen & Herbert, 2018; Stevens et al., 2000).

Additionally, because of the documented suppression of frontal activity during REM sleep (Cote, 2002; Hobson et al., 1998; Maquet, 2000), temporo-parietal circuits, including the IPL, are known to take over some aspects of auditory processing typically mediated by frontal regions during wakefulness (e.g., see (Cote, 2002)). Therefore, the IPL was included as a potential candidate region for auditory processing during REM sleep. The coordinates of left A1 [MNI coordinates: -42; -22; 7], right A1 [MNI coordinates: 46; -14; 8], left STG [MNI coordinates: -61; -32; 8], right STG [MNI coordinates: 59; -25; 8] and right IFG [MNI coordinates: 46; 20; 8] were obtained from (Tyrer et al., 2020). Coordinates of left IFG [MNI coordinates: -56.2; 13.9; 15], left IPL [MNI coordinates: -51.3; -68.8; 31.2] and right IPL [MNI coordinates: 48.8; -64.1; 35] were derived from (P. Y. Chen et al., 2021). As they were originally provided in the Subject Coordinate System, we converted these coordinates to the MNI space using Brainstorm software (Tadel et al., 2011). The activity of each source was described using the event-related potentials neural mass model, comprising three neural subpopulations including spiny stellate cell in the granular layer, pyramidal cells, and inhibitory interneurons

in the supragranular layers (Moran et al., 2007). Driving inputs (i.e., tones) were considered to enter the network from the left and right A1. Based on scalp-analysis results, we assumed that the tones would activate the input region 50 ms after stimulus onset (with width of the input volley left at the default value of 16 ms).

2.3.4 Bayesian Model Comparison and Parametric Empirical Bayes

Through random effects Bayesian Model Selection (BMS), we conducted a comparative analysis of the ten abovementioned models on both individual participant groups (CC, DC, and awake) and combined groups (CC-DC and awake-CC). We first run BMS assuming all models belonged to the same family to ascertain the model with the best fit for each group's data. To elucidate architectural differences between groups, we employed family-based inference, categorizing models into distinct families based on the number of regions and type of connections. For the number-of-region family-inference, models were partitioned into five families: a 4-source model (Model 1), 5-source models (Models 2-3), 6-source models (Models 4-5), 7-source models (Models 7-8), and 8-source models (Models 6-9-10). For the type-of-connection family-inference, models were divided into two families: those with feedback, feedforward, and self connections (Models 1-2-3-4-5-7-8-10) and those with feedback and feedforward connections only (Models 6-9). The evidence for each model (or family of models) was approximated using negative variational free energy, yielding a value known as free energy (Friston et al., 2003). This metric reflects the balance between a model's predictive accuracy and its complexity. The winning model thus represents the optimal trade-off between fit and complexity, thereby mitigating both overfitting (complex models with high fit but poor generalizability) and underfitting (models inadequately explaining the data). The Bayesian Omnibus Risk (BOR) was computed to quantify the uncertainty associated with the winning model/family. A high BOR indicates that all models or families have a similar chance of being the true underlying model, i.e., BOR indicates the posterior probability that model frequencies are all equal.

The winning models in the CC, DC, CC-DC and CC-awake groups were selected for further analysis of individual connections using a second-level Parametric Empirical Bayes (PEB) analysis. PEB is a hierarchical approach (Friston et al., 2016; Zeidman et al., 2019) that allows to test for differences in DCM connections' strength between subjects, assuming a shared neural architecture across all participants. We estimated a second-level PEB within-group

on the BMS winning models for the CC and DC groups; and between groups on the BMS winning model for all CC-DC participants and for CC-awake participants. We exclusively modeled parameters from the DCM matrix B, which comprised intrinsic, forward, and backward connections modulated by the deviant effect and included (dis)connectedness as the between-subjects effect for the CC-DC group and wakefulness for the CC-awake group. The outcomes were 1) two group-level model PEBs which quantified the commonalities within the CC and DC groups in terms of connection strength for each of the 21 DCM connections specified for the CC group and each of the 24 DCM connections specified for the DC group; 2) two group-level model PEBs which quantified the effect of disconnectedness/wakefulness on each of the 24 DCM connections specified for the CC-DC group and each of 16 DCM connections specified for the CC-awake group. As we did not have strong hypotheses regarding the neural characterization of CC/DC states or the differences between CC and DC states or CC and awake states, we conducted an automatic search for model comparison. This search consisted of comparing 256 candidate PEB models, each with different combinations of DCM parameters switched on or off. Finally, the parameters from the best reduced models were averaged (Bayesian Model Averaging) and thresholded based on the free energy (very strong evidence Pp > .99).

2.4 Results

2.4.1 Greater prevalence of CC in males and no significant difference in sleepiness between CC and DC

Analyses were conducted on a total of 22 participants, with 11 participants in the CC group and 11 in the DC group. A chi-square test reveled a statistically significant gender disparity in connection rates, with males considerably more likely to be connected than females ($\chi^2(1, N = 22) = 9.2$, p = .05). SSS and VAS questionnaires were administered to participants before the start of the overnight recording session and again upon awakening in the morning to assess their sleepiness levels - refer to the SI sec.2.6.2 for the full versions of the questionnaires. Two participants' SSS and VAS questionnaires were lost due to technical issues with storage. Both participants were CC, leading to a comparison of sleepiness levels between 9 CC and 11 DC participants. A Mann-Whitney U test was conducted to compare CC and DC SSS sleepiness scores. The test revealed no statistically significant difference in sleepiness scores between the groups, neither before sleep onset (W = 60.5, p = 0.4051)

nor after awakening in the morning (W = 62.5, p = 0.31). Responses to VAS question 1 "overall, how would you describe your mood?" (VAS1), VAS question 2 "overall, how alert do you feel?" (VAS2) and VAS question 3 "overall, how sleepy do you feel?" (VAS3) were compared between the CC and DC groups to assess differences in mood, alertness, and sleepiness. As Shapiro-Wilk normality tests confirmed a normal distribuition of VAS1/2/3 scores within both CC and DC and F-tests equal variances, two-sample t-tests were used to investigate inter-group differences. No statistically significant differences were observed in mood (t = 0.92999, df = 18, p = 0.3647), altertness (t = -0.50839, df = 18, p = 0.6174) or sleepiness (t = 0.29617, df = 18, p = 0.7705) between CC and DC participants before sleep onset. Similarly, two-sample t-tests on VAS3 scores collected upon awakening revealed no significant differences in sleepiness (t = 0.87, df = 18, p = 0.3977). As VAS1 and VAS2 scores collected upon awakening were not normally distributed, a Mann-Whitney U test was employed to test for inter-group differences, revealing no significant differences in mood (W = 41.5, p = 0.5517) or alertness (W = 36, p = 0.3161) upon awakening. More detailed results of the SSS and VAS analyses are displayed in the SI, sec. 2.6.2.

2.4.2 Hypotheses I-VIII. Main findings of the scalp-level analyses

Hypotheses I-IV. CC participants show early differentiation between standard and deviant stimuli while DC show no differential processing

During wakefulness, in the 6-minute recordings, oddball tones elicited a classic ERP waveform with a delayed N1 (∼150-175 ms), followed by N2 (∼225 ms), and P3 (∼300-350 ms) components (see fig. 2.4, top panel). In contrast, standard tones produced a smaller amplitude N1 and a P2 component. Subtracting the standard from the deviant waveform in the 200-250 ms post-stimulus window revealed a typical MMN response, consistent with prior literature (Garrido et al., 2007, 2008). Significant differences between standard and deviant waveforms were observed in the MMN time window, peaking at 232 ms in a central cluster [x:-4, y:-3] (SPM, pFWE-corr: 0.000; T:4.82), showing increased negativity for deviant tones; and in the P3 window, with increased positivity for deviant tones peaking at 322 ms (SPM, pFWE-corr: 0.05; T:4.80) and 370 ms (SPM, pFWE-corr: 0.02; T:4.63) in a temporo-central cluster [x:21, y:-52 and x:-4, y:-3].

Within CC, in the two-minute recordings, one sample t-tests on subtracted deviant and standard (average) scalp-images revealed a right frontal cluster

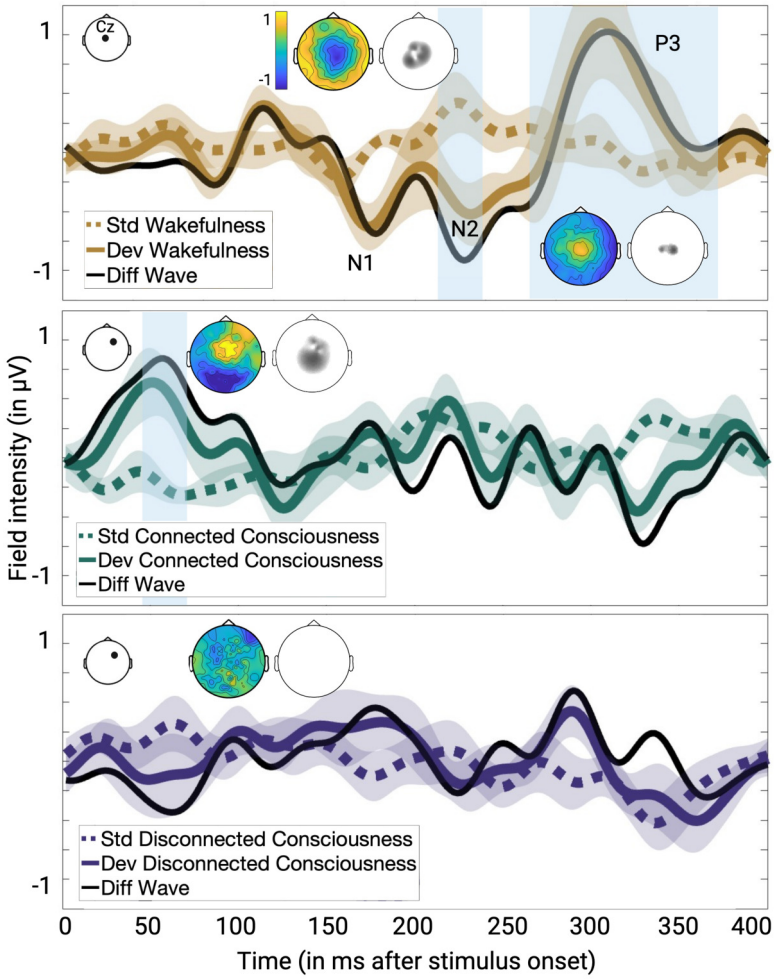

Figure 2.4: Scalp differences in deviant and standard sound processing during wakefulness, CC and DC.. Grand average time series of deviant evoked responses are shown during wakefulness (top panel) at channel Cz, CC (middle panel) and DC (bottom panel) both at channel 50. See next page. Time-series are shown from 0 ms (stimulus onset) to the end of the epoch (400 ms) and for recording duration of 6 minutes for wakefulness and 2 minutes for CC and DC groups. Blue highlighted region shows significance level (*p < 0.05). ERPs were bandpass filtered 1-30 Hz for visualization purposes. Yellow/green/purple shading indicates the standard error of the mean. Within each panel, SPM grand average T maps of the difference in deviant and standard sound processing are shown for the significant components of each group. See next page.

Figure 2.4: T maps are displayed unthresholded (left) and thresholded at p = 0.001 (uncorrected) at the peak latency. Figures were generated in MATLAB and assembled in BioRender.com.

[x:17, y:29] at 64 ms (see fig. 2.4, middle panel), indicating differential processing of standard and deviant sounds already at very early latencies during CC (SPM, pFWE-corr: 0.01; T:13,04). Within DC, no significant clusters were found (see fig.2.4, bottom panel). The same within-condition analysis conducted on the 6-minute recordings did not yield any significant clusters in either CC or DC participants.

Hypothesis V. Effect of physiological state on connected consciousness: frontal activity to deviant tones distinguishes awake participants from asleep, connected ones

No statistically significant difference was observed when comparing ERP waveforms in response to standard tones in CC with those of the same participants recorded during wakefulness. However, significant differences emerged in the processing of deviant sounds (see fig. 2.5): a two-sample t-test between deviant-ERP waveforms in CC versus awake participants found a frontally distributed cluster [x: 26, y: 67] characterized by increased positivity upon deviant tones presentation and peaking at 246 ms, more pronounced in awake participants than in CC ones (SPM, pFWE-corr: 0.02, T: 5.26).

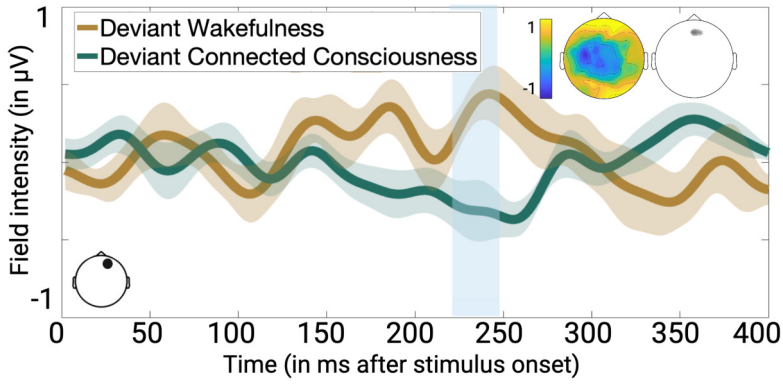

Figure 2.5: See next page.

Figure 2.5: Scalp differences in deviant sound processing between CC and wakefulness. Grand average time series of deviant evoked responses are shown in CC (green line) and during wakefulness (yellow line) at channel 25, which corresponds to one of the suprathreshold channels closest to the coordinates (26, 67) of the significant scalp positivity. Time-series are shown from 0 ms (stimulus onset) to the end of the epoch (400 ms) and for recording duration of 6 minutes. Blue highlighted region shows significance level (*p < 0.05). ERPs were bandpass filtered 1-30 Hz for visualization purposes. Green/yellow shading indicates the standard error of the mean. On the top right, SPM grand average T maps of the difference in deviant sound processing between CC and wakefulness. T maps are displayed unthresholded (left) and thresholded at p = 0.001 (uncorrected) at the peak latency. Figures were generated in MATLAB and assembled in BioRender.com.

Hypothesis VI-VII. Effect of (dis)connectedness within the same physiological state: asleep, connected and disconnected participants exhibit differences in standard and deviant stimulus processing

Scalp analyses revealed significant differences in the processing of standard and deviant sounds between CC and DC participants. The two-sample t-test on first-level contrast images from the six-minute recordings identified a temporal cluster [x:8, y:50] of increased positivity at 280 ms in both CC and DC groups upon presentation of deviant tones compared to standard ones (see fig. 2.6, top panel). This effect was significantly stronger in the CC group compared to the DC group and intensified as awakening approached more in CC than DC participants (SnPM, pFWE-corr: 0.004, T:4,46). No significant clusters were observed with SPM or SnPM when brain activity time-locked to standard-alone and deviant-alone events were contrasted in CC versus DC. However, the same analysis conducted on the 2-minute recordings found a cluster in the right fronto-temporal scalp region [x:60, y: -3] where the difference between CC and DC standard ERP waveforms peaked at 154 ms, with increased negativity in response to standard tones in CC compared to DC participants (SnPM, pFWE-corr: 0.004; T:6,21) – see fig. 2.6, bottom panel. Finally, no significant clusters were found for any analyses when all tones were pooled together, neither in the 6-minute nor the 2-minute recordings.

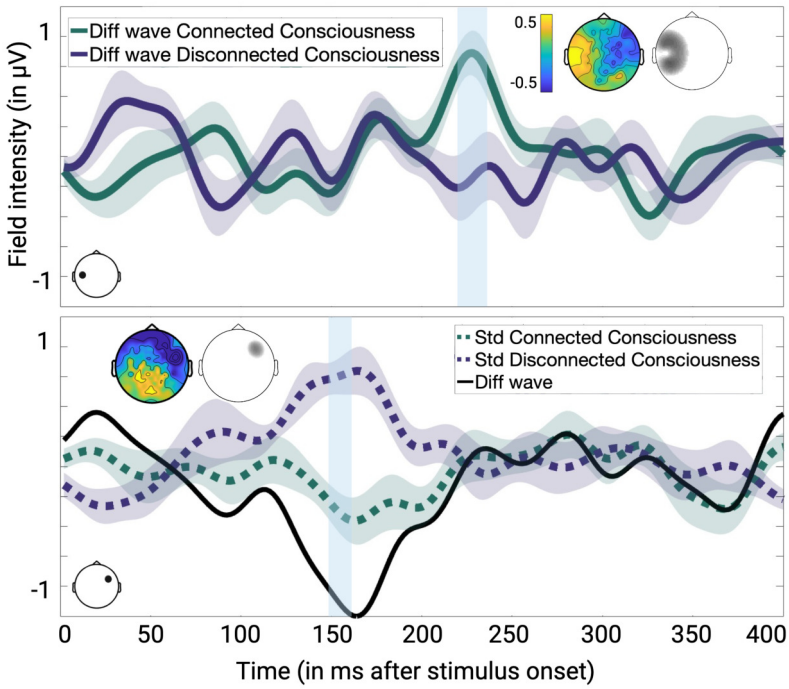

Figure 2.6: Scalp differences in deviant vs. standard sound processing between CC and DC states. On the **top panel**, grand average time series of "standard-deviant" difference waves in CC (green line) and DC (purple line) are displayed at channel 69, corresponding to the coordinates (8,50) of the significant scalp positivity. On the **bottom panel**, grand average time series of standard evoked responses in CC (green line) and DC (purple line), along with their difference wave, are displayed at channel 12, corresponding to the coordinates (60, -3) of the significant scalp negativity. Within each panel, SPM grand average T maps for the respective time series contrast are shown unthresholded (left) and thresholded at p = 0.001 (uncorrected) at the peak latency. Time-series are shown from 0 ms (stimulus onset) to the end of the epoch (400 ms) and for recording duration of 6 minutes (top) and 2 minutes (bottom). Blue highlighted region shows significance level (*p < 0.05). ERPs were bandpass filtered 1-30 Hz for visualization purposes. Green/purple shading indicates the standard error of the mean. Figures were generated in MATLAB and assembled in BioRender.com.

Hypothesis VIII. Asleep, connected participants exhibit increased beta2 and decreased delta power compared to disconnected ones

Comparison of power spectral density between CC and DC participants reveled a widespread increase in beta2 (20-30 Hz) power in both the 60-sec and 2-min recordings (paired t-test, p <0.05, SNPM corrected), alongside

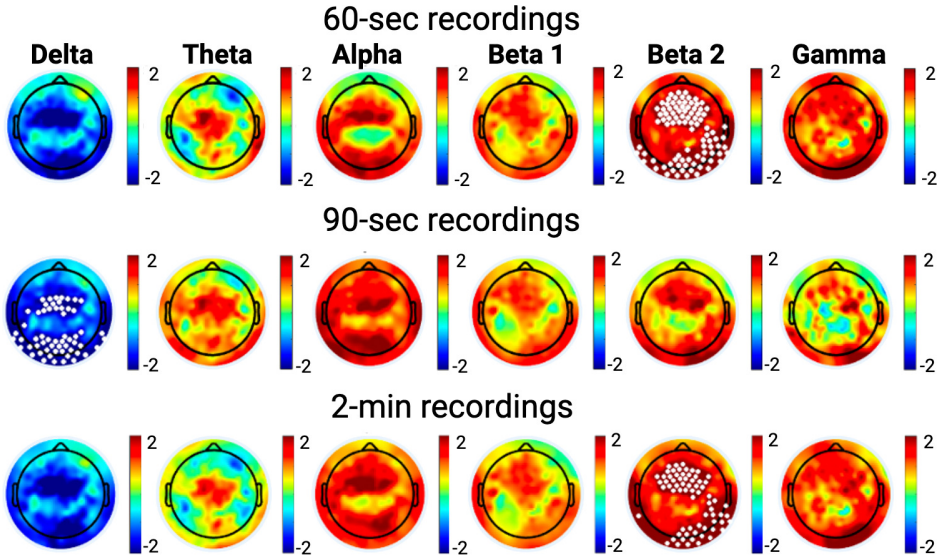

Figure 2.7: Differences in normalized power spectral density between CC and DC. The difference between CC and DC (i.e., CC-DC) in averaged power spectral density in the delta (1-4 Hz), theta (4-7.5 Hz), alpha (8-11.5 Hz), beta1 (12.5 – 18 Hz), beta2 (18–30 Hz), and gamma (30-50 Hz) frequency bands is shown for 60-90-second and 2-minute recordings. Widespread decrease in delta band and widespread increases in beta2 band were found in CC compared to DC. White dots, $p<0.05$ SNPM corrected. Figures were generated in MATLAB and assembled in BioRender.com

widespread decreases in delta (1-4 Hz) power in the 90-sec recordings (paired t-test, $p < 0.05$, SNPM corrected), for CC participants compared to DC ones – see fig. 2.7. No statistically significant clusters were observed for theta, alpha, beta1, or gamma power in any recording length.

Mean normalized percent power within CC and DC for each recording length is shown in the SI (see fig. 2.13).

Analyses of absolute, non-normalized power similarly revealed no statistically significant clusters for theta, alpha, beta1, or gamma power across any recording length. However, unlike the results for normalized power, no significant differences were found in the beta2 band, although a trend toward increased beta2 power in CC compared to DC participants was still observed in the uncorrected results (see fig. 2.14). The delta effect, with decreased power in CC compared to DC participants, was still detectable in the 2-min recording, albeit reduced (paired t-test, $p < 0.05$, SNPM corrected) - fig 2.14. See sec. 2.6.4 for further discussion of these findings.

2.4.3 Hypothesis IX-X. Main findings of the effective connectivity analyses

Most complex dynamic causal models best explain CC, DC, and awake states

Fig. 2.8B illustrates BMS analysis results by model, number of sources, and connection type for individual participant groups (CC, DC, awake) and combined groups (CC-DC, awake-CC).

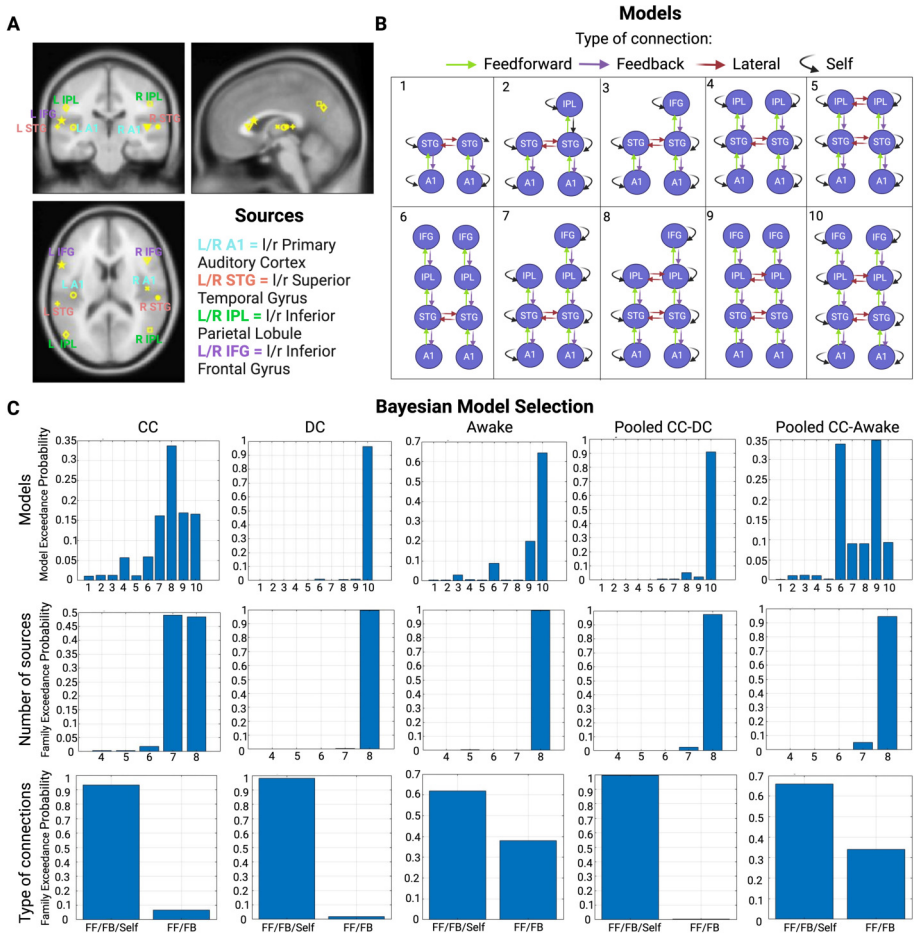

Figure 2.8: Panel A. Coronal, sagittal and axial view of the sources selected for the DCM models. MNI coordinates used for sources were left A1 [-42; -22; 7], right A1 46; -14; 8], left STG [-61; -32; 8], right STG [59; -25; 8], right IFG [46; 20; 8], left IFG [-56.2; 13.9; 15], left IPL [-51.3; -68.8; 31.2] and right IPL [48.8; -64.1; 35]. **See next page**.

Figure 2.8: (Previous page.) **Panel B**. DCM models estimated for each subject. The models were of increasing complexity and varied in the number of sources and type of connections. **Panel C**. Bayesian model selection results for CC, DC, Awake, pooled CC-DC and pooled CC-Awake groups. Results are shown per model (first row) and per family-based inference based on number of sources (second row) and type of connection (third row). Based on the number of sources, models were partitioned into five families: a 4-source model (Model 1), 5-source models (Models 2-3), 6-source models (Models 4-5), 7-source models (Models 7-8), and 8-source models (Models 6-9-10). Based on the type of connections, models were divided into two families: those with feedback, feedforward, and self connections (Models 1-2-3-4-5-7-8-10) and those with feedback and feedforward connections only (Models 6-9). FF= feedforward; FB = feedback; Self = intrinsic, self-connections. Figures were generated in MATLAB and assembled in BioRender.com.

The winning model varied across groups: model 8 prevailed in CC, with a probability of equal model frequencies (Bayes Omnibus Risk (BOR)) of 0.58; model 10 in DC (BOR = 0.00), the awake group (BOR = 0.04), and the CC-DC group (BOR=0.00); and model 9 prevailed in the CC-awake group (BOR= 0.42). Across all groups, models incorporating feedforward, feedback, and self-connections were consistently favored over those without self-connections. Families of models with 8 sources best explained the data in all groups except CC, where families with 7 and 8 sources were equally probable (see fig. 2.8C, first row).

Hypothesis IX. Awake, connected participants exhibit increased feedback and feedforward connectivity in fronto-parietal loop compared to asleep, connected participants

To examine the impact of the physiological state on model connectivity, we conducted a second-level PEB analysis on the winning model (model 9) from the CC-awake group, wherein participants were phenomenologically connected in both groups but in distinct physiological states. Fig. 2.9 illustrates commonalities (top panel) and differences (bottom panel) between connected wakefulness and connected dreaming in response to deviant sounds. In both CC and connected wakefulness, we observed an increase in feedback and feedforward connectivity in the IPL-STG temporo-parietal loop: specifically, increased feedforward connectivity from left and right IPL to left and right STG, respectively, and increased feedback connectivity from right IPL to right STG (free energy, very strong evidence >.99). This loop displayed interhemispheric connectivity in both states, evidenced by increased lateral

connections observed from the left to right IPL, right to left IPL, and from right STG to left STG (free energy, very strong evidence >.99). Additionally, a rise in feedback connectivity from left STG to left A1 was observed in both conditions (free energy, very strong evidence >.99).

Conversely, during connected wakefulness, we found an increase in connectivity in the IFG-IPL fronto-parietal loop, with increases in both feedforward and feedback connectivity between the left IFG and left IPL compared to CC (free energy, very strong evidence >.99). Connectivity within the auditory-temporal pathway exhibited greater strength during wakefulness, evidenced by increased feedforward connectivity from left A1 to left STG and increased feedback connectivity from right STG to right A1 (free energy, very strong evidence >.99). Connected wakefulness displayed also heightened interhemi-

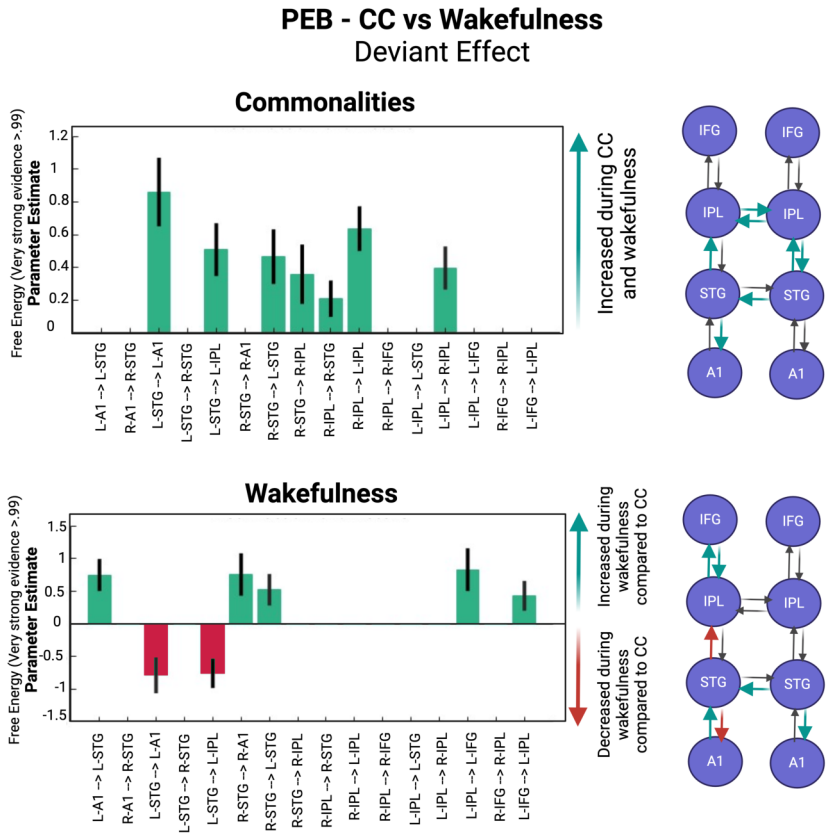

Figure 2.9: See next page.

Figure 2.9: (Previous page.) **Commonalities and differences in model connectivity between CC and Wakefulness.** PEB results are shown for the CC vs Wakefulness comparison on the BMS CC-Awake group winning model 9. Only parameters from the DCM matrix B were modelled, corresponding to self, feedforward, and feedback connections modulated by deviant sounds. The x-axis of the two histogram plots depicts the 16 DCM connections specified for the CC-Awake group. Common connectivity changes in response to deviant sounds across both groups (top) as well as changes in connectivity modulated by wakefulness are depicted in the histogram plots with free energy threshold (very strong evidence >.99). (Previous page.) For ease of the reader, significant connections are highlighted within the corresponding model visualization on the right (green: increased connectivity strength, red: decreased connectivity strength). Black error bars are 90% credible intervals. Figures were generated in MATLAB and edited in BioRender.com.

spheric connectivity at the level of the STG, specifically from right STG to left STG (free energy, very strong evidence >.99). Interestingly, some connectivity decreases were observed during connected wakefulness compared to CC. These included a reduction in connectivity strength from the left STG to both left IPL and left A1 free energy, very strong evidence >.99).

Hypothesis X. Asleep, connected participants exhibit increased feedback and feedforward connectivity in temporo-parietal loop compared to disconnected participants

Second-level PEB analysis on the winning model (model 10) from the CC-DC group revealed both similarities and differences in model connectivity between CC and DC states (fig. 2.7). In both states, in response to deviant sounds, there was a reduction in feedforward connectivity from the left A1 to the left STG and from the left STG to the left IPL (free energy, very strong evidence >.99), as well as a decrease in feedback connectivity from the right STG to the right A1 (free energy, very strong evidence >.99) - fig. 2.10, top panel.

Additionally, we found an increase in left IPL and left A1 self-connectivity (free energy, very strong evidence >.99). As in EEG DCM between-sources connections are modelled as excitatory and self-connections as inhibitory, this observed increase in self-connectivity indicates a reduction in the sensitivity of these regions to inputs from other areas within the network. In comparison to DC, CC exhibited heightened connectivity strength within the IPL-STG temporo-parietal loop (fig. 2.10, middle panel): specifically, we observed

increased feedback connectivity from the left and right IPL to the left and right STG, respectively, alongside increased feedforward connectivity from the left STG to the left IPL (free energy, very strong evidence >.99). When disconnectedness was utilized as a covariate, symmetrical results were found

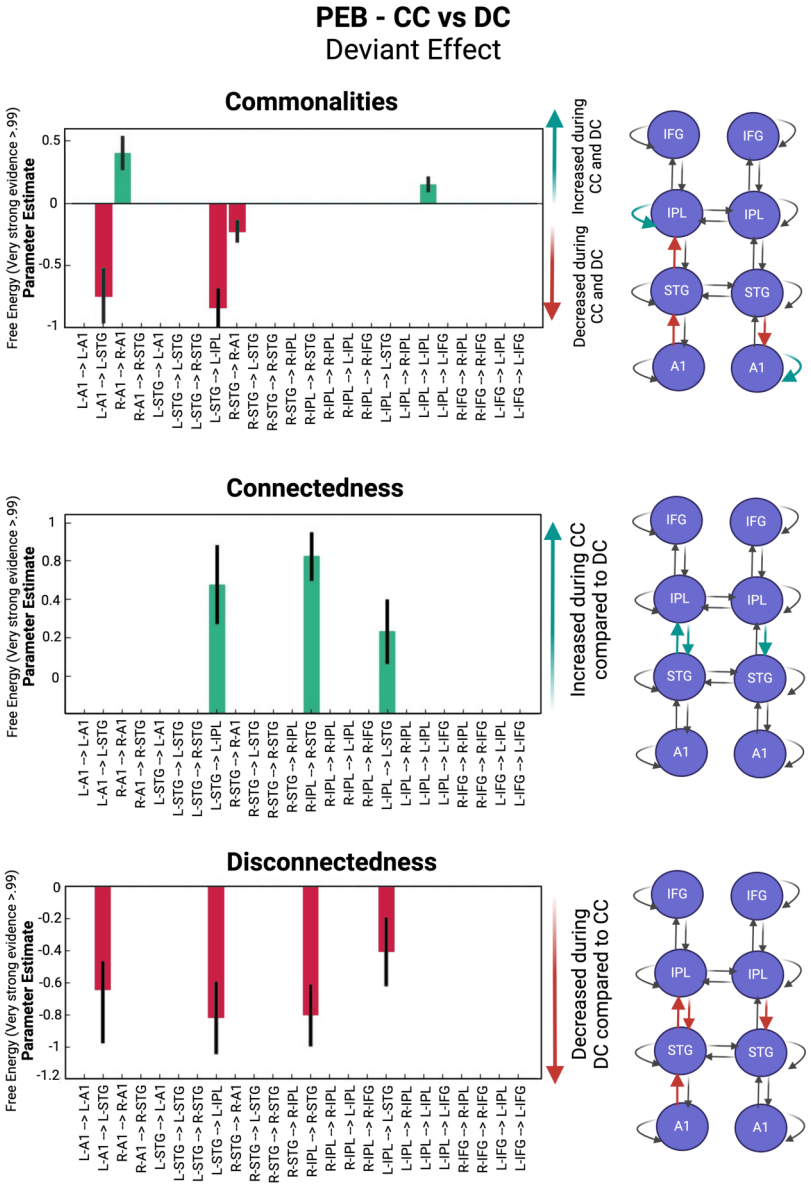

Figure 2.10: See next page.

Figure 2.10: (Previous page.) **Commonalities and differences in model connectivity between CC and DC.** PEB results are shown for the CC vs DC comparison on the BMS CC-DC group winning model 10. Only parameters from the DCM matrix B were modelled, corresponding to self, feedforward, and feedback connections modulated by deviant sounds. The x-axis of the two histogram plots depicts the 24 DCM connections specified for the CC-DC group. Common connectivity changes in response to deviant sounds across both groups (**top panel**) as well as changes in connectivity modulated by connectedness (**middle panel**) and disconnectedness (**bottom panel**) are depicted in the histogram plots with free energy threshold (very strong evidence >.99). For ease of the reader, significant connections are highlighted within the corresponding model visualization on the right (green: increased connectivity strength, red: decreased connectivity strength). Black error bars are 90% credible intervals. Figures were generated in MATLAB and edited in BioRender.com.

with an additional decrease in feedforward connectivity from the left A1 to the left STG (free energy, very strong evidence >.99) - fig. 2.10, bottom panel. For PEB results within CC and DC states, see SI (fig. 2.15).

2.5 Discussion

In this study, we investigated the neural correlates of auditory disconnection in a cohort of 22 participants (11 CC, 11 DC), employing a combination of neuroimaging and experience sampling. We recorded participants' brain activity with hd-EEG while exposing them to an auditory roving paradigm during late-night REM sleep. Upon awakening, participants provided subjective reports indicating whether they had heard the sounds during the preceding sleep period (classified as CC) or not (classified as DC).

At the scalp level, within-group analyses revealed early differentiation between standard and deviant sounds within CC, although without significant middle-latency components; thus, only partially supporting our initial hypothesis (II), which had also anticipated delayed middle-to-late latency components in response to deviant sounds. In the DC group, no specific components reached significance, indicating an overall poorly organized signal. This result partially aligns with hypothesis IV, in which we expected an absence of structured middle-to-late latency components but anticipated early components in DC which were not observed. Neither within-state nor between-group (CC vs. DC) analyses supported hypotheses I, III, or VI, which posited distinct components within each state and differences between groups in response to all sounds. However, corroborating hypothesis VII -

which predicted reduced middle-to-late latency components in DC compared to CC - the CC group exhibited more pronounced middle-latency ERP components associated with conscious processing, suggesting a more elaborate processing and differentiation of standard and deviant sounds during CC compared to DC. Additionally, relative to DC, the CC group demonstrated decreases in delta power and increases in beta2 power, supporting hypothesis VIII. DCM analyses suggested that these scalp-level differences likely stemmed from distinct connectivity patterns in CC and DC states. Specifically, DC displayed a reduction in feedback and feedforward connectivity within a temporo-parietal circuit, encompassing the IPL and STG, compared to CC - in line with hypothesis XI, which anticipated stronger connectivity between primary and secondary regions in the CC group relative to DC. When comparing CC to wakefulness, we observed greater positivity in an ERP component in response to deviant sounds during wakefulness, while no differences were observed for standard sounds, corroborating hypothesis V. DCM analyses indicated that this distinct processing of deviant sounds was likely supported by stronger feedback and feedforward connectivity within a fronto-parietal network during wakefulness compared to CC, consistent with hypothesis X. Finally, no significant differences in sleepiness, alertness, or mood emerged between CC and DC participants, either before sleep onset or upon awakening. However, we observed a gender effect, with males more likely to be in a CC state compared to females - this finding will be discussed in the general discussion of this thesis (see sec. 4.4).

2.5.1 Electrophysiological signatures of (dis)connection

DC participants displayed attenuated ERP components compared to CC participants, who exhibited more complex responses. A temporal positive component, peaking around 280 ms in response to deviant tones, was significantly more pronounced in CC compared to DC participants, possibly reflecting a delayed P200 response. This aligns with the association of the P200 with higher-order sensory processing, confirming this component as an indicator of enhanced processing of environmental stimuli (Campbell & Kenny, 2002). Consistent with this finding, CC participants also exhibited a fronto-temporal cluster of negativity around 154 ms in response to standard tones, significantly more pronounced compared to DC participants. Subtraction of the standard waveforms between CC and DC revealed a difference wave (see fig. 2.6, bottom panel) closely resembling the auditory awareness negativity, which is increasingly recognized as a physiological correlate of sensory consciousness, typically observed 120–200 ms after stimulus onset

(Dembski et al., 2021). The distinctive processing of standard and deviant sounds in CC was further evidenced by the significant difference between standard and deviant waveforms observed in CC participants as early as at 64 ms, whereas DC participants showed no such difference. While absence of evidence is not evidence of the absence, the early differentiation between deviant and standard tones observed in CC suggests that differences between these two states might manifest at very early stages of sound processing.

Finally, to elucidate the effect of physiological state on connectedness, we compared ERPs of CC participants with those of the same individuals recorded during wakefulness. Interestingly, the sole difference observed was an increased prefrontal positivity around 246 ms to deviant tones in awake participants. The lack of difference in standard waveforms between CC and wakefulness suggests similar processing (and potentially suppression) of redundant sounds. Conversely, deviant sounds may engage additional cognitive resources during wakefulness compared to CC, specifically recruiting prefrontal regions involved in cognitive control, which are known to be suppressed during REM sleep (Maquet, 2000; Muzur et al., 2002).

Interestingly, pooling standard and deviant sounds eliminated ERP differences between CC and DC. This may be explained by deviant sounds serving as a catalyst for connectedness. That is, deviant tones may act as triggers for CC, partially disrupting sleep-protective mechanisms trough their saliency. Some accounts of sensory disconnection propose, in fact, that sleepers exist in a perpetual "standby mode", balancing continuous monitoring of their environment with sensory isolation (Andrillon & Kouider, 2020). The detection of salient stimuli, known to be preferentially processed during sleep (Blume et al., 2018; Hennevin et al., 2007; Perrin et al., 1999), could, on occasion, prompt the dreamer to surpass a critical threshold and transition into a state of CC. Differences in baseline between CC and DC may elucidate why the saliency of deviant tones failed to induce connectedness in DC participants. The observed decrease in delta power and increase in beta2 power during CC suggests that CC and DC participants have distinct background activity profiles[2], with CC resembling wakefulness more closely. As discussed earlier, SWA has been proposed to play a pivotal role in inducing DC (Andrillon & Kouider, 2020; Funk et al., 2016), while beta-band coherence has been

[2]However, note that when conducting the same analyses on non-normalized power, differences in beta2, although showing a trend, did not survive correction, and the delta effect while remaining significant, with decreased power in CC compared to DC, was reduced. See 2.6.4 for a detailed discussion.

reported to increase during stimulus processing and to predict subject's responsiveness (Hipp et al., 2011). Given the short inter-stimulus interval, contrastive analyses on CC versus DC baselines could not be conducted. However, future studies may offer insights into the differences in background activity between these two states.

2.5.2 A tempo-parietal circuit promotes CC during sleep while a fronto-parietal circuit subserves wakefulness rather than CC

The scalp differences observed between CC and DC participants likely originated from distinct connectivity changes within each group. We will first discuss the shared connectivity patterns and then highlight the key differences. DCM analysis revealed a general increase in inhibition within primary regions (A1) and higher-order areas (IPL) in both CC and DC participants, with a strengthening of inhibitory self-connections on these sources (see fig. 2.10, top panel). Information transfer from primary regions also exhibited reduced forward propagation, evident in the overall decrease in connectivity from A1 to STG to IPL, in both groups. This overall increase in inhibition within the circuit is expected during sleep, indicative of the markedly different physiology relative to wakefulness, aimed at protecting sleep - such as the drastic decrease of activity in monoaminergic systems (e.g., the noradrenergic "arousal" system) compared to wake (Hayat et al., 2020; Scammell et al., 2017; Tononi et al., 2024). However, when comparing CC and DC participants, a circuit including IPL and STG exhibited increased feedback and feedforward connectivity in CC compared to DC participants (see fig. 2.10, middle panel). This circuit – as evidenced by the CC vs awake comparison (see fig. 2.9, top panel) – was also interhemispherically connected during CC. These findings suggest that in CC, information not only reaches higher-order areas (i.e., STG to IPL) but also that higher-order regions (i.e., IPL) actively relay this information back to lower-order areas and to corresponding regions in the opposite hemisphere.

The enhanced information flow from lower to higher-order areas in CC might stem from a decrease in SWA within primary regions. Compared to DC, CC participants displayed in fact lower delta power, potentially suggesting a role for SWA in establishing a cortical gate during disconnected REM, limiting further sound propagation. The weakening of this cortical gate in CC would explain the heightened feedback connectivity (IPL to STG) observed in this group. As feedback connectivity is known to be crucial for consciousness, by sustaining over time and amplifying information, it would account for

the sensory connection in CC participants (Mashour, 2019). Alternatively, DC could be due to a failure to attend to stimuli. Given the increasing evidence implicating IPL in auditory selective attention (Bareham et al., 2018; Bolognini et al., 2009; Igelström & Graziano, 2017; Westerhausen et al., 2010), its decreased connectivity with the rest of the circuit during DC could suggest a lack of attentional resources allocated to incoming sounds.

Interestingly, when comparing CC vs awake participants, we found increased feedback and feedforward connectivity from IFG to the IPL-STG loop during wakefulness. Previous studies comparing REM sleep vs wakefulness consistently reported deactivation of IFG, along with other frontal and prefrontal regions, during REM sleep (Nir & Tononi, 2010; Tononi et al., 2024). This led some to propose fronto-parietal interactions as the neural correlate of auditory consciousness. However, our findings, employing a within-state contrast, seem to suggest a stronger involvement of parieto-occipital regions in conscious perception of simple sounds, compared to prefrontal circuits. This aligns with recent evidence highlighting recurrent interactions in parietal, occipital, and lateral temporal lobes as the substrate of consciousness (e.g., Boly et al., 2017; Deco et al., 2021).

2.5.3 Which gating hypothesis aligns with our findings?

In summary, do our findings favor a specific gating hypothesis? While our data rule out the thalamic gating hypothesis, since stimuli reach the cortex also in DC, the early ($\sim$64 ms) differentiation between standard and deviant sounds observed in CC but not in DC suggests a potentially different modulation of external inputs already at the thalamic level. Saliency detection (i.e., recognition of deviant sounds) might be more efficient in CC compared to DC due to a 'more open' thalamic gate in CC. Recent studies implicated in fact certain thalamic nuclei in sensory (dis)connection. These included intralaminar nuclei such as the central lateral thalamus, higher order nuclei such as the pulvinar, dorsomedial thalamus and sensory nuclei such as the ventral posteromedial and ventroposterolateral thalamus (Feng et al., 2017; Liu et al., 2015). These nuclei might compromise thalamocortical communication in DC, leading to reduced cortical function. Future studies employing tecniques with higher spatial resolution might elucidate differences in thalamic nuclei's activity between CC and DC.

As mentioned above, our findings align with the cortical gating hypothesis. The observed decreased propagation of information to higher-order regions

in DC might have in fact arised from increased SWA in DC, impeding sensory stimuli from percolating further in the cortical hierarchy. Alternatively, or perhaps in conjunction with the influence of SWA, the abovementioned thalamic modulation of stimuli might be responsible for weakening sensory stimuli in DC, making propagation to higher-order regions less likely. By quantifying the regional and temporal distribution of SWA in DC compared to CC, alongside more precise monitoring of thalamic nuclei activity, we could gain a clearer understanding of the relative contributions of these mechanisms.

Finally, certain hypotheses on the mechanisms of sensory disconnection could not be explored with the current dataset. Although our data do not rule out the informational gating hypothesis, they also do not provide confirmation. To elucidate whether DC stemmed from heightened dream absorption compared to CC, more detailed dream content reports and comparisons of activity in brain regions associated with e.g., visual imagery between the groups would have been necessary. For instance, future studies could characterize and compare activity in the high-order occipito-temporal visual cortex between CC and DC. If an informational gate underlies DC, we would anticipate observing greater activation in this region among DC participants, indicative of a more vivid visual imagery. Similar considerations applies to other gating hypotheses. For instance, it has been theorized that disconnection might be the result of environmental stimuli being incongruent with the activation endogenously triggered by the dream (Andrillon & Kouider, 2020). Conversely, when a stimulus aligns with the ongoing activation, it can be incorporated into the dreaming experience. To investigate this possibility, detailed questioning about dream content upon awakening should have been included. Future research addressing sensory perception during sleep would benefit from using more detailed experience sampling, allowing to better characterize the subjective experience of both CC and DC participants.

2.5.4 No variations in sleepiness, mood or alertness between CC and DC participants

No significant differences in sleepiness, alertness, or mood were observed between CC and DC participants, either before sleep onset or upon awakening. This finding suggests that selective auditory processing during REM sleep (CC) does not arise from pre-existing differences in sleepiness or alertness levels nor that conscious auditory processing led to a less restorative sleep in CC compared to DC participants. While it is self-evident that sleep promotes

post-sleep alertness and reduce sleepiness (Cirelli & Tononi, 2008; Medic et al., 2017), future research could explore how the presence or absence of conscious auditory processing during REM sleep modulates these restorative functions. Similarly, given REM sleep's role in enhancing memory consolidation and task performance (Plihal & Born, 1997; Rasch & Born, 2015; Stickgold et al., 2000), future studies could investigate potential modulations of these cognitive benefits by conscious auditory perception during REM sleep.

2.5.5 Limitations

In the present study, participants were not questioned about their state of consciousness upon awakening (i.e., whether they were dreaming), but were only asked if they had perceived the sounds during the preceding sleep period. An objection might be raised that DC participants not only failed to consciously perceive the sounds, but were also not conscious at all, i.e., not dreaming. This would have framed our comparison as between unconsciousness and CC, rather than CC versus DC. However, it is unlikely that DC participants were unconscious, as all participants were in stage REM sleep throughout the auditory stimulation (see sleep scoring criteria in SI, 2.6.1). Studies involving serial awakenings during the night and subsequent collection of reports show that nearly all subjects awakened from REM sleep report dreaming (Siclari et al., 2017; Stephan et al., 2021; Tononi et al., 2024). In (Siclari et al., 2017), where the serial awakening methods were identical to those used in this study, the incidence of awakenings from unconsciousness during REM sleep was found to be only 9.4%, based on data from both experiments 1 and 2. This estimate aligns with a more recent finding of 12% from a study employing similar methodologies (Stephan et al., 2021). By contrast, white reports — instances where participants recall having dreamed but cannot recall the content — may be more common in awakenings from REM sleep, yet they denote consciousness, albeit with impaired memory recall.

A potential concern may arise regarding the number of events available after pre-processing for the 2-minute recordings, averaging 32 deviant and 58 standard events. While a larger number of trials is generally desirable, there are reports suggesting that a smaller number of deviants can still be adequate. Studies on the internal consistency of ERPs have indicated that 20-30 trials are sufficient for components like N2/P300 (Rietdijk et al., 2014), while others recommended a minimum of 30 trials for early latency ERPs and 60 trials for late latency components (Huffmeijer et al., 2014). Of note, (Boudewyn et al.,

2018) found that increasing the number of trials only modestly enhances power in between-subject designs but significantly boosts it in within-subject designs. To improve power in between-subject designs, increasing the sample size was suggested as preferable.

In this study, subjective reports collected upon awakening served as the basis for identifying CC and DC groups. This approach may be challenged, with some advocating for objective measures of consciousness over subjective ones (Irvine, 2012; Tsuchiya et al., 2015). However, employing task performance to infer consciousness would necessitate in our study to instruct participants to perform a specific task e.g., upon hearing a sound during sleep. While it has been shown that this can be achieved without disrupting sleep, by training subjects beforehand (e.g., Konkoly et al., 2021), task performance and the cognitive resources required to execute it (including behavioral responsiveness) would inevitably alter the very state of consciousness under investigation. Task execution would render it impossible to isolate brain activity solely related to the conscious perception of sounds from that associated with the task and its associated consequences and prerequisites. Furthermore, it has been extensively demonstrated that unresponsiveness does not necessarily indicate unconsciousness (Sanders et al., 2012). Presently, in the absence of a definitive biological model of consciousness, subjective reports remain the gold standard for conscious assessment (Ellia et al., 2021).

A still unsolved challenge in using subjective reports lies in their retrospective nature. Can we confidently assume that a participant reporting sound perception upon awakening was in the state of CC not just seconds before, but also 1, 2, or even 6 minutes prior? In this study, CC participants exhibited a clear time-dependent effect, with responses becoming more pronounced closer to awakening. While some analyses can be conducted on shorter time segments, analyses like ERP require a minimum number of events, making it infeasible to solely focus on very brief pre-awakening periods. However, all our analyses within these constraints consistently identified significant differences between the CC and DC groups. This consistency argues against the possibility that CC participants were instead in a DC state minutes before awakening, or vice versa.

Moreover, it is worth mentioning that a between-groups effect was detected in the present study despite the relatively small sample size, indicating a robust effect (Cohen's D = 0.85) and sufficient statistical power to detect it. The sample size is comparable to that of previous studies investigating

dreaming using hd-EEG (Siclari et al., 2017). Nevertheless, the between-subject design employed here may have limited the detection of smaller effects, potentially resulting in false negatives and only capturing the most pronounced between-condition differences. Further studies are therefore essential to validate and expand these findings.

Finally, in the DCM analysis, as with any hypothesis-driven approach, the model space had to be constrained to a manageable set of testable hypotheses. This inherently limited the exploration of the full range of potential models, allowing us to identify the optimal model only from the predefined subset of models considered. In this study, the choice of network architectures was informed by prior research on MMN generators (Doeller et al., 2003; Garrido et al., 2007, 2008; Grau et al., 2007; Opitz et al., 2002; Rinne et al., 2000). And, as written in sec. 2.3.3, the inclusion of the IPL source was justified by its reported role in bottom-up perceptual processing (Igelström & Graziano, 2017) and its involvement in deviant detection, as indicated by evidence from both EEG and fMRI studies (Justen & Herbert, 2018; Stevens et al., 2000). Moreover, due to the documented suppression of frontal activity during REM sleep (Cote, 2002; Hobson et al., 1998; Maquet, 2000), temporo-parietal circuits — including the IPL — are thought to take over some aspects of auditory processing typically mediated by frontal regions during wakefulness (e.g., (Cote, 2002)). Thus, our model selection was grounded in well-established literature regarding MMN generators, providing a robust basis for the hypotheses being examined. Ultimately, the present work will need to be placed in the broader context of existing and future research employing other modalities and analysis approaches, to integrate findings in a common, most plausible, explanatory framework.

2.6 Supplementary Information

2.6.1 Sleep scoring criteria

As described in sec. 2.2.5, the segments of recordings during which auditory stimulation occurred were scored by a certified American Board of Sleep Medicine Sleep Technologist using standard 30-second epochs, based on the criteria established by the American Academy of Sleep Medicine (AASM) Manual for the Scoring of Sleep and Associated Events (version 2.5) (American Academy of Sleep Medicine, 2020). For reference, the main AASM criteria used to score different sleep stages are summarized in table 2.1. Although the table provides a general overview, more detailed rules and exceptions for scoring each epoch exist, and their explanation falls beyond the scope of this section. For those details, readers are encouraged to consult the AASM Manual (version 2.5) (American Academy of Sleep Medicine, 2020). Rather, this section focuses on detailing how stage REM was scored, specifically including recordings that contained definite REM stage epochs and adjacent epochs that met all criteria for definite REM sleep, except for the presence of REMs.

The AASM manual defines an epoch as definite stage REM sleep based on the simultaneous presence of the following phenomena: low-amplitude, mixed-frequency (LAMF) EEG activity without K complexes or sleep spindles, low chin EMG tone, and rapid eye movements (REMs). LAMF EEG activity refers to low-amplitude signals predominantly in the 4-7 Hz range (American Academy of Sleep Medicine, 2020). K complexes are defined as well-delineated, negative sharp waves immediately followed by a positive component, standing out from the background EEG for a duration $\geq$0.5 sec, with maximal amplitude in pre-frontal and frontal derivations (American Academy of Sleep Medicine, 2020). Sleep spindles are characterized as trains of distinct sinusoidal waves with a frequency of 11-16 Hz (most commonly 12-14 Hz), a low amplitude, and a duration of $\geq$0.5 sec, with maximal amplitude in central derivations (American Academy of Sleep Medicine, 2020). Sawtooth waves, which are also commonly observed during REM sleep - but are not required for the scoring of definite REM stage - are defined as trains of sharply contoured or triangular, serrated 2-6 Hz waves, with maximal amplitude over the central head region (American Academy of Sleep Medicine, 2020).

In cases where REMs were absent, adjacent epochs to those scored as

Stage	Eye movements	EMG tone	Predominant rhythms
N1	Slow eye movements	Variable	·Low-amplitude mixed frequency (LAMF) activity ·Vertex sharp waves
N2	No eye movements*	Variable	·K complexes (total duration $\geq$ 0.5 sec) ·Spindles (duration $\geq$ 0.5 sec)
N3	No eye movements*	Variable	SWA with peak-to-peak amplitude $>$ 75 μV
REM	REMs	·Low(est) ·Short irregular bursts of EMG activity	·Low-amplitude mixed frequency (LAMF) activity ·Sawtooth waves ·No K complexes nor spindles
Wake	·Eye blinks ·Reading eye movements ·REMs ·Slow eye movements	Normal or high	·Low-amplitude activity (alpha and beta) ·Posterior dominant alpha rhythm

Table 2.1: Sleep scoring criteria based on AASM guidelines. This table summarizes the main characteristics used for scoring different sleep stages according to the AASM guidelines (version 2.5). Included characteristics are eye movements, EMG tone, and predominant EEG rhythms. LAMF: predominantly 4-7 Hz; K complexes: negative sharp waves followed by a positive component, duration $\geq$0.5 sec; Sleep spindles: trains of distinct sinusoidal waves of 11-16 Hz (commonly 12-14 Hz), duration $\geq$0.5 sec; Sawtooth waves: serrated 2-6 Hz waves; SWA: 0.5-2 Hz, amplitude >75 μV; Alpha: 8-13 Hz; Beta: >13 Hz. * = in some individuals, slow eye movements (but not REMs) may persist during stage N2 sleep. Table was created with BioRender.com.

definite stage REM were also classified as REM, only if LAMF activity without K complexes nor spindles was present and EMG tone was low (American Academy of Sleep Medicine, 2020). To further ensure that the recordings represented only stage REM sleep, recordings containing intervening arousals were excluded. Arousals are defined as abrupt shifts in EEG frequency, including alpha, theta, and/or frequencies greater than 16 Hz (excluding spindles), lasting for at least 3 sec, and preceded by at least 10 sec of stable

sleep (American Academy of Sleep Medicine, 2020). This exclusion criterion was applied to ensure continuous, uninterrupted periods of stage REM sleep for both CC and DC conditions, eliminating any ambiguity in sleep stage classification.

Regarding how REM sleep was differentiated from other stages, its distinct EEG activity sets it apart from N2 and N3 stages. Scoring of N2 specifically requires the presence of K complexes or sleep spindles, whereas scoring of stage N3 requires the presence of slow-wave activity (SWA), which is defined as waves with a frequency of 0.5-2 Hz and a peak-to-peak amplitude greater than 75 μV, measured over frontal regions (American Academy of Sleep Medicine, 2020). Even though LAMF activity can also be found during N1 and wakefulness, REM sleep can be differentiated from these stages by several factors. During N1, LAMF activity is accompanied by vertex sharp waves (absent during REM), which are defined as sharply contoured waves with a duration of less than 0.5 sec, maximal over the central region, and distinguishable from the background activity (American Academy of Sleep Medicine, 2020). During wakefulness, LAMF activity typically occurs at a higher frequency than during REM, usually in the alpha (8-13 Hz) and beta (>13 Hz) ranges, and is accompanied by a posterior dominant alpha rhythm (American Academy of Sleep Medicine, 2020) - absent during REM. Moreover, REM sleep is distinguished by consistently low chin EMG tone, whereas during N1 and wakefulness, chin tone is generally variable or high (American Academy of Sleep Medicine, 2020). This feature also sets REM sleep apart from all other sleep stages, where chin tone is typically variable (American Academy of Sleep Medicine, 2020). Additionally, REMs, which are absent during stages N2 and N3, can occasionally occur during wakefulness but are replaced by slow eye movements during stage N1 (American Academy of Sleep Medicine, 2020).

Finally, it is important to note that during the REM sleep stage, delta activity - defined by the AASM manual as activity in the 0-3.99 Hz frequency range, and in our spectral analysis, in the 1-4 Hz range - can still occur. Studies in both rodents and humans have demonstrated that regional delta activity is, in fact, an integral part of REM sleep, indicating that regional brain activity during REM sleep can deviate from the global pattern that traditionally defines REM sleep from a sleep-scoring perspective (Bernardi et al., 2019; Funk et al., 2016; Langille, 2019; Siclari & Tononi, 2017). For instance, (Bernardi et al., 2019) showed that, in humans, REM delta waves can manifest as sawtooth waves, distributed across occipital-temporal and

frontal-central regions, as well as medial-occipital slow waves. Therefore, our spectral analysis results, which show increased delta band power in CC compared to DC, do not contradict the classification of the included recordings as REM sleep.

2.6.2 Sleepiness, alertness and mood in CC vs. DC participants

The Stanford Sleepiness Scale (Shahid et al., 2011) and the Visual Analog Scale for sleepiness (Alqurashi et al., 2021) are presented below in fig. 2.11. Participants completed these questionnaires before the start of the overnight recording and after awakening in the morning.

Degree of Sleepiness	Scale Rating
Feeling active, vital, alert, or wide awake	1
Functioning at high levels, but not at peak; able to concentrate	2
Awake, but relaxed; respnosive but not fully alert	3
Somewhat foggy, let down	4
Foggy; losing interest in remaining awake; slowed down	5
Sleepy, woozy, fighting sleep; prefer to lie down	6
No longer fighting sleep, sleep onset soon; having dream-like thoughts	7
Asleep	X

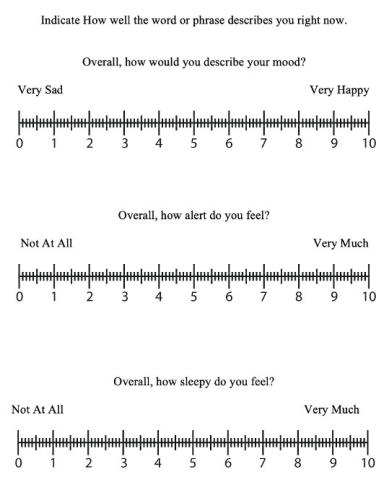

Figure 2.11: Left: **The Stanford Sleepiness Scale (SSS)**. Right: **The Visual Analog Scale VAS**

Analysis of SSS and VAS scores revealed no significant differences between CC and DC groups. Neither the Mann-Whitney U test for SSS scores (before sleep: $W = 37$, $p = 0.282$; after awakening: $W = 41.5$, $p = 0.552$) nor t-tests/ Mann-Whitney U test for VAS scores (mood, alertness, sleepiness; all $p > 0.31$) showed group differences in mood, alertness, or sleepiness, either before sleep onset or upon awakening (see fig. 2.12).

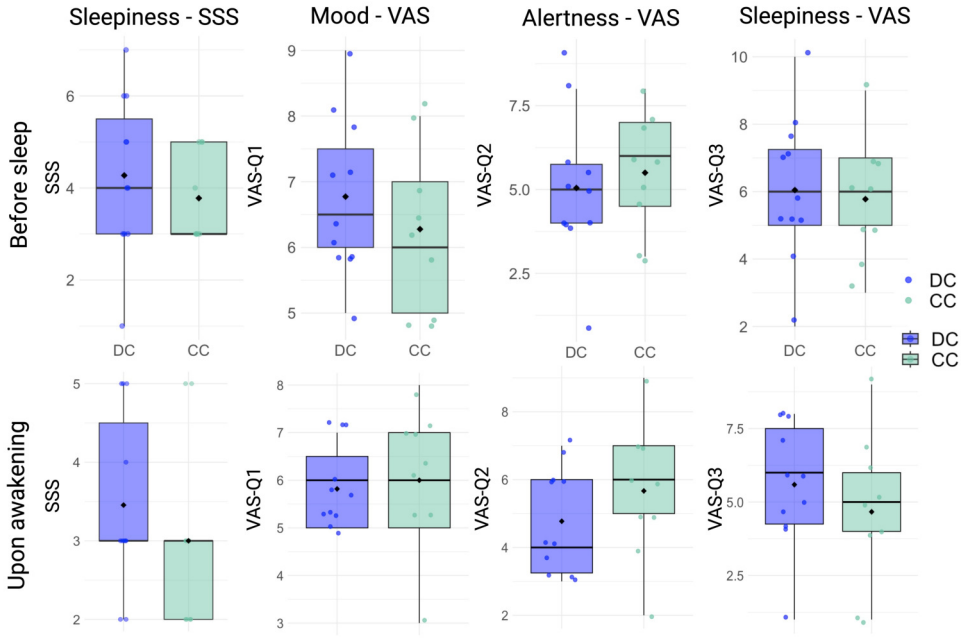

Figure 2.12: Variations in sleepiness, mood, and alertness in CC and DC participants. Distribution of SSS and VAS scores for the three questions (VAS-Q1, VAS-Q2, and VAS-Q3) before sleep (top panel) and upon awakening (bottom panel) within CC and DC groups. Each boxplot represents the median, quartiles, and outliers of SSS/VAS scores within each group. Dots represent individual data points. Blue and green colors indicate the DC and CC groups, respectively. Figures were generated in R and assembled in BioRender.com.

2.6.3 Within-CC and within-DC normalized power results

As illustrated in fig. 2.13, across all recording durations, power in high-frequency bands was consistently higher in CC compared to DC. Conversely, delta power was generally higher in DC compared to CC. Interestingly, the CC group also exhibited localized delta power increases, primarily observed in prefrontal regions (e.g., 60-second recordings), aligning with the documented frontal suppression during REM sleep (Cote, 2002; Hobson et al., 1998; Maquet, 2000). In DC, however, increases in delta power were more widespread, covering frontal, central, and temporal regions. Notably, delta power remained low in both CC and DC states in parieto-occipital regions. This aligns with findings by (Siclari et al., 2017): parieto-occipital regions,

which support endogenously generated content, are active in both CC and DC states, as participants are dreaming in both states. However, in DC, additional increases in delta power in more anterior regions likely disrupt environmental connection, potentially creating a cortical gate (see sec. 2.5).

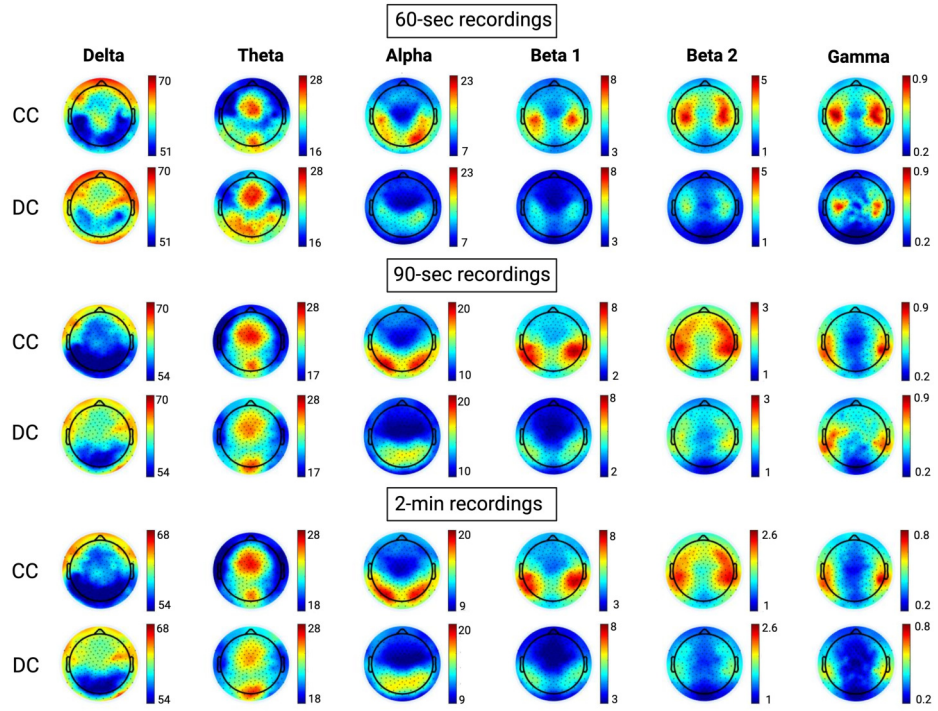

Figure 2.13: Mean normalized percent power, within CC and DC, for different recording lengths and frequency bands. Delta: 1-4 Hz; theta: 4-7.5 Hz; alpha: 8-11.5 Hz; beta1: 12.5 – 18 Hz; beta2: 18–30 Hz; gamma: 30-50 Hz. Colormap limits are the minimum and maximum value found for each frequency band. Figures were generated in MATLAB and assembled in BioRender.com

2.6.4 Differences in absolute, non-normalized power between CC and DC

To avoid confounding between-subject variability with between-group effects, we normalized the PSD in each frequency band by its total power. Through this normalization, we observed decreased delta power and increased beta2 power in CC participants compared to DC participants.

However, this normalization may have shifted or skewed the group effects in specific frequency bands due to large group differences. Therefore, we

also analyzed the PSD data without normalizing by total power (see figure below). As depicted in fig. 2.14, in the non-normalized data, the delta effect remained significant, though reduced, in the 2-min recordings (paired t-test, $p < 0.05$, SNPM corrected). In contrast, while beta2 power was still higher in CC compared to DC in the uncorrected results, it did not survive SNPM correction. This discrepancy may reflect a redistribution of power when normalization by total power is omitted, with the power from one band potentially being injected into another.

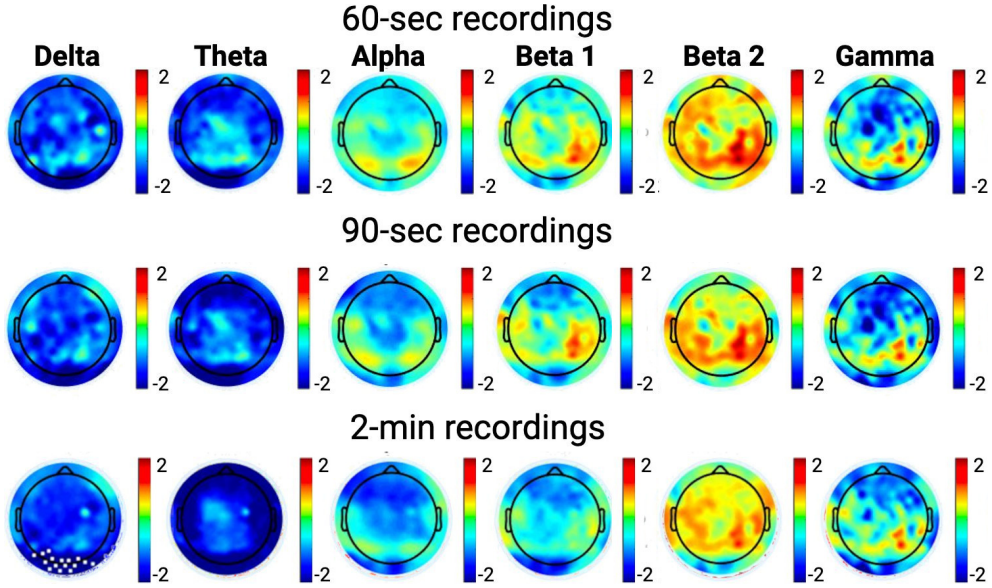

Figure 2.14: Differences in non-normalized power spectral density between CC and DC. The difference between CC and DC (i.e., CC - DC) in averaged, absolute power spectral density in the delta (1-4 Hz), theta (4-7.5 Hz), alpha (8-11.5 Hz), beta1 (12.5 – 18 Hz), beta2 (18–30 Hz), and gamma (30-50 Hz) frequency bands is shown for 60-90-second and 2-minute recordings. White dots, $p<0.05$ SNPM corrected. Figures were generated in MATLAB and assembled in BioRender.com

However, normalizing by total power may offer two important advantages. First, as previously mentioned, it might help reduce the inter-individual variability in EEG data, which can be substantial due to differences in scalp conductivity, electrode placement, or intrinsic amplitude, all of which might greatly influence absolute power. Second, normalization might enhance sensitivity to group differences in specific frequency bands, allowing more subtle variations to become detectable. By dividing each band by the total power, the proportional contribution of each band is emphasized, making the overall power spectrum more comparable across participants by focusing

on relative rather than absolute differences. This approach can reveal shifts that might be obscured when only considering absolute power, particularly if one group shows much higher power in dominant bands (such as delta), which can overshadow comparisons of other frequencies. Hence, the fact that beta2 increases in CC vs. DC are still observed in the uncorrected data but did not survive correction in the non-normalized data, while they did in the normalized data, could be used to argue that normalization enhances the sensitivity of the analysis to more subtle group differences.

Nonetheless, the delta band effect, though reduced, remained consistent across both normalized and non-normalized data, indicating that delta band group differences are robust and unaffected by normalization, further supporting their validity regardless of processing steps.

2.6.5 Within-CC and within-DC PEB results

Fig. 2.15 depicts commonalities in connectivity within CC, on the BMS CC group winning model 8, and within DC on the BMS DC group winning model 10. Connectivity changes in response to deviant sounds within each model are thresholded using free energy with very strong evidence >.99. CC participants exhibited enhanced information flow, characterized by increased feedforward connectivity (left A1 to left STG) and feedback connectivity (left STG to left A1) along with increased interhemispheric connectivity between left and right STG. Additionally, we found increased inhibition of right IPL and right A1 sources, accompanied by decreased connectivity from right IPL to right STG. Conversely, DC participants displayed diminished information flow, evidenced by decreased feedforward connectivity (left A1 to left STG, left STG to left IPL) and decreased feedback connectivity (right STG to right A1). Inhibition of left A1 was also observed in the DC group, together with inhibition of left STG.

Overall, the CC state was characterized by more elaborate information processing. Enhanced feedforward, feedback and lateral connectivity suggests increased information propagation from primary (A1) to higher-order regions (STG) and across hemispheres (left/right STG). In contrast, the DC state exhibited a dampened information flow with inhibition encompassing both feedforward and feedback connections between primary and higher-order regions (A1, STG and IPL). Interestingly, both states displayed inhibition of primary auditory regions (A1), likely reflecting sleep-protective mechanisms.

However, this inhibition extended to relay regions (STG) in the DC state,

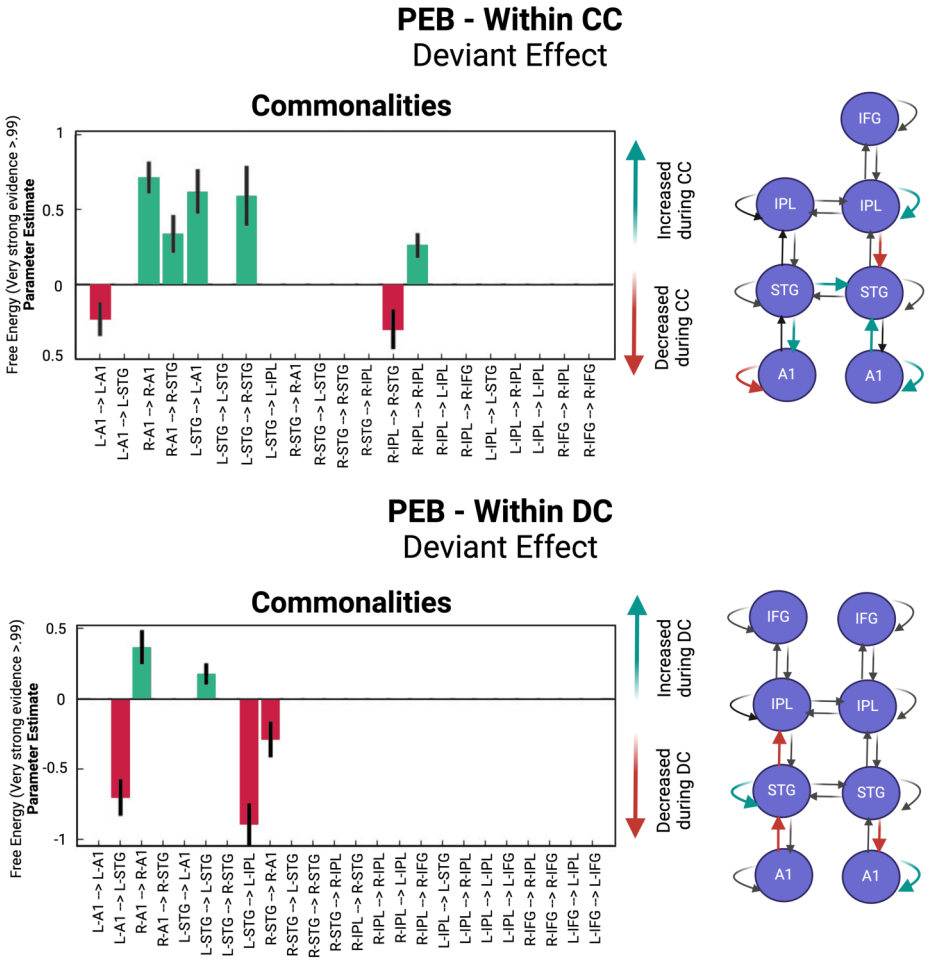

Figure 2.15: Commonalities in model connectivity within CC and DC participants. PEB results are shown within CC on the BMS CC group winning model 8 (top panel) and within DC on the BMS DC group winning model 10 (bottom panel). Only parameters from the DCM matrix B were modelled, corresponding to self, feedforward, and feedback connections modulated by deviant sounds. The x-axis of the two histogram plots depicts the 21 DCM and 24 DCM connections specified for the CC and DC group, respectively. Common connectivity changes in response to deviant sounds within both groups are depicted in the histogram plots with free energy threshold (very strong evidence >.99). For ease of the reader, significant connections are highlighted within the corresponding model visualization on the right (green: increased connectivity strength, red: decreased connectivity strength). Black error bars are 90% credible intervals. Figures were generated in MATLAB and edited in BioRender.com.

potentially hindering further information propagation. In contrast, the CC state exhibited inhibition only in higher-order regions (IPL), suggesting different levels of information processing and more thorough processing in CC participants.

Notably, PEB analysis on the combined CC-DC group (see fig. 2.10) revealed increased right IPL to right STG connectivity as a key difference between these two states. However, in this analysis decreased connectivity between these regions was found in the CC group, while the DC group showed no connectivity changes between these regions. This difference might be due to employing different models for CC and DC group in the within-state PEB analysis - model 8 for the CC group and model 10 for the DC group (see fig.2.15, top and bottom right for models' description). PEB results on the CC-DC group were based on the BMS winning model for the (pooled) CC-DC group, i.e., model 10, which might account for this discrepancy between the two analyses. Our finding of increased right IPL-STG connectivity as a key difference between CC and DC states (fig. 2.10) remains consistent with these results. While the CC group did not exhibit elevated left IPL-left STG connectivity on its own, when contrasting CC and DC, changes in IPL-STG connectivity might still emerge as the main difference between the two states.

Chapter 3

Cerebral characterization of sensory gating in disconnected dreaming states during propofol sedation using fMRI

"It was the hour when things lose the consistency of shadow that has clung to them throughout the night and little by little regain their colors [..], the hour when one is least sure of the existence of the world."

Italo Calvino
The Nonexistent Knight

Based on:

Cecconi, B., Montupil, J., Mortaheb, S., Panda, R., Sanders, R. D., Phillips, C., Alnagger, N., Remacle, E., Defresne, A., Boly, M., Bahri, M. A., Lamalle, L., Laureys, S., Gosseries, O., Bonhomme, V., & Annen, J. (2024). Study protocol: Cerebral characterization of sensory gating in disconnected dreaming states during propofol anesthesia using fMRI. *Frontiers in Neuroscience*, *18*, 1306344. https://doi.org/10.3389/FNINS.2024.1306344/BIBTEX

Cecconi, B., Mortaheb, S., Bahri, M. A., Boly, M., Laureys, S., Gosseries, O., Bonhomme, V., & Annen, J. (2024). *Cerebral characterization of sensory gating in disconnected dreaming states during propofol sedation using fMRI* [In preparation]

In this chapter, we examined fMRI BOLD responses to an auditory oddball paradigm in CC and DC participants under propofol sedation. DC, relative to CC participants, exhibited unexpected activation increases primarily in temporal regions in response to all-sound blocks. In contrast, CC participants showed overall decreases in activation, with focused increases observed in the precuneus, and extending to middle cingulate/paracingulate gyri, prefrontal regions, hippocampal gyrus, and middle occipital gyrus. This pattern reversed during deviant blocks, where CC participants displayed widespread activation, while DC participants showed minimal changes compared to their response to standard/all-sound blocks, possibly indicating that deviant perception may be exclusive to CC states. Spectral analysis revealed increased high-frequency oscillations in sensory and attention-related regions in DC relative to CC, potentially suggesting higher slow-wave activity compared to CC. Interestingly, differences in sound processing between CC and wakefulness emerged only in response to all-sound/standard blocks, with similar deviant processing in both states.

Keywords: *fMRI, activation, BOLD oscillations, sensory disconnection*

3.1 Introduction

In this study, we identified unresponsive connected and disconnected dream-like states by delivering auditory stimuli during propofol-induced mild sedation and serially awaking healthy participants. We collected subjective reports about mental activity prior to awakening (assessing dreaming/consciousness) and stimulus perception (assessing connectedness), while ensuring unresponsiveness throughout the experiment and minimizing the risk of arousals. The cerebral activity of participants was recorded by means of fMRI. During the auditory stimulation session, we played series of sounds following the oddball rule, in which trains of beeps of the same frequency (i.e., standard sounds) are occasionally interrupted by a beep of a different frequency (i.e., the deviant or 'oddball' sound). This way, we were able to investigate not only differences in the perception of sounds during DC and CC, but also whether standard and deviant sounds are processed differently in the two conditions. Additionally, prior to administering propofol, an auditory stimulation session was recorded while participants were awake. This allowed us to compare the brain activity of participants who reported being in a CC state during sedation with their brain activity during wakefulness, enabling

an investigation into the impact of physiological state on phenomenologically similar conditions, as in both cases participants heard the sounds.

Capitalizing on the enhanced spatial resolution of BOLD fMRI, we first conducted an exploratory, whole-brain analysis aimed at identifying regions involved in sensory disconnection (CC vs DC), independent of arousal or cognitive functions associated with wakefulness (CC vs wakefulness). These analyses were also conducted separately on CC and DC groups and, to validate our approach, on wakefulness recordings alone, in order to replicate known findings on auditory and oddball perception.

Voxel-wise activation analyses were complemented by a Region Of Interest (ROI) analysis aimed at characterizing stimulus processing within several thalamic nuclei, primary and secondary cortices during CC vs DC and during CC vs wakefulness. Both voxel-wise and ROI-wise activation analyses were conducted for all-sounds versus silence and for deviant versus standard blocks. In general, for both types of analyses, in the CC vs wakefulness all-sounds versus silence comparison, we hypothesized that brain activation in CC would show a general reduction compared to wakefulness in response to all-sounds blocks, largely driven by the sedative effects of propofol (Fiset et al., 1999; Saxena et al., 2019; H. Zhang et al., 2010). This widespread reduction was expected to be particularly pronounced in frontal regions, consistent with the findings from the REM sleep study (*Hypothesis I*). A similar reduction in CC activity compared to wakefulness was also hypothesized in response to deviant blocks whereas for standard sounds, we anticipated a smaller decrease in activity — or even potentially higher activation — compared to wakefulness, reflecting weaker inhibition/habituation mechanisms in CC (*Hypothesis II*).

For the CC vs DC comparison, we hypothesized that activation in DC would remain localized to primary auditory regions in response to all-sounds blocks, reflecting elementary sensory processing. In contrast, during CC, we anticipated activation not only in primary auditory areas but also in higher-order integration regions, indicative of more complex sensory processing (*Hypothesis III*). Similarly, for the deviant versus standard contrast, we hypothesized that in CC, deviant blocks would elicit more widespread activation compared to DC, but with increased deactivation during standard blocks, reflecting enhanced habituation mechanisms, as seen during wakefulness. Conversely, during DC, we expected no significant activation differences in response to deviant and standard blocks, with activity in both cases mostly

confined to the primary auditory cortex with minimal or no involvement of secondary regions, reflecting participants' inability to differentiate between the two types of sounds (*Hypothesis IV*).

Finally, we quantified, in the CC and DC groups, the regional distribution of high-frequency BOLD oscillations, which have been suggested to correlate with sleep slow waves (Song et al., 2022) and potentially lead to states of DC (Funk et al., 2016; Mhuircheartaigh et al., 2013). This analysis was conducted independently of the auditory events, on the whole brain (parcellated into 400 ROIs) - see fig. 3.4 for an overview of the analyses. In this context, we hypothesized that high-frequency BOLD oscillations would be lower in the thalamic region and in both primary auditory cortex and secondary regions during CC compared to DC (*Hypothesis V*).

In conclusion, we propose an fMRI experiment that systematically differentiates CC and DC states by delivering auditory stimuli and serially awakening participants sedated with propofol to assess the conscious state and stimulus perception through subjective reports. Through activation analyses of collected fMRI data, we investigated whether sensory disconnection is caused by altered activity at the level of the thalamus, primary regions, or, higher up, due to a lack of stimulus integration in associative areas. Spectral analyses elucidated the potential role of SWA in influencing these mechanisms. Comparisons between CC and awake states clarified the impact of physiological state on CC.

3.2 Methods

3.2.1 Ethics

The study was approved by the University of Liege Hospital Ethics Committee (2020–707) and was registered at the European Union Drug Regulating Authorities Clinical Trials Database (identifier: 2020-003524-17). All study subjects were informed in writing of the objectives, methods and potential risks of the experiment. They were given two documents: a general information form on MRI acquisition and a specific form containing information on the study itself. All participants provided written informed consent according to the Declaration of Helsinki and received financial compensation (300 euros).

To ensure participant's safety, vital parameters were continuously moni-

tored, and an anesthesiologist was present in the MRI room for the entire duration of the experiment. Subjects received additional oxygen through a plastic facemask at a rate of 3 L min^{-1}. Monitored vital signs included electrocardiography and heart rate, non-invasive blood pressure, peripheral saturation in oxygen, inspired and expired CO2, thoracic movements amplitude, and respiratory rate. All material and medications needed to ensure safety of the sedation were immediately available.

3.2.2 Subjects

Participants were screened through an online form, an in-person interview and a medical examination. The initial phase of screening using the online form selected healthy, right-handed, non-smoking, MRI-compatible subjects without psychiatric and neurological disorders, propensity for nausea, recurrent nightmares, memory and hearing impairments, substance abuse, cannabis use in the three months preceding the study and regular alcohol consumption (i.e., everyday). During the in-person interview it was verified that the above inclusion/exclusion criteria were fulfilled to avoid oversights or errors in filling out the form.

We selected participants with a low risk of obstructive sleep apnea through the StopBang questionnaire (Low Risk: Yes to 0–2 questions) (Chung et al., 2012; Chung et al., 2008) and low levels of anxiety through the scales 'Novelty Seeking' and 'Harm Avoidance' of the Temperament and Character Inventory self-rating questionnaire (Cloninger et al., 1993). We included participants with average or above average scores on the 'Novelty Seeking' scale (i.e., $\geq$ 16.5 for men and $\geq$ 16.3 for women) and participants with average or below average scores on the 'Harm Avoidance' scale (i.e., $\geq$ 14.5 for men and $\geq$ 17.5 for women) (Pélissolo & Lépine, 2000). We controlled for obstructive sleep apnea because of the known respiratory depression effects of propofol. We took into account the predisposition to anxiety as anxious participants might require higher propofol concentrations to achieve loss of responsiveness compared to non-anxious participants, impairing subsequent recovery of responsiveness and report collection.

Participants who met these criteria were visited by an anesthesiologist with an evaluation similar to a pre-anesthesia examination, including a physical examination, full review of the patient's medical, surgical and allergological history, treatment and intubation score and any potential contraindication to propofol sedation. Finally, alcohol consumption was forbidden for 48h

preceding the experiment. A proper sleep hygiene was encouraged in the 2 to 3 days prior to the study. Participants were required to refrain from drinking and eating six hours before the start of the experiment.

3.2.3 Experimental protocol

In short, the present experiment comprised four main phases (schematic representation in fig. 3.1): (1) acquisition of MRI data in awake participants during rest and auditory stimulation, (2) gradual sedation with propofol (∼45 min), (3) training session of sedated participants for ∼20 min (see below for an explanation) and (4) acquisition of MRI data in sedated participants during rest and auditory stimulation, both repeated twice. During the awake phase, a structural (T1) image was collected prior to the acquisition of functional scans during rest (∼10 min) and auditory stimulation (∼15 min; for a detailed description of the auditory paradigm, see sec. 3.2.5). Awake participants were instructed to passively listen to the sounds. To prevent the comparison of CC and DC from being contaminated by correlates of (un)responsiveness we ensured that participants were unresponsive prior to the start of the experimental sessions and awakening. We also assessed their state of wakefulness before and after the experimental sessions to minimise the risk of arousals and confounding correlates of wakefulness with those of (dis)connected consciousness.

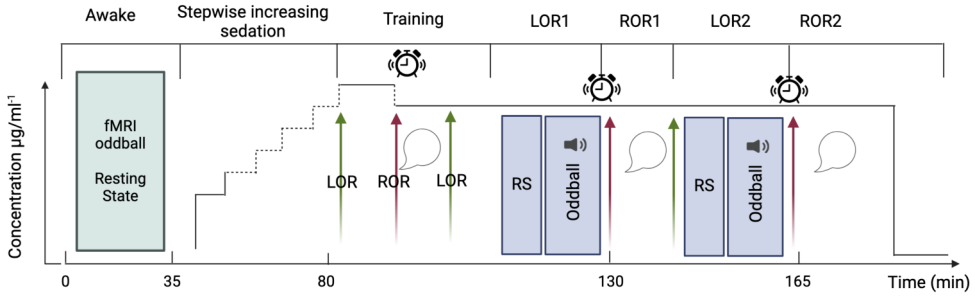

Figure 3.1: Schematic representation of the experimental design. Green arrows indicate loss of responsiveness (LOR); red arrows, regain of responsiveness (ROR); sound symbol, auditory oddball stimulation; alarm clock, awakening attempt; speech bubble, collection of subjective reports. fMRI acquisitions were conducted throughout LOR1 and LOR2 and concluded prior to the initiation of the awakening attempt. Created with BioRender.com.

From the beginning of the sedation, to monitor responsiveness, participants were instructed to perform a continuous task of alternately pressing the left

and right keys of a box-shaped keypad. Propofol was infused until loss of volitional motor activity which was used as a proxy for loss of responsiveness (LOR). LOR was defined as three consecutive minutes in which the participant had stopped pressing keys and neither spoke nor moved spontaneously. Propofol was administered by a computer-controlled continuous infusion (target-controlled infusion—TCI) using a pharmacokinetic model to achieve stable plasma and effect-site propofol concentration (Schnider et al., 1999). The initial target for induction was set at 1 μg.ml^{-1}, and progressively increased (waiting five minutes between each increase in concentration) until LOR as follows: from the initial target, propofol concentration was increased by a step of 0.5 μg.ml^{-1} to 1.5 μg.ml^{-1}; if LOR was not reached at 1.5 μg.ml^{-1}, propofol was increased by a step of 0.2 μg.ml^{-1} until 1.9 μg.ml^{-1}. If LOR was not reached at 1.9 μg.ml^{-1}, propofol was increased by steps of 0.1 μg.ml^{-1} until LOR. This ensured to determine, for each subject, the precise concentration at which LOR occurs. This approach minimizes the risk to exceed the dose required to reach LOR. The higher the dose, the more difficult the recovery of responsiveness may become. Since the aim is to target LOR and not loss of consciousness, the maximum propofol concentration was set at 4 μg.ml^{-1}. This sedative dosage also allowed the participants to remain in spontaneous ventilation.

When participants lost responsiveness, we waited 5 min for the drug to stabilize, and then we began the training session. The goal of the training session was to fine-tune the propofol concentration to maximize the chances of having both LOR and intelligible reports upon regain of responsiveness (ROR) at the same propofol concentration. During the training session (outside the MRI scanner bore, but on the MRI table), we attempted to awaken participants by performing an arousal protocol that consisted of (1) calling the volunteer aloud through the MRI microphone for up to two times, (2) if unsuccessful, lightly shaking volunteer's shoulders for up to two times, (3) if unsuccessful, applying moderate painful stimulation, i.e., pinching the skin of the forearm for up to two times. If, after three runs of the protocol, participants were still not responsive, we decreased the propofol concentration by 0.1 μg.ml^{-1}, waited five minutes and repeated the arousal protocol a second time. This process was repeated until the participants were able to recover responsiveness.

Once responsiveness had been recovered, participants were asked questions (see sec. 3.2.4) to verify their state of CC/DC and consciousness/unconsciousness. If participants were unable to speak intelligibly, the concentration of

propofol was reduced by steps of 0.1 μg.ml^{-1} (always waiting 5 min between steps) until reports became intelligible. Once the right concentration had been identified, we waited for participants to spontaneously lose responsiveness again, and ended the training session with participants unresponsive (i.e., LOR1). LOR1 marked the beginning of the experimental session. After LOR1, we acquired 10 min of resting-state (RS) fMRI followed by 15 min of task-based fMRI, i.e., passive listening to a sequence of oddball auditory stimuli. After concluding the fMRI acquisition and without altering the drug concentration, we attempted to awake participants by performing the arousal protocol described above. If the participant did not regain responsiveness after one execution, the protocol was repeated a maximum of two times. If the participant did not regain responsiveness after three executions, the participant was defined unarousable.

In case of ROR, participants were questioned about their experience during the period of unresponsiveness to determine whether they were (un)conscious and (dis)connected (see sec. 3.2.4). After the first ROR (ROR1), we waited a maximum of 10 min for the participant to spontaneously lose responsiveness a second time (LOR2). If the participant did not lose responsiveness in the 10 min following ROR1, we increased the propofol concentration up to three times in 0.1 μg.ml^{-1} increments. If, after increasing the concentration, the participant did not reach LOR2, the LOR attempt was considered unsuccessful, and the experiment was terminated. In the case that LOR2 succeeded, the procedure described above for ROR1 was repeated for ROR2. Finally, the end of the experiment was marked by termination of the drug infusion. This protocol was fine-tuned based on previous work of our team (Bonhomme et al., 2016).

3.2.4 Interviews following ROR

After every successful ROR, participants were subjected to the following 6-question interview (and provided with the following possible answers):

1. Did you have any sensations or thoughts before you were awakened? Yes/No/Not sure/Nothing
2. Did you hear the tones? Yes/No/Not sure
3. Do you think you were awake, having a dream, or unconscious? Awake/Dream/Unconscious/Not sure

4. Did you hear one or two different tones? One/Two/Not sure/Nothing
5. Was this experience more centered on yourself or on the environment? Myself/Environment/Nothing
6. Did you rather think, or did you see many things? Think/See/Not sure/Nothing

The first and third questions verified that participants were (un)conscious during the period of unresponsiveness and the second question verified the (dis)connectedness of participants during the period of unresponsiveness. The last three questions served two purposes: to gather more detailed information on the experience during the period of unresponsiveness and to check the consistency of the reports. Probing the presence of the experience/perception of sounds strengthened the reliability of the answers to the first two questions (e.g., the participant might answer that he/she did not hear any sounds, but then answer the question "did you hear one or two tones?" with "two"). This interview identified four different states: (1) awakening without any recall of experiences; (2) connected dreaming; (3) disconnected dreaming and (4) wakefulness. State 1 was discarded as it could not be classified in either of the two categories of interest in this study. CC (i.e., connected dreaming) was considered to have occurred during the unresponsive period if participants answered "Yes" to questions number 1–2 and disconnected consciousness if participants replied "Yes" to question 1 and "No" to question 2. In the case of conflicting answers, we considered participants to have been CC if they provided a positive response to at least one question amongst numbers 1,5,6 or if they responded with "Having a dream" to question number 3, in addition to a positive response to at least one question amongst numbers 2 and 4. Participants responding with "Awake" to question number 3 were excluded, as they were considered not to be in a state of CC during a dream-like state but rather awake. If participants replied with "No/Nothing" to question number 2–4 and positively to at least one of the questions investigating their experience (i.e., question number 1,3,5,6) they were considered having been DC during the unresponsive period. See fig. 3.2 for a schematic illustration of the classification of reports into CC and DC groups.

Participants were acquainted in advance with the different questions and possible answers to ensure full understanding of each question. To rule out potential arousals during fMRI acquisitions, subjects were monitored continuously throughout the acquisition via an eye-tracking camera (EyeLink 1000plus system from SR Research, Ltd) – the eye-tracker was used for online monitoring but not for offline analysis. In case of eye opening, the MRI

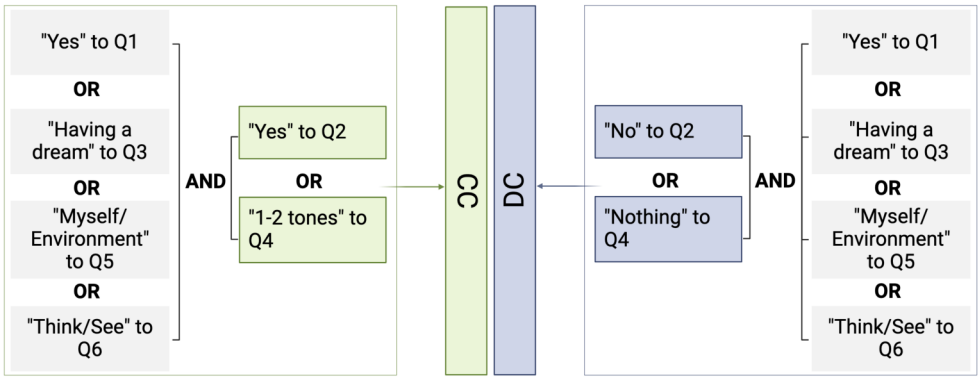

Figure 3.2: Classification of reports into CC and DC. The flow chart illustrates the possible combinations of responses to questions 1-6 used to classify participants into CC and DC groups. Grey boxes represent questions aimed at verifying the state of consciousness, while green and blue boxes indicate questions aimed at verifying the state of connectedness or disconnectedness, respectively. For details on how conflicting answers were handled, see the text. OR: inclusive "or" statement, i.e., A or B or both. Q: question. Created with BioRender.com.

acquisition was interrupted, and we waited for participants to spontaneously fall unresponsive again. If, after 15 min, LOR did not occur, we increased the propofol concentration up to three times in 0.1 μg.ml^{-1} increments.

3.2.5 fMRI experimental design and auditory paradigm

We chose a mixed block/event-related design (see fig. 3.3), in which trials of auditory stimuli are interspersed with blocks of silence of varying durations (15 blocks in total, each lasting 45 sec and containing 30 trials on average).

This design allows for the simultaneous modeling of the transient, trial-related activity, and the sustained, task-related BOLD activity. That is, by alternating silence blocks with task blocks (i.e., blocks with trials with auditory stimuli) we can optimize the sensitivity for discriminating events within trials and all events combined within a block.

Blocks with only standard events were alternated with blocks containing both standard and deviant events. Standard and deviant blocks were alternated in pseudorandomized order (ABBA...), in which no more than two identical types of blocks can follow one another. The length of the silence blocks was randomized in 1-sec steps in intervals of 7–10 sec. Based on previous studies (Bekinschtein et al., 2009), each event (both standard and

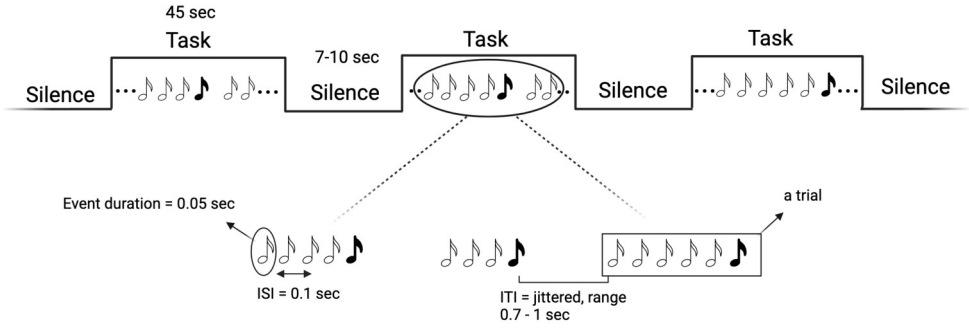

Figure 3.3: Schematic representation of the mixed block/event-related design (top) and of the 'Mixed35' oddball rule (bottom). White musical notes denote standard sounds, black notes deviant sounds. Created with BioRender.com.

deviant sounds) lasted 0.05 sec; the inter-stimulus interval was fixed at 0.1 sec and inter-trial interval was jittered in 0.05-sec steps between 0.7 to 1 sec. We used a variant of the 'classic oddball' paradigm (see fig. 3.3), in which trials consisted of a randomized number of repetitions (i.e., 3–5) of standard events plus one deviant event. Standard sounds had a frequency of 100 Hz and deviants of 500 Hz. The total length of the auditory stimulation was 15 min. Each task block lasted 45 sec (to have both a frequency still below the recommended 128 sec high-pass filter, but also a reasonable number of trials). The parameters selected for the auditory stimulation were the result of the efficiency and collinearity analyses we performed to optimize the efficiency of our design (see SI, sec. 3.14). Sounds were delivered via a Serene Sound Digital MRI-compatible system.

3.2.6 MRI data acquisition

MRI data were collected with a 3T Magnetom Prisma Fit scanner (Siemens, Erlangen, Germany) equipped with a 20-channel array receiver head–neck coil. For rs-fMRI and task based-fMRI, the scanning parameters were defined as follows: echo-planar imaging with multi-band acceleration factor of 6, 7/8 phase partial Fourier, 2.25 mm slice thickness, no gap between slices, 2.25 mm x 2.25 mm in-plane spatial resolution, 842 ms repetition time (TR), 30 ms echo time (TE), 52° flip angle, 207 mm x 225 mm field of view and a matrix size of 92 × 100. For anatomical reference, a high-resolution T1-weighted image was acquired for each subject during the awake session (T1-weighted 3D magnetization-prepared rapid gradient echo (MPRAGE) sequence, TR=1900 ms, TE = 2.19 ms, inversion time (TI)=900 ms, sagittal orientation, 224 slices,

1 mm slice thickness, field of view=256×240 mm2, matrix size=256x240x224, voxel size=1x1x1 mm3, GRAPPA R=2 acceleration factor in phase-encoding direction (AP).

3.2.7 Pre-processing

fMRI data were bidsified (Gorgolewski et al., 2016) and then preprocessed in software SPM12 (Statistical Parametric Mapping, version 12, UCL Institute of Neurology, London, Britain, http://www.fil.ion.ucl.ac.uk/spm) and FSL 6.3. The preprocessing pipeline included standard steps of realignment (FSL MCFLIRT (Jenkinson et al., 2002)), susceptibility-induced distortions correction (FSL topup (Andersson et al., 2003; Smith et al., 2023)), coregistration, brain tissue segmentation, spatial normalization to the Montreal Neurological Institute stereotaxic template and smoothing using the Gaussian filter method with an isotropic kernel of size 6 mm. Outlier volumes, due to excessive head and body motion, were detected using Artifact Detection Tools (ART) toolbox (http://web.mit.edu/swg/software.htm) and regressed out in the first-level general linear model (GLM) analysis. An image was defined as an outlier image or artifact if the global mean intensity in the image deviated by more than 9 standard deviations from the mean image intensity for the entire scan session, or if the head motion exceeded 2.0 mm in the x-, y-, or z-direction. For each run of the 15-min auditory paradigm, the first five volumes were discarded to allow magnetization to reach dynamic equilibrium.

3.3 Analyses

Activation analyses were conducted on the preprocessed BOLD time-series at the block level. We contrasted (1) task/all-sounds blocks (i.e., standard and deviant blocks combined) vs silence blocks and (2) standard vs. deviant blocks. Analysis of rs-fMRI data, collected as an ancillary investigation of sedation effects, falls outside the scope of this thesis, focused on the neural mechanisms of sensory disconnection; due to a 25-minute temporal gap between subjective report collection and the start of resting-state data recording these reports cannot be meaningfully extended to the resting-state period. Spectral analyses were conducted independently of the auditory events - see fig. 3.4 for an overview of the analyses.

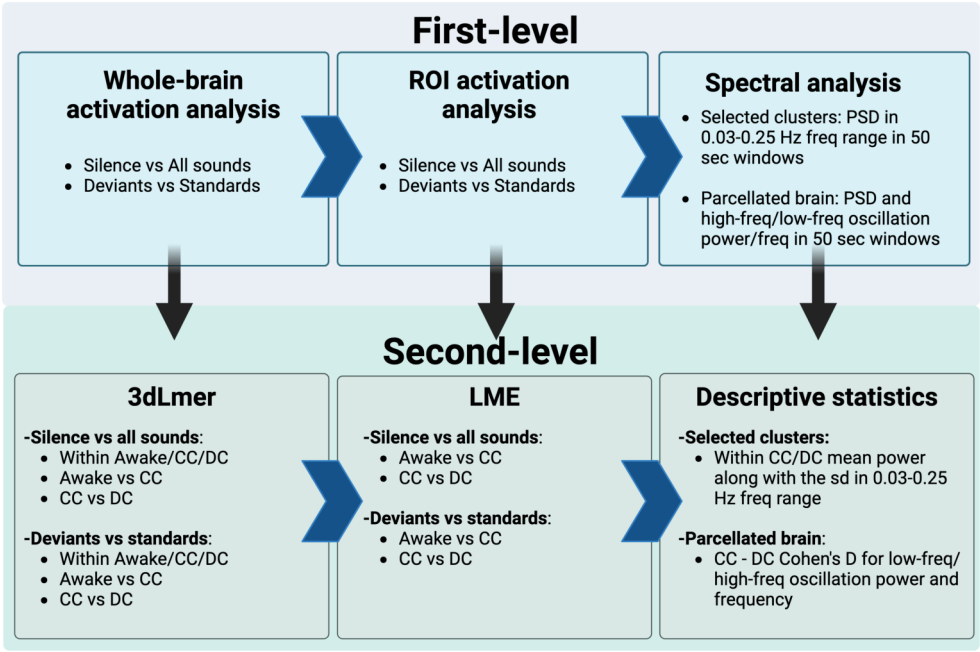

Figure 3.4: Analyses overview. This figure illustrates the single-subject, first-level (top) and group, second-level (bottom) analyses. It details the types of stimuli used, the contrasts specified, and the statistical methods applied at the group level. LME = Linear Mixed-Effects Models, 3dLmer = AFNI software for Voxelwise Linear Mixed-Effects Analysis, PSD = power spectral density, freq = frequency. Created with BioRender.com.

3.3.1 Voxel- and ROI-wise activation analyses

We performed voxel-wise and Region Of Interest (ROI)-wise activation analyses. All first-level activation analyses were conducted in SPM12 by specifying a first-level general linear model (GLM). The GLM design matrix included six movement parameters, outlier volumes (identified by Artifact Detection Tools (ART) toolbox) and the onsets of deviant/standard or all-sounds-combined/silence blocks. Regressors were convolved with the canonical hemodynamic response function and filtered with a high-pass filter of 128 sec. To minimize noise contamination, the voxel-wise activation analysis was restricted to gray matter only. This involved removing white matter and cerebrospinal fluid from the whole-brain mask. Activation values within each ROI were computed by estimating separate GLMs on implicit masks corresponding to each ROI. The ROIs included primary auditory cortices (Heschl's gyrus (HG), including HG1 and HG2)

and secondary auditory cortices (planum polare and planum temporale) extracted from the Harvard-Oxford cortical and subcortical structural atlases (https://identifiers.org/neurovault.collection:262); and thalamic ROIs extracted from the 'Oxford thalamic connectivity atlas', in which sub-striatal regions are segmented according to their white-matter connectivity to cortical areas (Behrens, Johansen-Berg, et al., 2003; Behrens, Woolrich, et al., 2003). We included the areas of the thalamus labeled in the atlas as posterior-parietal, occipital, sensory, and prefrontal. For both voxel- and ROI-wise analyses, we defined a series of contrasts to separately quantify brain activation during standard, deviant, all-sounds-combined and silence blocks. The contrast images obtained were used as inputs in second-level analyses (see sec. 3.3.2).

3.3.2 Activation - Group analyses

For group-level voxel-/ROI-wise activation analyses we performed a linear mixed effect model. For the voxel-wise analysis, we employed the 3dLMEr program (G. Chen et al., 2013) from AFNI (Cox, 1996) (AFNI version = AFNI 24.1.17), with contrast images from the first-level analysis as input[1]. For CC vs. DC comparisons, fixed effects and interactions were included for group (CC vs. DC), propofol concentration, and block type (all sounds vs. silence or deviant vs. standard), along with the main effects of gender and session (first or second oddball session during sedation). Random intercepts were specified at the subject level to account for individual variability. Specifically, random intercepts were included for each subject, nested within block type, and within session. This approach ensured that the model adjusted for how each subject's responses may differ depending on the type of blocks presented and the experimental session number. In the CC vs. awake model, fixed effects and interactions were included only for group (CC vs awake) and block type, along with the main effect of gender. Random intercepts were included for each subject and nested only within block type. The CC vs. awake model included only the corresponding wakefulness sessions for participants classified as CC. For the within-group analyses, due to the smaller sample size of the within-group models, the model formula had to be simplified. For the within-group analyses of CC and DC, we included fixed effects and interactions for propofol concentration and block type, along with the main effect of gender and random intercepts for subject, nested within

[1]Group analyses were conducted in AFNI and R instead of SPM, as SPM currently lacks support for linear mixed-effects models, which were preferred for our experimental design due to the inclusion of multiple mixed-type variables (within- and between-subject factors, as well as a quantitative variable).

block type. For the within-awake group analysis, fixed effects were specified for block type and gender, with random intercepts for subject, nested within block type. The within-awake model was run on the wakefulness recordings corresponding to all the CC and DC participants included in the dataset.

To correct for multiple comparisons, for all voxel-wise activation analyses, we first estimated noise smoothness for each subject using the AFNI program 3dFWHMx. This program outputs three values for constructing the auto-correlation function, which models the correlation between each voxel and its neighbors. Each of these values were then averaged across subjects and used as input in AFNI's 3dClustSim program. We set the alpha threshold at 0.05 and the uncorrected cluster-forming p-threshold at 0.001. 3dClustSim calculated the minimum number of voxels required for a cluster to be considered significant. We used the cluster size threshold obtained with two-sided testing and third-nearest neighbor clustering (where faces, edges, or corners need to touch) for cluster definition. Group results were visualized using the highlight-but-not-hide approach (Taylor et al., 2023), with clusters outlined at a z-threshold of ±3.29 (p=0.001) and opacity decreased for clusters at a z-threshold of ±1.96 (p=0.05) to enhance transparency. This approach mitigates the risks associated with overly conservative, traditional thresholding, which can obscure meaningful sub-threshold effects, hindering reproducibility - defined as the ability to replicate scientific findings under consistent conditions in different studies. It has been shown, in fact, that there is no straightforward link between a specific significance threshold and the probability of achieving comparable results in future studies (McShane et al., 2019). By showing the full range of effects rather than focusing only on the most significant findings, this method ensures a more comprehensive view of the data, reducing selection bias and providing a clearer picture of underlying biological processes. Ultimately, this approach enhances reproducibility, verification, and quality control, while also facilitating more robust meta-analyses (Taylor et al., 2023). Effect size maps thresholded with this approach were visualized using BrainNet Viewer (http://www.nitrc.org/projects/bnv/) (Xia et al., 2013).

For the ROI-wise activation analyses, we used lmer function from lme4 package (Bates et al., 2015) in software R, with ROI activity mean from the first-level analysis as input. For the CC vs DC comparison, we employed a reduced model due to constraints in the number of observations for the previously specified random effect structure. The model specified for all-sounds/silence and deviant/standard blocks mirrored the voxel-wise model

but excluded the random intercept for subject nested within block type and within session (retaining only the random - but not nested - intercept for subject). The model used for the CC vs. awake comparison was identical to the CC vs. DC model, except it did not include the fixed effects of propofol concentration and session.

3.3.3 Spectral analysis

Preprocessed BOLD time-series (see sec. 3.2.7) were high-pass filtered at 0.01 Hz and further cleaned to remove head movements (see below). The change in BOLD frequency content during DC and CC conditions was estimated in each of the 400 pre-defined regions derived from parcellation. We used the atlas (Schaefer et al., 2018) with 400 regions, each annotated from the parcellation with a 17-network solution.

Spectral changes were quantified using Short Time Fourier Transform. A sliding Hamming window was applied to calculate the spectrogram of each voxel's time series, with a window length of 50 sec, corresponding to 238 volumes. For each ROI/cluster, the power spectral density PSD was calculated by averaging the PSD across all voxels within the region. To ensure that different voxels within a brain region contributed equally to the PSD of the region, the PSD of individual voxels was normalized by each voxel's total power (across windows). To identify and exclude time points potentially contaminated by head movement, for each ROI/cluster, we computed the accumulated power across all frequencies in each time window. We then calculated the mean and standard deviation of these accumulated power values and identified time windows where the accumulated power deviated from the mean by more than ± 2 standard deviations in 80% or more of the ROIs or clusters. These outlier time points were flagged as potentially affected by motion and were excluded from subsequent analyses. The peak frequency at each time point was estimated based on a method similar to that introduced in (Song et al., 2022). From the average PSD of each ROI, we extracted the high-frequency oscillation power by identifying, for each ROI and time window, the maximum power value within a predefined high-frequency range (0.10–0.25 Hz). We then averaged these peak power values across all time windows to obtain a single representative power value for the high-frequency band in each ROI. These averaged values were used to characterize oscillatory activity within each ROI.

For the group level analysis, as in (Song et al., 2022), we employed de-

scriptive statistics. We computed Cohen's D to quantify the effect size of the difference between CC and DC groups in high-frequency oscillatory power for each ROI. This allowed us to visualize the magnitude of differences between the groups per ROI. Cohen's D results were visualized with BrainNet Viewer (http://www.nitrc.org/projects/bnv/) (Xia et al., 2013).

3.4 Results

3.4.1 Motion

In total, 47 participants were initially recruited for the study. However, the experiment was prematurely halted before the start of the sessions under sedation for 7 participants. This interruption occurred due to scanner malfunctions in two cases and concerns over participant safety, arising from adverse reactions to propofol (e.g., obstructive apnea), in five cases. Among the remaining 40 subjects, 35 completed both experimental sessions under sedation. For the remaining 5 participants, only the first sedation session was

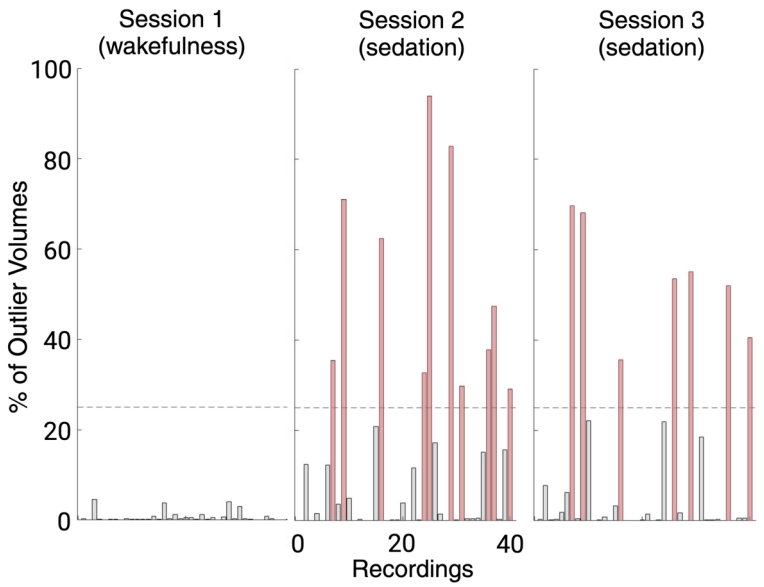

Figure 3.5: Percentage of outlier volumes for each recording. Histograms display the percentage of outlier volumes for each recording, grouped by session. Red bars highlight recordings excluded due to excessive motion, with the dotted line representing the 25% exclusion threshold. Figures were generated in MATLAB and assembled in BioRender.com.

completed due to health reasons that necessitated stopping the experiment before the beginning of the second sedation session. As described in section 3.2.7, outliers images were identified based on head motion and global mean intensity for each subject and session. Sessions exceeding 25% outlier volumes were excluded from further analysis (see fig. 3.5). This resulted in the exclusion of 17 out of 75 total sessions (10 second sessions and 7 third sessions), amounting to a motion-related rejection rate of approximately 22.67% - see fig. 3.5.

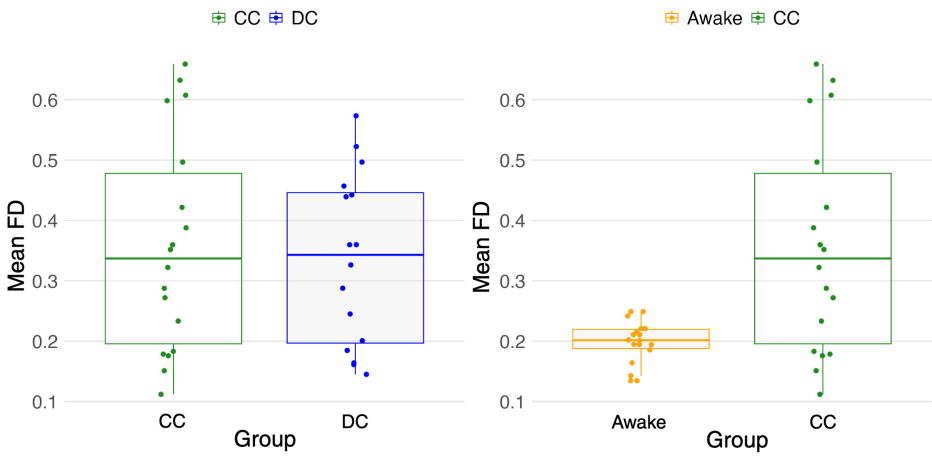

Figure 3.6: Mean framewise displacement in CC vs DC, and CC vs wakefulness. The boxplots represent the distribution of mean framewise displacement for the CC and DC groups (left) and CC and awake groups (right). The boxes indicate the interquartile range, the horizontal line inside each box represents the median, and the whiskers extend to 1.5 times the interquartile range. Individual points represent the mean framewise displacement for each recording. No significant difference was observed between the CC and DC groups, while the awake group exhibited a significant reduction in movement compared to CC. Mean FD = mean framewise displacement. Figures were generated in R and assembled in BioRender.com.

For each of the remaining usable recordings, we calculated the mean framewise displacement (i.e., the movement of the head from one volume to the next). A two-sample t-test showed no significant difference between the CC and DC groups (t = 0.39, p = 0.697, $M_{CC} = 0.357$, $M_{DC} = 0.335$), indicating comparable head movement - see fig. 3.6, left. However, for the awake[2] and CC groups, we found a significant difference in mean framewise

[2]Only the corresponding wakefulness sessions for participants classified as CC were included under 'awake'.

displacement (t = -3.72, p = 0.0007, $M_{\text{Awake}} = 0.198$, $M_{\text{CC}} = 0.357$) - see fig. 3.6, right.

This result was to some extent expected, as the CC group was sedated with propofol, while the awake group consisted of alert individuals who were explicitly instructed to remain still. Despite this difference, the preprocessing pipeline, incorporating standard procedures like realignment and coregistration, was likely sufficient to account for its impact. Additionally, movement was included as a covariate in our statistical models (i.e., the six movement parameters and outlier volumes), ensuring that any residual movement effects were addressed in the analysis.

3.4.2 Percentage of types of report

The usable sessions were classified into CC and DC groups based on the responses provided upon awakening, as detailed in section 3.2.4. In the second session, 16.6% and in the third session, 25% of participants provided conflicting responses, suggesting potential categorization under both CC and DC ('conflicting subjects'), and were consequently excluded from further analyses.

These conflicting responses were due to inconsistencies during the interview, such as reporting dreams and sounds initially but then denying any sounds when asked for the total number. 6.6% of participants in the second session and 7.1% in the third session denied any subjective experience ('unconscious'), while 7.1% in the third session reported wakefulness during the unresponsive period. These participants were excluded from the analysis. Finally, 16.6% of participants in the second session and 3.5% in the third session were unarousable, which precluded the collection of reports and necessitated their exclusion from further analyses. Fig. 3.7 depicts the proportion of conflicting, unarousable, unconscious, CC and DC participants for each sedation session. A total of 34 sedation sessions (18 CC, 16 DC) involving 25 participants were included in this study.

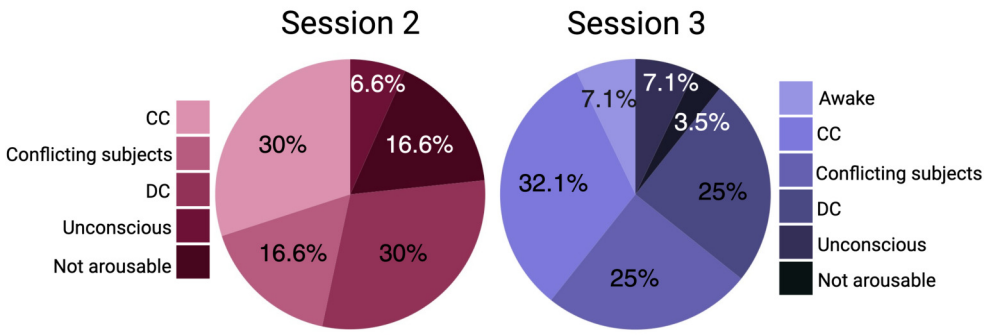

Figure 3.7: Proportion of report types per session. The pie charts depict the percentages of report types upon regaining responsiveness in session two (left) and session three (right). Participants were categorized as 'conflicting' if their responses to the six-question interview suggested possible classification into both CC and DC groups. Participants were categorized as 'unconscious' if they reported no experience upon awakening. 'Not arousable' participants could not be awakened, precluding the interview. Figures were generated in R and assembled in BioRender.com.

3.4.3 77% of CC participants report perceiving multiple tones

Question four, "did you hear one or two different tones?", aimed to assess whether CC participants detected the deviant sounds in the oddball paradigm, where deviant and standard tones were presented at different frequencies. 77.8% of CC participants, across both ROR1 and ROR2, reported hearing two or more tones, while only 5.56% (one participant) reported hearing just one tone - see table 3.1.

Table 3.1: Counts and percentages of number of tones reported by CC participants

Reported	Session 2	Session 3	Across Sessions
One	0 (0%)	1 (11.1%)	1 (5.56%)
Two	6 (66.7%)	4 (44.4%)	10 (55.6%)
Three	2 (22.2%)	2 (22.2%)	4 (22.2%)
Not sure	0 (0%)	1 (11.1%)	1 (5.56%)
NA	1 (11.1%)	1 (11.1%)	2 (11.1%)

Question number five "was this experience more centered on yourself or on the environment?", was designed to investigate the focus of participants' experiences — whether it was more centered on oneself or on being im-

mersed in an environment. 'Environment' here referred to the dream-like context rather than external surroundings, as clarified to participants before the beginning of the experiment. A slightly higher proportion of DC participants (56.2%) reported being more focused on the (dream-like) environment compared to 38.9% in the CC group (see table 3.2). In contrast, 44.4% of CC participants reported being more centered on themselves, compared to 37.5% of DC participants. This difference, however, was not statistically significant ($\chi^2(2, N = 34) = 0.96$, p = .62), confirming that the only notable variation in phenomenological state between the two groups was their (dis)connectedness to the environment.

Table 3.2: Counts and percentages of content of experience (self-focused vs. environment-centered) reported by CC and DC participants

	Reports	Session 2	Session 3	Across Sessions
CC	myself	4 (44.4%)	4 (44.4%)	8 (44.4%)
	environment	4 (44.4%)	3 (33.3%)	7 (38.9%)
	both	0 (0%)	1 (11.1%)	1 (5.56%)
	NA	1 (11.1%)	1 (11.1%)	2 (11.1%)
DC	myself	2 (22.2%)	4 (57.1%)	6 (37.5%)
	environment	6 (66.7%)	3 (42.9%)	9 (56.2%)
	both	0 (0%)	0 (0%)	0 (0%)
	NA	1 (11.1%)	0 (0%)	1 (6.25%)

Finally, building on question five, question six, "did you rather think, or did you see many things?", aimed to characterize the type of participants' experiences, distinguishing between thought-like and visual experiences. An equal proportion of CC participants reported their experiences as either visual or thought-like (33.3% for each). In contrast, a higher percentage of participants in the DC group described their experiences as more visual (43.8%) rather than thought-like (37.5%) - see table 3.3. However, the relation between group (CC vs. DC) and type of experience reported ("seeing," "thinking," or "not sure") was not significant - $\chi^2(2, N = 29) = 1.04$, $p = .59$.

Table 3.3: Counts and percentages of types of experience (visual vs. thought-like) reported by CC and DC participants

	Reports	Session 2	Session 3	Across Sessions
CC	Seeing	3 (33.3%)	3 (33.3%)	6 (33.3%)
	Thinking	3 (33.3%)	3 (33.3%)	6 (33.3%)
	Not sure	2 (22.2%)	1 (11.1%)	3 (16.67%)
	NA	1 (11.1%)	2 (22.2%)	3 (16.7%)
DC	Seeing	4 (44.4%)	3 (42.9%)	7 (43.8%)
	Thinking	4 (44.4%)	2 (28.6%)	6 (37.5%)
	Nothing	0 (0%)	1 (14.3%)	1 (6.25%)
	NA	1 (11.1%)	1 (14.3%)	2 (12.5%)

3.4.4 No significant differences in demographics, propofol concentration or time to ROR between CC and DC

In the final dataset, no statistically significant differences were found between CC and DC sessions for BMI (Wilcoxon rank sum test, W = 177.5, p-value = 0.25), age (Wilcoxon rank sum test, W = 105.5, p-value = 0.19), or gender (Pearson's Chi-squared test, X-squared = 0, df = 1, p-value = 1) - see table 3.4.

Table 3.4: Summary of BMI, age, and female percentage by group

Group	BMI	Age	Female_Percentage
CC	22.88 ± 2.44	24.06 ± 4.85	50%
DC	21.88 ± 2.06	24.62 ± 2.96	50%

Propofol concentration did not differ significantly between CC and DC across sessions (Welch Two Sample t-test, t = 0.78, df = 30.7,df = 12.443, p-value = 0.44), nor within session 2 (Welch Two Sample t-test, t = 15.35, df = 15.348, p-value = 1) or session 3 (Welch Two Sample t-test, t = 1.31, df = 12.44, p-value = 0.21). Similarly, no significant differences were found in propofol concentration between session 2 and 3 for either CC (Welch Two Sample t-test, t = -0.44, df = 15.907, p-value = 0.66) or DC (Welch Two Sample t-test, t = 0.82, df = 13.201, p-value = 0.42) - see table 3.5.

Finally, no significant difference was found between CC and DC groups in the time needed to achieve ROR - computed as elapsed time from the

Table 3.5: Average propofol concentration by group and session

Group	Session 2	Session 3	Across sessions
CC	2.03 μg.ml^{-1} ± 0.44	2.12 μg.ml^{-1} ± 0.41	2.08 μg.ml^{-1} ± 0.43
DC	2.03 μg.ml^{-1} ± 0.36	1.91 μg.ml^{-1} ± 0.21	1.97 μg.ml^{-1} ± 0.29

first ROR attempt to the time of ROR - neither for ROR1 (Welch Two Sample t-test, t = -0.36, df = 15.19, p-value = 0.72), nor for ROR2 (Wilcoxon rank sum test, W = 38.5, p-value = 0.48), nor across sessions (Wilcoxon rank sum test, W = 147, p-value = 0.93) - see table 3.6.

Table 3.6: Average time to ROR for CC and DC groups

Group	Time to ROR1	Time to ROR2	Across Sessions
CC	4.00 min ± 3.64	5.11 min ± 5.18	4.56 min ± 4.41
DC	4.56 min ± 2.88	2.86 min ± 2.67	3.71 min ± 2.77

3.4.5 Hypotheses I-IV. Main findings of the activation analyses

Group-level results were visualized using the highlight-but-not-hide approach (Taylor et al., 2023), with clusters outlined at a z-threshold of ±3.29 (p = 0.001) and opacity decreased for clusters at a z-threshold of ±1.96 (p = 0.05). This method mitigates the limitations of traditional thresholding, promoting a more comprehensive view of the data, supporting reproducibility, verification, and quality control - see section 3.3.2 for more details on this approach.

Typical auditory processing patterns in awake participants

To validate our methodology, we first analyzed data from awake participants for both all-sounds versus silence and deviant versus standard blocks. These analyses served as a positive control, replicating established findings on general auditory and oddball perception in awake individuals.

Figure 3.8 (top panel) shows activation differences between silence and all-sound blocks (cluster-forming threshold: p<0.001, 20 voxels; FWE-corrected at p<0.05). At a stringent z-threshold of ±3.29 (p<0.001), we observed strong, localized activations in the bilateral superior temporal gyri (including bilateral Heschl's gyri) and the right middle temporal gyrus. At a less stringent z-

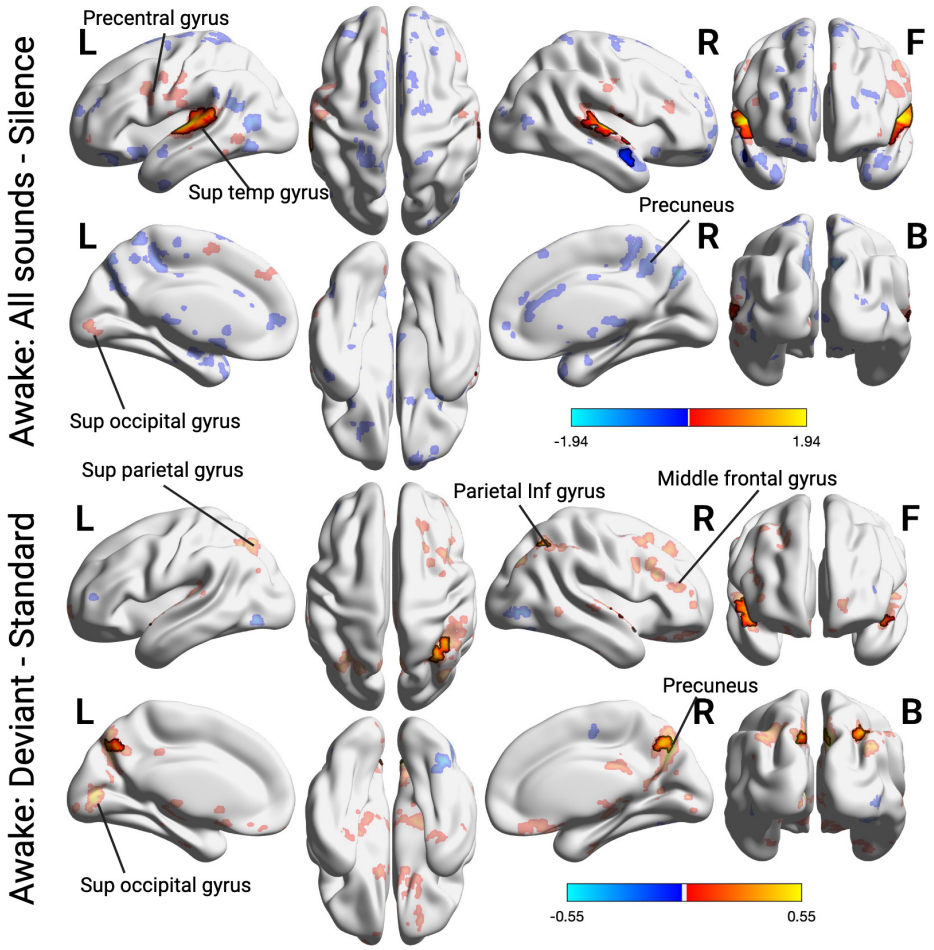

Figure 3.8: Activation differences in awake participants in response to all sounds vs silence blocks and in response to deviant vs standard blocks. Voxel-wise effect size maps showing activation differences in response to all-sounds vs silence blocks **(top panel)** and deviant vs standard blocks (bottom panel), thresholded by z-scores. Results are cluster-corrected (k=20 for top panel, k=19 for the bottom panel with $p<0.05$) with a cluster-defining threshold of $p<0.001$. Clusters are visualized at a z-statistic threshold of 1.96 for transparent clusters and 3.29 for outlined clusters, following a highlight-but-not-hide approach to present results at both conservative and less stringent thresholds. L = left, R = right, F = front, B = bottom views. Inf = inferior; Sup = superior; Temp = temporal.

threshold of ±1.96 ($p<0.05$), these temporal clusters appeared as part of a larger network, extending to the left Supplementary Motor Area (SMA), bilateral precentral regions, and the left superior occipital gyrus near the

calcarine fissure. These activations were accompanied by deactivations in various portions of the left superior, middle, and inferior temporal gyri, bilateral precuneus, anterior cingulate gyrus, bilateral middle frontal gyri, right superior frontal gyrus, and left inferior frontal gyrus (z-threshold, $p<0.05$).

In response to deviant vs standard blocks (see fig. 3.8, bottom panel), activation in the bilateral superior temporal gyri was accompanied by additional clusters, commonly linked to oddball processing, including the bilateral precuneus and the left inferior parietal gyrus (Calhoun et al., 2006; Kiehl et al., 2005; Stevens et al., 2000) (cluster-forming threshold: $p<0.001$, 19 voxels; FWE-corrected at $p<0.05$; z-threshold of ± 3.29, $p<0.001$). At the less stringent z-threshold of ± 1.96 ($p<0.05$), these regions appeared to be embedded in the canonical network underlying deviant perception, comprising temporal, occipito-parietal and frontal regions, consistent with previous fMRI studies on auditory oddball processing (Calhoun et al., 2006; Kiehl et al., 2005; Stevens et al., 2000). Parieto-occipital activations were identified in the left lingual gyrus, bilateral middle occipital gyrus, bilateral angular gyrus, bilateral superior parietal gyrus, bilateral precuneus and bilateral middle cingulate gyrus (z-threshold of ± 1.96, $p<0.05$). Frontal regions exhibiting increased activity included the right middle frontal gyrus, bilateral superior frontal gyrus and right inferior frontal gyrus (fig. 3.8) - z-threshold of ± 1.96, $p<0.05$. Temporal activations were observed in the bilateral temporal superior gyrus accompanied by deactivation in the right inferior temporal gyrus. Other activations previously reported in response to deviants were found in the bilateral parahippocampal gyrus, hippocampus, and right insula (z-threshold of ± 1.96, $p<0.05$).

The thalamus and the caudate, key structures in deviant perception (Calhoun et al., 2006; Kiehl et al., 2005; Stevens et al., 2000; Strobel et al., 2008), showed increased activation in response to deviant compared to standard blocks at z-threshold of ± 1.96 ($p<0.05$) but not of ± 3.29 ($p<0.001$). Conversely, in response to standard and all-sounds blocks they exhibited deactivation, likely reflecting inhibitory processes associated with habituation (z-threshold of ± 1.96, $p<0.05$).

Hypothesis I-II. Effect of physiological state on connected consciousness

Hypothesis I: extensive decreases in response to sounds with focused reductions in the auditory cortex and SMA during CC compared to wakefulness

Next, we compared recordings of CC participants with those obtained from the same individuals during wakefulness. Although both conditions involved similar phenomenological states, as in both cases participants heard the sounds, their physiological state was markedly different. This contrast explored the impact of the physiological state on auditory connectedness.

As expected, during all-sounds blocks, CC participants exhibited widespread decreases in activity compared to their wakeful state (cluster-forming threshold: $p<0.001$, 20 voxels; FWE-corrected at $p<0.05$; z-threshold of ± 3.29, $p<0.001$) - see fig. 3.9. These reductions were localized to the occipital regions, including portions of the bilateral calcarine fissure and surrounding cortex and bilateral lingual gyrus; in parietal regions, covering areas in the bilateral superior parietal gyri, precentral gyri, postcentral gyri; in frontal regions, particularly portions of the bilateral middle and superior frontal gyri and left inferior frontal gyrus; and in temporal regions, notably the bilateral Heschl's gyri and temporal superior gyri (z-threshold of ± 3.29, $p<0.001$). Additional decreases were observed in the right hippocampus, the right SMA, and in the bilateral middle and right anterior portions of the cingulate gyrus (z-threshold of $p<0.001$) - see sec. 3.6.3 of SI for cluster tables. At the less stringent z-threshold of $p<0.05$, these activations expanded to cover larger parts of the previously mentioned areas, as well as additional regions, including the bilateral anterior and posterior cingulate gyrus and bilateral caudate. Interestingly, some regions also exhibited increased activation in CC compared to wakefulness. These included the bilateral cuneus, bilateral precuneus, left parahippocampal gyrus, bilateral inferior temporal gyrus and frontal clusters primarily in the right middle frontal gyrus (z-threshold of ± 1.96, $p<0.05$) - see fig. 3.9, top panel.

During silence blocks, no clusters survived at the z-threshold of ± 3.29 ($p<0.001$). However, at the less stringent threshold, some negative clusters were found in the left superior, middle and inferior temporal gyrus, the bilateral SMA, the right anterior cingulate gyrus and hippocampus and, predominantly the left-lateralized middle and inferior frontal gyri - see fig. 3.9, middle panel. In contrast, in the all-sounds vs. silence contrast, decreased activity in CC relative to wakefulness was also observed at the z-threshold of $p<0.001$, in a small cluster in the left superior temporal gyrus. This activation

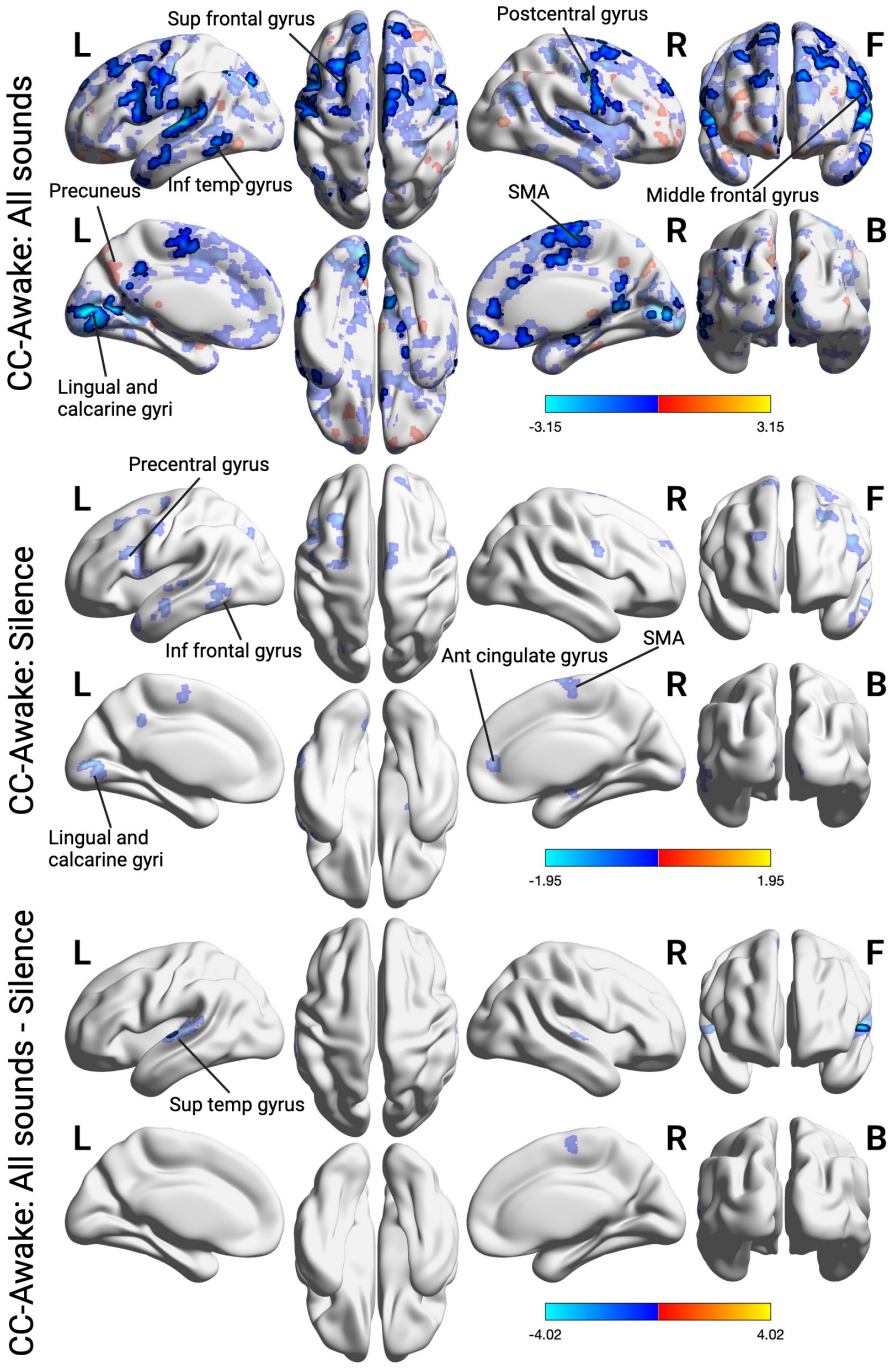

Figure 3.9: See next page

Figure 3.9: (Previous page.) **Activation differences between CC and wakefulness in response to sounds vs silence**. Voxel-wise effect size maps, thresholded by z-scores, showing activation differences between CC and wakefulness in response to all sounds combined (top), silence blocks (middle) and to the difference between the two (bottom). Specifically, bottom row shows regions with stronger sound versus silence responses in the CC group (red) relative to wakefulness, and vice versa (blue). Results are cluster-corrected (k=20, at $p<0.05$) with a cluster-defining threshold of $p<0.001$. Clusters are visualized at a z-statistic threshold of ±1.96 for transparent clusters and ±3.29 for outlined clusters, following a highlight-but-not-hide approach to present results at both conservative and less stringent thresholds. SMA = supplementary motor area; L = left, R = right, F = front, B = bottom views. Inf = inferior; Sup = superior; Temp = temporal.

expanded to cover a larger portion of this area at the less stringent threshold and was accompanied by deactivation in the left SMA (z-threshold of ±1.96, $p<0.05$)- see fig. 3.9, bottom panel.

Finally, differences in thalamic and caudate activity between CC and wakefulness were observed only at the least conservative threshold, with some thalamic activation increases and caudate decreases in CC compared to wakefulness in response to all-sounds blocks (z-threshold of ±1.96, $p<0.05$). This potential thalamic involvement was also suggested by the ROI analyses, where the thalamus (all parts combined into a single ROI) and the prefrontal portion of the thalamus were found to be the regions where the difference in activation between all-sounds and silence conditions was more pronounced for the CC group compared to wakefulness ($p<0.05$). The ROI analysis also corroborated the general decrease in activation to all sounds observed in CC compared to wakefulness - see 3.6.4 for more details on the ROI results and see 3.6.5 for summary of model coefficients and p-values.

Hypothesis II: extensive decreases to deviant and standard sounds in occipital, temporal and frontal regions during CC compared to wakefulness

Similar decreases in activation observed in response to all sounds were also found when examining differences in deviant and standard sound processing between CC and wakefulness (cluster-forming threshold: $p<0.001$, 20 voxels; FWE-corrected at $p<0.05$; z-threshold of ±3.29, $p<0.001$). As illustrated in fig. 3.10 (top and middle panel), in response to both standard and deviant blocks, activity reductions encompassed occipital (bilateral calcarine gyri, lingual gyri) and temporal regions (predominantly bilateral superior and

middle temporal gyrus) at the z-threshold of $p<0.001$. In the frontal regions, reductions were observed in the bilateral inferior and middle frontal gyri in response to deviant blocks, and in the left inferior and middle frontal gyri in response to standard blocks (z-threshold of ± 3.29, $p<0.001$). At the less conservative threshold, these deactivations broadened to cover larger portions of these areas, along with additional regions such as the bilateral postcentral and precentral gyri, inferior parietal gyrus, bilateral SMA, and bilateral anterior cingulate gyrus. Notably, decreases in the right parahippocampal gyrus and left hippocampus were observed only in response to deviant blocks (z-threshold of ± 1.96, $p<0.05$) - see sec. 3.6.3 of the SI for cluster tables.

Increases in activity in CC compared to wakefulness were detected only at the less stringent threshold. In response to deviant blocks, these increases were localized to the right middle and inferior temporal gyrus, right middle frontal gyrus, and right inferior parietal gyrus. In contrast, standard blocks elicited more widespread activations in the right middle frontal gyrus, bilateral precuneus, and left superior temporal gyrus. No significant differences emerged between CC and wakefulness in the deviant vs. standard block contrast, at either the most stringent or the more lenient threshold - see fig. 3.10 (bottom panel).

ROI analyses further supported the widespread decreases observed in CC compared to wakefulness, showing reduced activation across ROIs and stimulus types ($p<0.05$). Additionally, the ROI analysis revealed that the difference in activation between wakefulness and CC was less pronounced in the planum polare, thalamus, and sub-thalamic regions including occipital, posterior/parietal, prefrontal, and sensory sub-thalamic regions ($p<0.05$) - see 3.6.4 for more details on the ROI results and see 3.6.5 for summary of model coefficients and p-values.

In summary, compared to wakefulness, CC exhibited widespread decreases in occipital, temporal, and frontal regions in response to all-sounds versus silence blocks, with more localized deactivations, primarily in the SMA, precentral, and temporal regions, in response to standard versus deviant blocks (z-threshold of ± 3.29, $p<0.001$). Increased activity in CC relative to wakefulness was observed only at the more lenient threshold, and appeared more pronounced during standard blocks than deviant ones, potentially indicating reduced inhibition to standard sounds in CC.

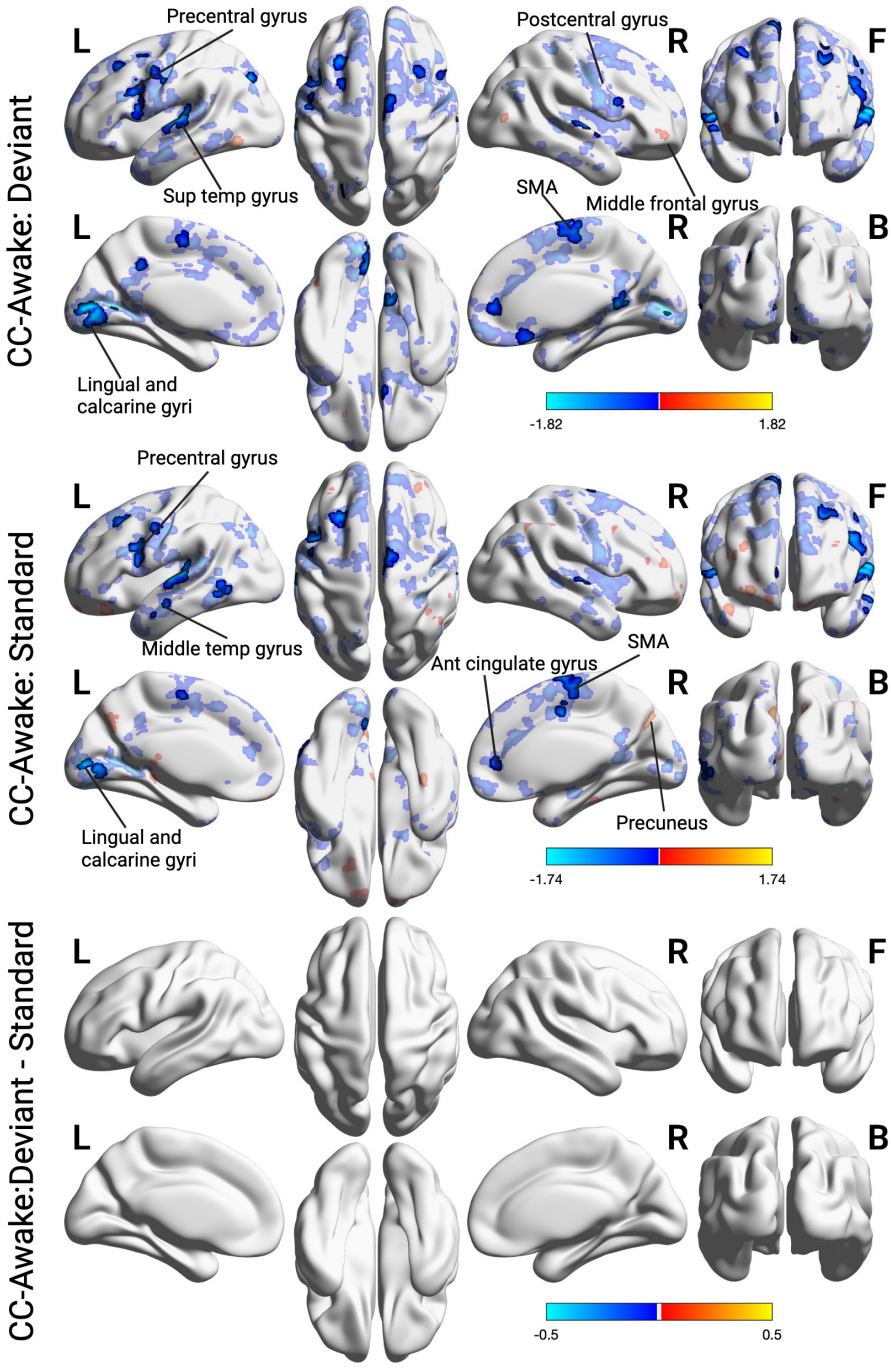

Figure 3.10: See next page

Figure 3.10: (Previous page.) **Activation differences between CC and wakefulness in response to deviant vs standard blocks**. Voxel-wise effect size maps, thresholded by z-scores, showing activation differences between CC and wakefulness in response to deviant (top), standard blocks (middle) and to the difference between the two (bottom). Specifically, bottom row shows regions with stronger deviant versus standard responses in the CC group (red) compared to wakefulness, and vice versa (blue). Results are cluster-corrected (k=20, at $p<0.05$) with a cluster-defining threshold of $p<0.001$. Clusters are visualized at a z-statistic threshold of ±1.96 for transparent clusters and ±3.29 for outlined clusters, following a highlight-but-not-hide approach to present results at both conservative and less stringent thresholds. L = left, R = right, F = front, B = bottom views. SMA = supplementary motor area; Inf = inferior; Sup = superior; Temp = temporal.

Hypothesis III-IV. Effect of (dis)connectedness within the same physiological state

Hypothesis III: increased activation to sounds in temporal regions in DC vs. focused activation in the precuneus in CC

In this section, we compared brain activation patterns between CC and DC states in response to all-sounds vs silence blocks (cluster-forming threshold: $p<0.001$, 16 voxels; FWE-corrected at $p<0.05$). Unlike the previous contrast, both groups were under identical physiological conditions — propofol sedation with similar anesthetic concentrations. However, their phenomenological states differed substantially, as DC participants did not hear the sounds while CC participants did. This contrast therefore explored the neural correlates of conscious auditory perception unbiased by physiological state.

At the most stringent z-threshold of ±3.29 ($p<0.001$), DC exhibited widespread increases in temporal activation in response to all sounds compared to CC, particularly in the left middle and superior temporal gyri, as well as the bilateral inferior temporal gyri (see fig. 3.11, top panel). This temporal activation was accompanied by additional increases in a smaller cluster in the right precentral gyrus (z-threshold of ±3.29, $p<0.001$). At the less stringent threshold, these activation increases in DC relative to CC appeared to be part of a broader pattern of widespread (paradoxical) activation - with 69 positive clusters and 78 negative clusters identified (see cluster table in Sec. 3.6.3 of the SI). These increases in DC extended across the bilateral inferior and middle temporal gyri, middle and inferior frontal gyri, precentral regions, the left superior frontal gyrus, and SMA (z-threshold of ±1.96, $p<0.05$). In contrast, CC participants showed focused activation increases restricted to the bilateral

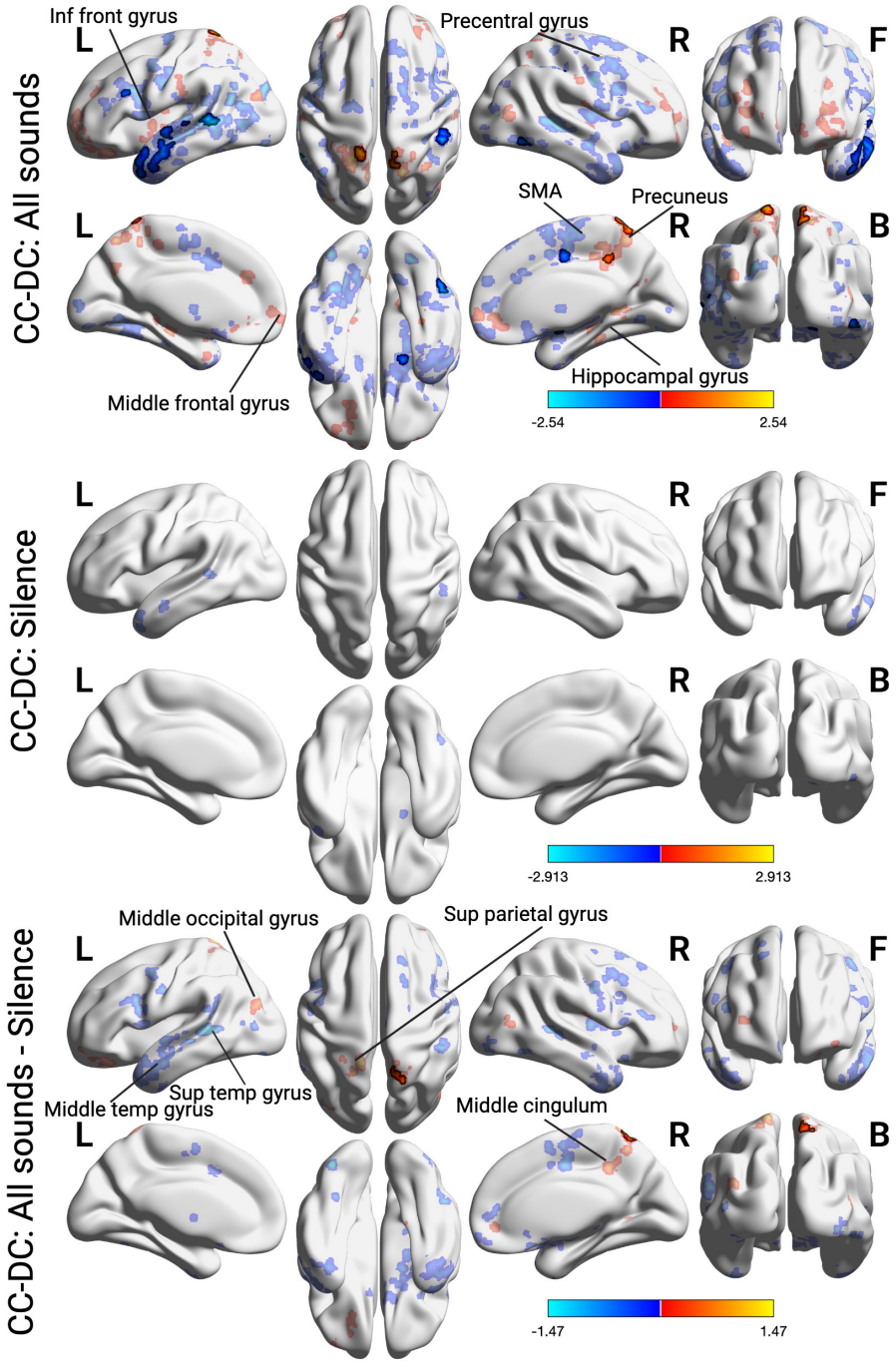

Figure 3.11: See next page

Figure 3.11: (Previous page.) **Activation differences between CC and DC in response to all sounds vs silence**. Voxel-wise effect size maps, thresholded by z-scores, showing activation differences between CC and DC in response to all sounds combined (top), silence blocks (middle) and to the difference between the two (bottom). Specifically, bottom row shows regions with stronger sound versus silence responses in the CC group (red) compared to the DC group, and vice versa (blue). Results are cluster-corrected (k=16, at $p<0.05$) with a cluster-defining threshold of $p<0.001$. Clusters are visualized at a z-statistic threshold of ±1.96 for transparent clusters and ±3.29 for outlined clusters, following a highlight-but-not-hide approach to present results at both conservative and less stringent thresholds. L = left, R = right, F = front, B = bottom views. SMA = supplementary motor area; Inf = inferior; Sup = superior; Temp = temporal.

precuneus (z-threshold of ±3.29, $p<0.001$). At the less conservative threshold (z-threshold of ±1.96, $p<0.05$), this activation seemed to integrate into a larger network, which included the right middle cingulate and paracingulate gyri, bilateral middle frontal gyri, hippocampal gyrus, superior parietal gyrus, and middle occipital gyrus (fig. 3.11, top panel)

Notably, none of the activation increases in DC relative to CC withstood the most stringent threshold during both the silence blocks and the all-sound versus silence contrast (see fig. 3.11, middle and bottom panels). Conversely, the enhanced activation in the right precuneus region in CC persisted in the all-sound versus silence contrast at the z-threshold of ±3.29, ($p<0.001$). Interestingly, at the less stringent threshold, the same regions in the DC group that showed increased activation during all-sounds blocks were also active during silence blocks. In the temporal regions, these increases were more scattered compared to the more concentrated activations seen during the all-sounds blocks, but they still encompassed the superior, middle, and inferior sections (z-threshold of ±1.96, $p<0.05$). In the precentral region, these activation increases included a cluster remarkably similar in both size and location to the one observed during all-sounds blocks (z-threshold of ±1.96, $p<0.05$) - see fig. 3.11, middle panel. This overall pattern of reduced activation in CC relative to DC was further supported by the ROI analyses, which revealed significant main effects of group and propofol concentration (see fig. 3.19), with the CC group showing significantly ($p<0.05$) lower activation across ROIs and stimulus types compared to the DC group - see 3.6.4 for more details on the ROI results and see 3.6.5 for summary of model coefficients and p-values.

The contrast between all sounds and silence, at the less conservative threshold, revealed broader activation differences between CC and DC, substantially overlapping with the network of regions observed in the all-sounds condition (z-threshold of ±1.96, $p<0.05$) - including 30 positive clusters and 47 negative clusters (see cluster table in Sec. 3.6.3 of the SI). Specifically, CC participants exhibited heightened activation within a network encompassing the right precuneus, right middle cingulate/paracingulate gyri, a small cluster in the prefrontal right middle frontal gyrus, the right superior frontal gyrus, and the bilateral middle occipital gyrus (z-threshold of ±1.96, $p<0.05$). Notably, the prefrontal activation increases in CC participants relative to DC, observed during sound blocks at the less stringent threshold, were markedly reduced (z-threshold of ±1.96, $p<0.05$).

Similarly, DC participants showed greater activation increases at the less stringent threshold, in regions comparable to those activated during the all-sounds blocks, including the left middle/superior temporal gyrus, precentral regions, and SMA (primarily in the right hemisphere).

In summary, DC participants exhibited widespread, paradoxical activation increases compared to CC participants in response to sounds, primarily concentrated in the left temporal region (z-threshold of ±3.29, $p<0.001$). Conversely, CC participants displayed more focused activation increases in the precuneus (z-threshold of ±3.29, $p<0.001$), which, at the less stringent threshold, appeared to be part of a more extensive network which included the middle cingulate/paracingulate gyri, superior parietal gyrus, middle occipital gyrus, and the middle/superior frontal gyrus (z-threshold of ±1.96, $p<0.05$).

Hypothesis IV: enhanced processing of deviant vs. standard sounds in CC compared to DC in fusiform and lingual gyri

Further analysis separated sound blocks into deviant and standard types, investigating CC-DC differences in processing each category (cluster-forming threshold: $p<0.001$, 15 voxels; FWE-corrected at $p<0.05$). As depicted in fig. 3.12, the overall pattern of results resembled those observed for all sounds combined, although the extent of activation differences was reduced. At the most stringent threshold, DC continued to exhibit increased activation in a small cluster within the left middle temporal gyrus (z-threshold of ±3.29, $p<0.001$), consistent with the findings for all sounds. Activation increases in CC relative to DC remained localized in the left precuneus but were

only present during deviant blocks, not standard ones (z-threshold of ±3.29, p<0.001). At the less stringent threshold, these clusters appeared to be part of broader networks similar to those seen in response to all sounds combined. In response to deviant blocks, at a z-threshold of ±1.96 (p<0.05), DC showed increased activation in the bilateral superior and middle temporal gyri, precentral regions, inferior frontal gyrus, and right SMA. Conversely, CC participants exhibited increased activation in a network, consistent with the all-sounds versus silence analysis, involving the right precuneus, right middle cingulate/paracingulate gyri, bilateral middle frontal gyrus, and superior parietal gyrus.

The activation decreases observed in CC compared to DC during deviant blocks reappeared in response to standard blocks (z-threshold of ±1.96, p<0.05).DC participants exhibited the same network of regions as seen for deviant blocks, but with additional activation increases in the precentral area, bilateral middle frontal gyrus, and left superior frontal gyrus compared to CC (z-threshold of ±1.96, p<0.05). And, overall, DC participants showed greater activation in response to standard blocks compared to deviant blocks, with 71 positive clusters for standard blocks versus 56 for deviant blocks (z-threshold of ±1.96, p<0.05) - see table 3.24 in SI.

However, when comparing the difference in processing deviant versus standard blocks between groups, a distinct set of regions emerged from the standard and deviant analyses, at both z-thresholds (see fig. 3.12, bottom panel). At the most stringent threshold, CC participants exhibited greater activation compared to DC in the right fusiform gyrus (cluster size: 31 voxels), right lingual gyrus (cluster size: 20 voxels), and left precentral region (cluster size: 19 voxels)[3]. No significant activation increases were observed in DC relative to CC at this stringent threshold. At the more lenient threshold, the activation increases found in CC at the z-threshold of ±3.29 (p<0.001), appeared to extend into a more broader network, consisting exclusively of activation increases in CC, encompassing parieto-central regions such as the right inferior parietal gyrus, left superior parietal gyrus, and SMA; frontal and prefrontal areas including the left middle frontal gyrus and right inferior frontal gyrus; and temporal regions such as the bilateral inferior and left superior temporal gyri, along with the right angular gyrus (z-threshold of ±1.96, p<0.05). Of note, the deviant-standard contrast at z-threshold of ±1.96 (p<0.05) also revealed scattered activation increases in DC compared to CC.

[3]Note that these clusters may appear smaller in surface brain images due to their crossing multiple slices

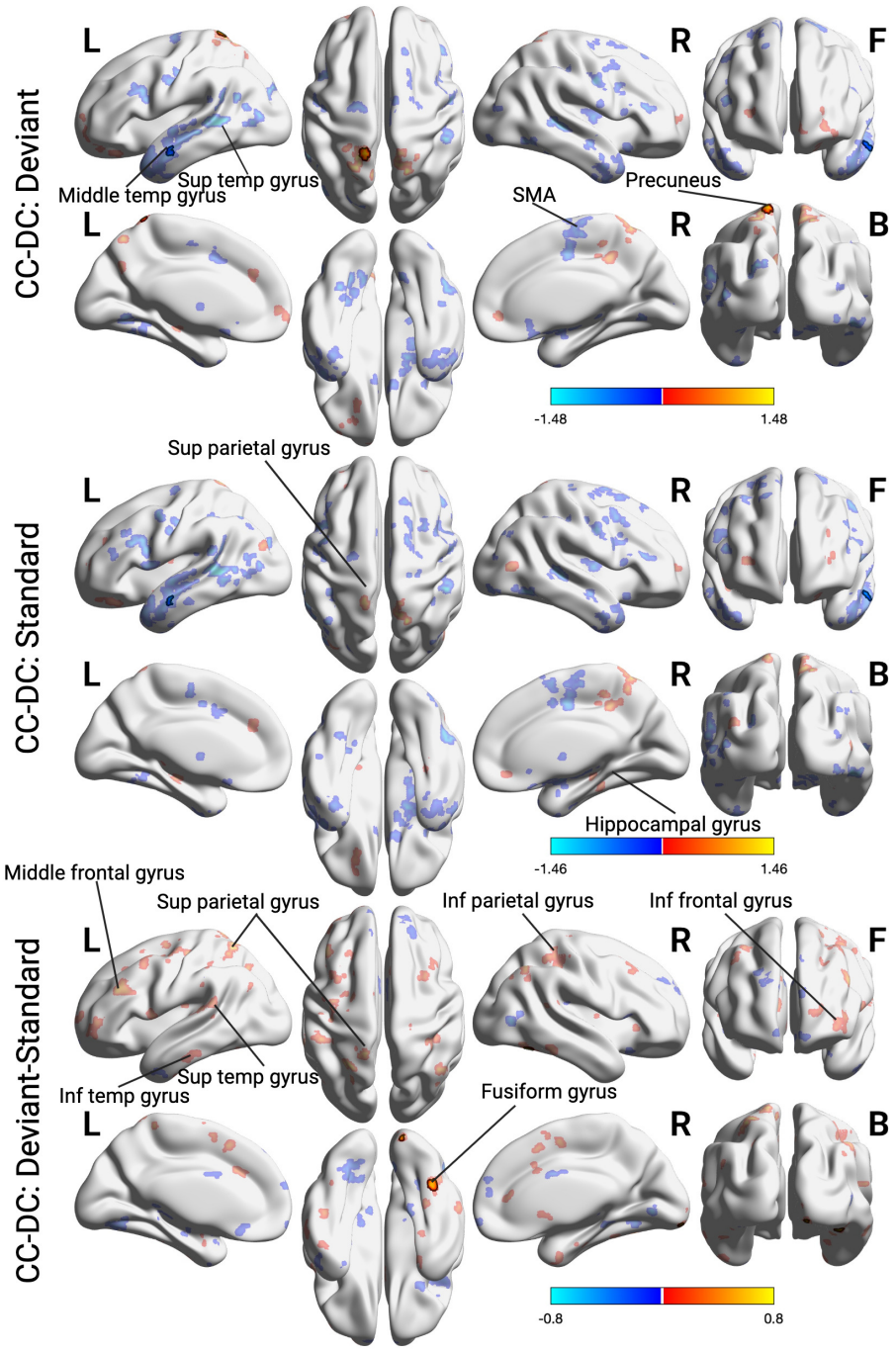

Figure 3.12: See next page

Figure 3.12: (Previous page.) **Activation differences between CC and DC in response to deviant vs standard sounds**. Voxel-wise effect size maps, thresholded by z-scores, showing activation differences between CC and DC in response to deviant (top), standard sounds (middle) and to the difference between the two (bottom). Specifically, bottom row shows regions with stronger deviant versus standard responses in the CC group (red) compared to the DC group, and vice versa (blue). Results are cluster-corrected (k=15, at $p<0.05$) with a cluster-defining threshold of $p<0.001$. Clusters are visualized at a z-statistic threshold of ±1.96 for transparent clusters and ±3.29 for outlined clusters, following a highlight-but-not-hide approach to present results at both conservative and less stringent thresholds. L = left, R = right, F = front, B = bottom views. SMA = supplementary motor area; Inf = inferior; Sup = superior; Front = frontal; Temp = temporal.

These activations included regions in the left lingual gyrus, bilateral fusiform gyri, cingulate/paracingulate gyri, and parts of the superior and inferior frontal gyri (z-threshold of ±1.96, $p<0.05$).

Interestingly, the increase in precuneus activity observed in CC was suppressed in the deviant-standard contrast, potentially indicating that this region plays a role in general conscious auditory processing rather than in detection of deviant sounds. In contrast, prefrontal activation increases in CC compared to DC were more widespread in the deviant-standard contrast than in the all-sounds analysis, predominantly affecting the left hemisphere and involving the inferior and middle frontal gyri (z-threshold of ±1.96, $p<0.05$).

Finally, the overall pattern of reduced activation in CC compared to DC, observed during both standard and deviant blocks, was further supported by the ROI analyses. These analyses revealed significant main effects for both group and propofol concentration (see fig. 3.19), with the CC group exhibiting significantly lower activation ($p<0.05$) across ROIs and stimulus types compared to the DC group. However, no significant ROI findings specific to between-group differences during deviant blocks were found. For more details on the ROI results, refer to sec. 3.6.4, and see 3.6.5 for a summary of model coefficients and p-values.

In summary, the networks identified in CC and DC participants in response to all sounds combined were similarly observed during both standard and deviant blocks. However, when comparing the difference in processing of deviant versus standard blocks between groups, CC participants exhibited increased activation in the right fusiform and lingual gyri, as well as the left

precentral region, compared to DC. The less stringent threshold suggested that these clusters were part of a broader network of diffuse activation increases in CC, involving frontal, prefrontal, and temporal regions, along with superior and inferior parietal gyri. These results might potentially be interpreted as suggesting that detection of deviant sounds occurs in CC but not DC participants.

3.4.6 Hypothesis V. Spectral analysis of parcellated brain: higher high-frequency power in DC compared to CC in the visual, sensorimotor, executive and attention networks

We then examined the differences between CC and DC (DC-CC) in high-frequency (0.10-0.25 Hz) oscillation power across the whole brain, analyzing 400 ROI from the (Schaefer et al., 2018) atlas.

Fig. 3.13 illustrates the Cohen's D effect size for the difference in high-frequency power between the CC and DC groups. The effect size ranges from -1.3 to -0.3, suggesting no overall global trend in high-frequency power across the whole brain for either CC or DC. Instead, different regions exhibit distinct patterns of high-frequency power in CC and DC states. To avoid displaying Cohen's D values near 0, which could be misleading and lead to inappropriate interpretations, we included only effect sizes from -/+ 0.1 onward.

From fig. 3.13, we observe increases in high-frequency power in CC relative to DC in the bilateral frontal, occipital, right precuneus and precentral/post-central regions. Conversely, DC participants show localized increases in high-frequency power relative to CC in various portions of the bilateral temporal gyri (middle, inferior, and superior); in the bilateral superior precentral gyrus; left occipital middle gyrus; right supramarginal gyrus and left lingual gyrus. Notably, the temporal and precentral regions with higher-frequency power in DC overlapped substantially with the clusters that showed increased activation in DC compared to CC in the voxel-wise activation analysis (see sec. 3.4.5).

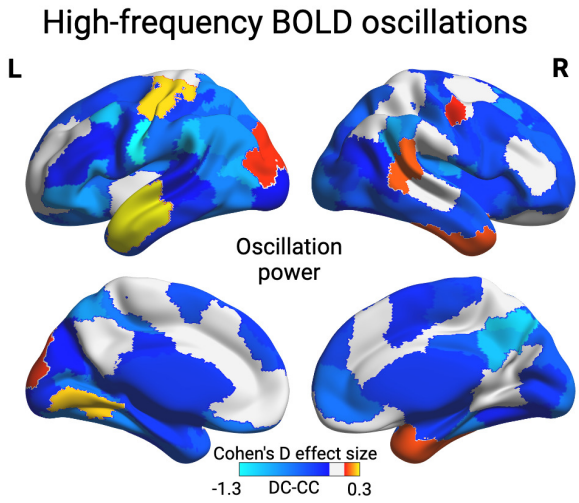

Figure 3.13: Regional distributions of high-frequency BOLD oscillation power in CC and DC groups. Cohen's D effect size (DC-CC) for oscillation power in the high-frequency range (0.10-0.25 Hz).

3.5 Discussion

In this study, we aimed to elucidate the neural correlates of sensory disconnection within-state, avoiding contrastive approaches to minimize bias stemming from physiological differences. We recorded brain activity in participants exposed to an auditory oddball paradigm during propofol sedation and prior to sedation, during wakefulness. During sedation, participants were serially awakened to report on their subjective experience and sound perception prior awakening. Based on these reports, they were categorized as CC, if they reported perceiving the sounds, or DC if they did not. By contrasting CC and DC, we sought to identify differences in sound processing between distinct phenomenological states yet similar physiological conditions (comparable propofol concentrations). By contrasting CC with wakefulness, we aimed to determine the impact of physiological state on sensory connection, as CC and wakefulness represent similar phenomenological states (both involving sound perception) but different physiological conditions.

Contrary to expectations outlined in hypothesis III, we observed paradoxical activation increases in DC compared to CC in response to all-sound blocks (see fig. 3.11), predominantly in the temporal region. Conversely, CC participants displayed localized activity in the precuneus, which appeared,

under a less stringent threshold, integrated into a network comprising the middle cingulate/paracingulate gyri, prefrontal areas, hippocampal gyrus, and middle occipital gyrus (fig. 3.11). This paradoxical pattern in DC reversed during deviant blocks, where activity increases were observed only in CC participants, localized in the fusiform, lingual, and precentral gyri and extending into frontal and parieto-central areas at the less conservative threshold. In contrast, DC participants showed minimal differences from their response to standard/all-sound blocks, potentially suggesting that deviant perception may be exclusive to the CC state. Supporting deviant perception during CC, the majority of CC participants (i.e., 77%) reported hearing two or more distinct sounds upon awakening (see 3.4.3). These findings corroborated Hypothesis IV, which proposed similar processing patterns for standard and deviant blocks in the DC group, contrasted by activation increases in CC during deviant blocks. Interestingly, contrary to hypothesis II — which posited reductions in CC activity compared to wakefulness in response to deviant blocks — we found no significant differences between these states in response to such stimuli. This could imply that the processing of deviant sounds in CC may closely resemble that observed in wakefulness. However, in line with hypothesis I, widespread activity reductions in CC relative to wakefulness were observed in response to all sounds - as shown in figs. 3.9-3.10.

Finally, the spectral analysis revealed enhanced high-frequency oscillation power in CC compared to DC in frontal, occipital, and precentral/postcentral regions, with this enhancement partially overlapping key nodes of the Default Mode Network DCM. Conversely, in DC, high-frequency oscillations were predominantly localized in discrete clusters within temporal, precentral, and occipital regions, encompassing auditory, somatosensory, and attention networks. These results partially confirmed Hypothesis V, as increased oscillation power was observed in DC within auditory regions but not in the thalamic area.

3.5.1 Paradoxical activation increases in DC: a reflection of disrupted inhibition and increased feedforward prediction error?

When comparing two physiologically equivalent groups, one aware of the presented sounds and one not, we might intuitively expect greater BOLD activation (particularly in the temporal lobes) in those who perceived the sounds. However, contrary to this expectation, we observed activity increases in DC relative to CC in response to all-sound blocks, notably in the mid-

dle/superior temporal gyrus, and at a more lenient threshold, in precentral regions, and SMA. This increased activation in DC was consistently observed across different stimulus types and regions, indicating a general pattern of greater activation in DC compared to CC (see sec. 3.19). One possible explanation for these findings, although speculative, lies in the concept of excitation-inhibition balance (EIB).

The importance of maintaining EIB for normal sensory processing is well-established across various fields (Isaacson & Scanziani, 2011; Z. Zhang & Sun, 2011). Experimental manipulation of this balance — by selectively increasing or decreasing inhibition/excitation — has been shown to disrupt sensory processing (Dudek & Sutula, 2007). For example, reducing GABA receptor levels, which mediate inhibitory control in the brain, decreases stimulus selectivity of neurons by diminishing their sensitivity across various sensory cortices (Isaacson & Scanziani, 2011; Wood et al., 2017), including auditory (J. Wang et al., 2000), visual (Katzner et al., 2011; Li et al., 2023), somatosensory (Kyriazi et al., 1996), and olfactory (Poo & Isaacson, 2009) cortices. This indicates that appropriate inhibition reduces neuronal noise, which in turn "reduces the randomness of cortical operations and increases temporal precision" (Z. Zhang & Sun, 2011). Thus, when inhibition is suboptimal, cortical excitability rises, leading to disorganized neural responses that can potentially disrupt conscious perception.

Indeed, as illustrated in fig. 3.8, awake participants displayed restricted activations, confined to key regions involved in auditory processing, with the highest activation localized in the primary auditory regions, specifically the Heschl's gyri. These activations, at a less stringent threshold, appeared to be accompanied by deactivations in temporal, frontal, and parietal regions. Similarly, in the CC vs DC comparison, activity increases in CC appeared specifically localized in the precuneus (see fig. 3.11). In addition, within CC, responses were distinctly localized to primary auditory regions, although apparent only at the more lenient threshold (fig. 3.15). In contrast, DC participants displayed a much broader pattern of temporal activation, which was not confined to primary/secondary auditory areas but extended across nearly the entire left temporal lobe and substantial portions of the right (figs. 3.11 and 3.16), suggesting hyperexcitability to external perturbations without focused activation. This increased excitability in DC was further evidenced by heightened activity in temporal, precentral, and frontal regions during silence blocks, compared to CC, indicating more unconstrained, unregulated activity - although these activations were only evident at a more liberal threshold.

These findings might align with previous observations of increased stimulus representation in the auditory cortex under sedation compared to wakefulness (Banks et al., 2018) and heightened alpha power, reflecting increased excitability, reported during presumed disconnected states of ketamine anesthesia and REM sleep (Darracq et al., 2018). This paradoxical heightened excitability observed during DC states, as discussed in sec. 1.7, may be explained by increased prediction error signaling due to a mismatch between feedforward and feedback information. It is possible that, as the DC brain generates top-down predictions that do not align with incoming sensory stimuli, the resulting feedforward prediction error continues to propagate to the cortex, failing to trigger correct prediction updates and potentially leading to the greater activation observed (Sanders et al., 2021).

Yet, it could be argued that increases in BOLD activation could reflect inhibitory neuronal populations rather than excitatory ones. Indeed, recent research underscores that the BOLD signal is not solely a marker of excitatory activity; instead, it captures a blend of both excitatory and inhibitory processes (Howarth et al., 2021; Moon et al., 2021). In particular, the activation of inhibitory neurons can lead to a biphasic BOLD response, featuring an initial positive signal followed by a negative phase (Moon et al., 2021). However, it is important to note that excitatory synapses remain the most energy-intensive part of neuronal signaling due to the significant ion fluxes involved in generating excitatory post-synaptic potentials (Howarth et al., 2021). Moreover, during task fMRI, task-related BOLD signal increases are typically observed in brain regions where excitatory activity is expected to be predominant, further supporting the likelihood that, in our experiment, such increases reflect excitatory rather than inhibitory neuronal activity (Howarth et al., 2021).

In summary, the widespread increases observed in DC compared to CC may indicate that auditory conscious perception could rely not only on activating the 'correct' brain areas but also on appropriately inhibiting or suppressing other regions. This balance between excitation and inhibition might play an important role in conscious sensory processing.

3.5.2 Processing of sounds during CC: enhanced surprise to all sounds and reduced habituation compared to wakefulness

As mentioned earlier, when comparing CC and DC states, the precuneus emerged as a key region in CC for the processing of all sounds and appeared

part of a distinct network which emerged at the less stringent threshold. This network encompassed the cingulate and paracingulate gyri, a small cluster in the prefrontal portion of the middle frontal gyrus, the superior frontal gyrus, the middle occipital and hippocampal gyri. As shown in figs. 3.11-3.4.5, this temporo-fronto-parietal network was consistently engaged in CC during the processing of all sounds, being activated during both deviant and standard blocks.

Interestingly, during wakefulness the precuneus was one of the clusters surviving the most stringent threshold in response to deviant blocks and, at a more liberal threshold, appeared nested within a network that resembled the one used during CC to process all sounds (see figs. 3.11 - 3.8). The wakeful state network encompassed nearly all the same regions as the CC network, with a few additional nodes in the parahippocampal gyrus, insula, angular gyri, and inferior frontal gyrus. Although only at the more liberal threshold, when comparing CC to wakefulness in response to all sounds, several regions within this network, such as the precuneus and middle frontal gyrus, exhibited increased activation in CC. This suggests a potential role for the network's in processing all sounds during CC, contrasting with its more selective use for deviant sounds during wakefulness. This possibility is further supported by the observation that, in the wakeful state, many of these regions (e.g., the precuneus, middle frontal gyrus, cingulate gyrus, and hippocampus) were deactivated in response to standard blocks (see fig. 3.8), highlighting how these regions may typically be suppressed during wakefulness when processing standard sounds. A potential interpretation of these findings could involve decreased habituation mechanisms in CC compared to wakefulness, leading CC participants to process standard/all-sounds blocks with increased surprise, hence reusing the network typically employed for deviant perception in awake individuals.

However, this might not necessarily imply that CC participants perceived all sounds as deviants. The fact that the majority of CC participants reported hearing two or more sounds upon awakening and the additional increases in activation observed in response to deviant blocks in CC (see sec. 3.5.3) would seem to suggest otherwise. While awake participants likely rapidly habituate to standard sounds[4] habituation in CC might occur more slowly. Consequently, it is possible that the network continues to be engaged for processing all sounds, not just deviant ones. Potentially supporting this interpretation,

[4]Short-term decreases resulting from habituation can be observed within seconds in the primary auditory cortex of awake individuals (Merchie & Gomot, 2023; Mutschler et al., 2010).

the hippocampus — typically activated during deviant perception to detect mismatches between incoming stimuli and sensory memory traces (Näätänen et al., 2001) — showed greater activation during all-sounds blocks in CC compared to DC at the more lenient threshold. However, this hippocampal increase in CC was not observed in the CC vs. wakefulness comparison, likely due to global suppression in CC caused by sedation[5], which may have resulted in reduced baseline hippocampal activation in CC compared to the awake state. Additionally, the precuneus — another key node in this network, used for processing deviants during wakefulness and all sounds in CC — has been positively correlated with deviant trials (Collier et al., 2014; Justen & Herbert, 2018; Kiehl et al., 2005; Linden et al., 1999), reinforcing the possibility that habituation in CC might be slower than during wakefulness.

3.5.3 Deviant perception in CC but not DC: detection of local irregularities as a sign of sensory connection

A noteworthy finding was that 77% of CC participants reported hearing two or more sounds upon awakening (sec. 3.4.3). These reports may have a potential, corresponding neural correlate in the increased activation observed in CC participants, compared to DC, in response to deviant blocks. Specifically, in the 'deviant-standard' contrast, CC exhibited increased activation in areas which have been implicated in deviant perception, such as the fusiform gyrus, which have been documented to correlate with target detection in both visual and auditory modalities (Baudena et al., 1995; Clark et al., 2000; D. Friedman et al., 2001; Halgren et al., 1995; Wronka et al., 2012). Furthermore, at a more liberal threshold, this region seemed to contribute to a broader network involving parieto-central regions (see fig. 3.12. This network included the SMA, frontal and prefrontal areas, temporal regions, and the right angular gyrus. These additional regions were also engaged during deviant perception in wakefulness (sec. 3.3.2) and have been identified as key regions for processing deviant stimuli (Kiehl et al., 2005; Stevens et al., 2000). Notably, when comparing CC to wakefulness, no significant difference was found in the 'deviant-standard' contrast, potentially suggesting a similar processing of deviant sounds between CC and awake states.

In contrast, DC participants showed minimal differentiation between the processing of standard and deviant blocks, as evidenced by the direct com-

[5] As shown by the decreased activation in CC compared to wakefulness in response to all sounds across regions in the ROI analyses, indicating a general pattern of greater activation to sounds during wakefulness compared to CC (sec. 3.17).

parison of CC and DC, where the difference between these two states was nearly identical in response to both types of blocks. This effect was also reflected in the within-DC results (fig. 3.15), where there was little to no distinction between the processing of standard and deviant blocks. Conversely, within-CC (fig. 3.15), activation was primarily restricted to primary and secondary auditory regions in response to all sounds, whereas a distinct network — resembling the one observed during wakefulness in response to deviant blocks, predominantly involving occipital and temporal regions — appeared to be recruited specifically for deviant stimuli. These results could suggest that DC participants neither detected the deviancy nor, as argued in sec. 3.5.1, processed all sounds as deviants. Rather, it is possible that they did not perceive any sounds, consistent with what they reported upon awakening.

If confirmed, these findings suggest that the detection of local deviance may rely on the conscious perception of standard sounds, positioning the detection of local irregularities as a significant indicator of consciousness. This aligns with recent (re-)interpretations of the meaning of local deviancy detection, which in EEG studies elicits the MMN, as discussed in sec. 1.6. The classic interpretation posits that detection of local irregularities reflects automatic and pre-attentive responses, while the detection of global irregularities is associated with conscious processing (see sec. 1.2). This view was based mostly on observations that the MMN response, but not the P300[6], could be detected during sleep or anesthesia (Fitzgerald & Todd, 2020), states in which participants were assumed to be unconscious. However, as discussed in sec. 1.7 and 1.6, states of CC can occur during these altered states of consciousness. Moreover, the preconscious interpretation of local deviancy detection has been challenged by a growing body of research showing that the MMN response occurs only when participants are conscious of the sounds (Dykstra et al., 2017; Fitzgerald & Todd, 2020; Sussman et al., 2014). For instance, a study by (Dykstra & Gutschalk, 2015) using informational masking and magnetoencephalography found that the MMN was only observed when the preceding regularity (i.e., standard sounds) was consciously perceived. The authors concluded that their results "raise the possibility that [local deviance detection] might index partial awareness in the absence of overt behavior" (Dykstra & Gutschalk, 2015). Consistent with this, studies on comatose patients have found an association between the MMN response and recovery

[6]The P300 response is associated with detection of global irregularities, as discussed in sec. 1.2.

of consciousness. For example, (Fischer et al., 1999) reported that 91% of comatose patients exhibiting the MMN recovered consciousness. Our results, suggesting deviant detection only in CC participants, align with the new interpretation of detection of local irregularities as a marker of conscious perception.

3.5.4 Brain activity during silence blocks: can we draw conclusions on resting activity?

During silence blocks, across all states and comparisons, we observed either no significant results, or few significant clusters which emerged solely under the more liberal threshold. It is important to clarify that in all models, the baseline against which activity during silence blocks was compared was the pooled activation of both all-sounds and silence blocks together. These results indicate that our measures to prevent contamination of oddball paradigm-related activity with background MRI noise were effective. However, due to the baseline used, these findings cannot be interpreted as reflective of the resting-state mental activity of participants, as this would require a different type of analysis.

It is however worthy to note that even during silence blocks, CC participants showed decreased activation primarily in the temporal lobe compared to DC (fig. 3.11) and more widespread decreases in fronto-temporal regions compared to wakefulness (fig. 3.9). The decreased activation in CC compared to DC aligns with the increased inhibition generally observed in CC, which may potentially be explained by a more balanced EIB in CC compared to DC, as speculated in sec. 3.5.1. The reduced activation in CC compared to wakefulness is consistent with the ROI-wise analysis results, which showed overall decreased activation to sounds in CC relative to wakefulness (see sec. 3.17). Awake participants, being alert and unsedated, might still have processed background noise during silence blocks, whereas in CC participants, the increased inhibition may have filtered out these feeble background sounds, preventing them from percolating through the cortex.

In summary, the activity pattern observed during silence blocks supports the overall finding of decreased inhibition in DC compared to CC and the general suppressive effect of propofol sedation on CC.

3.5.5 Increased high-frequency power in DC compared to CC in auditory, somatosensory, and attention networks: a marker of sensory gating?

Spectral analysis revealed no overall reduction or increase in high-frequency BOLD oscillation power between the CC and DC groups. Instead, we observed region-dependent spectral differences between these two conditions. Notably, regions with increased high-frequency oscillation power in DC overlapped with areas that showed increased activation for all sounds vs. silence in the DC vs. CC comparison (sec. 3.4.6). These regions included the bilateral temporal gyri and, at a more lenient threshold, superior precentral gyri, the left occipital middle gyrus and the right supramarginal gyrus, belonging to networks such as the auditory network, the salience/ventral attention, visual network[7], sensorimotor network and dorsal attention network. Conversely, CC participants exhibited increased high-frequency BOLD oscillation power in the bilateral frontal, occipital, right precuneus and precentral/postcentral regions relative to DC, with some of the regions overlapping with the DMN nodes.

To interpret these findings, we must first consider the potential role of BOLD oscillations within this frequency range. Preliminary evidence suggests that high-frequency oscillation power tends to increase from wakefulness to sleep or anesthesia, with these increases becoming more pronounced as sleep or anesthesia deepens (Fukunaga et al., 2006; Guldenmund et al., 2016; Song et al., 2022). For example, (Song et al., 2022) reported a positive correlation (r = 0.5) between SWA and high-frequency BOLD oscillation power in healthy participants during sleep, simultaneously recorded with hd-EEG and fMRI. Additionally, (Guldenmund et al., 2016) found that increases in high-frequency BOLD oscillations within the DMN led to network disruption. Thus, preliminary evidence suggests that high-frequency BOLD oscillation power may reflect increased SWA - which is typically observed during states of unconsciousness or presumed disconnection (Funk et al., 2016; Mhuircheartaigh et al., 2013; Siclari et al., 2018) - and/or may contribute to disruptions in cortical dynamics and network integrity.

In light of these emerging findings, our high-frequency power results could represent a plausible outcome. Indeed, the majority of regions showing increased high-frequency power in DC are involved in sensory processing,

[7]For a discussion of increased high-frequency power in visual networks during DC, see sec. 3.5.6

which are likely to be compromised in a state of disconnection. Notably, we also observed increases in high-frequency power in DC relative to CC within the attention networks. This could imply that attentional resources are involved in sensory connection. Whether attention is necessary for conscious perception remains a topic of ongoing debate (see Scholarpedia entry for 'Attention and Consciousness' for a review), and it is beyond the scope of this experiment to provide a definitive answer. However, a potential approach to investigate this further would be to apply DCM to the present fMRI dataset, exploring effective connectivity differences within attention and sensory networks between CC and DC states. This could shed light on the role, if any, that attention plays in sensory perception.

The increased high-frequency BOLD power observed in CC compared to DC within certain nodes of the DMN could similarly be interpreted as evidence that these oscillations contribute to disruptions in cortical dynamics within this "intrinsic" network. It is possible that CC participants, having heard the sounds, were less focused on inward, self-referential processes (Fox et al., 2005). This interpretation echoes the findings of (Vanhaudenhuyse et al., 2011), which showed a significant anticorrelation between internal and external awareness, with specific DMN nodes relating to internal awareness and lateral fronto-parietal cortices correlating with external awareness.

However, to date, the functional significance of high BOLD oscillations remains largely speculative and relatively unexplored. Future studies combining simultaneous EEG and fMRI with sensory stimulation could clarify the specific cortical dynamics reflected or caused by these BOLD oscillations. Should these findings be corroborated by future research, high-frequency BOLD oscillations could potentially be developed into a reliable measure for anesthesia monitoring, with significant implications for clinical practice.

3.5.6 Which gating hypothesis align with our findings?

Which of the gating hypotheses discussed in sec. 1.6-1.7 best aligns with the findings of the present study? The hypothesis proposed by (Sanders et al., 2021), which suggests that feedforward prediction error propagation in DC leads to increased neural excitability, appears to be the most consistent with our results, as discussed in sec. 3.5.1. In addition, while still highly speculative, our spectral findings may lend some support to the cortical gating hypothesis. However, the mechanisms behind this gating may involve not only increases in SWA but also disruptions in EIB, potentially impeding

information propagation to higher cortical areas due to disrupted functional connectivity resulting from heightened excitability.

Direct support from our findings for the informational gating hypothesis proposed by (Andrillon & Kouider, 2020; Nir & Tononi, 2010) does not appear to be evident. One might argue that the widespread activation increases observed in DC relative to CC reflected higher dreaming activity in DC rather than increased excitability. However, this explanation is difficult to reconcile with the fact that there was almost no activation in DC during silence blocks. If DC participants were intensely dreaming, it is unlikely that this would occur only during sound presentation. Even though, as discussed in sec. 3.5.4, activity during silence blocks was computed against a baseline that included both task and silence blocks, if DC participants were more engaged in dreaming than CC participants, we would still expect to see increased activation during both silence and task blocks, without a drop to almost no significant activations during silence blocks. Our spectral findings also do not seem to align with the predictions of the informational gating hypothesis — although, as previously mentioned, strong conclusions should not be drawn from these results. If DC participants had been disconnected due to an overflow of top-down information over bottom-up, we would have expected to find increased high-frequency power in DC only in sensory or attention-related regions. Instead, some of the regions showing the highest increases were located within visual network. If DC participants were highly absorbed in dreaming activity, which is predominantly visual (Nir & Tononi, 2010), we would have expected to find decreased high-frequency power in these regions compared to CC.

These findings raise the intriguing question of whether sensory connection and the overall state of consciousness are tightly linked. It is possible that individuals deeply engaged in hallucinatory experiences during dreaming, which requires significant cortical resources, may also be more connected to their environment. In such a scenario, more organized cortical dynamics could position the brain in a state more akin to normal functioning, making it better able and more receptive to perceiving sounds. To explicitly test the information gating hypothesis, future studies should include more detailed questioning about mental activity prior to awakening. For example, a briefer version of the Tellegen Absorption Scale (Tellegen & Atkinson, 1974), which assesses imaginative involvement, could be adapted for use immediately upon awakening. Mental absorption could then be compared between CC and DC groups. Additionally, decoding models trained on stimulus-induced

brain activity in visual cortical areas could be applied to identify dreaming content and compare it between CC and DC states. However, as this experiment demonstrated (see sec. 3.4.2), upon awakening from propofol confabulation and contradictory reports are frequent. Extending the number of questions asked upon awakening could increase this trend, leading to higher rates of discarded data due to conflicting answers. Moreover, significantly lengthening the questioning period — thus increasing the time since awakening — may heighten the likelihood of amnesic effects, with participants forgetting the experience they had while unresponsive. Therefore, while additional questions could provide greater detail on participants' experiences, a careful balance must be struck between gathering richer reports and minimizing the potential for increased amnesic effects or confabulation due to extended time from awakening.

3.5.7 Criticality of CC and DC states: is sensory disconnection a super-critical state?

An intriguing hypothesis, which warrants further investigation, is that both CC and DC represent primary states of consciousness, with CC leaning towards sub-criticality and DC towards super-criticality. This interpretation stems from the entropic brain hypothesis proposed by R. Carhart-Harris in 2014 (Carhart-Harris et al., 2014), inspired by their work on psychedelics. This theory posits that the entropy of spontaneous brain activity indexes the informational richness of conscious states. According to this theory, the quality of any conscious state depends on the system's entropy, defined as the degree of uncertainty or randomness/disorder within the brain's dynamics. Based on entropic levels, two modes of consciousness are identified: primary and secondary consciousness.

Primary consciousness, associated with higher entropy, is characterized by more fluid, unconstrained (sometimes bizarre) mental states, reflecting a regressive style of cognition with significantly diminished metacognition. Examples of primary consciousness include psychedelic states, sleep dreaming and sedation. In contrast, secondary consciousness, linked with lower entropy, is more structured and ordered, typical of normal waking states.

The concept of criticality explains the brain's optimal functioning state, existing between order and chaos. Within this critical zone, a narrow range where the brain's activity is neither too stable (sub-critical) nor too unstable (super-critical), the brain is most responsive and adaptable, processing infor-

mation efficiently and responding to various stimuli in a flexible and effective manner. Wakefulness is positioned within this critical zone (or 'criticality proper') in the center of a spectrum ranging from high-entropic, flexible states (e.g., super-criticality, as seen in psychedelic states or infant consciousness or dreaming) to low-entropic, rigid states (e.g., coma, depression, or obsessive-compulsive disorder). According to the entropic brain hypothesis, conscious states can vary along this entropy spectrum in a continuous way. Of note, high-entropic states are posited to be hypersensitive to perturbations, aligning with their phenomenology.

We therefore propose that both DC and CC are primary states of consciousness, as participants in both conditions are in a dream-like state, with regressed metacognition and cognition. However, as CC participants seemed to display more consistent and organized brain activity, likely had lower entropy levels than DC, which enabled them to perceive external stimuli. Conversely, DC's neurodynamics appeared to be characterized by heightened excitability, which may align with the hypersensitivity to perturbations associated with high-entropic states. To test this hypothesis - i.e., if awake, CC and DC states are ordered from sub-critical to super-critical - entropy measures could be calculated, as done in psychedelic studies reviewed in (Carhart-Harris, 2018). Specifically, a resting-state analysis on silence blocks could quantify the deviation of voxels from the mean signal, assessing signal variation within canonical networks.

3.5.8 Limitations

In this study, the differentiation between CC and DC groups was based on subjective reports. As discussed in sections 2.5.5 and 1.2, the limitations of introspection, and thus of subjective reports in verifying the state of consciousness, have been widely discussed (Irvine, 2012; Tsuchiya et al., 2015). The question of which measure best captures awareness remains open. Nonetheless, our experimental design did not allow for the use of objective measures, as participants were sedated and expected to remain unresponsive during auditory stimulation, making task performance unfeasible.

The collection of subjective reports during propofol sedation may raise the concern that amnesic effects led participants to forget the experiences they had during the unresponsive period, potentially biasing their reports. While the absence of dream report upon awakening does not necessarily imply unconsciousness or disconnection (Windt et al., 2016), collecting retrospective

reports remains the only way to access participants' subjective experience during unresponsive periods such as sleep or sedation. Moreover, amnesic effects on subjective reports are significantly reduced the closer they are collected to the experience under investigation. Indeed, compared to post-anesthesia collection of reports, the serial awakening paradigm has been shown to minimize the lack of explicit recall, as participants are awakened and questioned about their experience immediately before regaining responsiveness (Siclari et al., 2013, 2017).

As discussed in section 3.5.5, this study would have greatly benefited from the simultaneous acquisition of EEG, which was unfortunately not feasible due to logistical and financial constraints. The EEG signal could have provided valuable insights into the interpretation of BOLD frequency oscillations by analyzing correlations with well-known EEG phenomena, such as SWA, spindles, and activity in different bands. EEG would have also offered a more adaptable method to identify (and exclude) data containing brief arousals. In the present study, potential arousals during fMRI acquisitions were ruled out by continuously monitoring participants via an eye-tracking camera. If eye opening was detected, acquisitions were interrupted and restarted once the participants had spontaneously fallen unresponsive again.

Finally, another limitation of the present study pertains to its generalizability to alternative sensory modalities and different anesthetic agents. Our study explored sensory disconnection induced by the anesthetic agent propofol within the auditory modality. The extent to which our findings can be extended to other sensory modalities and anesthetics remains unknown. Future studies incorporating a range of anesthetics and sensory modalities will be necessary to validate and extend the applicability of these findings.

3.6 Supplementary Information

3.6.1 Efficiency analysis. Optimising the oddball paradigm to detect standard and deviant events

With the following analyses, we sought to maximize the efficiency of the auditory paradigm. Estimation of the efficiency can be defined as "a measure of the reliability with which model parameters are estimated" (Mechelli et al., 2003). The efficiency of a design strongly "affects the sensitivity with which experimental effects are detected" (Mechelli et al., 2003). In order to find the (a priori) most efficient design to detect our effects of interest, we manipulated the temporal distribution of events, resulting in several designs whose efficiency was estimated a priori and then compared.

The variables manipulated were the length of the silence blocks (i.e., randomized in 1-sec steps in intervals of 7–20 sec, 7–10 sec, 15–20 sec, 10–15 sec), the ordering of standard and deviant blocks (i.e., interleaved order or pseudorandomized order in which no more than two identical types of blocks can follow one another), the type of oddball paradigm. We selected four different types of oddball paradigms for comparing their efficiency, of which only one was chosen for the experiment. In the 'classic oddball' paradigm (Squires et al., 1975), trials consist of four standard sounds and one deviant, where the deviant is defined by a change in frequency. The 'roving oddball' (Garrido et al., 2007) differs with each trial presenting sounds of the same frequency and starting a new trial with a different frequency, making the first event of a trial a deviant. We also designed two 'mixed oddballs', in which trials follow the 'classic oddball' rule but with the difference that the number of repetitions of standard events is randomized, between three and five ('Mixed Oddball35') or between three and seven repetitions of standards ('Mixed Oddball37').

The efficiency analysis was conducted by comparing all possible combinations of parameters (i.e., inter-stimulus interval, inter-trial interval, stimulus and block duration) for the different oddball paradigm designs. The efficiency calculation is related to the number of scans (i.e., to a given TR and duration of experiment), and specific to a given contrast. We calculated the efficiency for TR=0.842 sec, 900 sec duration of the experiment and for the following three contrasts: main effect of the standard response, main effect of the deviant response and the difference between standard and deviant responses. For more information on how we computed efficiency, see our

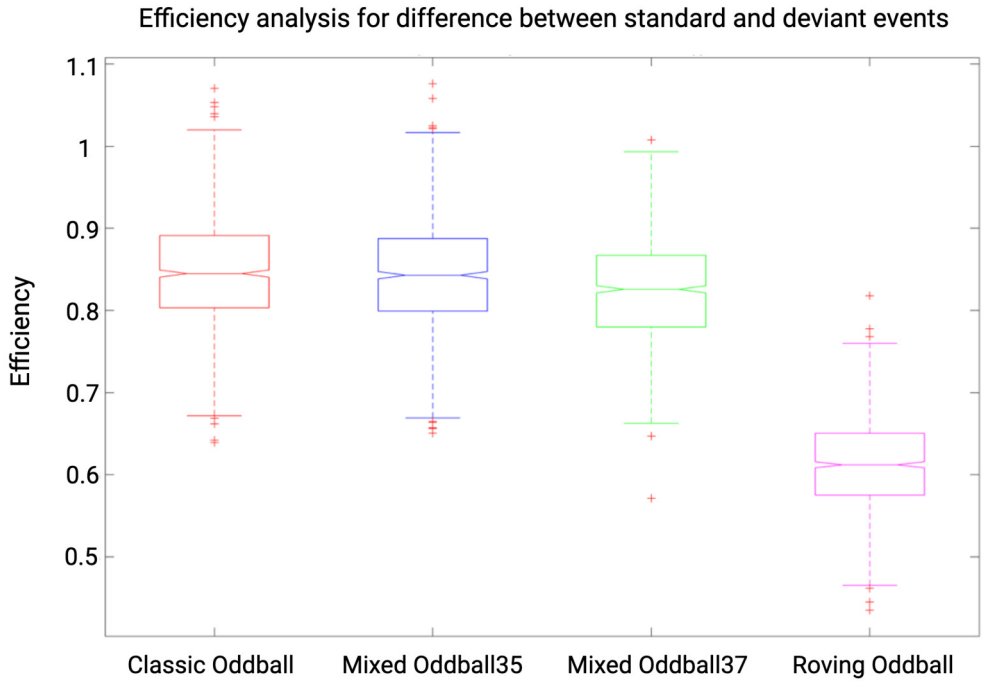

Figure 3.14: Efficiency results for four auditory oddballs. Results shown are for contrast standard-deviant, TR = 0.842 sec and for an experiment duration of 900 sec (i.e., 1,125 scans). Efficiency values are reported for 'Classic oddball', 'Mixed Oddball35', 'Mixed Oddball37', and 'Roving oddball' with silence blocks of duration 7-10 sec and in pseudorandomized order (ABBA). Whiskers corresponds to approximately +/-2.7σ and 99.3 percent coverage. We selected the 'Mixed Oddball35' for its combination of high efficiency and the reduction of expectation achieved through the randomization of standard sounds.

repository on GitHub 'Efficiency-Analysis-fMRI-mixed-design', where each step of the analysis is detailed: https://doi.org/10.5281/zenodo.8117861.

In addition to the efficiency analysis, we also performed a collinearity analysis in SPM12 to estimate the extent to which our two events (standard and deviant) were collinear (i.e., whether their responses correlated with each other) — see our GitHub repository for more details on how to compute collinearity in SPM. The design that was most efficient and with least collinearity was the 'Mixed Oddball35' with 7–10 sec silence blocks and pseudorandomized order (mean efficiency for the difference between standard and deviant events = 0.843). As depicted in fig. 3.14, 'Mixed Oddball35' was found to have comparable efficiency with the 'Classic oddball' (mean

efficiency for the difference between standard and deviant events = 0.845). We chose the 'Mixed Oddball35' for the experiment as randomizing the number of repetitions of the standard sounds has the advantage of decreasing expectation.

3.6.2 Within-CC and within-DC: temporal activation in DC and widespread suppression in CC in response to all sounds, but widespread activation to deviant sounds observed only in CC

In what follow, I will present activation results within CC and DC conditions in response to all-sounds versus silence blocks, as well as deviant versus standard blocks. It is important to note that comparisons between the two groups should not be drawn from these within-state results, due to different intercepts for each model. Comparisons results between the two states will be described in section 3.4.5 where both groups were modeled together using a common baseline, allowing for valid inferences on between-group differences.

At the most conservative threshold (z-threshold of ±3.29, $p<0.001$), in response to all auditory stimuli vs silence, both CC and DC participants displayed pre-central deactivations, which extended to occipital, parietal, temporal, and frontal regions at more lenient threshold (z-threshold of ±1.96, $p<0.05$) (see figs. 3.15 and 3.16, top panels). In CC, the most extensive negative cluster encompassed nearly the entire parieto-frontal region of the brain, comprising 13098 voxels, and in DC, the largest negative cluster, including similar regions, consisted of 1260 voxels (fig. 3.15, top panel) - both at the z-threshold of ±3.29, $p<0.001$. In line with the CC vs DC findings (sec. 3.4.5, at the more lenient threshold, DC participants showed diffuse activations in the bilateral inferior and middle temporal gyri as well as the right superior temporal gyrus, with a dominance in the left hemisphere (fig. 3.16, top panel). These activations were markedly reduced in the CC group. CC participants exhibited only minimal activations in these temporal regions, with small clusters located in the bilateral inferior and middle temporal gyri and the right superior temporal gyrus (z-threshold of ±1.96, $p<0.05$). Additional activations in the CC group were observed in the bilateral parahippocampal gyrus, rolandic operculum, and postcentral gyrus (z-threshold of ±1.96, $p<0.05$).

Interestingly, in response to deviant vs standard sounds the inverse pattern emerged (see figs. 3.15 and 3.16, bottom panels), although only at the less stringent threshold: CC participants exhibited widespread activations

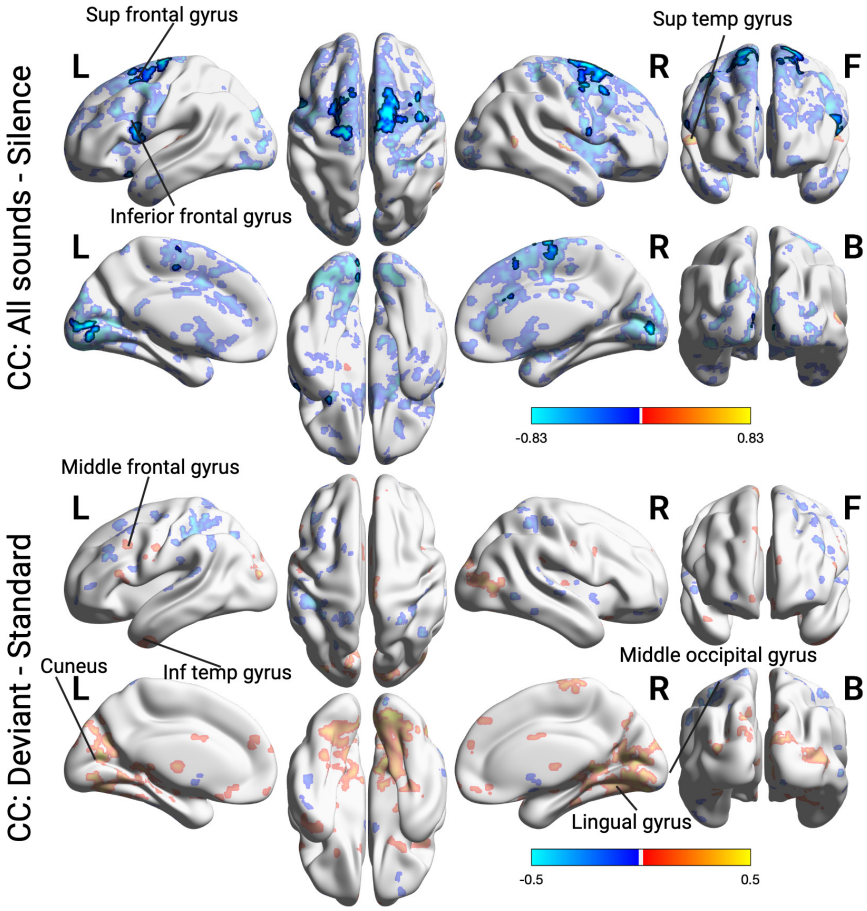

Figure 3.15: Activation differences within CC in response to sounds vs silence and deviants vs standards. Voxel-wise effect size maps, thresholded by z-scores, of voxel-wise activation differences in response to all-sounds-combined vs silence blocks (**top panel**) and in response to deviant vs standard blocks (**bottom panel**). Results are cluster-corrected (k = 16 for top panel and k = 15 for bottom panel) with a cluster-defining threshold of p<0.001. Clusters are visualized at a z-statistic threshold of ±1.96 for transparent clusters and ±3.29 for outlined clusters, following a highlight-but-not-hide approach to present results at both conservative and less stringent thresholds. L = left, R = right, F = front, B = bottom views. Inf = inferior; Sup = superior; Temp = temporal.

predominantly distributed in occipital and temporal regions, while DC participants showed few significant clusters and mostly negative - 14 positive and 33 negative clusters in DC versus 58 positive and 33 negative clusters in CC (z-threshold of ±1.96, p<0.05). In particular, CC participants showed positive

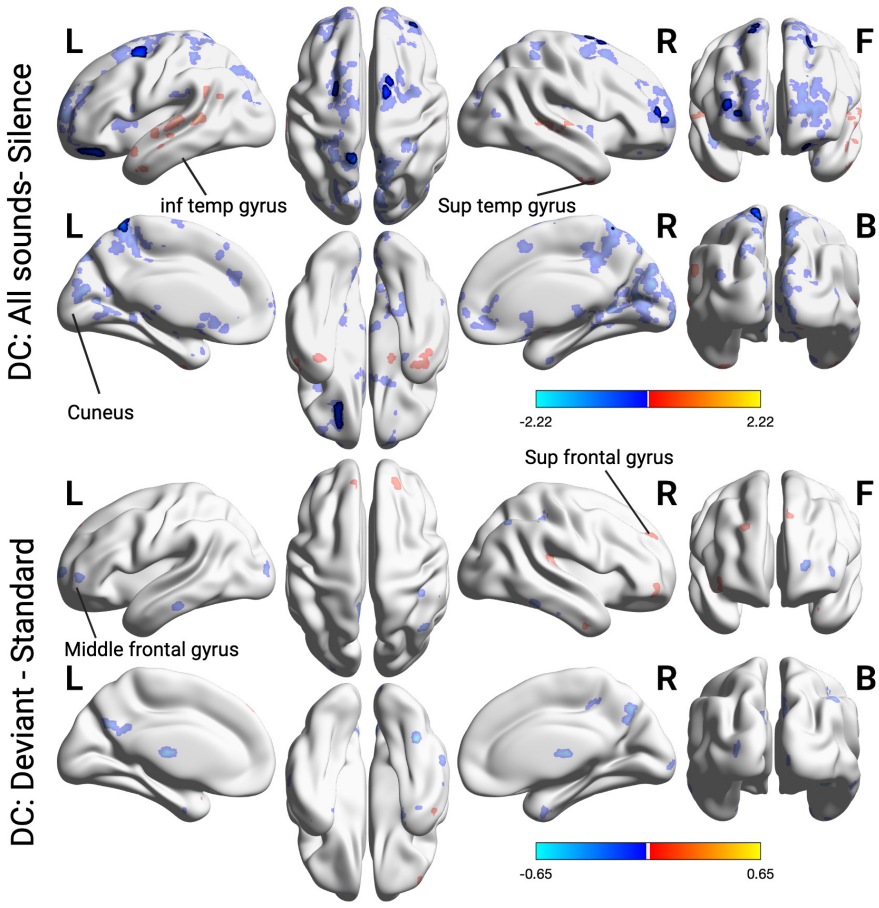

Figure 3.16: Activation differences within DC in response to sounds vs silence and deviants vs standards. Voxel-wise effect size maps, thresholded by z-scores, of voxel-wise activation differences in response to all-sounds-combined vs silence blocks (**top panel**) and in response to deviant vs standard blocks (**bottom panel**). Results are cluster-corrected (k = 16 for top panel and k = 15 for bottom panel) with a cluster-defining threshold of p<0.001. Clusters are visualized at a z-statistic threshold of ±1.96 for transparent clusters and ±3.29 for outlined clusters, following a highlight-but-not-hide approach to present results at both conservative and less stringent thresholds. L = left, R = right, F = front, B = bottom views. Inf = inferior; Sup = superior; Temp = temporal.

clusters in temporo-occipital regions at the level of the right fusiform gyrus, left cuneus, bilateral middle occipital gyrus, left superior occipital gyrus, and bilateral superior and inferior temporal gyri (z-threshold of ±1.96, p<0.05). Additional clusters in CC were observed in parieto-central and frontal regions

(z-threshold of ±1.96, $p<0.05$). Parieto-central activations included the right paracentral lobule, left precentral gyrus, and right postcentral gyrus, with deactivations in the bilateral superior parietal gyrus and left inferior parietal gyrus (z-threshold of ±1.96, $p<0.05$). Frontal activations were observed in the right middle and orbital frontal gyrus (near the midline) while deactivations occured in the left middle and bilateral orbital frontal gyrus (further from the midline) - (z-threshold of ±1.96, $p<0.05$). The bilateral superior frontal gyrus was primarily deactivated, showing only a few positive clusters in its medial portion (z-threshold of ±1.96, $p<0.05$). Similarly, the bilateral inferior frontal gyrus mostly included negative clusters, except for some positive in its orbital and opercolar parts (z-threshold of ±1.96, $p<0.05$). Finally, additional frontal activations were observed in the right medial frontal gyrus (z-threshold of ±1.96, $p<0.05$) - see fig. 3.15, bottom panel.

In DC participants, the few significant positive clusters were located in the left cuneus, bilateral superior temporal gyri, right superior frontal gyrus, and the triangular part of the right inferior frontal gyrus (z-threshold of ±1.96, $p<0.05$). Deactivations were observed in the left middle occipital gyrus, bilateral inferior temporal gyri, left parahippocampal gyrus, right fusiform gyrus, bilateral precuneus, right inferior parietal gyrus, and the left middle and superior frontal gyri as well as the right middle frontal gyrus (z-threshold of ±1.96, $p<0.05$) - see fig. 3.16, bottom panel.

3.6.3 Voxel-wise analyses - Cluster tables

Cluster results for contrasts CC-Awake all sound/silence blocks

Volume	CM_RL	CM_AP	CM_IS	minRL	maxRL	minAP	maxAP	minIS	maxIS	Mean	SEM	Max_Int	MI_RL	MI_AP	MI_IS
18177	-0.7	3.2	23.9	-70	68	-68	64	-50	78	-1.4923	0.0055	-7.4234	62	20	10
4166	1	73.1	4.4	-42	38	20	104	-40	42	-2.1291	0.0139	-5.9747	0	90	4
859	30.6	68.8	44.8	2	56	54	88	8	68	-2.3735	0.038	-7.08	30	70	52
398	-50.2	66.2	27.9	-60	-36	50	84	14	44	-1.7457	0.024	-3.0849	-56	66	22
345	-14.1	-51.6	35.8	-32	-4	-64	-32	26	50	-1.4138	0.0341	-3.4792	-4	-58	32
208	-5.2	52.4	-52.7	-16	6	44	64	-60	-44	1.106	0.0275	2.148	-8	50	-54
180	19	80.8	-29.9	8	32	64	88	-42	-22	0.9903	0.025	1.9975	12	84	-24
155	-38.8	64.7	-34	-48	-30	56	76	-44	-22	-1.0453	0.0314	-2.8017	-46	70	-22
140	46.7	-43.4	-2.9	30	54	-62	-30	-10	10	-1.2454	0.0303	-2.3674	46	-50	-4
105	-20.1	47.6	-20	-28	-12	36	58	-28	-12	0.9732	0.0291	1.9071	-22	56	-14
101	-14.7	69.1	56.4	-28	-2	64	74	48	64	-2.9113	0.0792	-5.1002	-2	66	52
95	-15.4	68.2	38.3	-22	-10	58	80	28	44	2.0716	0.046	3.0045	-16	68	36
93	21	28	64	12	38	22	34	50	78	-1.398	0.0629	-3.7532	14	28	76
91	-46.8	-33.1	32.5	-52	-40	-40	-24	18	42	1.1948	0.0413	2.1746	-48	-28	40
85	-22.4	-59.4	-10.6	-36	-8	-64	-54	-22	0	0.8788	0.036	1.8151	-28	-60	-8
82	-46.4	51.3	-30.1	-58	-34	44	62	-36	-26	0.8817	0.0273	1.6942	-52	48	-26
82	28.5	33.4	-2.1	22	36	26	40	-10	10	0.9024	0.0252	1.5073	36	36	-8
81	14.3	-17.9	5.4	6	22	-22	-14	-8	14	-0.8092	0.0243	-1.2357	14	-18	8
79	12.3	78.3	-47.4	4	20	72	84	-54	-42	-1.0299	0.0314	-1.7299	18	78	-50
76	-29.3	81.4	-41.7	-38	-22	72	86	-46	-32	0.8872	0.0268	1.468	-30	84	-38
76	-48.5	67.5	-38.9	-54	-40	56	78	-44	-32	-0.8639	0.0346	-1.8833	-52	60	-42
75	-21.9	70	-25	-26	-20	56	80	-30	-20	0.8828	0.0353	1.9371	-22	76	-20
74	-27	49.6	-49.2	-36	-20	42	56	-52	-46	0.8624	0.0251	1.3875	-28	52	-48
71	13.4	43.8	-53.6	6	24	36	50	-62	-44	1.1089	0.0427	2.0321	10	46	-60
71	31.8	-27.4	3.9	26	40	-32	-22	0	8	-0.9414	0.0328	-1.5932	32	-26	4
68	22.7	-35	-14.9	18	32	-40	-28	-22	-8	0.8577	0.0319	1.4753	22	-38	-14
67	9.2	67.8	40.5	6	14	58	74	28	52	1.9124	0.0709	3.1344	8	72	40
64	-61.4	50.4	-15.5	-66	-56	42	62	-24	-10	-1.1319	0.0537	-2.2589	-58	58	-20
63	-11.2	76.3	-23.9	-16	-4	70	82	-32	-18	1.0236	0.0404	2.0684	-12	80	-18
62	-50.7	73.4	2.4	-56	-44	68	78	-8	12	1.5501	0.0635	2.6464	-48	74	8

Table 3.7: All Sounds CC-Awake Part 1. Cluster results for the contrast 'all sounds CC-Awake'. Nvoxel = Number of voxels in the cluster; CM RL = Center of mass (CM) for the cluster in the Right-Left direction; CM AP = Center of mass (CM) for the cluster in the Anterior-Posterior direction; CM IS = Center of mass (CM) for the cluster in the Inferior-Superior direction; minRL, maxRL = Bounding box coordinates for the cluster in the Right-Left direction (minimum and maximum); minAP, maxAP = Bounding box coordinates for the cluster in the Anterior-Posterior direction (minimum and maximum); minIS, maxIS = Bounding box coordinates for the cluster in the Inferior-Superior direction (minimum and maximum); Mean = Mean value for the volume cluster; SEM = Standard Error of the Mean for the volume cluster; Max Int = Maximum Intensity value for the volume cluster; MI RL = Coordinate of the Maximum Intensity value in the Right-Left direction; MI AP = Coordinate of the Maximum Intensity value in the Anterior-Posterior direction; MI IS = Coordinate of the Maximum Intensity value in the Inferior-Superior direction.

Volume	CM_RL	CM_AP	CM_IS	minRL	maxRL	minAP	maxAP	minIS	maxIS	Mean	SEM	Max_Int	MI_RL	MI_AP	MI_IS
62	-57	35	50.1	-62	-54	30	40	46	56	1.9715	0.0627	2.9195	-56	34	52
61	-42.2	44.9	-42.9	-48	-36	38	58	-56	-36	-0.6302	0.0361	-1.6119	-46	46	-46
61	-10.4	78.9	-45.6	-14	-4	72	86	-52	-38	-0.9332	0.0346	-1.5707	-10	78	-48
61	-14.6	-21.3	4	-20	-10	-26	-14	-2	12	-0.9154	0.0449	-1.9454	-12	-22	4
60	-23.7	66.6	-56.3	-30	-16	62	70	-60	-52	-0.9878	0.0357	-1.6114	-28	66	-60
59	25.1	10	-17.7	20	30	4	20	-24	-10	-1.1898	0.0648	-2.4874	28	8	-22
58	41.9	61	-52.2	36	48	48	68	-60	-46	0.696	0.0283	1.2144	36	62	-60
57	21.9	-62.2	-8.4	18	26	-66	-58	-16	-2	-1.1627	0.039	-1.7221	20	-64	-10
52	35.1	-39.8	20.4	30	40	-44	-36	16	26	1.1058	0.0379	1.8687	36	-38	22
50	-37	77.6	-29.1	-42	-34	70	82	-32	-26	1.326	0.0613	2.3135	-38	78	-28
50	39.8	-32.8	-14.7	36	44	-42	-26	-20	-10	-0.919	0.0305	-1.3285	40	-32	-14
45	25	-52.1	4.5	20	32	-60	-48	0	10	-0.8269	0.0226	-1.1346	26	-50	4
43	-41.3	62.4	14.9	-46	-38	54	70	6	20	-1.456	0.0354	-1.8223	-42	64	16
43	-17.2	-10.7	15.2	-20	-12	-16	-2	10	20	-0.9389	0.0253	-1.3146	-20	-14	14
42	46.5	57.5	-30.7	40	50	50	64	-38	-26	0.8428	0.0283	1.2425	50	52	-30
42	-42	51.6	40	-48	-34	44	56	36	46	1.2804	0.0496	2.0626	-40	50	40
41	44.4	64	-8.5	42	48	60	68	-14	-4	1.2837	0.0459	1.8008	44	64	-6
35	-40.9	-47.6	-5.1	-44	-38	-54	-40	-10	0	1.0208	0.0386	1.5249	-40	-48	-6
35	-34.1	74.1	-50.5	-42	-26	72	78	-54	-44	-1.0582	0.0582	-1.8505	-36	74	-54
34	33.1	3.4	1.6	30	36	-6	12	-2	6	-0.6114	0.0137	-0.8119	34	8	2
33	47	78.8	13.9	44	54	72	84	10	22	-1.2634	0.0507	-1.831	46	80	12
32	34.3	-4.1	-20.9	26	42	-8	2	-24	-18	1.1551	0.0662	2.1449	36	-6	-20
32	-33.1	-49.2	5.8	-40	-28	-52	-44	-2	14	0.7859	0.0189	0.9725	-34	-52	6
32	41.3	43.5	-39.1	36	48	38	50	-46	-36	-0.7308	0.0525	-1.1848	38	42	-36
31	49.6	52.7	22.4	40	54	48	56	18	30	1.1691	0.0625	1.7943	52	54	24
31	-36.5	-10.4	39	-40	-32	-12	-6	32	42	0.827	0.0325	1.1853	-36	-10	40
31	28.2	24.6	-28.6	22	36	18	28	-32	-24	-0.6639	0.0391	-1.3297	26	26	-30
31	-21.8	25.6	-25.3	-26	-18	18	32	-28	-18	-1.0532	0.0383	-1.664	-18	20	-26
30	-39.7	-49.4	17.2	-44	-36	-52	-46	14	20	1.0517	0.0501	1.6269	-42	-50	18
29	-30.9	-45.1	21.2	-34	-28	-48	-40	18	26	1.0969	0.0434	1.5404	-30	-46	22
28	-29.8	36	-33.9	-38	-24	32	40	-38	-30	0.7685	0.066	1.8136	-26	36	-38
27	32.7	-20.2	-37	26	38	-22	-14	-44	-32	0.8508	0.0674	1.6026	32	-20	-38
27	-30.1	-49.5	-13.2	-34	-28	-54	-46	-18	-10	0.9078	0.0362	1.2692	-30	-50	-14
27	1.9	96.7	-7.2	0	4	92	100	-16	-2	3.591	0.2252	6.2136	2	96	-6
27	5.7	68	-37.6	4	8	64	72	-40	-32	-0.78	0.042	-1.2484	6	68	-38
27	29.9	86.4	3.7	24	34	82	92	0	10	-1.5566	0.0539	-2.0308	32	84	4
26	-5.7	28.4	7.2	-12	-2	24	32	2	14	1.4214	0.1094	2.9077	-4	32	4
26	8.6	30.3	9.1	2	14	28	32	6	12	0.9092	0.043	1.3612	8	30	12
26	-10.7	52.7	42.9	-14	-8	46	56	40	48	1.0145	0.0376	1.4283	-8	56	44
26	-48.7	56.3	-17.9	-54	-42	52	60	-22	-14	-1.4837	0.0605	-2.0381	-50	58	-18
25	14.3	-54.4	-17.6	6	18	-56	-52	-22	-14	0.5981	0.0283	0.8774	16	-54	-16
25	15.6	6.9	10.9	12	18	4	10	6	16	0.7274	0.0258	1.0125	16	8	14
24	34	46.9	-50.9	30	38	40	52	-54	-48	0.6942	0.0488	1.1015	32	42	-52
24	29.5	35.4	-34.9	24	34	30	38	-40	-30	0.7417	0.0548	1.3158	26	36	-38
24	-20.2	9.4	-29.1	-24	-16	6	16	-34	-26	-0.6233	0.0392	-0.9264	-22	6	-28
24	-0.5	83.2	27.7	-4	4	80	86	26	30	-3.58	0.142	-4.7067	-2	86	28
23	31.5	-15.7	-8.3	26	36	-20	-14	-12	-6	-0.5948	0.0197	-0.7672	34	-16	-10
23	22.9	85.3	25.3	20	28	84	88	20	28	-1.8304	0.0897	-2.586	24	86	28
22	-35.5	32	-24	-38	-32	28	38	-30	-20	0.9996	0.048	1.4843	-36	32	-24
22	29.7	-51.6	-10.8	26	34	-56	-48	-14	-8	0.6216	0.0259	1.0249	28	-56	-8
21	12.8	56.2	-47.9	8	18	50	60	-52	-40	0.6719	0.0245	0.8623	14	54	-50
21	-15.8	72.4	-48.7	-20	-12	70	74	-50	-46	0.8278	0.0361	1.1273	-16	72	-50
21	-10.5	-3.6	3.5	-16	-6	-6	-2	0	8	-0.9516	0.0589	-1.3445	-6	-2	2
21	8.2	90.7	32.7	2	18	88	94	28	38	-2.5749	0.1388	-3.4573	10	92	32
20	-41.7	-12.3	-21.8	-44	-40	-16	-10	-26	-20	1.3145	0.1036	2.2712	-42	-12	-20
20	16.8	63.2	-56.7	14	20	60	66	-60	-54	-1.0274	0.0544	-1.4488	16	62	-58
20	-44.7	83.1	-13.1	-48	-38	80	88	-20	-8	-1.6202	0.0865	-2.1713	-46	82	-14
20	28.5	52.3	-12	24	32	50	54	-18	-8	-1.06	0.0364	-1.2632	28	52	-18
20	23.1	39.4	-16.1	20	26	36	42	-18	-14	-1.0679	0.0585	-1.5925	24	40	-16
20	51.9	74.8	-4.2	48	54	70	78	-12	2	-1.1523	0.0745	-1.6367	52	76	-6
20	-53.2	52.1	49.4	-56	-50	48	54	46	52	-1.7116	0.0712	-2.3849	-52	52	50

Table 3.8: All Sounds CC-Awake Part 2.

Volume	CM_RL	CM_AP	CM_IS	minRL	maxRL	minAP	maxAP	minIS	maxIS	Mean	SEM	Max_Int	MI_RL	MI_AP	MI_IS
247	43.6	-11.2	22.8	32	58	-26	-2	6	32	-0.9869	0.0162	-1.8469	40	-20	22
96	57.7	51.2	-6.5	50	64	42	60	-18	10	-1.0347	0.0229	-1.5974	62	50	-8
96	7.5	79.6	2.8	0	12	72	90	-4	8	-1.7563	0.0456	-2.7814	12	82	4
86	28.6	-23.8	47.4	20	36	-28	-18	40	56	-1.1356	0.0313	-1.8911	28	-24	46
84	-7.4	7.7	69.7	-14	-2	-4	18	56	76	-1.3416	0.0509	-2.4967	-6	4	74
78	57.5	9.8	-16.4	50	64	2	14	-24	-12	-0.9105	0.0237	-1.3825	60	10	-16
73	-8	-44.3	5.8	-14	-2	-48	-40	2	10	-0.7389	0.0137	-0.988	-6	-46	6
57	51.1	6.7	46.1	48	54	-2	12	40	56	-1.0449	0.0223	-1.5214	48	8	56
54	31.9	10.1	62.5	24	40	6	12	50	68	-0.8706	0.0242	-1.2453	40	10	64
46	63.5	24	-0.8	58	68	12	32	-4	2	-1.002	0.0368	-1.531	64	28	-2
42	3.2	9.4	62.9	2	8	4	14	54	70	-0.9715	0.0388	-1.5056	2	12	62
38	-56.5	0.8	28.8	-60	-48	-6	4	24	38	-0.9989	0.0204	-1.3069	-58	0	24
36	-7	49.8	-54.7	-10	-2	46	54	-58	-52	0.8474	0.0226	1.0758	-8	48	-54
29	25.2	-6.3	53.2	22	28	-8	-4	48	58	-0.7464	0.0197	-1.0202	28	-4	58
27	46.1	-8.5	-28.5	42	50	-12	-4	-34	-24	-0.5944	0.0154	-0.7254	46	-10	-30
27	-30.6	13.6	-15.3	-36	-24	10	18	-18	-12	-0.7936	0.0292	-1.136	-36	14	-16
27	-19.5	-50.4	31.5	-24	-16	-54	-44	30	34	-0.6236	0.0258	-0.9529	-18	-54	34
25	28.2	77	40	24	32	72	80	36	46	-1.6859	0.0738	-2.3842	28	78	46
23	-7	99.4	-3.2	-12	-4	96	102	-8	2	-2.1218	0.115	-3.3885	-4	98	-2
22	11.9	43	37.5	10	14	40	46	34	42	-0.9043	0.0366	-1.1667	12	44	36

Table 3.9: Silence CC-Awake

Volume	CM_RL	CM_AP	CM_IS	minRL	maxRL	minAP	maxAP	minIS	maxIS	Mean	SEM	Max_Int	MI_RL	MI_AP	MI_IS
436	55.9	20.8	7.2	34	68	6	38	-4	16	-2.2067	0.0408	-5.6211	62	22	10
218	-60.1	12.5	5.3	-70	-44	4	28	-2	10	-2.6295	0.0575	-4.8572	-58	10	4
20	-3.6	14.9	60.4	-6	-2	12	18	54	66	-1.5726	0.1026	-2.629	-2	16	60

Table 3.10: All sounds-Silence CC-Awake

Cluster results for contrasts CC-Awake deviant/standard blocks

Volume	CM_RL	CM_AP	CM_IS	minRL	maxRL	minAP	maxAP	minIS	maxIS	Mean	SEM	Max_Int	MI_RL	MI_AP	MI_IS
4228	-46.7	2.9	10.1	-70	20	-66	44	-42	70	-0.8615	0.0069	-3.3768	-58	8	4
3370	52.5	12.8	15.8	32	68	-26	56	-26	58	-0.9352	0.0066	-3.8162	62	22	10
2955	1.5	70.1	6.3	-32	38	20	104	-22	42	-1.2163	0.0089	-2.9965	0	90	4
2385	-12.1	-3.9	53.5	-48	12	-66	34	0	78	-0.8852	0.0086	-3.1492	-6	0	74
368	24.3	-26.8	49.4	6	36	-38	-14	32	64	-0.8211	0.0139	-1.8464	28	-32	52
343	27.2	74.5	46.6	8	44	62	88	24	66	-1.5595	0.0384	-3.953	30	70	52
238	-16.1	-51.2	36.2	-30	-6	-62	-32	28	50	-0.7931	0.021	-1.7132	-10	-62	32
213	43.4	-9.1	-35.3	30	52	-22	2	-46	-26	-0.4583	0.0089	-0.898	46	-18	-32
209	29.4	-6.7	55.2	20	44	-16	2	42	64	-0.725	0.0124	-1.4203	40	0	60
191	9.6	-49	41.3	2	22	-58	-38	28	52	-0.9215	0.0187	-1.6939	2	-48	44
189	-50	66.3	28.8	-60	-36	56	84	16	44	-0.963	0.0188	-1.6393	-56	66	22
181	58.3	53.3	-12.6	50	66	42	64	-22	-2	-0.8412	0.0202	-1.5937	56	60	-20
141	24.9	10.6	64.7	10	36	2	16	50	76	-0.6712	0.0212	-1.8672	16	14	76
139	42.6	59.9	44.9	36	48	54	64	22	58	-1.1294	0.0301	-2.221	42	60	54
95	-4.7	50.7	-52.9	-12	6	46	54	-60	-44	0.6295	0.018	1.0528	2	52	-50
92	16.4	-59.8	22.8	10	24	-66	-54	16	32	-0.733	0.0186	-1.285	14	-64	22
89	-30	-6.8	-38.5	-40	-24	-22	8	-50	-28	-0.2855	0.0159	-1.0257	-28	-8	-28
86	-14.6	69.2	56.3	-28	-2	64	74	48	62	-1.6886	0.0513	-2.9449	-2	66	52
85	-37.8	64.2	-34.2	-44	-32	58	68	-44	-24	-0.5824	0.0146	-0.9354	-40	64	-26
63	-51.7	73.2	0.2	-56	-46	68	78	-8	12	0.9922	0.0375	1.6718	-52	74	-4

Table 3.11: See next page

Table 3.11: Deviant CC-Awake Part 1. Cluster results for the contrast 'deviant CC-Awake'. Nvoxel = Number of voxels in the cluster; CM RL = Center of mass (CM) for the cluster in the Right-Left direction; CM AP = Center of mass (CM) for the cluster in the Anterior-Posterior direction; CM IS = Center of mass (CM) for the cluster in the Inferior-Superior direction; minRL, maxRL = Bounding box coordinates for the cluster in the Right-Left direction (minimum and maximum); minAP, maxAP = Bounding box coordinates for the cluster in the Anterior-Posterior direction (minimum and maximum); minIS, maxIS = Bounding box coordinates for the cluster in the Inferior-Superior direction (minimum and maximum); Mean = Mean value for the volume cluster; SEM = Standard Error of the Mean for the volume cluster; Max Int = Maximum Intensity value for the volume cluster; MI RL = Coordinate of the Maximum Intensity value in the Right-Left direction; MI AP = Coordinate of the Maximum Intensity value in the Anterior-Posterior direction; MI IS = Coordinate of the Maximum Intensity value in the Inferior-Superior direction.

Volume	CM_RL	CM_AP	CM_IS	minRL	maxRL	minAP	maxAP	minIS	maxIS	Mean	SEM	Max_Int	MI_RL	MI_AP	MI_IS
58	32	-27.8	3.8	26	40	-32	-22	2	8	-0.5313	0.0174	-0.7908	32	-26	4
53	-9.3	77.8	-44.8	-14	-4	72	84	-50	-38	-0.5325	0.0163	-0.7847	-10	78	-48
50	-57	34.8	50.4	-62	-54	30	40	46	56	1.1226	0.0385	1.6083	-56	34	52
50	21.5	-62.4	-8	18	26	-64	-58	-18	-2	-0.6881	0.024	-0.9478	22	-64	-8
48	-23	-61.6	11.4	-32	-14	-66	-56	8	14	-0.5275	0.0149	-0.7965	-28	-62	12
46	-49.3	66.3	-39.2	-52	-40	56	78	-44	-32	-0.4997	0.0207	-0.9466	-52	60	-42
46	3.9	-25.4	34.8	2	10	-34	-20	28	42	-0.5885	0.0238	-1.023	2	-22	32
42	-42.5	51.1	-30.7	-50	-34	44	58	-36	-26	0.4899	0.0106	0.6871	-46	50	-32
42	25.2	89.2	-24.3	16	36	84	98	-26	-18	-1.3762	0.0626	-2.1227	30	88	-24
42	14.1	-18.2	6.9	8	18	-22	-14	2	12	-0.4534	0.0156	-0.6399	14	-18	6
39	24.1	79.4	-30.3	20	30	76	84	-34	-28	0.4759	0.0192	0.7075	24	80	-30
36	44.4	63.7	-8.9	42	48	60	68	-12	-4	0.7691	0.0265	1.0598	46	66	-10
36	-34.9	37.5	60.8	-40	-26	34	42	56	64	-1.1996	0.0703	-1.91	-36	36	62
34	7	-66.7	1.3	4	14	-68	-64	-8	10	-0.8819	0.0303	-1.26	6	-68	4
33	-23.8	66.2	-54	-28	-16	64	68	-56	-52	-0.5478	0.0215	-0.8591	-24	66	-54
33	2.7	-10.5	64.1	2	6	-14	-6	56	70	-1.2668	0.0832	-2.5211	2	-12	68
31	35	-39.5	20.3	30	38	-44	-36	16	24	0.5847	0.0199	0.8449	36	-38	22
31	56.5	44.1	1.5	48	60	38	48	0	4	-0.8438	0.0346	-1.2138	58	44	2
31	28.6	-43.3	34.1	26	32	-48	-40	30	36	-0.6995	0.0308	-1.044	30	-42	34
30	39.6	-56.2	-4	30	46	-62	-48	-10	0	-0.7894	0.0411	-1.2684	34	-62	-2
30	52	-34.5	-0.9	48	54	-38	-32	-8	8	-0.6756	0.0266	-1.0688	54	-32	6
30	-13.7	-20.7	4.6	-18	-10	-24	-16	2	8	-0.5779	0.038	-1.0368	-12	-22	4
29	-27.5	83.5	-43.5	-32	-22	80	86	-46	-38	0.5279	0.0215	0.7797	-26	82	-46
29	-37.3	78.1	-29.4	-40	-34	72	82	-32	-28	0.7694	0.0379	1.1706	-38	78	-28
29	23.5	14.6	-13.7	20	28	10	18	-18	-12	-0.601	0.0275	-0.9238	22	12	-12
28	-17.6	-11.7	14.4	-20	-12	-16	-4	10	18	-0.5259	0.0143	-0.6712	-20	-14	14
27	5.7	67.8	-37.6	4	8	64	72	-40	-32	-0.4687	0.0214	-0.6963	6	68	-38
27	26	-50.3	4.1	24	32	-54	-48	2	10	-0.4143	0.0143	-0.5492	26	-50	4
26	22.5	-36.5	-13.1	18	26	-40	-32	-16	-10	0.55	0.0308	0.7982	22	-38	-14
26	-11.4	90.3	-34	-16	-6	88	92	-38	-28	-0.5865	0.0221	-0.8508	-10	90	-34
25	-61.7	47.7	-14	-64	-60	44	52	-20	-10	-0.7009	0.0309	-0.9428	-64	50	-12
24	12	44.3	-54.5	8	16	42	48	-62	-48	0.6855	0.028	0.9756	10	46	-60
24	-30.2	50	-48	-36	-26	44	56	-50	-46	0.475	0.0235	0.6939	-28	52	-48
24	-44.3	-32.5	38.3	-48	-42	-36	-26	34	42	0.8001	0.0358	1.1223	-44	-32	40
24	-32.4	74.8	-49.2	-42	-26	72	78	-54	-44	-0.5551	0.0246	-0.8545	-36	74	-52
24	39.5	-32.3	-14	38	42	-36	-28	-18	-12	-0.5238	0.0158	-0.6545	40	-32	-12
24	41.9	-49	15.3	36	46	-52	-46	10	22	-0.8708	0.0425	-1.3168	46	-48	10
24	43.7	66	16.2	38	48	60	72	14	18	-0.6387	0.0287	-0.9135	46	68	16

Table 3.12: Deviant CC-Awake Part 2.

Volume	CM_RL	CM_AP	CM_IS	minRL	maxRL	minAP	maxAP	minIS	maxIS	Mean	SEM	Max_Int	MI_RL	MI_AP	MI_IS
23	-53.3	51.8	50	-58	-50	48	54	46	54	-1.0158	0.0407	-1.3999	-52	52	50
22	-23.4	39.6	-26.3	-28	-18	38	42	-28	-24	0.4916	0.0242	0.6762	-20	40	-26
21	61.8	38.6	-22.1	60	66	30	44	-24	-20	0.3274	0.0255	0.5399	62	44	-22
21	-41.8	13.1	-8.2	-44	-38	6	18	-16	-4	-0.5841	0.0317	-0.8313	-40	16	-4
20	14.6	85	-31.7	12	18	84	86	-34	-28	0.6714	0.0293	0.8889	14	86	-32
20	-41	-46.3	-4.6	-44	-38	-50	-40	-8	-2	0.5883	0.0227	0.7952	-40	-48	-6

Table 3.13: Deviant CC-Awake Part 3.

Volume	CM_RL	CM_AP	CM_IS	minRL	maxRL	minAP	maxAP	minIS	maxIS	Mean	SEM	Max_Int	MI_RL	MI_AP	MI_IS
3726	17.1	-3.2	48.5	-42	66	-42	28	0	78	-0.849	0.0056	-3.2363	-4	0	72
2987	-52.1	12.7	17.4	-70	-18	-28	48	-26	72	-0.9528	0.0078	-2.9347	-66	12	8
2164	55.7	28.2	5.2	24	68	-8	64	-26	28	-0.988	0.0091	-3.6518	62	20	10
1471	2.9	75.4	5.4	-26	26	34	104	-22	42	-1.2733	0.0121	-3.2278	-4	98	-2
311	-7.2	-35.5	17.9	-14	-2	-54	-16	0	40	-0.6299	0.0086	-1.0768	-2	-22	32
232	10.4	-52.6	35.9	2	22	-64	-42	16	50	-0.848	0.0164	-1.8281	6	-56	40
219	-10.5	50.5	-52	-36	6	44	62	-60	-44	0.613	0.0133	1.1785	-8	50	-54
216	42.7	60.4	39	36	50	54	72	10	60	-1.0956	0.0252	-2.1636	40	60	52
195	-49.8	67.6	28	-60	-42	54	84	16	36	-0.9983	0.016	-1.4532	-56	66	22
192	-13.4	-53.6	34.3	-28	-4	-62	-40	28	40	-0.7819	0.0232	-1.815	-4	-58	32
149	32	76.9	38.9	22	50	66	84	26	46	-1.2194	0.0293	-2.1608	28	78	46
118	16.7	68.5	58	2	32	54	76	44	68	-1.9399	0.0563	-3.4307	30	70	52
108	16.6	82.9	-30.1	6	30	74	88	-36	-24	0.6077	0.0207	1.0373	14	86	-32
108	-15.2	68	38.2	-22	-10	58	80	28	44	1.3271	0.0272	1.9432	-16	68	36
95	46.6	-7	-34	42	50	-14	0	-46	-24	-0.4479	0.0094	-0.6538	48	-2	-30
87	-51.3	-7.9	-31.8	-62	-44	-18	8	-40	-26	-0.5009	0.0141	-0.8379	-48	-16	-26
84	-7.8	-57.6	-11.5	-20	-4	-66	-44	-18	-6	-0.5583	0.0143	-0.8281	-6	-58	-10
79	-32.2	0.2	-44.4	-44	-26	-12	14	-50	-38	-0.2568	0.0096	-0.4681	-30	4	-44
78	29.2	33.8	-4.2	22	36	26	38	-10	10	0.5286	0.0162	0.9053	36	36	-8
78	-37.2	64	-37.2	-44	-32	56	68	-42	-30	-0.5552	0.0162	-0.8931	-38	66	-40
70	8.8	-40.5	14.3	4	12	-46	-36	8	20	-0.4963	0.0085	-0.6286	4	-38	18
67	-47.2	-33.2	31.6	-52	-42	-40	-26	16	42	0.6956	0.0224	1.1536	-48	-28	40
65	13.8	43.3	-52.9	6	24	36	50	-62	-44	0.6512	0.023	1.0822	10	46	-60
61	-19.5	28.5	-0.6	-26	-14	22	34	-6	6	-0.4919	0.0153	-0.7198	-18	30	0
58	8.9	68.5	39.4	6	14	58	74	30	48	1.1833	0.0448	1.9031	8	72	40
50	13.7	-17.8	7.1	8	18	-22	-14	2	14	-0.4861	0.014	-0.6962	14	-16	8
49	4.6	-49.5	-6.5	2	8	-56	-42	-10	-2	-0.8128	0.0336	-1.3785	2	-50	-6
49	31	-27.1	4.1	26	36	-32	-22	0	8	-0.5011	0.0213	-0.8363	32	-26	4
46	21.6	-35.5	-15.6	16	26	-40	-30	-22	-10	0.4709	0.0174	0.7066	22	-38	-14
44	4.9	-25.9	34.4	2	10	-34	-22	28	42	-0.5414	0.0202	-0.971	2	-22	32
43	-11.5	76.2	-24.9	-16	-4	70	80	-30	-18	0.6	0.0228	1.0507	-12	80	-18
42	-23.4	66.8	-56.6	-28	-16	64	70	-60	-52	-0.5468	0.0256	-0.8769	-26	70	-58
40	34.7	-39.7	20.6	30	38	-44	-36	16	24	0.6527	0.0239	1.0604	36	-38	22
39	-6	-13.7	50.8	-10	-4	-18	-10	44	56	-0.6805	0.033	-1.2688	-4	-12	52
37	-42.4	44.9	-43.2	-48	-36	38	58	-52	-36	-0.3596	0.027	-0.8332	-46	46	-46
37	-62.2	48.7	-15	-66	-60	44	58	-20	-12	-0.6636	0.0376	-1.0477	-64	50	-12
37	50.7	-35.9	-3.6	42	54	-44	-32	-6	0	-0.6239	0.0203	-0.8211	50	-44	-4
36	-56.2	-9.3	-13.9	-60	-52	-16	-6	-22	-8	-0.9711	0.0469	-1.6106	-58	-8	-12
35	-19.2	-9.8	-20.3	-22	-14	-14	-6	-24	-14	-0.7664	0.0418	-1.2908	-20	-8	-22
35	25.5	-54.8	27	20	34	-58	-52	22	32	-0.7947	0.0372	-1.3291	28	-54	28
34	29.9	-6.5	-39.8	22	36	-12	2	-44	-36	-0.2706	0.0167	-0.5095	32	-10	-40
33	-41.1	50.9	40.2	-48	-34	44	56	36	44	0.8232	0.0349	1.2921	-40	50	40
33	39.6	-32.7	-15.1	38	42	-38	-28	-20	-12	-0.5314	0.0154	-0.7035	40	-34	-16
33	41.3	-52.9	-6	32	46	-62	-44	-10	-2	-0.6845	0.0413	-1.1702	46	-50	-6
33	-14.2	-21.6	3.2	-18	-10	-26	-16	-2	6	-0.5597	0.0341	-0.9793	-12	-22	4
32	-56.9	35.5	50	-60	-54	32	40	46	54	1.0034	0.0408	1.3875	-58	34	50
32	25.5	-51	3.9	22	32	-56	-48	2	10	-0.4629	0.0144	-0.6083	24	-52	4
32	-31.5	14.7	70.2	-38	-22	10	20	66	74	-1.1444	0.0734	-1.8619	-30	20	70
31	-21.2	63.9	-24.8	-24	-20	58	72	-28	-20	0.4716	0.0132	0.6227	-22	68	-22
30	-4.1	-21.9	-13.7	-6	2	-26	-18	-20	-10	-0.4001	0.0096	-0.5612	0	-24	-10
29	-21.5	77.5	-27.7	-24	-18	76	80	-32	-22	0.5058	0.0232	0.9565	-22	76	-22
29	-19.3	52.7	-16.5	-22	-16	46	56	-24	-14	0.6062	0.0357	1.0384	-22	56	-14
29	-36.3	-10.9	38.6	-40	-32	-12	-8	30	42	0.5074	0.0185	0.6503	-36	-10	40
28	45.7	58.5	-29.8	40	50	54	64	-32	-26	0.5305	0.0183	0.7227	50	54	-32
28	8.1	30.7	8.7	2	14	28	34	6	12	0.6015	0.0274	0.9395	4	34	6
27	-11.3	79.7	-47.2	-14	-8	76	84	-50	-44	-0.5922	0.0242	-0.8714	-10	78	-50

Table 3.14: Standard CC-Awake Part 1.

Volume	CM_RL	CM_AP	CM_IS	minRL	maxRL	minAP	maxAP	minIS	maxIS	Mean	SEM	Max_Int	MI_RL	MI_AP	MI_IS
27	-60	18.7	-26.3	-64	-56	16	22	-30	-24	-0.3641	0.0235	-0.5718	-60	18	-26
27	51.8	74.6	-4.9	48	54	70	78	-12	2	-0.7233	0.0414	-1.0499	52	76	-6
26	-14.4	-59.8	-11.9	-20	-10	-62	-56	-20	-2	0.4641	0.021	0.6981	-16	-58	-10
26	-18	-11.3	15	-20	-12	-16	-2	10	18	-0.5061	0.0164	-0.673	-20	-14	14
25	21.3	94.2	-13.1	14	32	90	98	-14	-10	-1.0343	0.0491	-1.437	18	94	-14
24	-37	77.7	-29.1	-40	-34	74	82	-32	-28	0.8277	0.0426	1.1933	-38	78	-28
24	-37.7	-22.6	-31	-44	-30	-24	-18	-36	-26	-0.5785	0.0387	-0.8863	-42	-24	-28
23	14.3	-54.6	-17.3	8	18	-56	-52	-22	-14	0.3807	0.0155	0.532	16	-54	-16
23	-28.6	-59.5	-8.9	-34	-24	-60	-58	-12	-6	0.6584	0.0343	1.0249	-28	-60	-8
23	-5.2	-37.3	49.6	-8	-4	-42	-30	46	54	-0.7243	0.0358	-1.088	-4	-40	48
21	-4.1	63.2	-51.4	-8	-2	62	66	-56	-48	0.6456	0.0273	0.9488	-2	62	-56
21	-39.8	-49.4	16.3	-42	-36	-52	-46	14	18	0.6296	0.0329	0.923	-42	-50	18
21	-45	75.3	-36.2	-50	-40	72	78	-42	-32	-0.4707	0.0125	-0.574	-42	76	-36
21	40.9	-8.5	51.7	36	44	-10	-6	50	56	-0.8106	0.0334	-1.0946	42	-8	52
20	-33	31	-23.4	-36	-24	28	34	-26	-22	0.5775	0.029	0.8263	-36	32	-24
20	-41.4	-12.7	-22.1	-44	-40	-16	-10	-26	-20	0.7597	0.0516	1.1902	-42	-12	-20
20	-30.2	-44.5	20.5	-32	-28	-48	-40	18	24	0.6042	0.0271	0.8144	-30	-46	20

Table 3.15: Standard CC-Awake Part 2.

Cluster results for contrasts CC-DC all sound/silence blocks

Volume	CM_RL	CM_AP	CM_IS	minRL	maxRL	minAP	maxAP	minIS	maxIS	Mean	SEM	Max_Int	MI_RL	MI_AP	MI_IS
2981	54.9	34.8	-1	22	68	-22	90	-50	30	-1.4082	0.014	-6.8213	58	64	14
874	-25.1	-1	-7.1	-40	-2	-26	34	-26	14	-1.1304	0.0157	-2.7981	-28	-2	-12
786	-51.4	-0.1	-23	-70	-26	-26	20	-48	8	-0.902	0.0145	-2.8274	-58	-2	-16
774	-47.8	-3.1	32.1	-66	-20	-40	30	8	72	-1.4165	0.0177	-3.4732	-48	-14	30
545	-10.6	50.3	57.5	-30	-2	28	66	32	76	1.8377	0.0502	9.8657	-8	60	68
475	-34.6	-6.4	55.3	-52	-16	-18	16	38	70	-1.3199	0.0267	-4.0122	-34	-8	64
469	44.3	-14.2	25.3	32	60	-28	0	4	42	-1.403	0.0234	-5.3679	52	-20	36
468	34.9	53.3	-18.8	12	54	28	74	-38	-2	-1.2682	0.0213	-3.1051	48	64	-24
451	-2.8	4.1	50.3	-14	12	-16	24	32	74	-1.2049	0.0192	-2.8995	-8	12	74
432	-59.8	36.1	2.2	-70	-44	20	56	-12	18	-1.9432	0.0267	-4.0045	-66	46	8
403	-26.4	56.3	-47.7	-48	-8	32	84	-60	-32	0.7972	0.0119	1.6212	-24	58	-46
339	40.1	57.6	-48.5	24	54	44	78	-62	-30	0.8067	0.0123	1.5097	30	60	-58
301	16.6	49.7	66.2	2	36	32	62	42	78	2.0006	0.0532	5.1994	6	56	70
279	-48.8	44.6	49.8	-62	-34	28	70	40	58	-1.9314	0.0382	-3.9461	-54	34	56
254	-23.9	54.7	-21.2	-40	-8	38	74	-38	-10	0.8791	0.0189	2.3534	-36	66	-20
205	-44.8	67.5	-31.3	-56	-28	52	84	-40	-24	1.1865	0.0325	2.6264	-48	64	-30
197	29.2	-57.8	1.9	20	40	-66	-46	-16	12	0.8987	0.0251	2.241	28	-62	6
191	-1.5	-18.3	-17.1	-14	12	-28	-10	-26	-8	-0.5784	0.0162	-1.1777	0	-22	-12
181	-52.5	57.9	-15.1	-66	-44	44	76	-24	-6	-1.8474	0.0598	-4.495	-54	58	-20
170	30.9	30.7	-7.9	18	40	18	48	-18	10	0.941	0.0254	1.9597	34	36	-8
167	46.2	11.1	38.3	34	58	0	22	28	50	-1.2913	0.0223	-2.0918	40	14	36
158	-5.4	74.7	-29.9	-28	12	66	88	-44	-20	0.8084	0.0158	1.6456	-12	84	-30
122	-30.2	-58.2	9.7	-42	-20	-68	-46	2	20	0.9823	0.0328	2.218	-24	-66	6
113	38.5	62.6	53	28	50	54	72	46	64	-2.654	0.089	-4.9193	34	68	54
94	11	-10.6	8.3	6	18	-22	4	4	14	-0.8746	0.0248	-1.4912	10	0	12
89	23.3	-37.3	-19.2	18	30	-52	-30	-22	-14	0.7535	0.0242	1.277	26	-44	-18
82	35.5	46.6	40.7	26	44	38	56	36	46	-1.0986	0.0271	-1.7889	36	42	44
81	-12.2	-33.2	55.4	-20	-4	-40	-28	48	60	-1.1502	0.038	-2.2622	-6	-34	56
77	44.9	0.4	48.3	36	50	-4	6	42	56	-1.2552	0.0482	-2.5361	48	2	56
75	29.7	67.3	-31.4	20	42	64	74	-38	-28	0.7108	0.0189	1.1077	38	66	-34
74	-46.1	72.4	36.6	-58	-38	62	82	30	44	-1.4687	0.0352	-2.3938	-46	74	34
73	-4.3	50.9	-52.6	-14	6	44	54	-60	-44	0.9382	0.0269	1.5385	0	52	-48
72	-40.6	86.9	-10.8	-48	-32	80	96	-18	2	-1.8612	0.0626	-3.2659	-40	88	-12
71	22.8	84.5	26.9	14	28	78	92	20	36	-1.8905	0.07	-3.4866	22	88	32
70	4.8	9.8	52.1	2	8	2	14	46	58	-1.0092	0.03	-1.6233	2	12	54
69	0.3	90.9	3.3	-10	12	86	96	-2	8	-2.5272	0.1219	-4.712	-2	90	0
65	-17.5	-11.8	13.8	-20	-14	-20	-4	6	20	-0.8721	0.0218	-1.2597	-18	-14	14
62	43.3	59	31.7	38	52	52	64	22	40	-1.4628	0.0445	-2.0153	40	60	32
61	-7.2	-44.1	-7.6	-12	-2	-50	-36	-14	-2	0.6132	0.0201	1.0287	-8	-46	-4
61	-6.2	-6.4	62.4	-8	-4	-14	-2	52	70	-1.0432	0.0438	-2.106	-8	-10	70
60	36.1	-2.8	-13	28	44	-12	4	-20	-6	1.0542	0.0383	2.0545	44	0	-12

Table 3.16: See next page.

Table 3.16: All sounds CC-DC- Part 1. Cluster results for the contrast 'all sounds CC-DC'. Nvoxel = Number of voxels in the cluster; CM RL = Center of mass (CM) for the cluster in the Right-Left direction; CM AP = Center of mass (CM) for the cluster in the Anterior-Posterior direction; CM IS = Center of mass (CM) for the cluster in the Inferior-Superior direction; minRL, maxRL = Bounding box coordinates for the cluster in the Right-Left direction (minimum and maximum); minAP, maxAP = Bounding box coordinates for the cluster in the Anterior-Posterior direction (minimum and maximum); minIS, maxIS = Bounding box coordinates for the cluster in the Inferior-Superior direction (minimum and maximum); Mean = Mean value for the volume cluster; SEM = Standard Error of the Mean for the volume cluster; Max Int = Maximum Intensity value for the volume cluster; MI RL = Coordinate of the Maximum Intensity value in the Right-Left direction; MI AP = Coordinate of the Maximum Intensity value in the Anterior-Posterior direction; MI IS = Coordinate of the Maximum Intensity value in the Inferior-Superior direction.

Volume	CM_RL	CM_AP	CM_IS	minRL	maxRL	minAP	maxAP	minIS	maxIS	Mean	SEM	Max_Int	MI_RL	MI_AP	MI_IS
59	40	84.1	-14.2	34	46	78	92	-20	-6	-1.7246	0.0762	-3.0781	36	84	-14
57	-21	51.9	1.4	-30	-12	44	60	-4	6	1.5451	0.0439	2.2441	-28	58	2
56	-20.2	39.9	-27.5	-30	-10	34	44	-30	-26	0.783	0.0313	1.399	-14	40	-28
56	55	21.6	31.4	50	62	18	26	22	38	0.91	0.0229	1.3644	54	24	32
55	-33.6	31.6	-15.4	-38	-28	26	40	-22	-8	0.8531	0.025	1.3028	-32	34	-18
55	46.4	71.7	37.9	40	52	62	76	30	48	-2.3694	0.0855	-3.8689	44	72	40
53	10.9	62.3	-48.7	6	16	54	68	-56	-44	0.7235	0.0174	1.0464	8	64	-52
52	20.6	11.4	69	14	26	8	14	62	74	-1.0758	0.0391	-1.7124	20	10	72
51	-41.5	83.9	13.3	-46	-36	80	88	10	18	-1.1727	0.0342	-1.7237	-40	86	14
51	-15.4	10.5	19.2	-22	-4	4	16	12	22	-1.0848	0.0469	-1.8589	-18	10	22
50	-10.4	-1.6	5.4	-16	-4	-6	4	-4	10	-1.0488	0.0469	-1.7169	-12	0	8
49	-44.9	2	-11.5	-50	-42	-6	10	-22	-4	1.1961	0.0471	1.8505	-44	0	-14
49	-49.2	72.7	9.1	-52	-44	68	78	6	16	1.3076	0.0443	2.0591	-50	74	8
49	46.6	6.7	9.5	38	56	2	10	6	14	0.8867	0.0246	1.2609	44	8	10
48	42.8	-35.9	15.4	38	46	-40	-30	8	20	-0.8206	0.0338	-1.5255	44	-40	20
46	2.5	53.5	-7.1	-4	8	48	58	-14	-2	0.8007	0.0332	1.5081	-4	54	-4
46	-8.8	57.2	-47.6	-12	-4	46	66	-56	-42	-0.8224	0.0317	-1.5088	-10	62	-42
46	-24.4	21.1	10.4	-34	-18	14	26	2	18	-0.9262	0.0428	-1.6499	-28	18	4
43	8	-57.2	-1.4	2	14	-64	-52	-10	4	0.8076	0.0259	1.1912	4	-56	0
43	25.3	-41.2	26.2	20	30	-46	-38	22	32	0.6899	0.0203	1.012	24	-38	24
42	-46.2	43.9	-19.6	-58	-40	40	46	-28	-12	-0.9281	0.0292	-1.2891	-54	44	-26
41	18.9	43.5	-52.9	14	24	40	48	-58	-48	0.7811	0.0251	1.1025	24	44	-56
40	21.6	0.1	-33.5	14	30	-8	6	-38	-28	0.4232	0.0284	1.1203	28	-6	-32
40	-5.8	-61.4	-0.9	-10	-4	-68	-54	-4	4	0.8374	0.036	1.371	-4	-60	2
40	3.1	4.7	1.5	-4	14	2	8	-4	4	-0.8695	0.0451	-1.4791	4	4	2
39	13.6	86.5	-16.9	8	24	80	92	-28	-10	-2.1055	0.0937	-3.6028	10	86	-12
38	-21.3	64.8	22.7	-26	-16	54	74	20	26	1.1568	0.0395	1.662	-18	72	22
38	-4.9	-55.6	-13.6	-6	-4	-62	-48	-18	-10	-0.6001	0.0216	-0.9231	-4	-60	-12
36	-63.8	36.7	-21.6	-68	-58	30	42	-26	-18	0.7059	0.0483	1.4948	-64	38	-20
36	7	-35.2	27.9	4	12	-40	-30	24	32	0.7099	0.0252	1.0117	6	-36	28
36	7.7	76.2	-44.3	2	12	72	82	-54	-36	-0.9102	0.0507	-1.8868	2	82	-36
36	37.3	26.9	14.9	30	46	22	30	10	20	-1.1806	0.0412	-1.6034	42	24	14
35	1.6	98.1	-5.5	-4	8	92	102	-14	4	3.125	0.1879	5.1268	2	96	-6
35	16.4	8.3	-17.9	14	20	-4	16	-22	-14	-1.1839	0.0632	-1.9726	16	14	-22
34	-44.1	14.2	17.6	-50	-40	10	16	12	22	1.0036	0.0366	1.5176	-42	14	22

Table 3.17: All sounds CC-DC- Part 2.

Volume	CM_RL	CM_AP	CM_IS	minRL	maxRL	minAP	maxAP	minIS	maxIS	Mean	SEM	Max_Int	MI_RL	MI_AP	MI_IS
32	40.7	80.6	23.9	36	52	74	88	22	26	1.0849	0.0457	1.5364	40	80	24
32	-19.2	6.8	-32	-22	-16	-2	14	-38	-28	-0.5354	0.0437	-1.0531	-20	10	-34
32	24	-8.6	48.1	20	30	-16	-2	44	52	-0.7019	0.0215	-1.0762	22	-14	44
31	13.2	31.4	9.1	8	20	28	36	2	12	0.8406	0.0342	1.207	8	30	12
31	-10.3	-50.2	5.7	-12	-8	-54	-44	2	10	-0.7614	0.0259	-1.1254	-10	-52	4
30	-29.2	-44.4	21.9	-32	-28	-48	-38	18	28	0.7326	0.0192	0.9299	-30	-46	22
29	36.7	11.8	-2.2	34	40	8	18	-10	4	0.9603	0.0357	1.4323	36	14	-2
29	-46.2	-31.9	-14.9	-52	-42	-36	-26	-18	-10	-0.9037	0.0349	-1.2581	-46	-34	-18
28	-20.7	87.2	-28.4	-24	-18	82	92	-36	-24	1.204	0.0848	2.0476	-20	88	-24
28	6.4	31.6	48.7	2	12	28	34	42	54	0.9754	0.0326	1.3025	4	32	52
28	11.4	11.9	14	8	14	6	18	12	16	-0.8357	0.0328	-1.3579	10	10	14
27	8.3	86.5	-33.8	4	16	80	90	-38	-30	1.0238	0.0633	1.828	6	86	-36
27	-25	66.9	-55.3	-28	-20	64	70	-58	-54	-0.7751	0.0521	-1.4544	-26	68	-56
27	0	75.1	42.4	-4	4	72	80	38	46	-3.5628	0.1127	-4.4809	-4	74	40
26	58.3	47.8	-23.6	56	62	40	56	-26	-20	0.8322	0.0574	1.8348	56	56	-24
26	8.9	-35.7	-11.1	6	12	-46	-24	-14	-8	0.4678	0.0196	0.6423	10	-42	-10
26	12.7	64.4	54.5	8	22	62	68	50	58	1.5667	0.0662	2.2747	20	64	56
25	24.9	62.6	-52.6	22	26	58	68	-58	-48	-0.6361	0.0233	-0.9068	26	68	-58
25	-34.6	48.8	-21.4	-38	-30	46	52	-24	-16	-0.9826	0.0494	-1.5905	-34	48	-22
25	-15.2	64.5	-4.4	-20	-12	62	66	-8	0	-1.3439	0.0533	-1.821	-12	64	-6
24	-38.5	10.8	-2.4	-42	-36	8	16	-6	2	0.7892	0.0374	1.2407	-42	16	0
24	-7.7	77.2	-42.1	-14	-4	76	80	-48	-36	-0.8014	0.0268	-1.1671	-4	76	-38
24	4.4	59.7	6.2	2	8	56	62	0	10	-1.855	0.0946	-2.6151	4	58	6
23	9.4	64.9	33	6	12	62	68	30	36	1.3504	0.0539	1.8101	10	66	30
23	39.2	18.9	-23.2	36	44	16	24	-28	-20	-0.7462	0.0385	-1.114	42	20	-22
23	24.5	1.4	7.4	20	28	0	4	4	10	-0.7237	0.0265	-0.9532	24	2	8
22	40.2	76.8	-30.9	36	44	72	80	-34	-28	1.0861	0.0493	1.4612	40	78	-30
22	-31	34.4	2.6	-34	-28	28	40	-2	6	0.7699	0.0414	1.0973	-30	34	4
22	-55.5	17.6	35.3	-60	-50	16	22	34	38	1.0873	0.0446	1.5362	-58	16	36
22	-9.7	-25.4	31.8	-14	-4	-32	-20	30	38	-0.7921	0.0409	-1.1084	-10	-24	32
21	2.5	62.2	-11	-6	10	60	66	-14	-6	0.962	0.0512	1.4403	-2	62	-6
21	-33.2	-59.5	-6.6	-36	-30	-62	-56	-12	-4	0.8446	0.0518	1.3156	-34	-60	-6
21	-58	12.8	14.1	-60	-54	10	16	10	18	1.7624	0.0993	2.699	-58	14	14
21	63.2	21.6	-19.8	60	66	20	24	-22	-16	-0.6518	0.0339	-0.9638	66	20	-22
20	-29.2	-53.7	29.5	-32	-26	-58	-50	26	32	1.0806	0.0361	1.5436	-30	-52	32
20	-23.4	80.9	-11	-28	-20	78	88	-12	-8	-1.921	0.1528	-3.316	-24	80	-12
19	30.5	78.8	-40.2	28	34	76	80	-42	-38	1.1481	0.0606	1.4803	32	80	-40
19	-14.1	-22.7	-5	-16	-10	-26	-20	-8	-2	0.8073	0.0492	1.2923	-14	-22	-6
19	0.6	-37.3	-2.6	-2	4	-40	-36	-6	4	1.0006	0.0667	1.6558	0	-36	-4
19	-36.3	58.1	45.9	-40	-34	52	64	38	52	1.0757	0.0714	1.6402	-36	64	52
19	2.5	12.5	64.6	2	4	8	16	62	68	-1.1396	0.0732	-1.6965	2	14	64
18	19.4	53.8	-27.7	18	22	50	60	-30	-26	0.793	0.0412	1.109	18	52	-28
18	-50.3	-32.5	24.5	-54	-44	-36	-28	18	28	0.9036	0.0469	1.3052	-50	-34	24
18	-46.9	64	-42.7	-50	-44	60	68	-46	-40	-0.9259	0.0547	-1.3484	-44	62	-42
18	28.6	28.6	-23.4	24	32	24	34	-24	-22	-0.9087	0.0722	-1.5016	30	26	-22
18	19.2	-17.8	-4.9	18	22	-22	-16	-8	0	-0.615	0.0193	-0.7544	18	-18	-6
18	-6.9	-51.4	24.1	-10	-4	-54	-48	22	26	-0.7734	0.0404	-1.1581	-6	-52	24
17	38.3	-0.7	-0.2	36	42	-2	0	-6	4	0.9882	0.0435	1.2863	38	0	2
17	0.5	60.8	-33.4	-4	4	58	64	-38	-32	-0.5794	0.0305	-0.7282	-2	62	-34
17	25.4	-9.3	-21.7	20	30	-12	-4	-26	-18	-1.004	0.0476	-1.3742	28	-10	-22
17	23.8	20.7	15.3	18	28	18	24	8	22	-0.6977	0.0372	-0.9555	28	22	8
17	16.8	10.6	21.8	14	18	4	14	20	24	-0.9608	0.0451	-1.3191	18	12	22
17	-6.9	-30.3	25.4	-10	-4	-34	-28	24	28	-1.0707	0.0407	-1.3341	-6	-30	26
17	-5.7	-17.5	42.2	-10	-4	-22	-14	40	46	-0.8112	0.0498	-1.2327	-4	-16	42
16	18.2	-55	19.7	16	20	-58	-52	12	24	0.677	0.0379	0.9408	18	-56	18
16	-2.9	93.5	22.8	-6	0	90	96	20	26	4.34	0.3004	6.4771	-2	94	22
16	9.9	56.8	57.7	6	12	54	58	56	60	1.2121	0.0516	1.534	8	58	58
16	28.7	-21	-7.8	26	32	-24	-18	-10	-6	-0.7137	0.0432	-0.9723	30	-22	-8
16	56.7	17.6	21.9	52	64	16	22	20	24	-0.8434	0.0351	-1.0867	56	18	22
16	-34.7	35.7	58	-38	-30	34	38	56	60	-1.4059	0.0735	-1.9412	-36	36	60

Table 3.18: All sounds CC-DC- Part 3.

Volume	CM_RL	CM_AP	CM_IS	minRL	maxRL	minAP	maxAP	minIS	maxIS	Mean	SEM	Max_Int	MI_RL	MI_AP	MI_IS
73	56.2	9.4	-17	48	64	4	18	-22	-8	-0.9228	0.025	-1.5219	58	6	-18
39	-20.7	-0.8	-13.1	-24	-14	-8	6	-20	-10	-1.0147	0.047	-1.56	-22	-6	-12
27	56.3	65.6	13.4	52	60	62	70	10	16	-2.9836	0.1432	-4.0236	56	62	16
23	55.2	43.1	5.8	48	60	40	48	4	8	-1.4534	0.0524	-1.9767	58	44	4
22	47.9	-9.3	-26.6	44	52	-12	-4	-30	-24	-0.5999	0.019	-0.8431	52	-10	-30
21	-48.4	60	-12.9	-50	-46	56	62	-16	-8	-1.4485	0.0753	-2.0157	-48	60	-14
18	45.8	-10.2	-36.2	44	48	-14	-8	-38	-34	-0.7289	0.0289	-0.9661	46	-10	-36
18	-49.2	32	47.1	-52	-48	30	36	44	50	-1.3654	0.055	-1.7017	-48	32	46
16	45.6	52.8	-39.6	44	48	50	56	-44	-36	0.5522	0.0273	0.764	46	54	-40

Table 3.19: Silence CC-DC.

Volume	CM_RL	CM_AP	CM_IS	minRL	maxRL	minAP	maxAP	minIS	maxIS	Mean	SEM	Max_Int	MI_RL	MI_AP	MI_IS
667	55.8	5.6	-16	34	68	-22	30	-44	8	-0.6331	0.009	-1.6897	66	22	8
441	-26.1	-2.6	-6.4	-40	-4	-18	16	-26	14	-0.6485	0.0107	-1.4556	-28	-2	-12
317	57.2	50.1	11.8	48	66	34	70	0	30	-1.1524	0.0228	-2.8362	58	64	14
281	-47.6	-5.1	-33.6	-60	-32	-22	16	-46	-16	-0.4398	0.0068	-0.7536	-50	-22	-20
222	-51.8	-16.2	25.1	-58	-38	-34	-6	10	34	-0.9161	0.0202	-1.759	-48	-14	30
215	42.3	-12.8	25.2	32	56	-28	0	16	32	-0.8032	0.0136	-1.4382	40	-22	24
170	-11.9	57.6	65.6	-24	-2	48	68	52	76	1.5966	0.0682	4.6654	-8	60	68
163	-23.7	58.1	-49.8	-38	-10	46	78	-60	-42	0.4745	0.0091	0.7596	-24	58	-48
162	-40.9	-10.9	51.8	-48	-32	-18	0	40	64	-0.9389	0.0291	-2.1776	-34	-8	64
150	-53.7	3.8	34.2	-66	-38	-10	16	18	44	-0.8166	0.0154	-1.2468	-50	8	36
150	-5.5	7.6	51.3	-12	-2	-4	18	40	70	-0.8125	0.017	-1.4615	-2	12	64
110	-6.3	43.5	43.3	-16	-2	38	50	38	50	0.8112	0.0232	1.3372	-4	46	44
106	-57.9	6.8	-13.9	-64	-44	-4	18	-24	-6	-0.7124	0.0163	-1.4647	-58	-2	-16
93	14.9	52.8	70.2	6	28	42	62	64	76	1.6261	0.055	2.8398	22	58	68
92	-1.6	-18.1	-17.9	-14	8	-24	-10	-26	-8	-0.3563	0.0122	-0.6654	0	-22	-12
91	46.4	54.3	-38.5	38	54	48	62	-46	-30	0.4513	0.0122	0.7012	48	50	-36
88	34.7	58.7	-55.9	28	46	44	70	-60	-48	0.4548	0.0139	0.804	32	60	-60
80	-14.8	-7.7	11	-20	-8	-20	4	2	18	-0.5078	0.0134	-0.8554	-10	-4	8
78	-49.4	35.9	49.7	-58	-44	30	48	44	56	-1.0612	0.0288	-1.6988	-50	36	54
77	-56.5	35.8	1.9	-70	-44	30	44	-4	6	-1.0253	0.0226	-1.5837	-68	36	0
74	42.5	80	24.8	34	52	74	88	18	32	0.7455	0.0196	1.2754	48	78	26
67	23.6	-37.3	-19.3	18	32	-48	-30	-22	-14	0.4527	0.0146	0.6978	24	-46	-18
67	43.2	0.2	47.9	36	48	-4	4	42	56	-0.7818	0.0259	-1.2972	46	2	56
59	-3.1	50.7	-51.2	-14	6	44	54	-60	-42	0.5483	0.0148	0.827	0	52	-48
56	-50.8	58.8	-16.2	-56	-46	54	64	-20	-12	-1.3808	0.0514	-2.3191	-54	58	-20
55	-40.5	86.7	-10.7	-46	-36	82	92	-18	0	-1.0652	0.0348	-1.7366	-40	88	-12
51	4.1	-7.4	42	2	10	-16	0	36	48	-0.6197	0.0224	-0.9851	2	-4	40
49	-50.9	71.1	8.6	-58	-44	66	78	0	18	0.7948	0.0286	1.1256	-52	66	0
48	32	38.3	-6.1	24	36	32	48	-10	2	0.5773	0.0258	0.9567	36	34	-10
47	-28.4	-60.1	6.8	-38	-22	-68	-52	2	12	0.55	0.0283	1.2381	-24	-66	6
42	-51.6	12.8	13.6	-60	-40	10	16	8	20	0.8023	0.0447	1.4466	-58	14	14
41	-19.3	54.4	-14	-24	-14	52	60	-18	-10	0.6234	0.0197	0.9388	-18	54	-14
38	37.1	5	-41.8	30	40	0	12	-44	-38	-0.3835	0.0173	-0.6219	38	4	-44
36	7.1	5.2	1	2	18	2	8	-4	4	-0.4149	0.0199	-0.6362	2	4	2
35	-21.4	-15	63.5	-24	-18	-18	-12	60	66	-0.7835	0.0321	-1.1988	-22	-14	64
32	44.1	81.7	9.3	38	48	76	88	6	14	-0.68	0.0339	-1.18	44	76	8
32	-26.2	1.9	48.7	-32	-20	0	4	46	54	-0.5208	0.0228	-0.8091	-26	2	48
31	52.6	6.8	35.8	48	58	0	10	32	42	-0.7833	0.0172	-0.952	54	6	34
30	38.3	83.1	-14.8	34	44	80	90	-20	-10	-1.2215	0.0907	-2.0842	36	82	-14
28	-50.5	58.3	-34.4	-54	-46	52	64	-38	-30	0.4691	0.021	0.7083	-50	56	-34
28	-22.6	60.8	22.1	-26	-20	54	64	20	24	0.6589	0.0159	0.8113	-20	64	24
28	37.5	57.4	-21.8	32	46	54	62	-30	-14	-0.7551	0.0463	-1.246	42	58	-26
27	4.2	9	52	2	8	2	14	48	58	-0.6222	0.0321	-1.0011	2	10	52
26	-23.6	42.2	-16.8	-28	-18	38	48	-20	-12	0.5939	0.0137	0.753	-24	42	-18
25	-17.8	-30.9	54.1	-20	-16	-36	-26	50	56	-0.5406	0.0211	-0.722	-18	-30	56
24	55.5	-8.3	8.4	52	60	-14	-4	6	10	-0.5665	0.0255	-0.8176	54	-12	8
23	-40.9	77.1	-30.4	-46	-34	72	82	-34	-28	0.712	0.0314	0.9951	-38	78	-28

Table 3.20: All sounds-Silence CC-DC. Part 1.

Volume	CM_RL	CM_AP	CM_IS	minRL	maxRL	minAP	maxAP	minIS	maxIS	Mean	SEM	Max_Int	MI_RL	MI_AP	MI_IS
23	12	12.2	13.3	10	14	8	18	10	16	-0.4973	0.019	-0.6674	10	10	14
22	-63.9	37.8	-21.2	-68	-60	34	42	-26	-18	0.439	0.035	0.9035	-64	38	-20
22	-27	55.6	2.5	-30	-22	50	60	0	6	0.9181	0.0451	1.3569	-28	58	2
22	12	32.1	9.7	8	16	30	36	8	12	0.5067	0.0185	0.643	10	30	10
22	-25.1	19.9	9	-30	-20	16	24	2	16	-0.5144	0.0271	-0.8285	-28	16	4
21	-21.2	59.6	-22.5	-24	-16	56	66	-28	-20	0.4662	0.0213	0.615	-20	60	-20
21	34	-56.4	-10.1	32	36	-62	-50	-12	-8	0.4184	0.0274	0.6867	34	-60	-8
21	-10.1	-49.6	6	-12	-8	-54	-44	2	12	-0.4606	0.0178	-0.6337	-10	-52	4
20	-0.8	90.4	1.6	-2	2	86	92	-2	6	-1.937	0.122	-2.7962	-2	90	0
18	44.1	8.5	10.9	38	48	6	10	8	14	0.4773	0.0234	0.6323	44	8	10
18	28	45.4	69.3	24	32	42	48	64	72	1.1381	0.0894	2.0982	28	46	72
18	13.9	-16.1	6.2	10	16	-20	-12	2	10	-0.3907	0.0127	-0.4786	14	-18	6
18	-44.6	-31.9	15.8	-48	-40	-38	-28	12	18	-0.8208	0.0521	-1.1641	-46	-30	16
18	-17.4	11.1	19.7	-20	-14	8	16	14	22	-0.6343	0.0268	-0.8756	-18	10	22
18	-6.4	-4.7	56.6	-8	-4	-8	-2	52	60	-0.5647	0.0231	-0.769	-4	-4	60
18	37.6	59.6	58.3	34	40	56	64	56	62	-1.255	0.0549	-1.7391	38	60	58
17	24.8	1.6	-44.5	22	28	-4	6	-48	-42	-0.2056	0.0191	-0.3651	28	0	-46
17	-19.2	7.3	-31.4	-22	-18	2	12	-36	-28	-0.3764	0.0324	-0.5614	-18	6	-30
17	-4.8	-57.2	-12.7	-6	-4	-62	-50	-16	-10	-0.3607	0.0195	-0.5191	-4	-60	-12
17	-21.8	28.9	-0.3	-24	-20	26	32	-4	4	-0.4408	0.0117	-0.5499	-20	30	0
17	-28.6	23.3	55.4	-30	-26	22	24	50	60	-0.7575	0.0426	-1.2302	-30	24	56
17	-21.2	9.4	60.8	-22	-20	6	12	56	64	-0.4469	0.0133	-0.5458	-22	8	62
16	-13.8	39.7	-27.4	-20	-10	34	42	-30	-26	0.4968	0.0327	0.7779	-14	40	-28
16	-8.2	-45.7	-4.6	-10	-4	-48	-44	-6	-2	0.4398	0.0142	0.5862	-8	-46	-4
16	19.9	-17.6	-5.1	18	22	-20	-16	-10	-2	-0.3545	0.0099	-0.41	20	-18	-4
16	27.3	-20.6	-6	26	30	-24	-16	-8	0	-0.3712	0.0262	-0.5379	30	-22	-8

Table 3.21: All sounds-Silence CC-DC. Part 2.

Cluster results for contrasts CC-DC deviant/standard blocks

Volume	CM_RL	CM_AP	CM_IS	minRL	maxRL	minAP	maxAP	minIS	maxIS	Mean	SEM	Max_Int	MI_RL	MI_AP	MI_IS
1431	54.8	30.7	-3	30	68	-22	88	-46	28	-0.7994	0.0114	-3.5808	58	64	14
419	-24.5	-3	-8.8	-34	-12	-22	16	-24	10	-0.6823	0.012	-1.4445	-28	-2	-12
174	-13.3	56.4	65.9	-28	-2	44	66	52	76	1.4323	0.0621	4.7427	-8	60	68
162	17.2	51.4	68.1	6	30	42	62	52	76	1.3932	0.0419	2.9581	22	58	68
144	-50.2	6.2	36.9	-66	-34	-10	20	28	54	-0.8184	0.0152	-1.1983	-50	6	36
137	42	-15.5	26.6	34	52	-24	-2	18	38	-0.908	0.025	-2.7614	52	-20	36
131	-5.7	11.6	55.2	-12	-2	4	24	40	74	-0.7587	0.0197	-1.5318	-4	24	74
129	-49.2	0.6	-37	-60	-32	-12	8	-48	-28	-0.4028	0.0093	-0.6669	-56	0	-30
124	45.2	56.6	-44	36	54	48	68	-60	-34	0.4485	0.0102	0.7387	46	54	-40
116	-1.2	-18.1	-16.9	-10	12	-26	-10	-26	-8	-0.3601	0.0094	-0.6212	0	-24	-10
99	-49.2	-13.3	29.5	-56	-40	-18	-8	22	34	-1.0086	0.0302	-1.7653	-48	-14	30
98	-5.4	42.8	43.1	-12	-2	36	50	38	48	0.8691	0.0217	1.3333	-6	42	42
82	-51.2	35.2	1.7	-58	-44	24	42	-4	6	-0.9864	0.0195	-1.53	-48	34	2
77	-52	57.5	-16.4	-62	-46	44	64	-24	-10	-1.1568	0.0462	-2.2717	-54	58	-20
76	-49.9	35.1	50.1	-54	-46	28	46	44	58	-1.1603	0.0377	-2.4443	-54	34	56
73	25.8	52.5	-10.6	20	36	44	66	-20	-6	-0.6535	0.0167	-0.9918	26	62	-6
71	-44.8	-13.1	-26.9	-50	-32	-22	-6	-38	-16	-0.4762	0.0119	-0.8047	-44	-12	-32
70	-59	9.6	-12	-64	-50	4	18	-18	-6	-0.7303	0.0171	-1.0465	-60	8	-10
69	-24.5	55.1	-50.6	-32	-16	46	66	-60	-46	0.5057	0.0134	0.8019	-24	58	-46
66	-56.1	-22	16.9	-58	-52	-34	-12	10	22	-0.718	0.0194	-1.0706	-56	-20	20
66	-39.8	-10.8	55.5	-48	-34	-18	0	44	64	-0.9976	0.0402	-2.0226	-34	-8	64
62	-36.6	53	-47.2	-46	-30	44	60	-52	-42	0.3884	0.0097	0.6391	-34	50	-52
61	-40.2	75.2	-30.6	-48	-30	70	82	-34	-26	0.7026	0.0272	1.1937	-44	76	-30
59	30.9	59.1	-56.2	28	36	46	72	-60	-50	0.4985	0.0179	0.8446	30	60	-58
53	5.5	-7.3	41.7	2	10	-14	0	36	48	-0.5164	0.0141	-0.7486	2	-8	46
52	48.3	9.5	37.5	36	56	2	16	32	44	-0.7328	0.0158	-1.0541	40	14	38
47	-49.1	60.4	-32.6	-54	-46	52	68	-36	-28	0.6129	0.0363	1.3023	-48	64	-30
45	23.7	-37.1	-20	18	28	-48	-30	-22	-16	0.4466	0.0124	0.5829	26	-44	-18
41	26.6	-60.1	3.4	22	30	-66	-54	-8	12	0.5934	0.0402	1.2839	28	-62	6

Table 3.22: See next page.

Table 3.22: Deviant CC-DC - Part 1. Cluster results for the contrast 'deviant CC-DC'. Nvoxel = Number of voxels in the cluster; CM RL = Center of mass (CM) for the cluster in the Right-Left direction; CM AP = Center of mass (CM) for the cluster in the Anterior-Posterior direction; CM IS = Center of mass (CM) for the cluster in the Inferior-Superior direction; minRL, maxRL = Bounding box coordinates for the cluster in the Right-Left direction (minimum and maximum); minAP, maxAP = Bounding box coordinates for the cluster in the Anterior-Posterior direction (minimum and maximum); minIS, maxIS = Bounding box coordinates for the cluster in the Inferior-Superior direction (minimum and maximum); Mean = Mean value for the volume cluster; SEM = Standard Error of the Mean for the volume cluster; Max Int = Maximum Intensity value for the volume cluster; MI RL = Coordinate of the Maximum Intensity value in the Right-Left direction; MI AP = Coordinate of the Maximum Intensity value in the Anterior-Posterior direction; MI IS = Coordinate of the Maximum Intensity value in the Inferior-Superior direction.

Volume	CM_RL	CM_AP	CM_IS	minRL	maxRL	minAP	maxAP	minIS	maxIS	Mean	SEM	Max_Int	MI_RL	MI_AP	MI_IS
37	41.1	46.1	-29	36	46	42	50	-36	-24	-0.7018	0.0417	-1.1109	40	46	-28
34	32.8	37.7	-6.8	26	36	32	46	-10	-2	0.5955	0.0283	0.9609	34	36	-8
34	34.3	56.8	-18.5	30	40	54	60	-26	-12	-0.8558	0.0426	-1.3322	36	56	-20
33	20.4	11.7	69.1	14	26	10	14	64	72	-0.6415	0.0264	-0.9861	20	10	72
32	22.2	84.9	26.6	14	28	78	92	20	34	-1.1081	0.0537	-1.8473	22	88	32
31	-44.9	-33.6	14.5	-48	-40	-40	-30	12	18	-0.671	0.0452	-1.2388	-48	-30	16
30	-16.6	75.4	-50.6	-26	-10	70	78	-52	-48	0.5705	0.0271	0.9151	-14	76	-52
29	34.6	23.7	-15	26	40	20	28	-18	-12	0.678	0.0297	1.0129	36	24	-14
27	-58.3	-0.3	-19.8	-62	-56	-4	2	-24	-16	-0.7525	0.0377	-1.3086	-58	-2	-16
27	-41.6	86.5	-11.7	-46	-36	82	92	-18	-8	-1.084	0.0438	-1.5124	-40	88	-12
27	-64.6	33.5	-0.2	-70	-60	30	36	-4	2	-1.0699	0.0432	-1.5128	-68	36	0
27	-41.5	83.7	12.9	-46	-38	80	88	10	16	-0.6681	0.0249	-0.8974	-40	84	12
26	34.5	-7.5	-43.6	26	46	-16	0	-46	-40	-0.2373	0.0211	-0.5054	42	-2	-44
25	9.1	-57.1	-1.7	4	14	-62	-52	-10	2	0.4444	0.0156	0.5864	10	-54	0
25	-36.2	8.5	9	-40	-34	4	16	4	12	-0.7348	0.0424	-1.1511	-36	8	8
24	13.4	64.4	54.5	8	22	62	68	50	58	0.9457	0.0403	1.3476	20	64	56
24	-20.7	30	-1.2	-24	-16	28	34	-6	4	-0.4071	0.0152	-0.5527	-20	32	-4
24	-23.2	10.3	61.5	-28	-20	6	14	58	66	-0.4544	0.0195	-0.713	-28	12	62
23	-24.4	43.6	-18.6	-28	-22	40	48	-20	-16	0.609	0.0238	0.8087	-24	42	-18
23	50.6	74.5	-5.9	48	54	68	80	-12	-2	-0.9562	0.0609	-1.5166	52	76	-4
23	66.5	37.6	-0.1	62	68	32	44	-8	4	-0.9364	0.053	-1.3684	66	42	-2
23	-18.3	-13.3	13	-20	-16	-20	-8	6	18	-0.4729	0.0165	-0.6355	-18	-14	14
22	-63.9	36.2	-21.9	-66	-58	30	42	-26	-18	0.3928	0.0252	0.6348	-62	38	-22
22	-28.4	-56.5	6.3	-32	-26	-62	-52	4	10	0.4496	0.0181	0.5872	-28	-60	6
22	-45.1	43.8	-16.6	-48	-44	42	46	-22	-12	-0.5846	0.0134	-0.6877	-44	44	-16
22	24.6	1.4	7.6	22	28	-2	4	6	10	-0.4267	0.0144	-0.5681	24	2	8
22	-27.1	2	48.5	-32	-20	0	4	46	52	-0.4849	0.0258	-0.7271	-28	2	48
21	-0.1	52.3	-48.6	-4	4	50	54	-52	-46	0.581	0.0303	0.8516	0	52	-48
21	33.9	-54.6	-11.4	32	36	-60	-48	-16	-8	0.3831	0.0231	0.6568	34	-60	-8
21	25.5	2.4	-45.6	20	30	-2	6	-50	-42	-0.1646	0.0145	-0.257	24	4	-46
21	-1.2	90.5	2.3	-6	2	86	92	-2	8	-1.7424	0.1286	-2.5019	-2	90	0
21	-21.7	-11.3	63.9	-24	-20	-18	-4	62	66	-0.7026	0.0319	-1.0218	-22	-14	64
20	-9.3	34.4	48.1	-12	-8	30	40	40	52	0.6201	0.027	0.8219	-8	36	52
19	13.3	-15.2	7	10	16	-18	-12	4	10	-0.4528	0.0166	-0.5719	12	-14	10
19	-22.7	22	12.9	-28	-20	18	26	8	16	-0.4843	0.0263	-0.76	-20	24	16
19	-15.5	-33.6	55.8	-18	-10	-40	-30	54	58	-0.6346	0.0254	-0.8224	-10	-32	58
18	19.3	3.5	-33.7	14	22	-2	6	-38	-28	0.2507	0.0156	0.3804	22	4	-32
18	-17.1	52.5	-15.9	-22	-14	50	54	-20	-14	0.5306	0.0197	0.6778	-22	54	-14
18	15.5	62.8	-5.9	14	18	58	68	-8	-4	-0.7494	0.0332	-0.9986	16	66	-8
18	41.7	65.8	15.9	38	46	64	68	14	18	-0.6886	0.039	-0.9274	40	66	18

Table 3.23: Deviant CC-DC - Part 2

Volume	CM_RL	CM_AP	CM_IS	minRL	maxRL	minAP	maxAP	minIS	maxIS	Mean	SEM	Max_Int	MI_RL	MI_AP	MI_IS
18	-63.6	1.5	18.5	-66	-62	0	4	14	24	-0.7319	0.0209	-0.9413	-64	0	22
18	4.1	10.8	51.1	2	6	6	14	48	54	-0.6146	0.0268	-0.8256	4	12	52
17	9.1	73.2	-29.9	4	12	72	76	-32	-28	0.5146	0.0237	0.6798	10	72	-32
17	9.4	64.6	33.1	6	12	62	66	30	36	0.7828	0.0266	0.9215	10	64	32
17	41.9	83.6	-15.7	40	44	80	88	-20	-10	-0.9841	0.0723	-1.4617	40	80	-20
17	-10.8	-1	6.4	-14	-8	-6	4	2	10	-0.6584	0.0341	-0.9145	-10	2	8
16	-14.2	-22.5	-4.7	-16	-10	-26	-20	-8	-2	0.5012	0.0313	0.7669	-14	-22	-6
16	6.9	-35.5	28.1	4	10	-38	-34	24	30	0.4256	0.0144	0.5246	6	-36	28
16	-15	64.8	-4	-18	-12	62	66	-6	0	-0.7997	0.0329	-1.0366	-12	64	-6
16	4	5.2	1.7	2	6	4	8	-4	4	-0.534	0.0358	-0.8225	4	4	2
16	10.9	11.2	13.8	8	14	8	18	12	16	-0.4796	0.0274	-0.7513	10	10	14
16	-17.6	10	20.8	-20	-14	4	14	20	22	-0.6337	0.0332	-0.8615	-18	10	22
15	22.6	66.7	-31.5	20	28	64	70	-36	-28	0.3861	0.018	0.4693	20	68	-34
15	-8.4	-45.7	-4.5	-10	-6	-48	-44	-6	-2	0.4116	0.0164	0.5578	-8	-46	-4
15	12.6	31.8	9.9	8	18	30	36	8	12	0.4723	0.0192	0.5895	8	30	12
15	-37.3	-16.3	-41.5	-40	-32	-20	-14	-44	-40	-0.4129	0.0183	-0.5437	-34	-18	-42
15	-50.5	54.4	50.9	-54	-48	52	56	48	54	-1.2095	0.0534	-1.671	-52	54	50
15	-7.7	10	72.8	-12	-6	4	14	68	74	-0.9704	0.1169	-1.6934	-6	12	74

Table 3.24: Deviant CC-DC - Part 3

Volume	CM_RL	CM_AP	CM_IS	minRL	maxRL	minAP	maxAP	minIS	maxIS	Mean	SEM	Max_Int	MI_RL	MI_AP	MI_IS
832	56.6	8.6	-13.8	36	68	-22	42	-46	8	-0.6597	0.0082	-1.8492	64	22	8
589	55.8	53.3	9.8	38	68	34	80	-12	30	-1.1107	0.0202	-3.4732	58	64	14
372	-23.7	-3.5	-9.4	-34	-8	-18	12	-26	10	-0.6836	0.0132	-1.375	-28	-2	-12
225	42.2	-16.1	26.8	32	54	-28	0	16	40	-0.8751	0.0192	-2.8441	52	-20	36
192	-50.5	-13.9	26	-58	-34	-24	-4	10	34	-0.8653	0.0241	-1.8261	-50	-14	28
169	-40.9	-10.4	52.2	-50	-28	-18	0	40	64	-0.9561	0.0278	-2.1437	-34	-8	64
149	-59.3	35.1	1.3	-70	-44	28	42	-4	8	-1.1148	0.0212	-1.8782	-68	36	0
141	-11.2	57	64.7	-24	-2	46	66	52	74	1.4524	0.0743	5.0123	-8	60	68
136	-50.6	5.6	35.8	-62	-38	-10	16	30	44	-0.8155	0.0158	-1.3338	-40	14	38
134	-6.6	41.5	44.8	-16	-2	30	50	38	52	0.8029	0.0189	1.3442	-2	46	46
133	-6.2	9.6	51.9	-12	-2	4	22	40	68	-0.7505	0.0178	-1.2916	-2	12	64
105	-49.5	35.8	50.1	-58	-44	28	48	44	58	-1.1696	0.0303	-1.9916	-54	34	56
104	30.8	31.1	-8.3	18	38	20	48	-18	8	0.5548	0.0159	1.038	34	36	-8
98	-22.9	57.9	-48.4	-32	-10	48	72	-54	-42	0.5039	0.0126	0.8407	-24	58	-46
96	-49.9	60.6	-14.6	-56	-46	52	76	-22	-8	-1.2045	0.0434	-2.1565	-48	60	-14
87	3.8	-6.2	40.6	-2	10	-14	4	34	48	-0.6443	0.0195	-1.3055	0	-6	36
79	-40.2	3.6	-41.4	-52	-28	-12	16	-48	-34	-0.3212	0.013	-0.5737	-44	0	-42
77	-28.7	24	56.9	-36	-20	14	28	44	72	-0.8998	0.0238	-1.3791	-32	26	56
66	33.9	59.4	-55.8	28	46	46	72	-60	-50	0.4644	0.0159	0.7424	30	60	-58
66	-59.4	9.3	-12.3	-64	-52	6	14	-18	-6	-0.7419	0.0141	-1.0427	-60	8	-10
65	-49.1	61.2	-31.5	-54	-46	52	68	-38	-24	0.6917	0.0377	1.4271	-48	64	-28
65	-46.9	58.8	51	-54	-42	48	70	46	58	-1.2424	0.0306	-1.9057	-42	68	50
63	39.9	60.1	54.4	32	48	56	66	46	62	-1.4132	0.0449	-2.515	40	60	56
62	36.5	6.7	-39.2	30	42	0	14	-44	-28	-0.3683	0.0124	-0.5981	38	4	-44
58	23.3	-37.8	-19.4	18	30	-48	-30	-22	-14	0.4388	0.0146	0.699	26	-44	-18
56	47.3	54.3	-39.8	42	54	48	60	-46	-34	0.4561	0.0133	0.7037	46	54	-38
54	-45.2	73.4	36.6	-56	-38	62	82	30	44	-0.894	0.0251	-1.3523	-46	74	34
53	-44.7	-10.5	-29	-50	-34	-16	-4	-38	-22	-0.4898	0.0162	-0.8126	-44	-12	-32
52	-17.8	-11.6	14	-20	-14	-20	-2	6	20	-0.5255	0.0126	-0.7182	-18	-4	18
51	44.2	0.7	47.2	36	50	-2	4	42	56	-0.7199	0.0273	-1.2567	48	2	56
49	-21.3	5.7	63.3	-28	-18	-4	14	56	70	-0.5651	0.0255	-1.2345	-22	-2	70
48	-36.9	53.8	-46.7	-46	-30	46	60	-52	-40	0.3488	0.0092	0.5319	-42	58	-50
46	43.6	46.2	-26.8	36	50	40	50	-32	-22	-0.8335	0.0363	-1.2693	46	50	-26
45	-4.4	51	-53.4	-12	4	44	54	-60	-44	0.5325	0.0156	0.6907	-4	52	-54
44	-56.5	1	-31.2	-60	-50	-6	8	-36	-28	-0.4813	0.0149	-0.7023	-58	2	-30
43	-40.6	86.8	-11.6	-46	-32	82	96	-18	-6	-1.2272	0.054	-2.2037	-42	86	-12
43	24.8	19.7	17.4	16	38	6	30	8	24	-0.5028	0.02	-0.7963	36	28	18
42	-22	-12.5	63.2	-26	-18	-18	-4	60	66	-0.7686	0.0284	-1.1887	-22	-14	64
41	12.7	51.2	71.9	6	18	44	60	70	76	1.4119	0.0731	2.5348	6	56	70
40	-6.2	-18	-20.6	-14	-2	-22	-12	-24	-18	-0.3054	0.0168	-0.5087	-8	-18	-20
40	54.6	-8.1	8.4	50	60	-14	-2	6	12	-0.6174	0.0213	-0.8968	54	-12	8
35	11.1	61.7	-49	6	14	56	66	-56	-44	0.4278	0.0111	0.6132	8	64	-52
35	39.1	40.4	42.3	32	44	36	44	36	48	-0.6395	0.0223	-1.0479	36	42	44

Table 3.25: Standard CC-DC - Part 1

Volume	CM_RL	CM_AP	CM_IS	minRL	maxRL	minAP	maxAP	minIS	maxIS	Mean	SEM	Max_Int	MI_RL	MI_AP	MI_IS
35	-25.3	2.2	49.3	-30	-20	0	4	46	56	-0.5141	0.0196	-0.7639	-26	2	48
33	-22.3	62.4	-23.5	-26	-18	56	70	-28	-20	0.4223	0.0125	0.5723	-24	68	-20
33	0.7	-18.5	-15.1	-6	6	-24	-10	-24	-8	-0.349	0.0191	-0.5641	0	-20	-16
32	-33.3	31.3	-16	-36	-28	26	40	-24	-8	0.5142	0.0188	0.7097	-32	26	-12
32	46.8	6.8	9.6	38	56	2	10	6	14	0.5093	0.0172	0.6893	44	8	10
32	-61.7	48.3	-18.1	-66	-56	44	54	-24	-10	-0.8483	0.0422	-1.5563	-62	46	-20
32	4.9	11.4	51.3	2	8	4	14	46	58	-0.6341	0.0201	-0.8763	2	12	54
30	-19.2	54.3	-14.8	-26	-14	52	60	-20	-12	0.5947	0.0197	0.8772	-26	60	-16
30	47.1	71.8	36.9	44	52	66	74	30	42	-1.4257	0.0612	-2.0911	44	72	40
30	-5.7	-5.3	58.4	-8	-4	-12	-2	54	64	-0.5461	0.021	-0.844	-4	-4	60
29	-42.6	76.3	-31.1	-46	-38	72	82	-34	-28	0.7224	0.035	1.135	-44	76	-30
28	-48.1	71.7	7.3	-52	-42	68	74	4	10	0.8014	0.0287	1.1308	-50	74	8
28	11.9	-14	8.5	8	16	-16	-10	4	14	-0.4782	0.0152	-0.6701	10	-12	12
28	43.9	80.5	9.4	40	48	74	88	6	14	-0.6917	0.0365	-1.2895	44	76	8
27	25.2	2.3	-45.2	22	30	-2	6	-50	-40	-0.1875	0.0139	-0.3256	24	4	-46
27	-42	84	14	-46	-36	80	88	10	18	-0.6375	0.0206	-0.8969	-40	86	14
26	-35.6	-18.2	-37.7	-40	-28	-22	-14	-42	-32	-0.3943	0.0142	-0.5606	-32	-20	-32
26	-20.7	17.1	-10	-24	-18	10	24	-14	-4	-0.5691	0.0258	-0.8071	-22	10	-12
26	41.1	59.3	32.2	38	44	56	64	28	38	-0.9131	0.0282	-1.1997	38	58	32
26	32.4	51.6	38.7	28	38	48	54	36	42	-0.6791	0.0241	-0.8915	30	52	38
26	-5	-2.7	44.1	-12	-2	-6	0	42	46	-0.7468	0.0337	-1.0703	-2	-2	44
25	-28.4	-55.8	7.4	-32	-24	-62	-52	6	12	0.4166	0.0135	0.5304	-28	-56	6
24	-6.4	-41.6	-11.2	-10	-2	-46	-36	-14	-10	0.3161	0.0147	0.4699	-4	-44	-10
24	42.1	83.6	-15.7	38	44	78	92	-20	-8	-0.9611	0.0618	-1.6589	42	80	-20
24	-36.5	8.5	8.9	-40	-34	4	18	6	14	-0.7605	0.0425	-1.1185	-36	8	8
23	-17.2	10	20.3	-20	-14	4	14	18	22	-0.6906	0.0318	-1.0064	-18	10	22
23	23	11.1	67.4	20	26	8	14	62	72	-0.5524	0.0263	-0.7975	22	10	72
22	-28.1	36.3	-36.5	-32	-22	32	40	-42	-32	0.5071	0.0257	0.7511	-26	36	-38
22	-45	3.1	-10.2	-48	-42	-2	8	-14	-6	0.815	0.0403	1.08	-44	0	-14
22	40.7	80.6	24.3	36	50	76	88	22	26	0.6548	0.025	0.8159	40	76	22
22	27.5	-13.9	-39.9	26	30	-16	-10	-46	-34	-0.1999	0.0116	-0.3006	28	-16	-34
22	-10.8	-2.4	6.3	-16	-8	-6	2	2	10	-0.6469	0.0284	-0.8439	-12	0	8
22	36.9	17.4	43.6	34	38	14	22	36	48	-0.6377	0.03	-0.9381	38	16	44
21	28.9	-58.9	5.8	24	32	-62	-54	-2	12	0.5978	0.0206	0.7661	30	-58	10
21	25.5	-40.4	25.7	22	28	-42	-38	22	30	0.3957	0.0144	0.5114	24	-38	24
21	-21.6	28.7	1.4	-24	-16	26	30	-4	4	-0.3712	0.0092	-0.4411	-24	28	2
20	34.7	-2.6	-14.2	30	38	-6	2	-16	-10	0.5571	0.0214	0.7293	38	-2	-14
20	11.6	31.6	9.7	8	16	30	36	6	12	0.4942	0.0182	0.6359	12	32	10
20	-44.4	-31.8	15.6	-48	-40	-38	-28	12	18	-0.834	0.05	-1.2791	-48	-30	16
20	24.3	82.1	23.6	20	28	78	84	20	28	-0.8936	0.0378	-1.2657	26	84	28
20	51.1	8	35.1	48	54	6	10	32	42	-0.6683	0.0191	-0.8468	50	8	32
20	-36.6	44.3	41.9	-38	-34	40	48	40	44	-0.6094	0.0205	-0.7891	-36	44	42
19	-7.1	70.3	-26	-10	-6	66	72	-32	-20	0.4153	0.0193	0.6111	-6	72	-20
19	-14.2	39.3	-27.3	-20	-10	34	42	-30	-26	0.4335	0.0288	0.713	-14	40	-28
19	-21.6	23.1	14.2	-24	-18	20	26	10	16	-0.5079	0.0277	-0.7868	-20	24	16
18	7.7	-35.7	27.6	4	10	-38	-34	24	30	0.3925	0.0131	0.5011	6	-36	28
18	-19.4	8.5	-32.3	-22	-18	2	14	-36	-28	-0.3229	0.0295	-0.6185	-20	10	-34
18	33.4	56.7	-15.6	30	36	54	58	-20	-12	-0.7476	0.0421	-1.149	36	58	-20
18	41.1	32.4	-19.1	38	44	28	38	-20	-18	-0.5869	0.0282	-0.7895	42	32	-20
18	26.2	48.5	-10.3	22	30	46	52	-14	-8	-0.5655	0.0199	-0.7054	22	52	-10
18	58.2	59.7	-6.3	52	62	58	62	-10	-4	-0.8033	0.0334	-1.0506	58	60	-4
18	44.8	12.3	40.6	42	48	10	14	36	44	-0.748	0.0308	-1.0275	42	12	36
17	-24.9	67.1	-55	-28	-20	64	70	-56	-54	-0.4367	0.0295	-0.6525	-24	68	-56
17	2.3	4.6	2.1	-2	6	2	6	-2	4	-0.5766	0.0314	-0.8153	4	4	2
17	42.9	-35.9	17.3	38	46	-38	-30	14	20	-0.4456	0.0255	-0.6754	46	-38	20
16	22.3	65.4	-30	20	26	64	68	-34	-28	0.4113	0.0179	0.5157	22	64	-28
16	-8.2	55.8	-51.3	-12	-6	52	58	-56	-46	-0.4053	0.0163	-0.5151	-6	58	-52
16	63.2	21.8	-20.3	60	66	20	24	-22	-16	-0.3874	0.0212	-0.5083	64	22	-22
15	-30.4	33.4	3.5	-32	-28	28	38	0	6	0.4752	0.029	0.6748	-30	34	4
15	-17.1	-30.3	54.5	-20	-14	-34	-28	50	58	-0.5398	0.0279	-0.7361	-18	-30	56

Table 3.26: Standard CC-DC - Part 2

Volume	CM_RL	CM_AP	CM_IS	minRL	maxRL	minAP	maxAP	minIS	maxIS	Mean	SEM	Max_Int	MI_RL	MI_AP	MI_IS
189	22.5	61.1	-13.3	12	36	44	76	-28	-6	-0.2585	0.0044	-0.4577	22	68	-14
186	36.9	51.4	56	20	58	30	64	32	68	0.5141	0.0199	1.4081	28	58	64
138	-40	41.2	54.7	-46	-30	32	52	38	64	0.4236	0.0138	0.9618	-42	44	60
89	43.7	-29.3	29.6	36	52	-34	-20	20	42	0.3824	0.0101	0.6006	42	-30	28
86	54	33.5	13.3	46	66	24	44	8	22	0.5031	0.0154	0.9233	58	32	16
79	-10.4	96.2	-11.7	-16	-4	88	102	-20	2	0.9855	0.0423	1.9837	-14	96	-14
79	39.1	-49.3	0.2	34	44	-60	-40	-8	8	0.224	0.0059	0.3814	44	-48	4
75	39	10.5	60.8	34	42	4	22	50	68	0.624	0.0306	1.2686	40	6	62
73	-42.1	58.8	-18.6	-48	-34	52	64	-24	-14	0.8314	0.0422	1.8377	-44	60	-20
67	34.3	-11.3	55.3	20	46	-16	-8	44	68	0.3221	0.0128	0.5849	22	-10	66
59	-60.2	42.4	-19	-66	-54	28	52	-26	-14	0.2583	0.0108	0.4291	-60	42	-18
58	-45	-18.1	3.8	-50	-36	-26	-14	-4	10	-0.1934	0.0044	-0.2763	-46	-16	4
57	-47	10.6	6.7	-58	-38	2	18	4	10	0.3787	0.0125	0.6133	-56	6	6
56	15	35	-1.7	8	26	28	40	-8	6	-0.2441	0.012	-0.4888	8	38	2
47	-16.6	75.5	-53.1	-26	-10	70	80	-58	-50	0.3347	0.0149	0.6552	-14	76	-52
46	17.2	46.8	69.1	12	22	38	52	60	74	0.5083	0.0195	0.8294	16	50	74
42	-14.8	-20.2	-1.5	-20	-10	-24	-12	-6	4	0.2678	0.0078	0.3793	-16	-20	-4
41	-17.7	-56.4	31.4	-22	-12	-60	-52	26	38	-0.2193	0.0077	-0.3225	-18	-56	32
40	-26.8	-1.5	-39.8	-32	-22	-10	6	-48	-32	0.1261	0.0088	0.301	-26	0	-36
40	6.4	-62.5	20.2	2	12	-68	-54	16	26	-0.2628	0.0095	-0.4517	4	-64	24
38	-22.7	65.7	-25.2	-26	-18	62	70	-30	-20	-0.2006	0.006	-0.2591	-22	64	-28
37	22.2	10.3	-22.2	18	26	2	20	-26	-20	0.3638	0.017	0.5933	24	4	-24
37	-43.6	61.8	47.8	-48	-40	56	66	42	52	0.5368	0.0169	0.7516	-42	64	52
36	-5.8	-12.7	50.7	-10	-4	-20	-6	44	62	0.3061	0.013	0.4795	-4	-8	58
36	26.8	9.4	68.8	20	32	2	14	60	72	0.6332	0.0376	1.1246	28	12	72
36	18.6	60.8	-53.9	14	24	56	66	-60	-50	-0.1927	0.0055	-0.2673	20	62	-54
34	-33.3	-10.4	55.8	-40	-28	-16	-2	48	60	0.357	0.0168	0.6291	-40	-2	60
34	4.3	42.4	64.9	2	12	38	50	62	68	0.6196	0.0215	0.8386	2	42	64
34	-19.8	38	-8.2	-26	-16	32	48	-14	-2	-0.2911	0.01	-0.444	-16	36	-6
33	44.9	36	-21.8	40	52	32	38	-28	-18	0.2353	0.0098	0.3737	44	36	-22
33	-47.5	-9.3	45.6	-50	-44	-12	-4	38	50	0.504	0.0299	0.8392	-48	-12	46
33	43.9	8.1	48.9	36	50	0	16	44	52	0.3491	0.0151	0.5058	48	12	52
30	10.1	-26.7	29.7	8	12	-36	-22	26	34	0.2655	0.0104	0.4002	10	-26	28
30	-28.8	-19	-18.3	-32	-26	-22	-16	-22	-12	-0.1736	0.0062	-0.2442	-30	-18	-20
30	-22.7	-46.6	35.6	-26	-20	-52	-42	34	38	-0.1732	0.0038	-0.229	-20	-46	38
29	48.9	0.9	-35.8	44	54	-6	6	-38	-34	-0.2004	0.0083	-0.3417	46	4	-36
29	-28	58	-9.2	-30	-24	54	62	-14	-4	-0.305	0.009	-0.4086	-24	58	-14
28	30.4	66.4	-48.6	26	34	60	72	-54	-46	0.2287	0.0096	0.3013	30	70	-48
28	46.1	53.5	-22.8	40	50	46	60	-28	-18	0.5498	0.0269	0.7903	48	54	-24
28	10.5	-12.4	-6.2	8	14	-16	-6	-10	-4	0.1735	0.0058	0.233	10	-14	-6
28	23.6	26.1	13.2	20	30	24	30	10	20	0.184	0.0072	0.2649	30	24	12
28	-58.7	45.2	15.5	-66	-52	36	50	14	18	0.4027	0.0219	0.6725	-64	48	14
28	30.3	41.1	38.9	28	34	38	46	36	44	0.2881	0.0129	0.3996	30	40	38
28	30.2	4.8	49.3	26	32	0	8	44	54	0.3276	0.0062	0.3927	32	6	50
28	-44.3	58.2	-2.1	-48	-42	56	60	-8	2	-0.2933	0.0068	-0.3642	-46	58	2
27	-27.4	21.3	-29	-32	-20	14	28	-30	-26	0.2781	0.0132	0.4425	-30	26	-30
27	8.5	-63.4	-12.7	4	14	-66	-62	-20	-10	-0.1954	0.0085	-0.2703	6	-64	-12
26	-31	-25.1	-2.1	-34	-28	-28	-22	-6	2	0.2416	0.0094	0.325	-32	-26	-2
25	-33.1	41.7	-25	-34	-30	36	46	-28	-20	0.419	0.0231	0.688	-34	40	-26
25	3.3	-2.7	50.2	2	8	-8	4	46	58	0.3737	0.0245	0.6403	2	-2	48
25	0.3	46.4	-23.5	-8	6	42	52	-26	-20	-0.2215	0.01	-0.3148	2	46	-24
25	-6.5	-62.9	-8.1	-10	-2	-68	-56	-12	-2	-0.2355	0.0076	-0.3151	-6	-68	-6
25	-4.7	-53.9	19.5	-8	-2	-58	-52	12	26	-0.2384	0.0114	-0.3568	-4	-54	24
25	-0.9	-4.1	28.5	-4	4	-10	6	26	30	-0.2802	0.0172	-0.4638	-2	-6	28
24	59.6	23.7	-22.9	56	62	18	30	-30	-20	0.1176	0.0054	0.1756	62	24	-20
24	13.7	14.1	18.4	10	16	6	20	16	20	0.2852	0.0113	0.3915	14	16	18
24	-41.3	72.6	42.4	-48	-36	72	74	34	48	0.4611	0.0175	0.6606	-38	72	48
24	-8.4	1.1	51.7	-12	-6	-4	4	48	56	0.3041	0.0159	0.4476	-6	2	52
24	30.3	16.3	-17.2	24	36	10	20	-22	-8	-0.2003	0.0094	-0.2769	24	14	-16
23	53.3	-5.6	8.9	50	56	-10	0	6	12	0.2557	0.0102	0.3548	54	-6	8
22	10.7	80	-41.5	4	18	76	82	-44	-38	0.2389	0.0082	0.3508	14	78	-42
22	3.4	3.1	70.8	2	6	-2	8	68	72	0.4999	0.0462	1.0568	2	4	72
22	-3.7	61.5	-38.7	-10	2	56	66	-44	-34	-0.22	0.0078	-0.3056	-4	62	-36
22	-43.9	63.7	8.8	-46	-40	60	66	4	12	-0.2898	0.0065	-0.3557	-44	64	10
21	35.9	24.7	20	32	40	18	30	16	22	0.3828	0.0161	0.5145	34	24	18

Table 3.27: Deviant-Standard CC-DC. Part 1

Volume	CM_RL	CM_AP	CM_IS	minRL	maxRL	minAP	maxAP	minIS	maxIS	Mean	SEM	Max_Int	MI_RL	MI_AP	MI_IS
21	-44.9	55.9	36.2	-48	-40	52	60	34	40	0.3458	0.0103	0.4459	-48	60	36
21	-52.7	25.5	51.5	-56	-48	22	30	48	54	0.3797	0.0161	0.5175	-52	28	54
21	-7.3	72.5	0.1	-10	-4	70	76	-4	6	-0.4247	0.0197	-0.5662	-4	72	4
21	-45.1	71.5	4.3	-48	-42	70	74	2	6	-0.4702	0.0197	-0.6791	-44	72	4
21	-55	-32.1	13	-58	-50	-38	-26	8	18	-0.2082	0.0053	-0.256	-54	-26	16
20	12.4	-9.2	16.2	8	16	-12	-4	12	20	0.1968	0.0062	0.2506	14	-8	18
20	-19.3	26.8	62	-26	-16	26	30	56	68	0.4775	0.0256	0.6478	-18	26	62
20	33.7	-6.1	-24.7	30	36	-8	-2	-28	-22	-0.3007	0.019	-0.4395	34	-6	-24
20	-58.3	6.3	42.7	-62	-56	-2	10	40	46	-0.2741	0.0098	-0.361	-58	4	42
19	43.6	-5	4.4	40	48	-6	-2	2	6	0.2292	0.0171	0.3708	42	-6	4
19	22.4	-62.9	7	14	28	-68	-60	4	10	0.2873	0.016	0.4646	26	-62	8
19	-6.4	-39.2	10.9	-8	-4	-44	-36	8	16	0.2552	0.0112	0.3577	-6	-38	12
19	5.6	-17.6	49.7	4	8	-20	-14	46	52	0.3117	0.0184	0.4553	6	-16	50
19	29.3	-25.7	50.7	26	32	-28	-20	48	54	0.2758	0.0089	0.3405	28	-26	50
19	4.2	-28.2	-14.4	2	8	-32	-24	-20	-10	-0.1425	0.0078	-0.196	2	-28	-12
18	43.8	12.8	-38.6	40	50	10	16	-44	-36	0.1027	0.0107	0.1607	40	12	-40
18	-4.7	-9.5	-4.2	-10	-2	-16	-4	-8	0	0.185	0.0103	0.3188	-4	-14	-2
18	43	66.2	29.3	40	46	64	70	28	32	0.485	0.0212	0.6422	44	66	28
18	-5.5	-17.9	32.5	-12	-2	-22	-14	30	36	0.308	0.0208	0.4821	-4	-18	32
18	-40	-23.2	44.3	-44	-36	-28	-18	42	48	0.2561	0.0107	0.3527	-42	-22	42
17	-50.6	7.5	-19.9	-54	-48	4	12	-22	-18	0.2712	0.0135	0.3652	-50	8	-20
17	-15.1	52.2	-49	-18	-12	50	56	-52	-46	-0.2171	0.011	-0.3163	-16	52	-48
17	28.7	-3.9	-44.5	24	34	-8	-2	-48	-42	-0.0805	0.0092	-0.1447	30	-2	-42
17	-38.3	31.9	18.1	-42	-36	28	34	16	20	-0.2569	0.0131	-0.3744	-38	32	18
16	-62.8	31.2	-23.7	-68	-60	26	36	-28	-20	0.139	0.0086	0.1842	-60	34	-22
16	29.8	-4.3	-15	28	32	-8	-2	-18	-12	-0.2093	0.0153	-0.3357	28	-4	-18
16	-1	83.2	43.4	-4	0	80	86	36	50	-1.0276	0.0434	-1.3015	0	82	46
16	6	-46.7	48.1	4	10	-50	-44	44	50	-0.2431	0.0099	-0.3118	6	-46	50
15	-35.9	74.5	-51.6	-38	-34	72	78	-54	-50	0.2808	0.0189	0.3901	-36	72	-54
15	24.2	-27.9	40.8	20	28	-32	-24	38	44	0.2437	0.0128	0.3292	24	-28	40
15	22.2	67.2	44.3	20	24	62	70	42	46	0.4606	0.0165	0.5695	22	68	44
15	-59.7	-4	-22.1	-62	-58	-6	-2	-24	-20	-0.2514	0.0053	-0.2836	-60	-2	-22
15	-45.4	3.3	-9.1	-48	-44	2	6	-16	-4	-0.344	0.0196	-0.4987	-46	4	-8
15	0	-39.6	-13.2	-2	2	-42	-36	-16	-10	-0.1525	0.0063	-0.2032	0	-40	-12
15	63.1	31.4	39.6	62	64	24	38	38	42	-0.3117	0.0168	-0.4228	64	36	40

Table 3.28: Deviant-Standard CC-DC. Part 2

3.6.4 Results of ROI-wise activation analyses

Voxel-wise activation analyses were supplemented by a detailed examination of activation patterns in key regions involved in sound processing. Our goal was to quantify activity changes in the primary auditory cortices (HG), secondary auditory cortices (planum polare and planum temporale), and sub-thalamic regions (including the posterior-parietal, occipital, sensory, and prefrontal thalamic areas). This analysis focused on comparing the CC and awake groups, and the CC and DC groups, with the aim of quantifying the effects of physiological state on CC and the effects of (dis)connectedness within the same physiological state, in selected key regions.

Effect of physiological state on connected consciousness: reduced response to all-sounds in CC vs. wakefulness with enhanced differential processing in the thalamus

The linear mixed-effects model comparing awake and CC states for all-sounds versus silence blocks revealed a significant ($p < 0.05$) main effect of stimulus

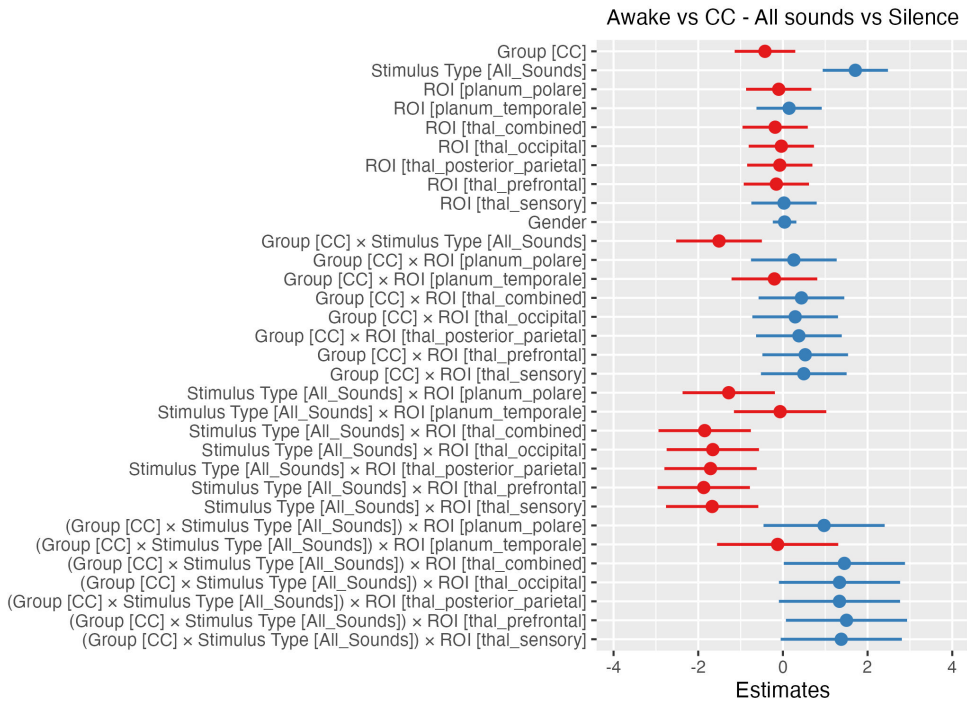

Figure 3.17: ROI activation differences between CC and wakefulness in response to all-sounds vs silence blocks. The plot displays the estimates for the main effects and interaction effects of group (CC vs. awake), stimulus type (all-sounds vs. silence), and ROI on brain activity. The awake group, the Heschl's gyrus ROI and the silence blocks were used as baselines. Error bars represent 95% confidence intervals. Red indicates negative estimates, while blue represents positive estimates.

type and several interactions between group, stimulus type, and ROIs (fig. 3.17). Overall, across groups and ROIs, all-sounds blocks were associated with higher ROI activation values compared to silence blocks (used as reference). This increase in activity in response to all-sounds was region-specific: across groups, the planum polare, thalamus (all sub-regions combined), and various sub-thalamic regions (occipital, posterior/parietal, prefrontal, and sensory sub-thalamic regions) showed less pronounced increases in response to all-sounds blocks compared to the HG (reference ROI). The negative coefficient of the two-way interaction between group and stimulus type revealed group differences in the processing of all-sounds versus silence blocks, with the increase in activation to all-sounds being less pronounced in CC compared to wakefulness. Finally, the positive coefficients of the three-way interactions among group, stimulus type, and ROI indicated that in the thalamus and the

prefrontal part of the thalamus the difference in activation between all-sounds and silence conditions was more pronounced for the CC group compared to wakefulness, relative to the reference region, the HG - see SI 3.6.5 for summary of model coefficients and p-values.

Effect of physiological state on connected consciousness: reduced activation differences between wakefulness and CC to deviant vs. standard blocks in the thalamus and planum polare

In the (awake-CC) deviant vs. standard model, we observed significant main effects of group and ROI - see fig. 3.18. The CC group showed a decrease in ROI activation values compared to wakefulness across ROIs and stimulus types. This difference in brain activity between wakefulness and

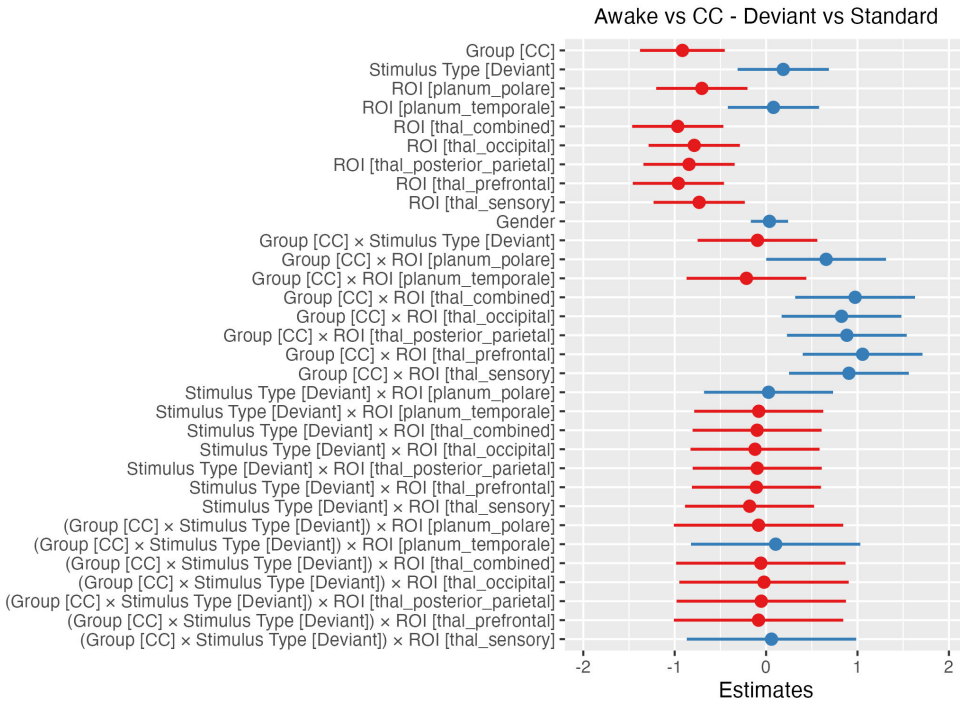

Figure 3.18: ROI activation differences between CC and wakefulness in response to deviant vs standard blocks. The plot displays the estimates for the main effects and interaction effects of group (CC vs. awake), stimulus type (deviant vs. standard), and ROI on brain activity. The awake group, the Heschl's gyrus ROI and the standard blocks were used as baselines. Error bars represent 95% confidence intervals. Red indicates negative estimates, while blue represents positive estimates.

CC was region-specific: the two-way interaction between group and ROI suggested, in fact, that the decrease in activation from wakefulness to CC was less pronounced in the planum polare, thalamus, and sub-thalamic regions (occipital, posterior/parietal, prefrontal, and sensory sub-thalamic regions) compared to the activity in the HG[8]. Finally, all regions, except the planum temporale, showed decreased activation, across all groups and stimulus types, compared to the primary auditory cortex (the HG) - see SI 3.6.5 for summary of model coefficients and p-values.

Effect of (dis)connectedness within the same physiological state: reduced activation to sounds in CC compared to DC and with higher propofol concentrations

The linear mixed-effects model comparing DC and CC states for both all-sounds versus silence and deviant vs standard blocks revealed significant main effects of group and propofol concentration (see figs. 3.19 and 3.20). Consistent with the voxel-wise activation results (sec.3.4.5), the CC group exhibited significantly ($p<0.05$) lower activation across ROIs and stimulus types compared to the DC group. Additionally, higher propofol concentrations were associated with reduced brain activation. No significant interactions between group, stimulus type, or ROI were found - see SI 3.6.5 for summary of model coefficients and p-values.

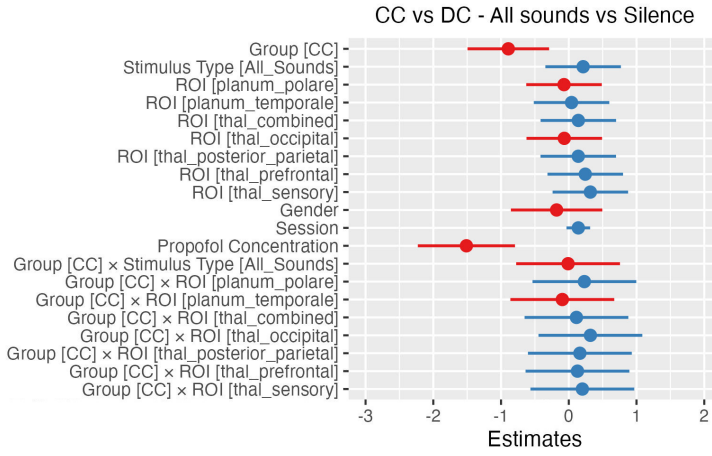

Figure 3.19: See next page.

[8]This means that, if the CC group shows a decrease in activation in the HG relative to the awake group, the e.g., planum polare shows a lesser decrease (or an increase) when comparing the CC group to the awake group.

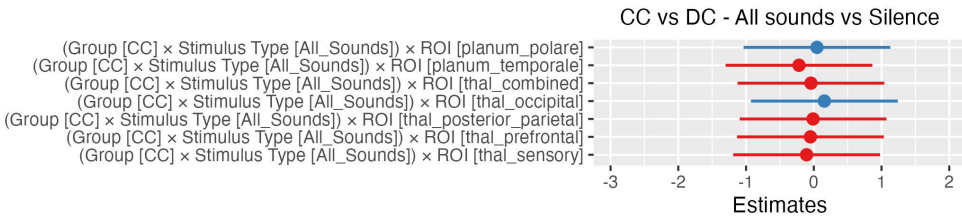

Figure 3.19: ROI activation differences between CC and DC in response to all-sounds vs silence blocks. The plot displays the estimates for the main effects and interaction effects of group (CC vs. DC), stimulus type (all-sounds vs silence), and ROI on brain activity. The DC group, the Heschl's gyrus ROI and the silence blocks were used as baselines. Error bars represent 95% confidence intervals. Red indicates negative estimates, while blue represents positive estimates.

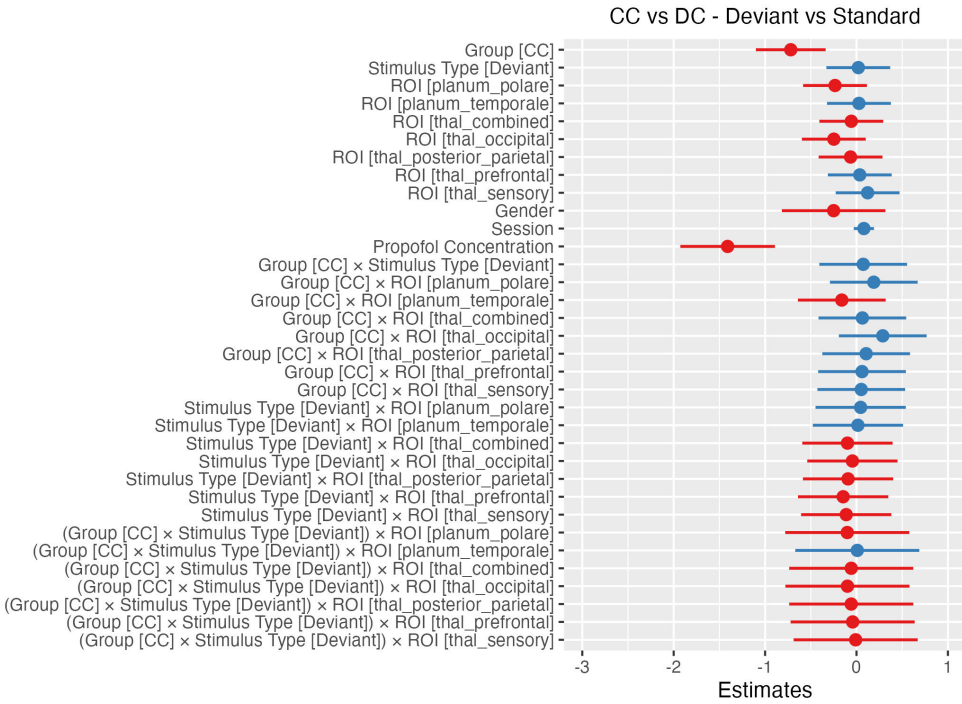

Figure 3.20: ROI activation differences between CC and DC in response to deviant vs standard blocks. The plot displays the estimates for the main effects and interaction effects of group (CC vs. DC), stimulus type (deviant vs standard), and ROI on brain activity. The DC group, the Heschl's gyrus ROI and the standard blocks were used as baselines. Error bars represent 95% confidence intervals. Red indicates negative estimates, while blue represents positive estimates.

3.6.5 ROI model coefficients tables

CC vs Awake model coefficients tables

Table 3.29: Summary of model coefficients and p-values - CC vs Awake - All sounds vs Silence

	Estimate	Std..Error	t.value	p.z
(Intercept)	0.0609393	0.3504612	0.1738831	0.8619573
GroupCC	-0.4239410	0.3643754	-1.1634732	0.2446375
Stimulus_TypeAll_Sounds	1.7103624	0.3924403	4.3582743	0.0000131
ROIplanum_polare	-0.0987717	0.3924403	-0.2516859	0.8012839
ROIplanum_temporale	0.1463996	0.3924403	0.3730494	0.7091117
ROIthal_combined	-0.1834399	0.3924403	-0.4674339	0.6401894
ROIthal_occipital	-0.0369752	0.3924403	-0.0942187	0.9249355
ROIthal_posterior_parietal	-0.0737975	0.3924403	-0.1880478	0.8508392
ROIthal_prefrontal	-0.1549766	0.3924403	-0.3949050	0.6929130
ROIthal_sensory	0.0260351	0.3924403	0.0663415	0.9471060
Gender	0.0400464	0.1416929	0.2826281	0.7774620
GroupCC:Stimulus_TypeAll_Sounds	-1.5088269	0.5150130	-2.9296871	0.0033930
GroupCC:ROIplanum_polare	0.2585516	0.5150130	0.5020293	0.6156469
GroupCC:ROIplanum_temporale	-0.2007428	0.5150130	-0.3897821	0.6966977
GroupCC:ROIthal_combined	0.4377982	0.5150130	0.8500721	0.3952850
GroupCC:ROIthal_occipital	0.2900459	0.5150130	0.5631818	0.5733111
GroupCC:ROIthal_posterior_parietal	0.3778165	0.5150130	0.7336057	0.4631891
GroupCC:ROIthal_prefrontal	0.5268920	0.5150130	1.0230655	0.3062769
GroupCC:ROIthal_sensory	0.4932629	0.5150130	0.9577679	0.3381798
Stimulus_TypeAll_Sounds:ROIplanum_polare	-1.2799334	0.5549944	-2.3062097	0.0210989
Stimulus_TypeAll_Sounds:ROIplanum_temporale	-0.0658617	0.5549944	-0.1186709	0.9055361
Stimulus_TypeAll_Sounds:ROIthal_combined	-1.8477687	0.5549944	-3.3293467	0.0008705
Stimulus_TypeAll_Sounds:ROIthal_occipital	-1.6556756	0.5549944	-2.9832296	0.0028522
Stimulus_TypeAll_Sounds:ROIthal_posterior_parietal	-1.7091581	0.5549944	-3.0795953	0.0020728
Stimulus_TypeAll_Sounds:ROIthal_prefrontal	-1.8699432	0.5549944	-3.3693012	0.0007536
Stimulus_TypeAll_Sounds:ROIthal_sensory	-1.6709592	0.5549944	-3.0107678	0.0026059
GroupCC:Stimulus_TypeAll_Sounds:ROIplanum_polare	0.9726180	0.7283383	1.3353931	0.1817477
GroupCC:Stimulus_TypeAll_Sounds:ROIplanum_temporale	-0.1244566	0.7283383	-0.1708774	0.8643202
GroupCC:Stimulus_TypeAll_Sounds:ROIthal_combined	1.4523416	0.7283383	1.9940480	0.0461468
GroupCC:Stimulus_TypeAll_Sounds:ROIthal_occipital	1.3373765	0.7283383	1.8362022	0.0663278
GroupCC:Stimulus_TypeAll_Sounds:ROIthal_posterior_parietal	1.3363743	0.7283383	1.8348263	0.0665314
GroupCC:Stimulus_TypeAll_Sounds:ROIthal_prefrontal	1.5022637	0.7283383	2.0625904	0.0391516
GroupCC:Stimulus_TypeAll_Sounds:ROIthal_sensory	1.3779346	0.7283383	1.8918881	0.0585059

Table 3.30: Summary of model coefficients and p-values - CC vs Awake - Deviant vs Standard sounds

	Estimate	Std..Error	t.value	p.z
(Intercept)	0.7672909	0.2388786	3.2120541	0.0013179
GroupCC	-0.9156633	0.2359251	-3.8811614	0.0001040
Stimulus_TypeDeviant	0.1877392	0.2540770	0.7389067	0.4599637
ROIplanum_polare	-0.7028090	0.2540770	-2.7661263	0.0056727
ROIplanum_temporale	0.0805823	0.2540770	0.3171569	0.7511246

Table 3.30: (Ctd.) Summary of model coefficients and p-values - CC vs Awake - Deviant vs Standard sounds

	Estimate	Std..Error	t.value	p.z
ROIthal_combined	-0.9664044	0.2540770	-3.8035891	0.0001426
ROIthal_occipital	-0.7858016	0.2540770	-3.0927698	0.0019830
ROIthal_posterior_parietal	-0.8429328	0.2540770	-3.3176275	0.0009079
ROIthal_prefrontal	-0.9596603	0.2540770	-3.7770454	0.0001587
ROIthal_sensory	-0.7321045	0.2540770	-2.8814278	0.0039588
Gender	0.0367798	0.1037144	0.3546259	0.7228699
GroupCC:Stimulus_TypeDeviant	-0.0943648	0.3334340	-0.2830089	0.7771700
GroupCC:ROIplanum_polare	0.6569706	0.3334340	1.9703166	0.0488021
GroupCC:ROIplanum_temporale	-0.2149588	0.3334340	-0.6446818	0.5191334
GroupCC:ROIthal_combined	0.9739855	0.3334340	2.9210740	0.0034883
GroupCC:ROIthal_occipital	0.8251203	0.3334340	2.4746134	0.0133380
GroupCC:ROIthal_posterior_parietal	0.8835849	0.3334340	2.6499543	0.0080503
GroupCC:ROIthal_prefrontal	1.0558750	0.3334340	3.1666682	0.0015420
GroupCC:ROIthal_sensory	0.9061008	0.3334340	2.7174816	0.0065781
Stimulus_TypeDeviant:ROIplanum_polare	0.0269128	0.3593191	0.0748994	0.9402947
Stimulus_TypeDeviant:ROIplanum_temporale	-0.0806268	0.3593191	-0.2243876	0.8224557
Stimulus_TypeDeviant:ROIthal_combined	-0.0983998	0.3593191	-0.2738507	0.7841993
Stimulus_TypeDeviant:ROIthal_occipital	-0.1210477	0.3593191	-0.3368809	0.7362067
Stimulus_TypeDeviant:ROIthal_posterior_parietal	-0.0970902	0.3593191	-0.2702061	0.7870017
Stimulus_TypeDeviant:ROIthal_prefrontal	-0.1055993	0.3593191	-0.2938873	0.7688440
Stimulus_TypeDeviant:ROIthal_sensory	-0.1807152	0.3593191	-0.5029380	0.6150078
GroupCC:Stimulus_TypeDeviant:ROIplanum_polare	-0.0827715	0.4715469	-0.1755319	0.8606617
GroupCC:Stimulus_TypeDeviant:ROIplanum_temporale	0.1047184	0.4715469	0.2220743	0.8242561
GroupCC:Stimulus_TypeDeviant:ROIthal_combined	-0.0578312	0.4715469	-0.1226414	0.9023910
GroupCC:Stimulus_TypeDeviant:ROIthal_occipital	-0.0228180	0.4715469	-0.0483898	0.9614056
GroupCC:Stimulus_TypeDeviant:ROIthal_posterior_parietal	-0.0529789	0.4715469	-0.1123512	0.9105449
GroupCC:Stimulus_TypeDeviant:ROIthal_prefrontal	-0.0825941	0.4715469	-0.1751557	0.8609573
GroupCC:Stimulus_TypeDeviant:ROIthal_sensory	0.0589959	0.4715469	0.1251114	0.9004353

CC vs DC model coefficients tables

Table 3.31: Summary of model coefficients and p-values - CC vs DC - All sounds vs Silence

	Estimate	Std..Error	t.value	p.z
(Intercept)	2.5357023	1.0608482	2.3902594	0.0168365
GroupDC_impure	0.9031883	0.3063346	2.9483718	0.0031945
Stimulus_TypeSilence	-0.2015355	0.2676020	-0.7531167	0.4513798
ROIplanum_polare	-0.1475355	0.2676020	-0.5513244	0.5814113
ROIplanum_temporale	-0.2446615	0.2676020	-0.9142737	0.3605731
ROIthal_combined	-0.1410688	0.2676020	-0.5271591	0.5980831
ROIthal_occipital	-0.0652284	0.2676020	-0.2437515	0.8074233
ROIthal_posterior_parietal	-0.0687648	0.2676020	-0.2569667	0.7972044
ROIthal_prefrontal	0.0042358	0.2676020	0.0158289	0.9873709
ROIthal_sensory	0.2262734	0.2676020	0.8455594	0.3977986
Gender	-0.1799137	0.3435080	-0.5237540	0.6004496
Session	0.1407728	0.0889275	1.5830068	0.1134199
Propofol_Concentration	-1.5113376	0.3650788	-4.1397568	0.0000348
GroupDC_impure:Stimulus_TypeSilence	-0.0103816	0.3900936	-0.0266130	0.9787684
GroupDC_impure:ROIplanum_polare	-0.2771120	0.3900936	-0.7103730	0.4774729

Table 3.31: (Ctd.) Summary of model coefficients and p-values - CC vs DC - All sounds vs Silence

	Estimate	Std..Error	t.value	p.z
GroupDC_impure:ROIplanum_temporale	0.3133295	0.3900936	0.8032162	0.4218498
GroupDC_impure:ROIthal_combined	-0.0713585	0.3900936	-0.1829265	0.8548557
GroupDC_impure:ROIthal_occipital	-0.4755904	0.3900936	-1.2191700	0.2227797
GroupDC_impure:ROIthal_posterior_parietal	-0.1535887	0.3900936	-0.3937228	0.6937857
GroupDC_impure:ROIthal_prefrontal	-0.0788755	0.3900936	-0.2021963	0.8397633
GroupDC_impure:ROIthal_sensory	-0.0949201	0.3900936	-0.2433265	0.8077525
Stimulus_TypeSilence:ROIplanum_polare	0.3073154	0.3784464	0.8120448	0.4167659
Stimulus_TypeSilence:ROIplanum_temporale	0.1903183	0.3784464	0.5028936	0.6150391
Stimulus_TypeSilence:ROIthal_combined	0.3954271	0.3784464	1.0448696	0.2960832
Stimulus_TypeSilence:ROIthal_occipital	0.3182991	0.3784464	0.8410680	0.4003098
Stimulus_TypeSilence:ROIthal_posterior_parietal	0.3727837	0.3784464	0.9850371	0.3246058
Stimulus_TypeSilence:ROIthal_prefrontal	0.3676795	0.3784464	0.9715499	0.3312745
Stimulus_TypeSilence:ROIthal_sensory	0.2930245	0.3784464	0.7742829	0.4387635
GroupDC_impure:Stimulus_TypeSilence:ROIplanum_polare	0.0469163	0.5516757	0.0850433	0.9322270
GroupDC_impure:Stimulus_TypeSilence:ROIplanum_temporale	-0.2180983	0.5516757	-0.3953380	0.6925935
GroupDC_impure:Stimulus_TypeSilence:ROIthal_combined	-0.0418855	0.5516757	-0.0759242	0.9394794
GroupDC_impure:Stimulus_TypeSilence:ROIthal_occipital	0.1561879	0.5516757	0.2831155	0.7770883
GroupDC_impure:Stimulus_TypeSilence:ROIthal_posterior_parietal	-0.0102853	0.5516757	-0.0186438	0.9851252
GroupDC_impure:Stimulus_TypeSilence:ROIthal_prefrontal	-0.0494811	0.5516757	-0.0896924	0.9285317
GroupDC_impure:Stimulus_TypeSilence:ROIthal_sensory	-0.1058290	0.5516757	-0.1918319	0.8478738

Table 3.32: Summary of model coefficients and p-values - CC vs DC - Deviant vs Standard sounds

	Estimate	Std..Error	t.value	p.z
(Intercept)	2.7493186	0.7916770	3.4727779	0.0005151
GroupDC_impure	0.6455956	0.1942821	3.3229808	0.0008906
Stimulus_TypeStandard	-0.0933744	0.1675923	-0.5571520	0.5774236
ROIplanum_polare	-0.1016971	0.1675923	-0.6068127	0.5439752
ROIplanum_temporale	-0.1102849	0.1675923	-0.6580546	0.5105031
ROIthal_combined	-0.1486500	0.1675923	-0.8869736	0.3750931
ROIthal_occipital	-0.1045471	0.1675923	-0.6238180	0.5327471
ROIthal_posterior_parietal	-0.1094169	0.1675923	-0.6528756	0.5138365
ROIthal_prefrontal	-0.0919788	0.1675923	-0.5488247	0.5831257
ROIthal_sensory	0.0522770	0.1675923	0.3119296	0.7550941
Gender	-0.2503379	0.2882058	-0.8686080	0.3850616
Session	0.0806208	0.0563419	1.4309195	0.1524533
Propofol_Concentration	-1.4097416	0.2634649	-5.3507755	0.0000001
GroupDC_impure:Stimulus_TypeStandard	0.0735302	0.2443057	0.3009762	0.7634326
GroupDC_impure:ROIplanum_polare	-0.0879884	0.2443057	-0.3601568	0.7187299
GroupDC_impure:ROIplanum_temporale	0.1523363	0.2443057	0.6235481	0.5329244
GroupDC_impure:ROIthal_combined	-0.0069143	0.2443057	-0.0283017	0.9774215
GroupDC_impure:ROIthal_occipital	-0.1883021	0.2443057	-0.7707645	0.4408465
GroupDC_impure:ROIthal_posterior_parietal	-0.0480433	0.2443057	-0.1966524	0.8440995
GroupDC_impure:ROIthal_prefrontal	-0.0183752	0.2443057	-0.0752139	0.9400445
GroupDC_impure:ROIthal_sensory	-0.0428060	0.2443057	-0.1752148	0.8609109
Stimulus_TypeStandard:ROIplanum_polare	0.0558587	0.2370113	0.2356795	0.8136814
Stimulus_TypeStandard:ROIplanum_temporale	-0.0240917	0.2370113	-0.1016478	0.9190362
Stimulus_TypeStandard:ROIthal_combined	0.1562310	0.2370113	0.6591710	0.5097860
Stimulus_TypeStandard:ROIthal_occipital	0.1438658	0.2370113	0.6069996	0.5438512

Table 3.32: (Ctd.) Summary of model coefficients and p-values - CC vs DC - Deviant vs Standard sounds

	Estimate	Std..Error	t.value	p.z
Stimulus_TypeStandard:ROIthal_posterior_parietal	0.1500691	0.2370113	0.6331727	0.5266209
Stimulus_TypeStandard:ROIthal_prefrontal	0.1881935	0.2370113	0.7940273	0.4271795
Stimulus_TypeStandard:ROIthal_sensory	0.1217193	0.2370113	0.5135592	0.6075602
GroupDC_impure:Stimulus_TypeStandard:ROIplanum_polare	-0.1011352	0.3455004	-0.2927208	0.7697355
GroupDC_impure:Stimulus_TypeStandard:ROIplanum_temporale	0.0086568	0.3455004	0.0250557	0.9800105
GroupDC_impure:Stimulus_TypeStandard:ROIthal_combined	-0.0575299	0.3455004	-0.1665118	0.8677542
GroupDC_impure:Stimulus_TypeStandard:ROIthal_occipital	-0.0989862	0.3455004	-0.2865008	0.7744946
GroupDC_impure:Stimulus_TypeStandard:ROIthal_posterior_parietal	-0.0575022	0.3455004	-0.1664316	0.8678173
GroupDC_impure:Stimulus_TypeStandard:ROIthal_prefrontal	-0.0421251	0.3455004	-0.1219250	0.9029584
GroupDC_impure:Stimulus_TypeStandard:ROIthal_sensory	-0.0093082	0.3455004	-0.0269411	0.9785067

Chapter 4
Conclusions

Ticket thrown away before not leaving
If I don't come home,
I want you to know that I never
left.
My travels
have all been staying
right here, where I never was.

Giorgio Caproni

4.1 Summary of research

The present work aimed to uncover the neural underpinnings of sensory disconnection during sleep and propofol sedation, employing EEG and fMRI, respectively. In both investigations, participants were exposed to an auditory oddball paradigm and subsequently awakened for questioning about their experience immediately prior to awakening. The ensuing reports enabled the classification of participants into two distinct groups: CC participants, who reported being conscious[1] (dreaming or dream-like experiences) and hearing sounds before awakening, and DC participants, who reported no conscious experience or perception of sounds prior to awakening. Notably, both CC and DC participants were in the same physiological state, either stable REM

[1] In the REM study, a specific question regarding conscious experience was not asked. However, it is well-established that dreaming almost always occurs during REM, with fewer than 5% of participants reporting no experience when awakened from REM. See section 2.5.5 for further discussion.

sleep or propofol sedation with comparable propofol concentrations[2]. This design allowed us to investigate sensory disconnection within the same state, minimizing biases associated with between-state comparisons. Additionally, in both studies, brain activity was recorded during wakefulness while participants were presented with an auditory oddball paradigm. By contrasting brain activity of CC participants with their brain activity while awake we were able to assess the impact of physiological state on CC. Our findings revealed distinct neural signatures of sensory (dis)connection which were largely consistent across the two studies.

During REM sleep, scalp-level differences emerged in the processing of both standard and deviant sounds between CC and DC states. Specifically, CC participants exhibited an increased positivity in the ERP response to deviant tones at ∼280 ms and increased negativity to standard tones at ∼154 ms, compared to DC participants. These findings suggest that both standard and deviant sounds were processed differently in these two states. The 154 ms component found in CC closely resembled the auditory awareness negativity, an increasingly recognized physiological correlate of sensory connection, indicating that the observed differences in deviant perception between the two states may be rooted in the absence of conscious perception of standard sounds during DC. Power analyses revealed decreased delta (1–4 Hz) power in CC relative to DC participants, corroborating previous findings implicating SWA in inducing DC states (Andrillon & Kouider, 2020; Funk et al., 2016). These scalp-level differences were found to be grounded in different connectivity profiles between CC and DC. In response to deviant sounds, CC participants exhibited increased feedback and feedforward connectivity within a temporo-parietal loop relative to DC, encompassing the Inferior Parietal Lobule (IPL) and Superior Temporal Gyrus (STG). When contrasting the brain activity of CC participants with their activity during wakefulness, differences were observed only in the processing of deviant sounds, suggesting similar processing (and possibly suppression) of standard sounds. During wakefulness, deviant tones elicited an increased positivity ∼246 ms after presentation compared to CC. This scalp difference in deviant processing was traced to a distinct circuit, with increased feedback and feedforward connectivity within a fronto-parietal loop during wakefulness compared to CC, involving the Inferior Frontal Gyrus (IFG) and IPL.

Under propofol sedation, we found unexpected increases in activation in

[2]There was no statistically significant difference in propofol concentrations between the CC and DC groups.

DC participants compared to CC in response to all-sound blocks, primarily in temporal and pre-/post-central regions. In contrast, CC participants showed broad reductions in activity accompanied by focused increases in the precuneus and a network that included the middle cingulate/paracingulate gyri, prefrontal regions, hippocampal gyrus, and middle occipital gyrus. This paradoxical pattern in DC participants reversed for deviant blocks, where CC participants exhibited widespread activation increases, while DC participants showed minimal changes from their response to standard/all-sound blocks, suggesting that deviant detection may only occur during CC. Spectral analysis of BOLD oscillations revealed heightened high-frequency oscillation power in sensory, attention-related and visual regions, in DC relative to CC participants, potentially indicating greater SWA in these regions. Interestingly, the observed differences between CC and wakefulness were restricted to all-sounds/standard blocks, with no differences observed in response to deviant sounds, suggesting that CC-sedation and wakeful states may share similar mechanisms for processing deviant stimuli.

To the best of our knowledge, this work represents the first investigation of the sensory gating mechanisms underlying auditory disconnection within-state, distinguishing between CC and DC through the collection of subjective reports. By leveraging the spatial precision of fMRI and the temporal accuracy of EEG (albeit acquired non-simultaneously), this work offers a comprehensive temporal and spatial characterization of the sensory gating mechanisms underlying auditory disconnection. Additionally, it examines sensory disconnection in two distinct physiological states of DC - REM sleep and propofol sedation — enhancing the generalizability of these findings across sleep and anesthesia. In the following sections, we will discuss potential discrepancies and commonalities between the two studies and discuss whether they converge on a neural signature of DC that could have potential clinical applications.

4.2 Potential conflicting evidence and possible explanations

4.2.1 Widespread activity increases in DC-sedation and reduced ERP components in DC-REM to standard sounds

A prominent pattern observed in sedated DC participants was the widespread increase in activation in response to all-sounds/standard blocks compared

to CC participants, who instead exhibited more localized activations in key regions associated with auditory processing. These widespread increases in DC were interpreted as indicative of a disrupted EIB (see sec. 3.5.1), coupled with increased prediction error signaling due to a mismatch between feedforward and feedback information. In contrast to these widespread activations, during REM sleep, DC participants displayed reduced amplitudes in ERP components. At first glance, these findings might appear contradictory. If the EIB disruption and increased feedforward error propagation account for the DC-sedation findings, should we not expect to observe similar increases in component amplitudes during DC-REM as well?

The apparent discrepancy between these findings can be potentially resolved by considering the different temporal resolutions of these studies. In the REM study, time-locked activity to deviant and standard sounds was analyzed at a 400-ms resolution, while in the propofol study, we analyzed blocks of deviant and standard tones, each lasting 45 sec. The widespread activation observed in DC-sedation, if reflecting EIB disruption and feedforward error propagation, was likely too unstructured to generate coherent ERP peaks at a millisecond scale. Indeed, in the within-DC-REM results (sec. 2.4), no coherent ERP peaks were observed, and the waveforms exhibited a poor signal-to-noise ratio. Over longer time periods, however, this disorganized activity accumulated and manifested as widespread BOLD activation. Therefore, the increased excitability in DC-sedation would seem to align with the decreased amplitude or absence of ERP components found during DC-REM.

Nonetheless, future analyses could enhance the comparability between the REM and propofol studies. For instance, trial-related BOLD activity could be examined. As described in section 3.2.5, we used a mixed block/event-related design, allowing for the simultaneous modeling of transient, trial-related activity, and sustained, block-related activity. In this study, as discussed in sec. 3.3, we focused on block-related activity. Analyzing trial-related activity would provide higher temporal resolution, although it would still not match the finer temporal scale of the REM study due to the 0.842-sec MRI repetition time. Nevertheless, this approach could improve the comparability with the REM study and potentially clarify whether the widespread activations observed in response to all-sounds *blocks* persist at the *trial* level. Finally, DCM of block- or trial-related BOLD activity could clarify the underlying causal architecture, if any, of the widespread activations observed in DC-propofol. This analysis could determine whether these activations merely reflect disorganized activity, as hypothesised, or are supported by coherent

causal networks.

4.2.2 No difference between CC and DC in response to all sounds during REM, but clear differences during sedation

During REM we found no significant differences between CC and DC states when we compared ERP responses to standard and deviant tones pooled together (i.e., all sounds). However, during sedation clear differences emerged between CC and DC in response to all-sounds blocks.

A possible explanation for this discrepancy may arise from the distinct nature of EEG and MRI signals. EEG records the summation of excitatory and inhibitory postsynaptic potentials from large groups of neurons firing synchronously. The ERP, in particular, reflects time-locked EEG activity in response to stimuli, in our case within a relatively short time window of about 400 ms. In contrast, the BOLD signal reflects changes in blood oxygenation, which are indirectly linked to neuronal activity. The BOLD signal results in a more spatially extensive and sustained measure of brain activity, capturing responses across a vast number of voxels - in our study covering the entire brain - on the scale of seconds.

Pooling ERP responses time-locked to standard and deviant tones could have caused the cancellation of effects if the responses exhibited peaks of opposite polarities at similar time points, resulting in the overall effect being averaged out. Alternatively, greater variability in response amplitude and latency across the two conditions may contribute to this effect: when these responses are averaged together, any misalignment in peak latencies could lead to a reduction in the apparent signal, effectively diminishing the observable difference between the conditions. In contrast, in the sedation study, the large number of voxels increases the number of data points, which in turn raises the probability of detecting persistent differences between CC and DC. Even if some voxel responses cancelled each other out when summing standard and deviant blocks (e.g., one voxel with a value of +1.4 and another with -1.4), the sheer number of voxels makes it unlikely that such cancellation would occur consistently across the entire brain. This might have reduced the likelihood of uniform cancellation and increased the chances that any significant effect could 'survive' when pooling standard and deviant blocks together in the propofol experiment.

4.2.3 Differences in deviant processing between CC-REM and wakefulness but no difference between CC-sedation and wakefulness

Our analysis of deviant responses revealed significant differences in both ERP activity and effective connectivity between CC during REM sleep and wakefulness. However, we observed no significant differences between CC during sedation and wakefulness. Several potential explanations may account for these findings.

One plausible explanation lies in the distinct mechanisms of action between propofol sedation and REM sleep. REM sleep is characterized by region-specific increases and decreases in brain activity. While regions such as the thalamus, amygdala, hippocampus, anterior cingulate cortex, and temporo-occipital areas show heightened activity during REM compared to wakefulness, the prefrontal cortex, precuneus, posterior cingulate gyrus, and inferior parietal cortex exhibit decreased activity (Braun et al., 1997; Dang-Vu et al., 2010; Maquet, 2000; Maquet et al., 2005; Nofzinger et al., 1997; Y. Wang et al., 2022). Propofol, at the sedative concentrations used in this study, has been reported to depress activity in several regions similar to REM, including the thalamus, precuneus, and posterior cingulate cortex, as well as the orbitofrontal gyri and the right angular gyrus (Fiset et al., 1999; Saxena et al., 2019; H. Zhang et al., 2010). However, unlike REM, which primarily depresses the fronto-parietal cortex (Dang-Vu et al., 2010; Y. Wang et al., 2022), propofol sedation appears to predominantly suppress activity in the parieto-occipital cortex (Fiset et al., 1999). Given that deviant sound processing typically involves the recruitment of frontal regions (Calhoun et al., 2006; Kiehl et al., 2005; Stevens et al., 2000), the greater suppression of these areas during REM compared to propofol sedation may explain the observed differences in ERP responses between CC-REM and wakefulness and the absence of differences between sedation and wakefulness in the voxel-wise activation analysis.[3]

Another consideration is that the observed differences in fronto-parietal circuit connectivity strength between CC-REM and wakefulness reflect changes in effective connectivity. The lack of observable differences between CC-propofol and wakefulness at the voxel-wise activation level does not necessarily indicate an absence of differences in the underlying causal architecture.

[3]Unfortunately, direct comparisons of brain activity during propofol sedation and REM sleep remain scarce.

Propofol may still induce disconnection between brain regions involved in deviant detection, but these changes may not be detectable in voxel-wise activation analyses. Effective connectivity, on the other hand, may capture such alterations in network dynamics.

Finally, the different temporal scale of the two studies, as discussed in sec. 4.2.1, may also contribute to these conflicting findings. Differences in deviant processing between CC states and wakefulness might be more detectable in ERP measures, where millisecond-level temporal changes can be detected.

4.3 Convergent evidence and shared signatures of sensory disconnection

4.3.1 Detection of local irregularities as a sign of sensory connection in both REM sleep and propofol anesthesia

Detection of local irregularities emerged as a specific signature of sensory connection during both REM sleep and propofol anesthesia. During REM, several findings suggested that deviant detection occurred in CC participants but not in DC. At the scalp level, CC participants exhibited increased positivity in the ERP response to deviant tones at $\sim$280 ms compared to DC. Within-group analyses revealed differential processing of standard and deviant sounds as early as at 64 ms in CC participants, whereas no differences between standard and deviant waveforms were observed in DC. The modeling analysis further revealed increased connectivity in the IPL-STG loop in response to deviant sounds in CC compared to DC participants, who also exhibited decreased connectivity strength from the primary auditory cortex to the STG. The enhanced amplitude of ERP components to deviant sounds in CC, in conjunction with the disconnection of key regions involved in processing auditory irregularities in DC - regions that were also found to be engaged in deviant processing during wakefulness - would seem to strongly suggest that DC participants were not detecting deviant sounds.

Similarly, during propofol anesthesia, DC participants showed almost no differential processing of standard and deviant blocks. While they exhibited widespread, non-organized activity increases in response to all-sounds and standard blocks, specific activation in response to deviant blocks was minimal or absent. Conversely, CC participants, who relied on a distinct fronto-occipital-parietal network for processing standard sounds, recruited additional network components (such as the fusiform gyrus, the SMA, frontal

and prefrontal areas, and the right angular gyrus) in response to deviant sounds. These additional components appeared to be part of the network used during wakefulness for deviant processing. Indeed, when comparing brain activity in response to deviant blocks between CC and wakefulness, no significant differences were found, indicating a similar neural signature of deviant detection in CC and awake participants.

Taken together, these findings seem to suggest that the detection of local irregularities is a defining feature of CC states during both REM sleep and propofol anesthesia.

4.3.2 Converging on gating mechanisms at play during DC states

The two present studies appear to converge on the gating mechanisms operative during DC states, refining and complementing each other's findings.

Both experiments support a potential involvement of a cortical gate during DC states. In the REM experiment, this conclusion was based on the observed decrease in effective connectivity between the primary auditory cortex and higher-order regions (such as the STG) in DC, along with increased delta power in DC compared to CC (sec. 2.7-2.10). We inferred that SWA may have prevented sensory stimuli from further propagating within the cortical hierarchy. During sedation, these findings were preliminary confirmed and complemented by the observed increased high-frequency BOLDoscillation power in sensory and attention-related regions in DC relative to CC. Notably, emerging evidence suggests that high-frequency BOLD oscillations correlate with SWA and may serve a similar role in inducing sensory disconnection (Song et al., 2022). However, we also found signs of increased excitability and/or error signaling during DC, suggesting that, during propofol sedation, this cortical gate may not solely be driven by high-frequency BOLD oscillations but also by disruption of EIB. This disruption could impede information flow to higher cortical areas by altering functional connectivity due to increased excitability.

Finally, as previously mentioned in sections 2.5.3 and 3.5.6, exploring other hypotheses on sensory disconnection mechanisms, such as the informational gating hypothesis, would require more detailed questioning about mental activity upon awakening.

4.4 Men are more likely to be connected during sleep: debunking anecdotal evidence?

In the REM study, we found that men were more likely to be CC compared to women. At first glance, this result may seem to contradict the common anecdotal belief that women are more likely to be CC due to biological factors related to childcare. However, the increased connectedness observed in men aligns with current empirical evidence from gender studies on sleep.

Research has consistently shown that women are more prone to insomnia, sleep disturbances, frequent awakenings, prolonged wakefulness during the night, and generally poorer self-reported sleep quality (Mawhinney et al., 2012; Perger et al., 2024). This evidence suggests that women are more likely to experience nighttime arousals and, one might infer, are also more easily disturbed by external stimuli, making them more prone to being CC. However, it is important to note that participants in the REM experiment were screened for sleep disorders, and those with any such condition were excluded. Moreover, our study only considered data acquired during stable REM sleep, with recordings containing brief arousals being discarded. Thus, the increased likelihood of sleep disturbances in women compared to men had likely no impact in our study.

A potential explanation for the observed gender difference, albeit remains speculative, lies in the differing polysomnographic characteristics of sleep in men and women. Research has shown that women have higher spindle density and higher spindle peak frequencies compared to men (Gaillard & Blois, 1981; Lok et al., 2024; Ujma et al., 2014). Additionally, higher SWA in temporal regions has been reported in women relative to men, although this study was conducted on a cohort of adolescents (Huupponen et al., 2002; Markovic et al., 2020). Since both spindles and SWA are widely regarded as sensory gating mechanisms (Bandarabadi et al., 2020; Funk et al., 2016), it is plausible that women, during stable sleep, are less likely to incorporate external stimuli into their ongoing experience. Supporting this, a study exposing both men and women to noise found that men's sleep duration was reduced by 1.5 hours, while women's sleep duration was unaffected by the noise (Röösli et al., 2014).

Nevertheless, the common knowledge that women are more likely to hear a crying baby may still hold, potentially reflecting a highly selective process that is fine-tuned to allow only specific meaningful stimuli to be

detected, such as an infant's cry. Several studies have indeed shown sex differences in the processing of infants' faces and cries. For instance, (K. Zhang et al., 2022) found that when men and women were exposed to infants' faces, rs-fMRI activity of women shows increased activation in emotional networks linked to empathy relative to men. Similarly, (Pisapia et al., 2013) reported that women tend to interrupt mind-wandering when exposed to infant hunger cries, while men tend to continue uninterrupted. Consistent with our findings, these results suggest that women may generally be more disconnected than men during sleep due to higher spindle density and SWA levels. However, this pattern could potentially reverse for certain stimuli to which the brain is primed to respond rapidly - although direct empirical evidence from neuroimaging or behavioral studies is currently lacking to validate this stimulus-specific responsiveness. It is important to emphasized that, to date, our interpretation of the observed higher rate of CC in males remains largely speculative.

The absence of a gender difference in the rate of CC in the propofol study may instead be explained by our experimental design, which carefully controlled for participants reaching the same unresponsive, dream-like state using a continuous behavioral task. It is well known that women generally require higher propofol concentrations than men due to factors such as higher clearance rates, faster metabolization, and/or a smaller volume of distribution[4] (Gan et al., 1999; Glass et al., 1997; Mawhinney et al., 2012; D. S. Ward et al., 2002). Additional contributing factors include various pharmacokinetic and pharmacodynamic differences between sexes. From a pharmacokinetic perspective, higher estrogen levels in women, particularly during the follicular phase of the menstrual cycle, may lead to increased protein binding of anesthetic agents, which in turn significantly affects drug bioavailability (Buchanan et al., 2009). The increased binding may, in fact, effectively reduce the free fraction of drugs available in the bloodstream. Furthermore, there are potential sex-based variations in enzymatic activity, which influences the metabolism of many anesthetic drugs, though the evidence remains to date inconclusive (Buchanan et al., 2009).

The potential interplay between these various factors results in an increased likelihood of intraoperative awareness in women compared to men, as reported in multiple studies (Adamus et al., 2008; Gan et al., 1999; Mawhinney et al., 2012; Sandin et al., 2000). Based on these findings, one might expect

[4]Volume of distribution refers to the ratio of the plasma concentration to the total amount of drug in the body.

women to exhibit higher rates of CC than men. However, in our study, the dosage of propofol was individually adjusted to ensure that both men and women reached the same behavioral endpoint. As a result, differences in propofol concentrations requirements were likely accounted for across genders, neutralizing gender-based differences in metabolism and required dosage. Once these factors are controlled for, it is possible that no inherent gender difference exists in the likelihood of experiencing connected consciousness under sedation.

4.5 Future directions

The current work represents one of the first proofs of concept demonstrating that differential sound processing occurs between self-reported CC and DC participants within the same physiological state. Our investigation of the neural correlates of sensory disconnection, in both REM sleep and propofol sedation, has yielded distinct signatures of CC that may hold promise for clinical translation, with potential applications in anesthesia monitoring and the diagnosis of patients with DoC.

In the context of anesthesia, current monitoring practices typically assess consciousness by tracking end-tidal anesthetic concentration — reflecting the concentration of anesthetic in the patient's exhaled breath at the end of expiration; physiological responses to surgical stimuli such as heart rate, blood pressure, and purposeful movements (Bullard et al., 2023); and through analyses of raw EEG data, such as the Bispectral Index monitor, which decomposes the EEG into different frequency bands, yielding a single value whose range is associated with various depths of anesthesia (Mathur et al., 2023). However, as discussed in section 1.3, these measures often miss episodes of intraoperative awareness. While they are intended to provide a general index of the state of consciousness, they do not offer any insight into the patient's level of CC, which could be more critical for effective anesthesia management. Our findings, validating a neural signature of CC in healthy participants, could pave the way for novel monitoring strategies that tackle the issue of intraoperative awareness from a different angle. For example, during surgical procedures, oddball sensory evoked potentials could be periodically employed to stimulate the patient and analyze her brain's response, with a focus on early components time-locked to deviant stimuli. The patterns observed in DC participants could serve as a baseline, with deviations from these patterns indicating the re-establishment of sensory connection and a

potential need to adjust the depth of anesthesia.

Similarly, the behavioral diagnosis of DoC patients (see Box 1.1) is typically complemented by neuroimaging measures aimed at assessing the general state of consciousness, such as brain metabolism preservation (Thibaut et al., 2021). However, while informative, these measures do not provide insight into the level of sensory connection in these patients. Sensory paradigms, such as the local-global paradigm (Bekinschtein et al., 2009) or responses to emotionally or semantically significant stimuli, are occasionally employed — primarily in university hospitals — for diagnosing DoC patients. Yet, they often lack a clear validation of the expected response in the healthy population. This study builds on these efforts by validating a neural signature of CC in healthy controls, offering a benchmark for comparison in more challenging clinical cases. Specifically, our findings suggest that early components in response to deviant stimuli should be prioritized over late components such as the P3 when assessing sensory connection. This study could serve as a proof-of-concept, providing a foundation for further research aimed at developing diagnostic tools specifically designed to quantify sensory connection in DoC patients, rather than focusing solely on their state of consciousness. By placing emphasis on sensory connection, we may gain a deeper understanding of these patients' lived experiences. An understanding of their level of CC brings us closer to answering the fundamental question "what is it like to be in an MCS?" (Gosseries et al., 2014), ultimately enhancing the quality of care provided to these vulnerable patients.

Bibliography

Adamus, M., Gabrhelik, T., & Marek, O. (2008). Influence of gender on the course of neuromuscular block following a single bolus dose of cisatracurium or rocuronium. *European journal of anaesthesiology*, *25*, 589–595. https://doi.org/10.1017/S026502150800402X

Alkire, M. T., Hudetz, A. G., & Tononi, G. (2008). Consciousness and anesthesia. *Science*, *322*, 876–880. https://doi.org/10.1126/SCIENCE.1149213

Alqurashi, Y., Dawidziuk, A., Alqarni, A., Kelly, J., Moss, J., Polkey, M., & Morrell, M. (2021). A visual analog scale for the assessment of mild sleepiness in patients with obstructive sleep apnea and healthy participants. *Annals of Thoracic Medicine*, *16*, 141. https://doi.org/10.4103/ATM.ATM_437_20

American Academy of Sleep Medicine. (2020). *The aasm manual for the scoring of sleep and associated events: Summary of updates in version 2.5* [Available from: https://aasm.org/]. American Academy of Sleep Medicine.

Andersson, J. L., Skare, S., & Ashburner, J. (2003). How to correct susceptibility distortions in spin-echo echo-planar images: application to diffusion tensor imaging. *NeuroImage*, *20*, 870–888. https://doi.org/10.1016/S1053-8119(03)00336-7

Andrillon, T., & Kouider, S. (2020). The vigilant sleeper: neural mechanisms of sensory (de)coupling during sleep. *Current Opinion in Physiology*, *15*, 47–59. https://doi.org/10.1016/J.COPHYS.2019.12.002

Aydin, M., Lucia, S., Casella, A., Bello, B. M. D., & Russo, F. D. (2024). Bayesian interpretation of the prefrontal p2 erp component based on stimulus/response mapping uncertainty. *International Journal of Psychophysiology*, *199*. https://doi.org/10.1016/j.ijpsycho.2024.112337

Bahmani, Z., Clark, K., Merrikhi, Y., Mueller, A., Pettine, W., Vanegas, M. I., Moore, T., & Noudoost, B. (2019). Prefrontal contributions to attention and working memory. https://doi.org/10.1007/7854_2018_74

Balsdon, T., & Clifford, C. W. G. (2018). Visual processing: Conscious until proven otherwise. *Royal Society Open Science*, *5*. https://doi.org/10.1098/rsos.171783

Bandarabadi, M., Herrera, C. G., Gent, T. C., Bassetti, C., Schindler, K., & Adamantidis, A. R. (2020). A role for spindles in the onset of rapid eye movement sleep. *Nature Communications 2020 11:1*, *11*, 1–12. https://doi.org/10.1038/s41467-020-19076-2

Banks, M. I., Moran, N. S., Krause, B. M., Grady, S. M., Uhlrich, D. J., & Manning, K. A. (2018). Altered stimulus representation in rat auditory cortex is not causal for loss of consciousness under general anaesthesia. *British Journal of Anaesthesia*, *121*, 605–615. https://doi.org/10.1016/J.BJA.2018.05.054

Bareham, C. A., Georgieva, S. D., Kamke, M. R., Lloyd, D., Bekinschtein, T. A., & Mattingley, J. B. (2018). Role of the right inferior parietal cortex in auditory selective attention: An rTMS study. *Cortex*, *99*, 30–38. https://doi.org/10.1016/J.CORTEX.2017.10.003

Barron, E., Riby, L. M., Greer, J., & Smallwood, J. (2011). Absorbed in thought: The effect of mind wandering on the processing of relevant and irrelevant events. *Psychological Science*, *22*, 596–601. https://doi.org/10.1177/0956797611404083

Bastuji, H., García-Larrea, L., Franc, C., & Mauguière, F. (1995). Brain processing of stimulus deviance during slow-wave and paradoxical sleep: a study of human auditory evoked responses using the oddball paradigm. *Journal of clinical neurophysiology : official publication of the American Electroencephalographic Society*, *12*, 155–167. https://doi.org/10.1097/00004691-199503000-00006

Bates, D., Mächler, M., Bolker, B., & Walker, S. (2015). Fitting Linear Mixed-Effects Models Using lme4. *Journal of Statistical Software*, *67*(1), 1–48. https://doi.org/10.18637/jss.v067.i01

Baudena, P., Halgren, E., Heit, G., & Clarke, J. M. (1995). Intracerebral potentials to rare target and distractor auditory and visual stimuli. iii. frontal cortex. *Electroencephalography and Clinical Neurophysiology*, *94*. https://doi.org/10.1016/0013-4694(95)98476-O

Behrens, T. E., Johansen-Berg, H., Woolrich, M. W., Smith, S. M., Wheeler-Kingshott, C. A., Boulby, P. A., Barker, G. J., Sillery, E. L., Sheehan, K., Ciccarelli, O., Thompson, A. J., Brady, J. M., & Matthews, P. M. (2003).

Non-invasive mapping of connections between human thalamus and cortex using diffusion imaging. *Nature Neuroscience 2003 6:7*, *6*, 750–757. https://doi.org/10.1038/nn1075

Behrens, T. E., Woolrich, M. W., Jenkinson, M., Johansen-Berg, H., Nunes, R. G., Clare, S., Matthews, P. M., Brady, J. M., & Smith, S. M. (2003). Characterization and propagation of uncertainty in diffusion-weighted MR imaging. *Magnetic resonance in medicine*, *50*, 1077–1088. https://doi.org/10.1002/MRM.10609

Bekinschtein, T. A., Dehaene, S., Rohaut, B., Tadel, F., Cohen, L., & Naccache, L. (2009). Neural signature of the conscious processing of auditory regularities. *Proceedings of the National Academy of Sciences of the United States of America*, *106*, 1672–1677. https://doi.org/10.1073/PNAS.0809667106/SUPPL_FILE/0809667106SI.PDF

Berger, R. J. (1963). EXPERIMENTAL MODIFICATION OF DREAM CONTENT BY MEANINGFUL VERBAL STIMULI. *The British journal of psychiatry : the journal of mental science*, *109*, 722–740. https://doi.org/10.1192/BJP.109.463.722

Bernardi, G., Betta, M., Ricciardi, E., Pietrini, P., Tononi, G., & Siclari, F. (2019). Regional delta waves in human rapid eye movement sleep. *Journal of Neuroscience*, *39*. https://doi.org/10.1523/JNEUROSCI.2298-18.2019

Bernat, J. L. (2006). Chronic disorders of consciousness. *Lancet (London, England)*, *367*, 1181–1192. https://doi.org/10.1016/S0140-6736(06)68508-5

Blume, C., del Giudice, R., Wislowska, M., Heib, D. P., & Schabus, M. (2018). Standing sentinel during human sleep: Continued evaluation of environmental stimuli in the absence of consciousness. *NeuroImage*, *178*, 638–648. https://doi.org/10.1016/J.NEUROIMAGE.2018.05.056

Bolognini, N., Miniussi, C., Savazzi, S., Bricolo, E., & Maravita, A. (2009). TMS modulation of visual and auditory processing in the posterior parietal cortex. *Experimental Brain Research*, *195*, 509–517. https://doi.org/10.1007/S00221-009-1820-7/FIGURES/3

Boly, M., Garrido, M. I., Gosseries, O., Bruno, M. A., Boveroux, P., Schnakers, C., Massimini, M., Litvak, V., Laureys, S., & Friston, K. (2011). Preserved feedforward but impaired top-down processes in the vegetative state. *Science (New York, N.Y.)*, *332*, 858–862. https://doi.org/10.1126/SCIENCE.1202043

Boly, M., Massimini, M., Tsuchiya, N., Postle, B. R., Koch, C., & Tononi, G. (2017). Are the Neural Correlates of Consciousness in the Front or in the Back of the Cerebral Cortex? Clinical and Neuroimaging Evidence. *The Journal of neuroscience : the official journal of the Society for*

Neuroscience, *37*, 9603–9613. https://doi.org/10.1523/JNEUROSCI.3218-16.2017

Bonhomme, V., Staquet, C., Montupil, J., Defresne, A., Kirsch, M., Martial, C., Vanhaudenhuyse, A., Chatelle, C., Larroque, S. K., Raimondo, F., Demertzi, A., Bodart, O., Laureys, S., & Gosseries, O. (2019). General Anesthesia: A Probe to Explore Consciousness. *Frontiers in Systems Neuroscience*, *13*, 464177. https://doi.org/10.3389/FNSYS.2019.00036/BIBTEX

Bonhomme, V., Vanhaudenhuyse, A., Demertzi, A., Bruno, M. A., Jaquet, O., Bahri, M. A., Plenevaux, A., Boly, M., Boveroux, P., Soddu, A., Brichant, J. F., Maquet, P., & Laureys, S. (2016). Resting-state Network-specific Breakdown of Functional Connectivity during Ketamine Alteration of Consciousness in Volunteers. *Anesthesiology*, *125*, 873–888. https://doi.org/10.1097/ALN.0000000000001275

Boudewyn, M. A., Luck, S. J., Farrens, J. L., & Kappenman, E. S. (2018). How many trials does it take to get a significant ERP effect? It depends. *Psychophysiology*, *55*. https://doi.org/10.1111/psyp.13049

Braun, A. R., Balkin, T. J., Wesensten, N. J., Carson, R. E., Varga, M., Baldwin, P., Selbie, S., Belenky, G., & Herscovitch, P. (1997). Regional cerebral blood flow throughout the sleep-wake cycle. An H2(15)O PET study. *Brain : a journal of neurology*, *120 (Pt 7)*, 1173–1197. https://doi.org/10.1093/BRAIN/120.7.1173

Brice, D. D., Hetherington, R. R., & Utting, J. E. (1970). A simple study of awareness and dreaming during anaesthesia. *British journal of anaesthesia*, *42*, 535–542. https://doi.org/10.1093/BJA/42.6.535

Brown, E. N., Lydic, R., & Schiff, N. D. (2010). General anesthesia, sleep, and coma. *The New England journal of medicine*, *363*, 2638–2650. https://doi.org/10.1056/NEJMRA0808281

Brown, R., Lau, H., & LeDoux, J. E. (2019). Understanding the Higher-Order Approach to Consciousness. *Trends in Cognitive Sciences*, *23*, 754–768. https://doi.org/10.1016/J.TICS.2019.06.009

Buchanan, F. F., Myles, P. S., & Cicuttini, F. (2009). Patient sex and its influence on general anaesthesia. *Anaesthesia and Intensive Care*, *37*. https://doi.org/10.1177/0310057x0903700201

Bullard, T. L., Cobb, K., & Flynn, D. N. (2023). Intraoperative and Anesthesia Awareness. *StatPearls*. https://www.ncbi.nlm.nih.gov/books/NBK582138/

Calhoun, V. D., Adali, T., Pearlson, G. D., & Kiehl, K. A. (2006). Neuronal chronometry of target detection: fusion of hemodynamic and event-

related potential data. *NeuroImage*, *30*, 544–553. https://doi.org/10.1016/J.NEUROIMAGE.2005.08.060

Campbell, D. T., & Kenny, D. A. (2002, December). *A primer on regression artifacts* (Vol. 53). Int J Psychophysiol. https://doi.org/10.1016/S0167-8760(02)00112-5

Carhart-Harris, R. L. (2018). The entropic brain - revisited. *Neuropharmacology*, *142*, 167–178. https://doi.org/10.1016/J.NEUROPHARM.2018.03.010

Carhart-Harris, R. L., Leech, R., Hellyer, P. J., Shanahan, M., Feilding, A., Tagliazucchi, E., Chialvo, D. R., & Nutt, D. (2014). The entropic brain: A theory of conscious states informed by neuroimaging research with psychedelic drugs. *Frontiers in Human Neuroscience*, *8*, 55875. https://doi.org/10.3389/FNHUM.2014.00020/BIBTEX

Casagrande, M., Violani, C., Lucidi, F., Buttinelli, E., & Bertini, M. (1996). Variations in sleep mentation as a function of time of night. *The International journal of neuroscience*, *85*, 19–30. https://doi.org/10.3109/00207459608986348

Casey, C. P., Tanabe, S., Farahbakhsh, Z., Parker, M., Bo, A., White, M., Ballweg, T., Mcintosh, A., Filbey, W., Saalmann, Y., Pearce, R. A., & Sanders, R. D. (2022). Distinct EEG signatures differentiate unconsciousness and disconnection during anaesthesia and sleep. *British Journal of Anaesthesia*, *128*, 1006–1018. https://doi.org/10.1016/j.bja.2022.01.010

Cecconi, B., Annen, J., & Laureys, S. (2019). Can human neurological tests of consciousness be applied to octopus? *Animal Sentience*, *4*. https://doi.org/10.51291/2377-7478.1667

Cecconi, B., Gorska, U., Mat, B., Aparicio, M. K., Cilento, R., Selte, A., Monai, E., Moffet, E., Laureys, S., Gosseries, O., Schnakers, C., Annen, J., Tononi, G., & Boly, M. (2024). *Ethical and neuroscientific implications of high perturbational complexity in patients in a minimally conscious state* [In preparation].

Cecconi, B., Laureys, S., & Annen, J. (2020). Islands of Awareness or Cortical Complexity? [Letter to the editor]. *Trends in Neurosciences*, *43*, 545–546. https://doi.org/10.1016/j.tins.2020.05.007

Cecconi, B., Montupil, J., Mortaheb, S., Panda, R., Sanders, R. D., Phillips, C., Alnagger, N., Remacle, E., Defresne, A., Boly, M., Bahri, M. A., Lamalle, L., Laureys, S., Gosseries, O., Bonhomme, V., & Annen, J. (2024). Study protocol: Cerebral characterization of sensory gating in disconnected dreaming states during propofol anesthesia using fMRI.

Frontiers in Neuroscience, *18*, 1306344. https://doi.org/10.3389/FNINS.2024.1306344/BIBTEX

Cecconi, B., Mortaheb, S., Bahri, M. A., Boly, M., Laureys, S., Gosseries, O., Bonhomme, V., & Annen, J. (2024). *Cerebral characterization of sensory gating in disconnected dreaming states during propofol sedation using fMRI* [In preparation].

Cecconi, B., Riedner, B., Smith, R., Annen, J., Laureys, S., Tononi, G., Boly, M., & Baird, B. (2024). *High density EEG signatures of connected vs disconnected consciousness during REM sleep* [In preparation].

Cecconi, B., van der Lande, G., & Sala, A. (2023). Neural Correlates of Consciousness. *Coma and Disorders of Consciousness*, 1–15. https://doi.org/10.1007/978-3-031-50563-8_1

Chalmers, D. J. (1996). The Conscious Mind: In Search of a Fundamental Theory. https://philpapers.org/rec/CHATCM

Chayer, C., & Freedman, M. (2001). Frontal lobe functions. https://doi.org/10.1007/s11910-001-0060-4

Chen, G., Saad, Z. S., Britton, J. C., Pine, D. S., & Cox, R. W. (2013). Linear mixed-effects modeling approach to FMRI group analysis. *NeuroImage*, *73*, 176–190. https://doi.org/10.1016/J.NEUROIMAGE.2013.01.047

Chen, P. Y., Hsu, H. Y., Chao, Y. P., Nouchi, R., Wang, P. N., & Cheng, C. H. (2021). Altered mismatch response of inferior parietal lobule in amnestic mild cognitive impairment: A magnetoencephalographic study. *CNS Neuroscience & Therapeutics*, *27*, 1136. https://doi.org/10.1111/CNS.13691

Chernik, D. A., Gillings, D., Laine, H., Hendler, J., Silver, J. M., Davidson, A. B., Schwam, E. M., & Siegel, J. L. (1990). Validity and reliability of the observer's assessment of alertness/sedation scale: Study with intravenous midazolam. *Journal of Clinical Psychopharmacology*, *10*, 244–251. https://www.unboundmedicine.com/medline/citation/2286697/Validity%5C_and%5C_reliability%5C_of%5C_the%5C_Observer's%5C_Assessment%5C_of%5C_Alertness/Sedation%5C_Scale:%5C_study%5C_with%5C_intravenous%5C_midazolam%5C_

Chun, M. M., Golomb, J. D., & Turk-Browne, N. B. (2011). A taxonomy of external and internal attention. *Annual review of psychology*, *62*, 73–101. https://doi.org/10.1146/ANNUREV.PSYCH.093008.100427

Chung, F., Subramanyam, R., Liao, P., Sasaki, E., Shapiro, C., & Sun, Y. (2012). High STOP-Bang score indicates a high probability of obstructive sleep apnoea. *British journal of anaesthesia*, *108*, 768–775. https://doi.org/10.1093/BJA/AES022

Chung, F., Yegneswaran, B., Liao, P., Chung, S. A., Vairavanathan, S., Islam, S., Khajehdehi, A., & Shapiro, C. M. (2008). STOP questionnaire: a tool to screen patients for obstructive sleep apnea. *Anesthesiology*, *108*, 812–821. https://doi.org/10.1097/ALN.0B013E31816D83E4

Cirelli, C., & Tononi, G. (2008). Is Sleep Essential? *PLoS Biology*, *6*, 1605–1611. https://doi.org/10.1371/JOURNAL.PBIO.0060216

Clark, V. P., Fannon, S., Lai, S., Benson, R., & Bauer, L. (2000). Responses to rare visual target and distractor stimuli using event- related fmri. *Journal of Neurophysiology*, *83*. https://doi.org/10.1152/jn.2000.83.5.3133

Cloninger, C. R., Svrakic, D. M., & Przybeck, T. R. (1993). A Psychobiological Model of Temperament and Character. *Archives of General Psychiatry*, *50*, 975–990. https://doi.org/10.1001/ARCHPSYC.1993.01820240059008

Collier, A. K., Wolf, D. H., Valdez, J. N., Turetsky, B. I., Elliott, M. A., Gur, R. E., & Gur, R. C. (2014). Comparison of Auditory and Visual Oddball fMRI in Schizophrenia. *Schizophrenia research*, *158*, 183. https://doi.org/10.1016/J.SCHRES.2014.06.019

Colrain, I. M., & Campbell, K. B. (2007). The use of evoked potentials in sleep research. *Sleep Medicine Reviews*, *11*, 277–293. https://doi.org/10.1016/j.smrv.2007.05.001

Cote, K. A. (2002). Probing awareness during sleep with the auditory oddball paradigm. *International Journal of Psychophysiology*, *46*, 227–241. https://doi.org/10.1016/S0167-8760(02)00114-9

Cox, R. W. (1996). AFNI: Software for Analysis and Visualization of Functional Magnetic Resonance Neuroimages. *Computers and Biomedical Research*, *29*, 162–173. https://doi.org/10.1006/CBMR.1996.0014

Dang-Vu, T. T., Schabus, M., Desseilles, M., Sterpenich, V., Bonjean, M., & Maquet, P. (2010). Functional Neuroimaging Insights into the Physiology of Human Sleep. *Sleep*, *33*, 1589. https://doi.org/10.1093/SLEEP/33.12.1589

Darracq, M., Funk, C. M., Polyakov, D., Riedner, B., Gosseries, O., Nieminen, J. O., Bonhomme, V., Brichant, J. F., Boly, M., Laureys, S., Tononi, G., & Sanders, R. D. (2018). Evoked Alpha Power is Reduced in Disconnected Consciousness During Sleep and Anesthesia. *Scientific Reports 2018 8:1*, *8*, 1–10. https://doi.org/10.1038/s41598-018-34957-9

David, O., Kiebel, S. J., Harrison, L. M., Mattout, J., Kilner, J. M., & Friston, K. J. (2006). Dynamic causal modeling of evoked responses in EEG

and MEG. *NeuroImage*, *30*, 1255–1272. https://doi.org/10.1016/J.NEUROIMAGE.2005.10.045

Deco, G., Vidaurre, D., & Kringelbach, M. L. (2021). Revisiting the global workspace orchestrating the hierarchical organization of the human brain. *Nature human behaviour*, *5*, 497–511. https://doi.org/10.1038/S41562-020-01003-6

Dehaene, S., Changeux, J. P., & Naccache, L. (2011). The global neuronal workspace model of conscious access: From neuronal architectures to clinical applications. *Research and Perspectives in Neurosciences*, *18*, 200–227. https://doi.org/10.1007/978-3-642-18015-6_4

Delorme, A., & Makeig, S. (2004). EEGLAB: An open source toolbox for analysis of single-trial EEG dynamics including independent component analysis. *Journal of Neuroscience Methods*, *134*, 9–21. https://doi.org/10.1016/j.jneumeth.2003.10.009

Dembski, C., Koch, C., & Pitts, M. (2021). Perceptual awareness negativity: a physiological correlate of sensory consciousness. https://doi.org/10.1016/j.tics.2021.05.009

Dement, W., & Kleitman, N. (1957). The relation of eye movements during sleep to dream activity: an objective method for the study of dreaming. *Journal of experimental psychology*, *53*, 339–346. https://doi.org/10.1037/H0048189

de Pesters, A., Coon, W. G., Brunner, P., Gunduz, A., Ritaccio, A. L., Brunet, N. M., de Weerd, P., Roberts, M. J., Oostenveld, R., Fries, P., & Schalk, G. (2016). Alpha power indexes task-related networks on large and small scales: A multimodal ECoG study in humans and a non-human primate. *NeuroImage*, *134*, 122–131. https://doi.org/10.1016/J.NEUROIMAGE.2016.03.074

Doeller, C. F., Opitz, B., Mecklinger, A., Krick, C., Reith, W., & Schröger, E. (2003). Prefrontal cortex involvement in preattentive auditory deviance detection: Neuroimaging and electrophysiological evidence. *NeuroImage*, *20*, 1270–1282. https://doi.org/10.1016/S1053-8119(03)00389-6

Dudek, F. E., & Sutula, T. P. (2007). Epileptogenesis in the dentate gyrus: a critical perspective. *Progress in Brain Research*, *163*, 755–773. https://doi.org/10.1016/S0079-6123(07)63041-6

Dueck, M. H., Petzke, F., Gerbershagen, H. J., Paul, M., Heßelmann, V., Girnus, R., Krug, B., Sorger, B., Goebel, R., Lehrke, R., Sturm, V., & Boerner, U. (2005). Propofol attenuates responses of the auditory cortex to acoustic stimulation in a dose-dependent manner: a FMRI study. *Acta*

anaesthesiologica Scandinavica, *49*, 784–791. https://doi.org/10.1111/J.1399-6576.2005.00703.X

Dykstra, A. R., Cariani, P. A., & Gutschalk, A. (2017). A roadmap for the study of conscious audition and its neural basis. *Philosophical transactions of the Royal Society of London. Series B, Biological sciences*, *372*. https://doi.org/10.1098/RSTB.2016.0103

Dykstra, A. R., & Gutschalk, A. (2015). Does the mismatch negativity operate on a consciously accessible memory trace? *Science Advances*, *1*. https://doi.org/10.1126/SCIADV.1500677/SUPPL_FILE/1500677_SM.PDF

Eklund, R., Gerdfeldter, B., & Wiens, S. (2020). Is auditory awareness negativity confounded by performance? *Consciousness and Cognition*, *83*, 102954. https://doi.org/10.1016/J.CONCOG.2020.102954

Eklund, R., Gerdfeldter, B., & Wiens, S. (2021). The early but not the late neural correlate of auditory awareness reflects lateralized experiences. *Neuropsychologia*, *158*, 107910. https://doi.org/10.1016/J.NEUROPSYCHOLOGIA.2021.107910

Eklund, R., & Wiens, S. (2019). Auditory awareness negativity is an electrophysiological correlate of awareness in an auditory threshold task. *Consciousness and Cognition*, *71*, 70–78. https://doi.org/10.1016/J.CONCOG.2019.03.008

Ellia, F., Hendren, J., Grasso, M., Kozma, C., Mindt, G., Lang, J. P., Haun, A. M., Albantakis, L., Boly, M., & Tononi, G. (2021). Consciousness and the fallacy of misplaced objectivity. *Neuroscience of Consciousness*, *2021*, 1–12. https://doi.org/10.1093/nc/niab032

Ellman, S. J., & Antrobus, J. S. (1991). The mind in sleep : psychology and psychophysiology, 588.

Engemann, D. A., Raimondo, F., King, J. R., Rohaut, B., Louppe, G., Faugeras, F., Annen, J., Cassol, H., Gosseries, O., Fernandez-Slezak, D., Laureys, S., Naccache, L., Dehaene, S., & Sitt, J. D. (2018). Robust EEG-based cross-site and cross-protocol classification of states of consciousness. *Brain*, *141*, 3179–3192. https://doi.org/10.1093/BRAIN/AWY251

Errando, C. L., Sigl, J. C., Robles, M., Calabuig, E., García, J., Arocas, F., Higueras, R., Rosario, E. D., López, D., Peiró, C. M., Soriano, J. L., Chaves, S., Gil, F., & García-Aguado, R. (2008). Awareness with recall during general anaesthesia: a prospective observational evaluation of 4001 patients. *British journal of anaesthesia*, *101*, 178–185. https://doi.org/10.1093/BJA/AEN144

Esser, S. K., Hill, S., & Tononi, G. (2009). Breakdown of effective connectivity during slow wave sleep: investigating the mechanism underlying a cortical gate using large-scale modeling. *Journal of neurophysiology*, *102*, 2096–2111. https://doi.org/10.1152/JN.00059.2009

Evers, K. (2016). Neurotechnological assessment of consciousness disorders: Five ethical imperatives. *Dialogues in Clinical Neuroscience*, *18*. https://doi.org/10.31887/dcns.2016.18.2/kevers

Farisco, M., Pennartz, C., Annen, J., Cecconi, B., & Evers, K. (2022). Indicators and criteria of consciousness: ethical implications for the care of behaviourally unresponsive patients. *BMC Medical Ethics*, *23*. https://doi.org/10.1186/s12910-022-00770-3

Faugeras, F., Rohaut, B., Weiss, N., Bekinschtein, T., Galanaud, D., Puybasset, L., Bolgert, F., Sergent, C., Cohen, L., Dehaene, S., & Naccache, L. (2012). Event related potentials elicited by violations of auditory regularities in patients with impaired consciousness. *Neuropsychologia*, *50*, 403–418. https://doi.org/10.1016/J.NEUROPSYCHOLOGIA.2011.12.015

Feng, L., Motelow, J. E., Ma, C., Biche, W., McCafferty, C., Smith, N., Liu, M., Zhan, Q., Jia, R., Xiao, B., Duque, A., & Blumenfeld, H. (2017). Seizures and Sleep in the Thalamus: Focal Limbic Seizures Show Divergent Activity Patterns in Different Thalamic Nuclei. *The Journal of neuroscience : the official journal of the Society for Neuroscience*, *37*, 11441–11454. https://doi.org/10.1523/JNEUROSCI.1011-17.2017

Fischer, C., Morlet, D., Bouchet, P., Luaute, J., Jourdan, C., & Salord, F. (1999). Mismatch negativity and late auditory evoked potentials in comatose patients. *Clinical Neurophysiology*, *110*, 1601–1610. https://doi.org/10.1016/S1388-2457(99)00131-5

Fiset, P., Paus, T., Daloze, T., Plourde, G., Meuret, P., Bonhomme, V., Hajj-Ali, N., Backman, S. B., & Evans, A. C. (1999). Brain Mechanisms of Propofol-Induced Loss of Consciousness in Humans: a Positron Emission Tomographic Study. *The Journal of Neuroscience*, *19*, 5506. https://doi.org/10.1523/JNEUROSCI.19-13-05506.1999

Fitzgerald, K., & Todd, J. (2020). Making Sense of Mismatch Negativity. *Frontiers in Psychiatry*, *11*, 538673. https://doi.org/10.3389/FPSYT.2020.00468/BIBTEX

Fosse, R., Stickgold, R., & Hobson, J. A. (2001). Brain-mind states: reciprocal variation in thoughts and hallucinations. *Psychological science*, *12*, 30–36. https://doi.org/10.1111/1467-9280.00306

Fox, M. D., Snyder, A. Z., Vincent, J. L., Corbetta, M., Essen, D. C. V., & Raichle, M. E. (2005). The human brain is intrinsically organized into dynamic, anticorrelated functional networks. *Proceedings of the National Academy of Sciences of the United States of America*, *102*. https://doi.org/10.1073/pnas.0504136102

Freud, S. (1899, September). *The Interpretation of Dreams*. Franz Deuticke, Leipzig & Vienna.

Freunberger, R., Klimesch, W., Doppelmayr, M., & Höller, Y. (2007). Visual P2 component is related to theta phase-locking. *Neuroscience letters*, *426*, 181–186. https://doi.org/10.1016/J.NEULET.2007.08.062

Friedman, D., Cycowicz, Y. M., & Gaeta, H. (2001). The novelty p3: An event-related brain potential (erp) sign of the brain's evaluation of novelty. https://doi.org/10.1016/S0149-7634(01)00019-7

Friedman, N. P., & Robbins, T. W. (2022). The role of prefrontal cortex in cognitive control and executive function. https://doi.org/10.1038/s41386-021-01132-0

Friston, K. J., Harrison, L., & Penny, W. (2003). Dynamic causal modelling. *NeuroImage*, *19*, 1273–1302. https://doi.org/10.1016/S1053-8119(03)00202-7

Friston, K. J., Litvak, V., Oswal, A., Razi, A., Stephan, K. E., Wijk, B. C. V., Ziegler, G., & Zeidman, P. (2016). Bayesian model reduction and empirical Bayes for group (DCM) studies. *NeuroImage*, *128*, 413–431. https://doi.org/10.1016/J.NEUROIMAGE.2015.11.015

Frith, C., & Dolan, R. (1996). The role of the prefrontal cortex in higher cognitive functions. *Cognitive Brain Research*, *5*. https://doi.org/10.1016/S0926-6410(96)00054-7

Fukunaga, M., Horovitz, S. G., van Gelderen, P., de Zwart, J. A., Jansma, J. M., Ikonomidou, V. N., Chu, R., Deckers, R. H., Leopold, D. A., & Duyn, J. H. (2006). Large-amplitude, spatially correlated fluctuations in BOLD fMRI signals during extended rest and early sleep stages. *Magnetic resonance imaging*, *24*, 979–992. https://doi.org/10.1016/J.MRI.2006.04.018

Funk, C. M., Honjoh, S., Rodriguez, A. V., Cirelli, C., & Tononi, G. (2016). Local Slow Waves in Superficial Layers of Primary Cortical Areas during REM Sleep. *Current biology : CB*, *26*, 396–403. https://doi.org/10.1016/J.CUB.2015.11.062

Gaillard, J. M., & Blois, R. (1981). Spindle density in sleep of normal subjects. *Sleep*, *4*, 385–391. https://doi.org/10.1093/SLEEP/4.4.385

Gan, T. J., Glass, P. S., Sigl, J., Sebel, P., Payne, F., Rosow, C., & Embree, P. (1999). Women emerge from general anesthesia with propofol/alfentanil/nitrous oxide faster than men. *Anesthesiology*, *90*, 1283–1287. https://doi.org/10.1097/00000542-199905000-00010

Garrido, M. I., Friston, K. J., Kiebel, S. J., Stephan, K. E., Baldeweg, T., & Kilner, J. M. (2008). The functional anatomy of the MMN: a DCM study of the roving paradigm. *NeuroImage*, *42*, 936–944. https://doi.org/10.1016/J.NEUROIMAGE.2008.05.018

Garrido, M. I., Kilner, J. M., Kiebel, S. J., Stephan, K. E., & Friston, K. J. (2007). Dynamic causal modelling of evoked potentials: a reproducibility study. *NeuroImage*, *36*, 571–580. https://doi.org/10.1016/J.NEUROIMAGE.2007.03.014

Gaskell, A. L., Hight, D. F., Winders, J., Tran, G., Defresne, A., Bonhomme, V., Raz, A., Sleigh, J. W., & Sanders, R. D. (2017). Frontal alpha-delta EEG does not preclude volitional response during anaesthesia: prospective cohort study of the isolated forearm technique. *British journal of anaesthesia*, *119*, 664–673. https://doi.org/10.1093/BJA/AEX170

Geselowitz, D. B. (1967). On Bioelectric Potentials in an Inhomogeneous Volume Conductor. *Biophysical Journal*, *7*, 1. https://doi.org/10.1016/S0006-3495(67)86571-8

Giacino, J. T., Ashwal, S., Childs, N., Cranford, R., Jennett, B., Katz, D. I., Kelly, J. P., Rosenberg, J. H., Whyte, J., Zafonte, R. D., & Zasler, N. D. (2002). The minimally conscious state: Definition and diagnostic criteria. *Neurology*, *58*. https://doi.org/10.1212/WNL.58.3.349

Giacino, J. T., Kalmar, K., & Whyte, J. (2004). The JFK Coma Recovery Scale-Revised: measurement characteristics and diagnostic utility. *Archives of physical medicine and rehabilitation*, *85*, 2020–2029. https://doi.org/10.1016/J.APMR.2004.02.033

Glass, P. S., Bloom, M., Kearse, L., Rosow, C., Sebel, P., & Manberg, P. (1997). Bispectral analysis measures sedation and memory effects of propofol, midazolam, isoflurane, and alfentanil in healthy volunteers. *Anesthesiology*, *86*, 836–847. https://doi.org/10.1097/00000542-199704000-00014

Gold, J., & Ciorciari, J. (2020). A Review on the Role of the Neuroscience of Flow States in the Modern World. *Behavioral Sciences*, *10*. https://doi.org/10.3390/BS10090137

Goodenough, D. R., Lewis, H. B., Shapiro, A., Jaret, L., & Sleser, I. (1965). Dream reporting following abrupt and gradual awakenings from

different types of sleep. *Journal of Personality and Social Psychology*, *2*, 170–179. https://doi.org/10.1037/H0022424

Gorgolewski, K. J., Auer, T., Calhoun, V. D., Craddock, R. C., Das, S., Duff, E. P., Flandin, G., Ghosh, S. S., Glatard, T., Halchenko, Y. O., Handwerker, D. A., Hanke, M., Keator, D., Li, X., Michael, Z., Maumet, C., Nichols, B. N., Nichols, T. E., Pellman, J., … Poldrack, R. A. (2016). The brain imaging data structure, a format for organizing and describing outputs of neuroimaging experiments. *Scientific Data 2016 3:1*, *3*, 1–9. https://doi.org/10.1038/sdata.2016.44

Gosseries, O., Di, H., Laureys, S., & Boly, M. (2014). Measuring Consciousness in Severely Damaged Brains. https://doi.org/10.1146/annurev-neuro-062012-170339

Gott, J. A., Stücker, S., Kanske, P., Haaker, J., & Dresler, M. (2024). Acetylcholine and metacognition during sleep. https://doi.org/10.1016/j.concog.2023.103608

Grau, C., Fuentemilla, L., & Marco-Pallarés, J. (2007). Functional neural dynamics underlying auditory event-related n1 and n1 suppression response. *NeuroImage*, *36*. https://doi.org/10.1016/j.neuroimage.2007.03.027

Gross, W. L., Lauer, K. K., Liu, X., Roberts, C. J., Liu, S., Gollapudy, S., Binder, J. R., Li, S. J., & Hudetz, A. G. (2019). Propofol sedation alters perceptual and cognitive functions in healthy volunteers as revealed by functional magnetic resonance imaging. *Anesthesiology*, *131*. https://doi.org/10.1097/ALN.0000000000002669

Guldenmund, P., Gantner, I. S., Baquero, K., Das, T., Demertzi, A., Boveroux, P., Bonhomme, V., Vanhaudenhuyse, A., Bruno, M. A., Gosseries, O., Noirhomme, Q., Kirsch, M., Boly, M., Owen, A. M., Laureys, S., Gómez, F., & Soddu, A. (2016). Propofol-Induced Frontal Cortex Disconnection: A Study of Resting-State Networks, Total Brain Connectivity, and Mean BOLD Signal Oscillation Frequencies. *Brain connectivity*, *6*, 225–237. https://doi.org/10.1089/BRAIN.2015.0369

Halgren, E., Baudena, P., Clarke, J. M., Heit, G., Marinkovic, K., Devaux, B., Vignal, J. P., & Biraben, A. (1995). Intracerebral potentials to rare target and distractor auditory and visual stimuli. ii. medial, lateral and posterior temporal lobe. *Electroencephalography and Clinical Neurophysiology*, *94*. https://doi.org/10.1016/0013-4694(95)98475-N

Hämäläinen, M. S., & Sarvas, J. (1989). Realistic conductivity geometry model of the human head for interpretation of neuromagnetic data. *IEEE*

transactions on bio-medical engineering, *36*, 165–171. https://doi.org/10.1109/10.16463

Harel, A. (2020). P2: A novel erp marker of global scene perception. *Journal of Vision*, *20*. https://doi.org/10.1167/jov.20.11.908

Hassin, R. R. (2013). Yes It Can: On the Functional Abilities of the Human Unconscious. *Perspectives on Psychological Science*, *8*. https://doi.org/10.1177/1745691612460684

Hayat, H., Regev, N., Matosevich, N., Sales, A., Paredes-Rodriguez, E., Krom, A. J., Bergman, L., Li, Y., Lavigne, M., Kremer, E. J., Yizhar, O., Pickering, A. E., & Nir, Y. (2020). Locus coeruleus norepinephrine activity mediates sensory-evoked awakenings from sleep. *Science advances*, *6*. https://doi.org/10.1126/SCIADV.AAZ4232

Heinke, W., Fiebach, C. J., Schwarzbauer, C., Meyer, M., Olthoff, D., & Alter, K. (2004). Sequential effects of propofol on functional brain activation induced by auditory language processing: an event-related functional magnetic resonance imaging study. *British journal of anaesthesia*, *92*, 641–650. https://doi.org/10.1093/BJA/AEH133

Hennevin, E., Huetz, C., & Edeline, J. M. (2007). Neural representations during sleep: From sensory processing to memory traces. *Neurobiology of Learning and Memory*, *87*, 416–440. https://doi.org/10.1016/J.NLM.2006.10.006

Hipp, J. F., Engel, A. K., & Siegel, M. (2011). Oscillatory synchronization in large-scale cortical networks predicts perception. *Neuron*, *69*, 387–396. https://doi.org/10.1016/J.NEURON.2010.12.027

Hobson, J. A., Pace-Schott, E. F., Stickgold, R., & Kahn, D. (1998). To dream or not to dream? Relevant data from new neuroimaging and electrophysiological studies. *Current opinion in neurobiology*, *8*, 239–244. https://doi.org/10.1016/S0959-4388(98)80146-3

Howarth, C., Mishra, A., & Hall, C. N. (2021). More than just summed neuronal activity: how multiple cell types shape the BOLD response. *Philosophical Transactions of the Royal Society B*, *376*. https://doi.org/10.1098/RSTB.2019.0630

Hsu, S. H., Pion-Tonachini, L., Palmer, J., Miyakoshi, M., Makeig, S., & Jung, T. P. (2018). Modeling brain dynamic state changes with adaptive mixture independent component analysis. *NeuroImage*, *183*, 47–61. https://doi.org/10.1016/J.NEUROIMAGE.2018.08.001

Huffmeijer, R., Bakermans-Kranenburg, M. J., Alink, L. R., & IJzendoorn, M. H. V. (2014). Reliability of event-related potentials: The influence

of number of trials and electrodes. *Physiology and Behavior*, *130*, 13–22. https://doi.org/10.1016/J.PHYSBEH.2014.03.008

Hughes, P., & Watson, J. B. (1926). Behaviorism. *The Journal of Philosophy*, *23*, 331. https://doi.org/10.2307/2014115

Huupponen, E., Himanen, S. L., Värri, A., Hasan, J., Lehtokangas, M., & Saarinen, J. (2002). A study on gender and age differences in sleep spindles. *Neuropsychobiology*, *45*, 99–105. https://doi.org/10.1159/000048684

Igelström, K. M., & Graziano, M. S. (2017). The inferior parietal lobule and temporoparietal junction: A network perspective. *Neuropsychologia*, 1–14. https://doi.org/10.1016/j.neuropsychologia.2017.01.001

Irvine, E. (2012). Old Problems with New Measures in the Science of Consciousness. *British Journal for the Philosophy of Science*, *63*, 627–648. https://doi.org/10.1093/BJPS/AXS019

Isaacson, J. S., & Scanziani, M. (2011). How Inhibition Shapes Cortical Activity. *Neuron*, *72*, 231–243. https://doi.org/10.1016/J.NEURON.2011.09.027

Jacobsen, T., Casco, C., & Werth, R. (2022). A Scientific Approach to Conscious Experience, Introspection, and Unconscious Processing: Vision and Blindsight. https://doi.org/10.3390/brainsci12101305

Jemel, B., George, N., Olivares, E., Fiori, N., & Renault, B. (1999). Event-related potentials to structural familiar face incongruity processing. *Psychophysiology*, *36*. https://doi.org/10.1017/S0048577299970853

Jenkinson, M., Bannister, P., Brady, M., & Smith, S. (2002). Improved optimization for the robust and accurate linear registration and motion correction of brain images. *NeuroImage*, *17*, 825–841. https://doi.org/10.1016/S1053-8119(02)91132-8

Jensen, O., & Mazaheri, A. (2010). Shaping functional architecture by oscillatory alpha activity: gating by inhibition. *Frontiers in human neuroscience*, *4*. https://doi.org/10.3389/FNHUM.2010.00186

Justen, C., & Herbert, C. (2018). The spatio-temporal dynamics of deviance and target detection in the passive and active auditory oddball paradigm: A sLORETA study. *BMC Neuroscience*, *19*. https://doi.org/10.1186/S12868-018-0422-3/FIGURES/4

Kahan, T. L., & LaBerge, S. P. (2011). Dreaming and waking: Similarities and differences revisited. *Consciousness and Cognition*, *20*, 494–514. https://doi.org/10.1016/J.CONCOG.2010.09.002

Kakigi, R., Naka, D., Okusa, T., Wang, X., Inui, K., Qiu, Y., Tran, T. D., Miki, K., Tamura, Y., Nguyen, T. B., Watanabe, S., & Hoshiyama, M. (2003). Sensory perception during sleep in humans: a magnetoencephalograhic

study. *Sleep Medicine*, *4*, 493–507. https://doi.org/10.1016/S1389-9457(03)00169-2

Kam, J. W. Y., & Handy, T. C. (2013). The neurocognitive consequences of the wandering mind: a mechanistic account of sensory-motor decoupling. *Frontiers in Psychology*, *4*. https://doi.org/10.3389/FPSYG.2013.00725

Katzner, S., Busse, L., & Carandini, M. (2011). GABAA inhibition controls response gain in visual cortex. *The Journal of neuroscience : the official journal of the Society for Neuroscience*, *31*, 5931–5941. https://doi.org/10.1523/JNEUROSCI.5753-10.2011

Kiebel, S. J., Garrido, M. I., Moran, R. J., & Friston, K. J. (2008). Dynamic causal modelling for eeg and meg. *Cognitive Neurodynamics*, *2*. https://doi.org/10.1007/s11571-008-9038-0

Kiehl, K. A., Stevens, M. C., Laurens, K. R., Pearlson, G., Calhoun, V. D., & Liddle, P. F. (2005). An adaptive reflexive processing model of neurocognitive function: supporting evidence from a large scale (n = 100) fMRI study of an auditory oddball task. *NeuroImage*, *25*, 899–915. https://doi.org/10.1016/J.NEUROIMAGE.2004.12.035

Killingsworth, M. A., & Gilbert, D. T. (2010). A wandering mind is an unhappy mind. *Science*, *330*, 932. https://doi.org/10.1126/SCIENCE.1192439/SUPPL_FILE/KILLINGSWORTH.SOM.PDF

Klimesch, W., Sauseng, P., & Hanslmayr, S. (2007). EEG alpha oscillations: the inhibition-timing hypothesis. *Brain research reviews*, *53*, 63–88. https://doi.org/10.1016/J.BRAINRESREV.2006.06.003

Koch, C. (2017). How to Make a Consciousness Meter. *Scientific American*, *317*, 28–33. https://doi.org/10.1038/SCIENTIFICAMERICAN1117-28

Konkoly, K. R., Appel, K., Chabani, E., Mangiaruga, A., Gott, J., Mallett, R., Caughran, B., Witkowski, S., Whitmore, N. W., Mazurek, C. Y., Berent, J. B., Weber, F. D., Türker, B., Leu-Semenescu, S., Maranci, J. B., Pipa, G., Arnulf, I., Oudiette, D., Dresler, M., & Paller, K. A. (2021). Real-time dialogue between experimenters and dreamers during REM sleep. *Current Biology*, *31*, 1417–1427.e6. https://doi.org/10.1016/J.CUB.2021.01.026

Koroma, M., Lacaux, C., Andrillon, T., Legendre, G., Léger, D., & Kouider, S. (2020). Sleepers Selectively Suppress Informative Inputs during Rapid Eye Movements. *Current Biology*, *30*, 2411–2417.e3. https://doi.org/10.1016/J.CUB.2020.04.047

Krom, A. J., Marmelshtein, A., Gelbard-Sagiv, H., Tankus, A., Hayat, H., Hayat, D., Matot, I., Strauss, I., Fahoum, F., Soehle, M., Bostrom, J., Mormann, F., Fried, I., & Nir, Y. (2020). Anesthesia-induced loss

of consciousness disrupts auditory responses beyond primary cortex. *Proceedings of the National Academy of Sciences of the United States of America*, *117*, 11770–11780. https://doi.org/10.1073/PNAS.1917251117/SUPPL_FILE/PNAS.1917251117.SAPP.PDF

Kyriazi, H. T., Carvell, G. E., Brumberg, J. C., & Simons, D. J. (1996). Quantitative effects of GABA and bicuculline methiodide on receptive field properties of neurons in real and simulated whisker barrels. *Journal of neurophysiology*, *75*, 547–560. https://doi.org/10.1152/JN.1996.75.2.547

Lange, J., Oostenveld, R., & Fries, P. (2013). Reduced occipital alpha power indexes enhanced excitability rather than improved visual perception. *The Journal of neuroscience : the official journal of the Society for Neuroscience*, *33*, 3212–3220. https://doi.org/10.1523/JNEUROSCI.3755-12.2013

Langille, J. J. (2019). Human rem sleep delta waves and the blurring distinction between nrem and rem sleep. *Journal of Neuroscience*, *39*. https://doi.org/10.1523/JNEUROSCI.0480-19.2019

Laureys, S. (2005). The neural correlate of (un)awareness: lessons from the vegetative state. *Trends in cognitive sciences*, *9*, 556–559. https://doi.org/10.1016/J.TICS.2005.10.010

Lennertz, R., Pryor, K. O., Raz, A., Parker, M., Bonhomme, V., Schuller, P., Schneider, G., Moore, M., Coburn, M., Root, J. C., Emerson, J. M., Hohmann, A. L., Azaria, H., Golomb, N., Defresne, A., Montupil, J., Pilge, S., Obert, D. P., van Waart, H., … Sanders, R. D. (2023). Connected consciousness after tracheal intubation in young adults: an international multicentre cohort study. *British journal of anaesthesia*, *130*, e217–e224. https://doi.org/10.1016/J.BJA.2022.04.010

Leslie, K. (2010). Dreaming during anesthesia. *Consciousness, Awareness, and Anesthesia*, 74–89. https://doi.org/10.1017/CBO9780511676291.005

Leslie, K., Skrzypek, H., Paech, M. J., Kurowski, I., & Whybrow, T. (2007). Dreaming during anesthesia and anesthetic depth in elective surgery patients: a prospective cohort study. *Anesthesiology*, *106*, 33–42. https://doi.org/10.1097/00000542-200701000-00010

Leslie, K., Sleigh, J., Paech, M. J., Voss, L., Lim, C. W., & Sleigh, C. (2009). Dreaming and electroencephalographic changes during anesthesia maintained with propofol or desflurane. *Anesthesiology*, *111*, 547–555. https://doi.org/10.1097/ALN.0B013E3181ADF768

Leslie, K., & Ogilvie, R. (1996). Vestibular dreams: The effect of rocking on dream mentation. *Dreaming*, *6*, 1–16. https://doi.org/10.1037/H0094442

Li, Y., Dai, W., Wang, T., Wu, Y., Dou, F., & Xing, D. (2023). Visual surround suppression at the neural and perceptual levels. *Cognitive Neurodynamics 2023 18:2*, *18*, 741–756. https://doi.org/10.1007/S11571-023-10027-3

Linassi, F., Zanatta, P., Tellaroli, P., Ori, C., & Carron, M. (2018). Isolated forearm technique: a meta-analysis of connected consciousness during different general anaesthesia regimens. *British journal of anaesthesia*, *121*, 198–209. https://doi.org/10.1016/J.BJA.2018.02.019

Linden, D. E., Prvulovic, D., Formisano, E., Völlinger, M., Zanella, F. E., Goebel, R., & Dierks, T. (1999). The functional neuroanatomy of target detection: An fmri study of visual and auditory/oddball tasks. *Cerebral Cortex*, *9*. https://doi.org/10.1093/cercor/9.8.815

Ling, L., Yang, T. X., & Lee, S. W. K. (2022). Effect of anaesthesia depth on postoperative delirium and postoperative cognitive dysfunction in high-risk patients: A systematic review and meta-analysis. *Cureus*. https://doi.org/10.7759/cureus.30120

Liu, J., Lee, H. J., Weitz, A. J., Fang, Z., Lin, P., Choy, M., Fisher, R., Pinskiy, V., Tolpygo, A., Mitra, P., Schiff, N., & Lee, J. H. (2015). Frequency-selective control of cortical and subcortical networks by central thalamus. *eLife*, *4*. https://doi.org/10.7554/ELIFE.09215.001

Lok, R., Qian, J., & Chellappa, S. L. (2024). Sex differences in sleep, circadian rhythms, and metabolism: Implications for precision medicine. *Sleep medicine reviews*, *75*. https://doi.org/10.1016/J.SMRV.2024.101926

Maquet, P. (2000). Functional neuroimaging of normal human sleep by positron emission tomography. *Journal of sleep research*, *9*, 207–231. https://doi.org/10.1046/J.1365-2869.2000.00214.X

Maquet, P., Ruby, P., Maudoux, A., Albouy, G., Sterpenich, V., Dang-Vu, T., Desseilles, M., Boly, M., Perrin, F., Peigneux, P., & Laureys, S. (2005). Human cognition during REM sleep and the activity profile within frontal and parietal cortices: a reappraisal of functional neuroimaging data. *Progress in brain research*, *150*, 219–227. https://doi.org/10.1016/S0079-6123(05)50016-5

Marcel, > (2003). Introspective Report: Trust, Self-Knowledge and Science.

Markovic, A., Kaess, M., & Tarokh, L. (2020). Gender differences in adolescent sleep neurophysiology: a high-density sleep EEG study. *Scientific*

Reports 2020 10:1, *10*, 1–13. https://doi.org/10.1038/s41598-020-72802-0

Mashour, G. A., & Avidan, M. S. (2015). Intraoperative awareness: controversies and non-controversies. *BJA: British Journal of Anaesthesia*, *115*, i20–i26. https://doi.org/10.1093/BJA/AEV034

Mashour, G. A. (2019). Role of cortical feedback signalling in consciousness and anaesthetic-induced unconsciousness. *British Journal of Anaesthesia*, *123*, 404–405. https://doi.org/10.1016/j.bja.2019.07.001

Mashour, G. A., Roelfsema, P., Changeux, J. P., & Dehaene, S. (2020). Conscious Processing and the Global Neuronal Workspace Hypothesis. *Neuron*, *105*, 776–798. https://doi.org/10.1016/J.NEURON.2020.01.026

Mason, S. E., Noel-Storr, A., & Ritchie, C. W. (2010). The impact of general and regional anesthesia on the incidence of post-operative cognitive dysfunction and post-operative delirium: A systematic review with meta-analysis. *Journal of Alzheimer's Disease*, *22*. https://doi.org/10.3233/JAD-2010-101086

Massimini, M., Ferrarelli, F., Huber, R., Esser, S. K., Singh, H., & Tononi, G. (2005). Breakdown of cortical effective connectivity during sleep. *Science (New York, N.Y.)*, *309*, 2228–2232. https://doi.org/10.1126/SCIENCE.1117256

Mathur, S., Patel, J., Goldstein, S., Hendrix, J. M., & Jain, A. (2023). Bispectral Index. *Journal of Experimental and Clinical Medicine (Turkey)*, *39*, 587–588. https://doi.org/10.52142/omujecm.39.2.60

Mawhinney, L. J., Mabourakh, D., & Lewis, M. C. (2012). Gender-Specific Differences in the Central Nervous System's Response to Anesthesia. *Translational Stroke Research 2012 4:4*, *4*, 462–475. https://doi.org/10.1007/S12975-012-0229-Y

Mazaheri, A., & Jensen, O. (2010). Rhythmic pulsing: linking ongoing brain activity with evoked responses. *Frontiers in human neuroscience*, *4*. https://doi.org/10.3389/FNHUM.2010.00177

Mazzi, C., Bagattini, C., & Savazzi, S. (2016). Blind-Sight vs. Degraded-Sight: Different Measures Tell a Different Story. *Frontiers in psychology*, *7*. https://doi.org/10.3389/FPSYG.2016.00901

McCormick, D. A., & Bal, T. (1994). Sensory gating mechanisms of the thalamus. *Current opinion in neurobiology*, *4*, 550–556. https://doi.org/10.1016/0959-4388(94)90056-6

McShane, B. B., Gal, D., Gelman, A., Robert, C., & Tackett, J. L. (2019). Abandon statistical significance. *American Statistician*, *73*. https://doi.org/10.1080/00031305.2018.1527253

Mechelli, A., Price, C. J., Henson, R. N. A., & Friston, K. J. (2003). Estimating efficiency a priori: a comparison of blocked and randomized designs. https://doi.org/10.1016/S1053-8119(02)00040-X

Medic, G., Wille, M., & Hemels, M. E. (2017). Short- and long-term health consequences of sleep disruption. *Nature and Science of Sleep*, *9*, 151. https://doi.org/10.2147/NSS.S134864

Merchie, A., & Gomot, M. (2023). Habituation, Adaptation and Prediction Processes in Neurodevelopmental Disorders: A Comprehensive Review. *Brain Sciences 2023, Vol. 13, Page 1110*, *13*, 1110. https://doi.org/10.3390/BRAINSCI13071110

Mhuircheartaigh, R. N., Warnaby, C., Rogers, R., Jbabdi, S., & Tracey, I. (2013). Slow-wave activity saturation and thalamocortical isolation during propofol anesthesia in humans. *Science translational medicine*, *5*. https://doi.org/10.1126/SCITRANSLMED.3006007

Miller, E. K. (2000). The prefontral cortex and cognitive control. *Nature Reviews Neuroscience*, *1*. https://doi.org/10.1038/35036228

Moerman, N., Bonke, B., & Oosting, J. (1993). Awareness and recall during general anesthesia. Facts and feelings. *Anesthesiology*, *79*, 454–464. https://doi.org/10.1097/00000542-199309000-00007

Moheimanian, L., Paraskevopoulou, S. E., Adamek, M., Schalk, G., & Brunner, P. (2021). Modulation in cortical excitability disrupts information transfer in perceptual-level stimulus processing. *NeuroImage*, *243*, 118498. https://doi.org/10.1016/J.NEUROIMAGE.2021.118498

Moon, H. S., Jiang, H., Vo, T. T., Jung, W. B., Vazquez, A. L., & Kim, S. G. (2021). Contribution of Excitatory and Inhibitory Neuronal Activity to BOLD fMRI. *Cerebral Cortex (New York, NY)*, *31*, 4053. https://doi.org/10.1093/CERCOR/BHAB068

Moran, R. J., Kiebel, S. J., Stephan, K. E., Reilly, R. B., Daunizeau, J., & Friston, K. J. (2007). A neural mass model of spectral responses in electrophysiology. *Neuroimage*, *37*, 706. https://doi.org/10.1016/J.NEUROIMAGE.2007.05.032

Mosher, J. C., Leahy, R. M., & Lewis, P. S. (1999). EEG and MEG: forward solutions for inverse methods. *IEEE transactions on bio-medical engineering*, *46*, 245–259. https://doi.org/10.1109/10.748978

Mudrik, L., & Deouell, L. Y. (2022). Neuroscientific Evidence for Processing Without Awareness. *https://doi.org/10.1146/annurev-neuro-110920-*

033151, *45*, 403–423. https://doi.org/10.1146/ANNUREV-NEURO-110920-033151

Mutschler, I., Wieckhorst, B., Speck, O., Schulze-Bonhage, A., Hennig, J., Seifritz, E., & Ball, T. (2010). Time Scales of Auditory Habituation in the Amygdala and Cerebral Cortex. *Cerebral Cortex*, *20*, 2531–2539. https://doi.org/10.1093/CERCOR/BHQ001

Muzur, A., Pace-Schott, E. F., & Hobson, J. A. (2002). The prefrontal cortex in sleep. *Trends in Cognitive Sciences*, *6*, 475–481. https://doi.org/10.1016/S1364-6613(02)01992-7

Näätänen, R., & Picton, T. (1987). The N1 wave of the human electric and magnetic response to sound: a review and an analysis of the component structure. *Psychophysiology*, *24*, 375–425. https://doi.org/10.1111/J.1469-8986.1987.TB00311.X

Näätänen, R., Tervaniemi, M., Sussman, E., Paavilainen, P., & Winkler, I. (2001). "Primitive intelligence" in the auditory cortex. *Trends in neurosciences*, *24*, 283–288. https://doi.org/10.1016/S0166-2236(00)01790-2

Nagel, T. (1974). Philosophical Review What Is It Like to Be a Bat? *Source: The Philosophical Review*, *83*, 435–450. https://doi.org/10.2307/2183914

Nichols, T. E., & Holmes, A. P. (2002). Nonparametric permutation tests for functional neuroimaging: a primer with examples. *Human brain mapping*, *15*, 1–25. https://doi.org/10.1002/HBM.1058

Nielsen, T. A. (1993). Changes in the kinesthetic content of dreams following somatosensory stimulation of leg muscles during REM sleep. *Dreaming*, *3*, 99–113. https://doi.org/10.1037/H0094374

Nir, Y., & Tononi, G. (2010). Dreaming and the brain: from phenomenology to neurophysiology. *Trends in cognitive sciences*, *14*, 88–100. https://doi.org/10.1016/J.TICS.2009.12.001

Nofzinger, E. A., Mintun, M. A., Wiseman, M., Kupfer, D. J., & Moore, R. Y. (1997). Forebrain activation in REM sleep: an FDG PET study. *Brain Research*, *770*, 192–201. https://doi.org/10.1016/S0006-8993(97)00807-X

Noreika, V., Jylhänkangas, L., Móró, L., Valli, K., Kaskinoro, K., Aantaa, R., Scheinin, H., & Revonsuo, A. (2011). Consciousness lost and found: subjective experiences in an unresponsive state. *Brain and cognition*, *77*, 327–334. https://doi.org/10.1016/J.BANDC.2011.09.002

Nourski, K. V., Steinschneider, M., Rhone, A. E., Kawasaki, H., Howard, M. A., & Banks, M. I. (2018). Auditory Predictive Coding across Awareness States under Anesthesia: An Intracranial Electrophysiology Study.

Journal of Neuroscience, *38*, 8441–8452. https://doi.org/10.1523/JNEUROSCI.0967-18.2018

Ooms, F., Annen, J., Panda, R., Cecconi, B., Surlemont, B., & Laureys, S. (2024). Entrepreneurial neuroanatomy: Exploring gray matter volume in habitual entrepreneurs. *Journal of Business Venturing Insights*, *22*, e00480. https://doi.org/10.1016/J.JBVI.2024.E00480

Opitz, B., Rinne, T., Mecklinger, A., Cramon, D. Y. V., & Schröger, E. (2002). Differential contribution of frontal and temporal cortices to auditory change detection: Fmri and erp results. *NeuroImage*, *15*. https://doi.org/10.1006/nimg.2001.0970

Osterman, J. E., Hopper, J., Heran, W. J., Keane, T. M., & van der Kolk, B. A. (2001). Awareness under anesthesia and the development of posttraumatic stress disorder. *General hospital psychiatry*, *23*, 198–204. https://doi.org/10.1016/S0163-8343(01)00142-6

Overgaard, M., Fehl, K., Mouridsen, K., Bergholt, B., & Cleeremans, A. (2008). Seeing without Seeing? Degraded Conscious Vision in a Blindsight Patient. *PLOS ONE*, *3*, e3028. https://doi.org/10.1371/JOURNAL.PONE.0003028

Overgaard, M., & Sandberg, K. (2012). Kinds of access: Different methods for report reveal different kinds of metacognitive access. *Philosophical Transactions of the Royal Society B: Biological Sciences*, *367*, 1287. https://doi.org/10.1098/rstb.2011.0425

Panda, R., López-González, A., Gilson, M., Gosseries, O., Thibaut, A., Frasso, G., Cecconi, B., Escrichs, A., Deco, G., Laureys, S., Zamora-López, G., & Annen, J. (2023). Whole-brain analyses indicate the impairment of posterior integration and thalamo-frontotemporal broadcasting in disorders of consciousness. *Human Brain Mapping*, *44*, 4352–4371. https://doi.org/10.1002/HBM.26386

Pandit, J. J., Cook, T. M., Jonker, W. R., & O'Sullivan, E. (2013). A national survey of anaesthetists (NAP5 Baseline) to estimate an annual incidence of accidental awareness during general anaesthesia in the UK. *Anaesthesia*, *68*, 343–353. https://doi.org/10.1111/ANAE.12190

Pavlov, I. P. (1906). THE SCIENTIFIC INVESTIGATION OF THE PSYCHICAL FACULTIES OR PROCESSES IN THE HIGHER ANIMALS. *Science (New York, N.Y.)*, *24*, 613–619. https://doi.org/10.1126/SCIENCE.24.620.613

Pavlov, I. P. (1927). Conditioned reflexes: An investigation of the physiological activity of the cerebral cortex. *Annals of Neurosciences*, *17*, 136. https://doi.org/10.5214/ANS.0972-7531.1017309

Peels, R. (2016). The empirical case against introspection. *Philosophical Studies: An International Journal for Philosophy in the Analytic Tradition*, *173*, 2461–2485.

Pélissolo, A., & Lépine, J. P. (2000). Normative data and factor structure of the Temperament and Character Inventory (TCI) in the French version. *Psychiatry research*, *94*, 67–76. https://doi.org/10.1016/S0165-1781(00)00127-X

Perger, E., Silvestri, R., Bonanni, E., Perri, M. C. D., Fernandes, M., Provini, F., Zoccoli, G., & Lombardi, C. (2024). Gender medicine and sleep disorders: from basic science to clinical research. *Frontiers in Neurology*, *15*, 1392489. https://doi.org/10.3389/FNEUR.2024.1392489/BIBTEX

Perrin, F., García-Larrea, L., Mauguière, F., & Bastuji, H. (1999). A differential brain response to the subject's own name persists during sleep. *Clinical Neurophysiology*, *110*, 2153–2164. https://doi.org/10.1016/S1388-2457(99)00177-7

Picton, T. W., Hillyard, S. A., Krausz, H. I., & Galambos, R. (1974). Human auditory evoked potentials. I. Evaluation of components. *Electroencephalography and clinical neurophysiology*, *36*, 179–190. https://doi.org/10.1016/0013-4694(74)90155-2

Pisapia, N. D., Bornstein, M. H., Rigo, P., Esposito, G., Falco, S. D., & Venuti, P. (2013). Sex differences in directional brain responses to infant hunger cries. *Neuroreport*, *24*, 142–146. https://doi.org/10.1097/WNR.0B013E32835DF4FA

Plihal, W., & Born, J. (1997). Effects of early and late nocturnal sleep on declarative and procedural memory. *Journal of cognitive neuroscience*, *9*, 534–547. https://doi.org/10.1162/JOCN.1997.9.4.534

Plourde, G., Belin, P., Chartrand, D., Fiset, P., Backman, S. B., Xie, G., & Zatorre, R. J. (2006). Cortical Processing of Complex Auditory Stimuli during Alterations of Consciousness with the General Anesthetic Propofol. *Anesthesiology*, *104*, 448–457. https://doi.org/10.1097/00000542-200603000-00011

Plum, F., & Posner, J. B. (1972). The diagnosis of stupor and coma. *Contemporary neurology series*, *10*. https://doi.org/10.1001/jama.1981.03310320080042

Poo, C., & Isaacson, J. S. (2009). Odor representations in olfactory cortex: "sparse" coding, global inhibition and oscillations. *Neuron*, *62*, 850. https://doi.org/10.1016/J.NEURON.2009.05.022

Radek, L., Kallionpää, R. E., Karvonen, M., Scheinin, A., Maksimow, A., Långsjö, J., Kaisti, K., Vahlberg, T., Revonsuo, A., Scheinin, H., & Valli,

K. (2018). Dreaming and awareness during dexmedetomidine- and propofol-induced unresponsiveness. *British Journal of Anaesthesia*, *121*, 260–269. https://doi.org/10.1016/j.bja.2018.03.014

Ramsøy, T. Z., & Overgaard, M. (2004). Introspection and subliminal perception. *Phenomenology and the Cognitive Sciences 2004 3:1*, *3*, 1–23. https://doi.org/10.1023/B:PHEN.0000041900.30172.E8

Rasch, B., & Born, J. (2015). In search of a role of REM sleep in memory formation. *Neurobiology of learning and memory*, *122*, 1–3. https://doi.org/10.1016/J.NLM.2015.04.012

Riel-Salvatore, J., & Clark, G. A. (2001). Grave Markers. *https://doi.org/10.1086/321801*, *42*, 449–479. https://doi.org/10.1086/321801

Rietdijk, W. J., Franken, I. H., & Thurik, A. R. (2014). Internal consistency of event-related potentials associated with cognitive control: N2/P3 and ERN/Pe. *PloS one*, *9*. https://doi.org/10.1371/JOURNAL.PONE.0102672

Rinne, T., Alho, K., Ilmoniemi, R. J., Virtanen, J., & Näätänen, R. (2000). Separate time behaviors of the temporal and frontal mismatch negativity sources. *NeuroImage*, *12*. https://doi.org/10.1006/nimg.2000.0591

Romei, V., Rihs, T., Brodbeck, V., & Thut, G. (2008). Resting electroencephalogram alpha-power over posterior sites indexes baseline visual cortex excitability. *Neuroreport*, *19*, 203–208. https://doi.org/10.1097/WNR.0B013E3282F454C4

Röösli, M., Mohler, E., Frei, P., & Vienneau, D. (2014). Noise-related sleep disturbances: does gender matter? *Noise & health*, *16*, 197–204. https://doi.org/10.4103/1463-1741.137036

Russell, I. F., & Wang, M. (2015). The IFT (isolated forearm technique) and consciousness. *BJA: British Journal of Anaesthesia*, *114*, 532–532. https://doi.org/10.1093/BJA/AEV024

Rutiku, R., Martin, M., Bachmann, T., & Aru, J. (2015). Does the P300 reflect conscious perception or its consequences? *Neuroscience*, *298*, 180–189. https://doi.org/10.1016/J.NEUROSCIENCE.2015.04.029

Sakellariou, D. F., Nesbitt, A. D., Higgins, S., Beniczky, S., Rosenzweig, J., Drakatos, P., Gildeh, N., Murphy, P. B., Kent, B., Williams, A. J., Kryger, M., Goadsby, P. J., Leschziner, G. D., & Rosenzweig, I. (2020). Co-activation of rhythms during alpha band oscillations as an interictal biomarker of exploding head syndrome. *Cephalalgia*, *40*. https://doi.org/10.1177/0333102420902705

Salvesen, L., Capriglia, E., Dresler, M., & Bernardi, G. (2024). Influencing dreams through sensory stimulation: A systematic review. *Sleep Medicine Reviews*, *74*. https://doi.org/10.1016/J.SMRV.2024.101908

Sandberg, K., Bibby, B. M., Timmermans, B., Cleeremans, A., & Overgaard, M. (2011). Measuring consciousness: Task accuracy and awareness as sigmoid functions of stimulus duration. *Consciousness and Cognition*, *20*. https://doi.org/10.1016/j.concog.2011.09.002

Sanders, R. D., Casey, C., & Saalmann, Y. B. (2021). Predictive coding as a model of sensory disconnection: relevance to anaesthetic mechanisms. *British journal of anaesthesia*, *126*, 37–40. https://doi.org/10.1016/J.BJA.2020.08.017

Sanders, R. D., Gaskell, A., Raz, A., Winders, J., Stevanovic, A., Rossaint, R., Boncyk, C., Defresne, A., Tran, G., Tasbihgou, S., Meier, S., Vlisides, P. E., Fardous, H., Hess, A., Bauer, R. M., Absalom, A., Mashour, G. A., Bonhomme, V., Coburn, M., & Sleigh, J. (2017). Incidence of Connected Consciousness after Tracheal Intubation: A Prospective, International, Multicenter Cohort Study of the Isolated Forearm Technique. *Anesthesiology*, *126*, 214–222. https://doi.org/10.1097/ALN.0000000000001479

Sanders, R. D., Tononi, G., Laureys, S., & Sleigh, J. W. (2012, April). Unresponsiveness $\neq$ unconsciousness. https://doi.org/10.1097/ALN.0b013e318249d0a7

Sandin, R. H., Enlund, G., Samuelsson, P., & Lennmarken, C. (2000). Awareness during anaesthesia: a prospective case study. *Lancet (London, England)*, *355*, 707–711. https://doi.org/10.1016/S0140-6736(99)11010-9

Saxena, N., Gili, T., Diukova, A., Huckle, D., Hall, J. E., & Wise, R. G. (2019). Mild Propofol Sedation Reduces Frontal Lobe and Thalamic Cerebral Blood Flow: An Arterial Spin Labeling Study. *Frontiers in physiology*, *10*. https://doi.org/10.3389/FPHYS.2019.01541

Scammell, T. E., Arrigoni, E., & Lipton, J. O. (2017). Neural Circuitry of Wakefulness and Sleep. *Neuron*, *93*, 747. https://doi.org/10.1016/J.NEURON.2017.01.014

Schaefer, A., Kong, R., Gordon, E. M., Laumann, T. O., Zuo, X.-N., Holmes, A. J., Eickhoff, S. B., & Yeo, B. T. T. (2018). Local-Global Parcellation of the Human Cerebral Cortex from Intrinsic Functional Connectivity MRI. *Cerebral cortex (New York, N.Y. : 1991)*, *28*, 3095–3114. https://doi.org/10.1093/CERCOR/BHX179

Scheinin, A., Kantonen, O., Alkire, M., Långsjö, J., Kallionpää, R. E., Kaisti, K., Radek, L., Johansson, J., Sandman, N., Nyman, M., Scheinin, M.,

Vahlberg, T., Revonsuo, A., Valli, K., & Scheinin, H. (2021). Foundations of Human Consciousness: Imaging the Twilight Zone. *Journal of Neuroscience*, *41*, 1769–1778. https://doi.org/10.1523/JNEUROSCI.0775-20.2020

Schnider, T. W., Minto, C. F., Shafer, S. L., Gambus, P. L., Andresen, C., Goodale, D. B., & Youngs, E. J. (1999). The influence of age on propofol pharmacodynamics. *Anesthesiology*, *90*, 1502–1516. https://doi.org/10.1097/00000542-199906000-00003

Schredl, M., Atanasova, D., Hörmann, K., Maurer, J. T., Hummel, T., & Stuck, B. A. (2009). Information processing during sleep: the effect of olfactory stimuli on dream content and dream emotions. *Journal of sleep research*, *18*, 285–290. https://doi.org/10.1111/J.1365-2869.2009.00737.X

Schröder, P., Nierhaus, T., & Blankenburg, F. (2021). Dissociating Perceptual Awareness and Postperceptual Processing: The P300 Is Not a Reliable Marker of Somatosensory Target Detection. *The Journal of Neuroscience*, *41*, 4686. https://doi.org/10.1523/JNEUROSCI.2950-20.2021

Seli, P., Kane, M. J., Smallwood, J., Schacter, D. L., Maillet, D., Schooler, J. W., & Smilek, D. (2018). Mind-Wandering as a Natural Kind: A Family-Resemblances View. *Trends in Cognitive Sciences*, *22*, 479–490. https://doi.org/10.1016/J.TICS.2018.03.010

Sergent, C., Baillet, S., & Dehaene, S. (2005). Timing of the brain events underlying access to consciousness during the attentional blink. *Nature neuroscience*, *8*, 1391–1400. https://doi.org/10.1038/NN1549

Shahid, A., Wilkinson, K., Marcu, S., & Shapiro, C. M. (2011). Stanford Sleepiness Scale (SSS). *STOP, THAT and One Hundred Other Sleep Scales*, 369–370. https://doi.org/10.1007/978-1-4419-9893-4_91

Shanks, D. R. (2017). Regressive research: The pitfalls of post hoc data selection in the study of unconscious mental processes. *Psychonomic Bulletin and Review*, *24*. https://doi.org/10.3758/s13423-016-1170-y

Siclari, F., Baird, B., Perogamvros, L., Bernardi, G., LaRocque, J. J., Riedner, B., Boly, M., Postle, B. R., & Tononi, G. (2017). The neural correlates of dreaming. *Nature Neuroscience 2017 20:6*, *20*, 872–878. https://doi.org/10.1038/nn.4545

Siclari, F., Bernardi, G., Cataldi, J., & Tononi, G. (2018). Dreaming in NREM Sleep: A High-Density EEG Study of Slow Waves and Spindles. *The Journal of Neuroscience*, *38*, 9175. https://doi.org/10.1523/JNEUROSCI.0855-18.2018

Siclari, F., LaRocque, J. J., Postle, B. R., & Tononi, G. (2013). Assessing sleep consciousness within subjects using a serial awakening paradigm. *Frontiers in Psychology*, *4*, 542. https://doi.org/10.3389/FPSYG.2013.00542/BIBTEX

Siclari, F., & Tononi, G. (2017). Local aspects of sleep and wakefulness. https://doi.org/10.1016/j.conb.2017.05.008

Skinner, B. F. (1938). *The Behaviorof Organismms*.

Sklar, A. Y., Levy, N., Goldstein, A., Mandel, R., Maril, A., & Hassin, R. R. (2012). Reading and doing arithmetic nonconsciously. *Proceedings of the National Academy of Sciences of the United States of America*, *109*. https://doi.org/10.1073/pnas.1211645109

Smallwood, J., Beach, E., Schooler, J. W., & Handy, T. C. (2008). Going AWOL in the brain: mind wandering reduces cortical analysis of external events. *Journal of cognitive neuroscience*, *20*, 458–469. https://doi.org/10.1162/JOCN.2008.20037

Smallwood, J., Fitzgerald, A., Miles, L. K., & Phillips, L. H. (2009). Shifting moods, wandering minds: negative moods lead the mind to wander. *Emotion (Washington, D.C.)*, *9*, 271–276. https://doi.org/10.1037/A0014855

Smith, G., D'Cruz, J. R., Rondeau, B., & Goldman, J. (2023). General Anesthesia for Surgeons. *StatPearls*.

Song, C., Boly, M., Tagliazucchi, E., Laufs, H., & Tononi, G. (2022). fMRI spectral signatures of sleep. *Proceedings of the National Academy of Sciences of the United States of America*, *119*. https://doi.org/10.1073/PNAS.2016732119

Squires, N. K., Squires, K. C., & Hillyard, S. A. (1975). Two varieties of long-latency positive waves evoked by unpredictable auditory stimuli in man. *Electroencephalography and Clinical Neurophysiology*, *38*, 387–401. https://doi.org/10.1016/0013-4694(75)90263-1

Stephan, A. M., Lecci, S., Cataldi, J., & Siclari, F. (2021). Conscious experiences and high-density eeg patterns predicting subjective sleep depth. *Current Biology*, *31*. https://doi.org/10.1016/j.cub.2021.10.012

Stevens, A. A., Skudlarski, P., Gatenby, J. C., & Gore, J. C. (2000). Event-related fMRI of auditory and visual oddball tasks. *Magnetic Resonance Imaging*, *18*, 495–502. https://doi.org/10.1016/S0730-725X(00)00128-4

Stickgold, R., Malia, A., Fosse, R., & Hobson, J. A. (2001). Brain-mind states: I. Longitudinal field study of sleep/wake factors influencing mentation report length. *Sleep*, *24*, 171–179. https://doi.org/10.1093/SLEEP/24.2.171

Stickgold, R., Whidbee, D., Schirmer, B., Patel, V., & Hobson, J. A. (2000). Visual discrimination task improvement: A multi-step process occurring during sleep. *Journal of cognitive neuroscience*, *12*, 246–254. https://doi.org/10.1162/089892900562075

Strobel, A., Debener, S., Sorger, B., Peters, J. C., Kranczioch, C., Hoechstetter, K., Engel, A. K., Brocke, B., & Goebel, R. (2008). Novelty and target processing during an auditory novelty oddball: a simultaneous event-related potential and functional magnetic resonance imaging study. *NeuroImage*, *40*, 869–883. https://doi.org/10.1016/J.NEUROIMAGE.2007.10.065

Sussman, E. S., Chen, S., Sussman-Fort, J., & Dinces, E. (2014). The Five Myths of MMN: Redefining how to use MMN in basic and clinical research. *Brain topography*, *27*, 553. https://doi.org/10.1007/S10548-013-0326-6

Tadel, F., Baillet, S., Mosher, J. C., Pantazis, D., & Leahy, R. M. (2011). Brainstorm: a user-friendly application for MEG/EEG analysis. *Computational intelligence and neuroscience*, *2011*. https://doi.org/10.1155/2011/879716

Tasbihgou, S. R., Vogels, M. F., & Absalom, A. R. (2018). Accidental awareness during general anaesthesia - a narrative review. *Anaesthesia*, *73*, 112–122. https://doi.org/10.1111/ANAE.14124

Taylor, P. A., Reynolds, R. C., Calhoun, V., Gonzalez-Castillo, J., Handwerker, D. A., Bandettini, P. A., Mejia, A. F., & Chen, G. (2023). Highlight results, don't hide them: Enhance interpretation, reduce biases and improve reproducibility. *NeuroImage*, *274*. https://doi.org/10.1016/j.neuroimage.2023.120138

Tellegen, A., & Atkinson, G. (1974). Openness to absorbing and self-altering experiences ("absorption"), a trait related to hypnotic susceptibility. *Journal of Abnormal Psychology*, *83*, 268–277. https://doi.org/10.1037/H0036681

Thibaut, A., Panda, R., Annen, J., Sanz, L. R., Naccache, L., Martial, C., Chatelle, C., Aubinet, C., Bonin, E. A., Barra, A., Briand, M. M., Cecconi, B., Wannez, S., Stender, J., Laureys, S., & Gosseries, O. (2021). Preservation of Brain Activity in Unresponsive Patients Identifies MCS Star. *Annals of neurology*, *90*, 89–100. https://doi.org/10.1002/ANA.26095

Timmermans, B., Sandberg, K., Cleeremans, A., & Overgaard, M. (2010). Partial awareness distinguishes between measuring conscious perception and conscious content: Reply to Dienes and Seth. https://doi.org/10.1016/j.concog.2010.05.006

Tononi, G., Boly, M., & Cirelli, C. (2024). Consciousness and sleep. *Neuron*, *0*. https://doi.org/10.1016/J.NEURON.2024.04.011

Tononi, G., & Massimini, M. (2008). Why does consciousness fade in early sleep? *Annals of the New York Academy of Sciences*, *1129*, 330–334. https://doi.org/10.1196/ANNALS.1417.024

Tsuchiya, N., Wilke, M., Frässle, S., & Lamme, V. A. (2015). No-Report Paradigms: Extracting the True Neural Correlates of Consciousness. *Trends in Cognitive Sciences*, *19*, 757–770. https://doi.org/10.1016/J.TICS.2015.10.002

Türker, B., Musat, E. M., Chabani, E., Fonteix-Galet, A., Maranci, J. B., Wattiez, N., Pouget, P., Sitt, J., Naccache, L., Arnulf, I., & Oudiette, D. (2023). Behavioral and brain responses to verbal stimuli reveal transient periods of cognitive integration of the external world during sleep. *Nature Neuroscience*, *26*. https://doi.org/10.1038/s41593-023-01449-7

Tyrer, A., Gilbert, J. R., Adams, S., Stiles, A. B., Bankole, A. O., Gilchrist, I. D., & Moran, R. J. (2020). Lateralized memory circuit dropout in Alzheimer's disease patients. *Brain Communications*, *2*. https://doi.org/10.1093/BRAINCOMMS/FCAA212

Ujma, P. P., Konrad, B. N., Genzel, L., Bleifuss, A., Simor, P., Pótári, A., Körmendi, J., Gombos, F., Steiger, A., Bódizs, R., & Dresler, M. (2014). Sleep Spindles and Intelligence: Evidence for a Sexual Dimorphism. *The Journal of Neuroscience*, *34*, 16358. https://doi.org/10.1523/JNEUROSCI.1857-14.2014

Valli, K., Radek, L., Kallionpää, R. E., Scheinin, A., Långsjö, J., Kaisti, K., Kantonen, O., Korhonen, J., Vahlberg, T., Revonsuo, A., & Scheinin, H. (2023). Subjective experiences during dexmedetomidine- or propofol-induced unresponsiveness and non-rapid eye movement sleep in healthy male subjects. *British journal of anaesthesia*, *131*, 348–359. https://doi.org/10.1016/J.BJA.2023.04.026

Vanhaudenhuyse, A., Demertzi, A., Schabus, M., Noirhomme, Q., Bredart, S., Boly, M., Phillips, C., Soddu, A., Luxen, A., Moonen, G., & Laureys, S. (2011). Two distinct neuronal networks mediate the awareness of environment and of self. *Journal of Cognitive Neuroscience*, *23*. https://doi.org/10.1162/jocn.2010.21488

Vuyk, J., Mertens, M. J., Olofsen, E., Burm, A. G., & Bovill, J. G. (1997). Propofol anesthesia and rational opioid selection: determination of optimal EC50-EC95 propofol-opioid concentrations that assure adequate anesthesia and a rapid return of consciousness. *Anesthesiology*, *87*, 1549–1562. https://doi.org/10.1097/00000542-199712000-00033

Wang, J., Caspary, D., & Salvi, R. J. (2000). GABA-A antagonist causes dramatic expansion of tuning in primary auditory cortex. *Neuroreport*, *11*, 1137–1140. https://doi.org/10.1097/00001756-200004070-00045

Wang, M., Messina, A. G., & Russell, I. F. (2012). The topography of awareness: a classification of intra-operative cognitive states. *Anaesthesia*, *67*, 1197–1201. https://doi.org/10.1111/ANAE.12041

Wang, Y., Lu, L., Zou, G., Zheng, L., Qin, L., Zou, Q., & Gao, J. H. (2022). Disrupted neural tracking of sound localization during non-rapid eye movement sleep. *NeuroImage*, *260*, 119490. https://doi.org/10.1016/J.NEUROIMAGE.2022.119490

Ward, A. F., & Wegner, D. M. (2013). Mind-blanking: When the mind goes away. *Frontiers in Psychology*, *4*, 59718. https://doi.org/10.3389/FPSYG.2013.00650/BIBTEX

Ward, D. S., Norton, J. R., Guivarc'h, P. H., Litman, R. S., & Bailey, P. L. (2002). Pharmacodynamics and pharmacokinetics of propofol in a medium-chain triglyceride emulsion. *Anesthesiology*, *97*, 1401–1408. https://doi.org/10.1097/00000542-200212000-00011

Watakabe, A., Skibbe, H., Nakae, K., Abe, H., Ichinohe, N., Rachmadi, M. F., Wang, J., Takaji, M., Mizukami, H., Woodward, A., Gong, R., Hata, J., Essen, D. C. V., Okano, H., Ishii, S., & Yamamori, T. (2022). Local and long-distance organization of prefrontal cortex circuits in the marmoset brain. *bioRxiv*, 2021.12.26.474213. https://doi.org/10.1101/2021.12.26.474213

Westerhausen, R., Moosmann, M., Alho, K., Belsby, S. O., Hämäläinen, H., Medvedev, S., Specht, K., & Hugdahl, K. (2010). Identification of attention and cognitive control networks in a parametric auditory fMRI study. *Neuropsychologia*, *48*, 2075–2081. https://doi.org/10.1016/J.NEUROPSYCHOLOGIA.2010.03.028

Windt, J. M., Nielsen, T., & Thompson, E. (2016). Does Consciousness Disappear in Dreamless Sleep? *Trends in cognitive sciences*, *20*, 871–882. https://doi.org/10.1016/J.TICS.2016.09.006

Wittgenstein, L. (1967). Philosophische Untersuchungen [Philosophical Investigations] (3rd ed.), vii, 250.

Wood, K. C., Blackwell, J. M., & Geffen, M. N. (2017). Cortical inhibitory interneurons control sensory processing. *Current opinion in neurobiology*, *46*, 200. https://doi.org/10.1016/J.CONB.2017.08.018

Wronka, E., Kaiser, J., & Coenen, A. M. (2012). Neural generators of the auditory evoked potential components p3a and p3b. *Acta Neurobiologiae Experimentalis*, *72*. https://doi.org/10.55782/ane-2012-1880

Xia, M., Wang, J., & He, Y. (2013). BrainNet Viewer: A Network Visualization Tool for Human Brain Connectomics. *PLOS ONE*, *8*, e68910. https://doi.org/10.1371/JOURNAL.PONE.0068910

Yang, C. M., & Wu, C. S. (2007). The effects of sleep stages and time of night on nrem sleep erps. *International Journal of Psychophysiology*, *63*. https://doi.org/10.1016/j.ijpsycho.2006.08.006

Yanko, M. R., & Spalek, T. M. (2014). Driving with the wandering mind: The effect that mind-wandering has on driving performance. *Human Factors*, *56*, 260–269. https://doi.org/10.1177/0018720813495280/ASSET/IMAGES/LARGE/10.1177_0018720813495280-FIG3.JPEG

Young, M. J., Bodien, Y. G., Giacino, J. T., Fins, J. J., Truog, R. D., Hochberg, L. R., & Edlow, B. L. (2021). The neuroethics of disorders of consciousness: A brief history of evolving ideas. https://doi.org/10.1093/brain/awab290

Zeidman, P., Friston, K., & Parr, T. (2023). A primer on variational laplace (vl). *NeuroImage*, *279*. https://doi.org/10.1016/j.neuroimage.2023.120310

Zeidman, P., Jafarian, A., Seghier, M. L., Litvak, V., Cagnan, H., Price, C. J., & Friston, K. J. (2019). A guide to group effective connectivity analysis, part 2: Second level analysis with PEB. *NeuroImage*, *200*, 12–25. https://doi.org/10.1016/J.NEUROIMAGE.2019.06.032

Zhang, H., Wang, W., Zhao, Z., Ge, Y., Zhang, J., Yu, D., Chai, W., Wu, S., & Xu, L. (2010). The action sites of propofol in the normal human brain revealed by functional magnetic resonance imaging. *Anatomical record (Hoboken, N.J. : 2007)*, *293*. https://doi.org/10.1002/AR.21069

Zhang, K., Du, X., Liu, X., Su, W., Sun, Z., Wang, M., & Du, X. (2022). Gender differences in brain response to infant emotional faces. *BMC Neuroscience*, *23*, 1–13. https://doi.org/10.1186/S12868-022-00761-5/FIGURES/2

Zhang, K., Li, K., Zhang, C., Li, X., Han, S., Lv, C., Xie, J., Xia, X., Bie, L., & Guo, Y. (2023). The accuracy of different mismatch negativity amplitude representations in predicting the levels of consciousness in patients with disorders of consciousness. *Frontiers in Neuroscience*, *17*, 1293798. https://doi.org/10.3389/FNINS.2023.1293798/FULL

Zhang, Z., & Sun, Q. Q. (2011). The Balance Between Excitation And Inhibition And Functional Sensory Processing In The Somatosensory Cortex. *International Review of Neurobiology*, *97*, 305–333. https://doi.org/10.1016/B978-0-12-385198-7.00012-6